W&M ScholarWorks

Dissertations, Theses, and Masters Projects   Theses, Dissertations, & Master Projects

2013

Application of Acoustics and Optics for the Characterization of Suspended Particulate Matter within an Estuarine Observing System

Grace M. Cartwright

College of William and Mary - Virginia Institute of Marine Science

Follow this and additional works at: https://scholarworks.wm.edu/etd

Part of the Geology Commons

Application of Acoustics and Optics for the Characterization of Suspended Particulate Matter within an Estuarine Observing System

A Dissertation
Presented to
The Faculty of the School of Marine Science
The College of William and Mary in Virginia

In partial fulfillment
Of the requirement of
Doctor of Philosophy Degree

by

Grace M. Cartwright
Department of Physical Sciences
2013

APPROVAL SHEET

This dissertation is submitted in partial fulfillment of

The requirements for the degree of

Doctor of Philosophy
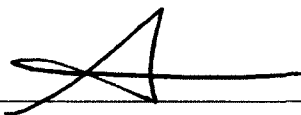
Grace M. Cartwright

Approved, by the Committee, July 2013

Carl T. Friedrichs, Ph.D.
Committee Chairman/Advisor
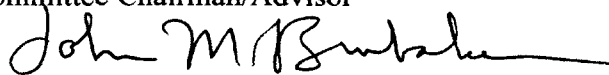
John M. Brubaker, Ph.D.

Courtney K. Harris, Ph.D.

Mark R. Patterson, Ph.D.

Lawrence P. Sanford, Ph.D.

Paul D. Panetta, Ph.D.

To my Mom and Dad,

For telling me I could be whatever I wanted to be.

To Rose and Bruce,

For living with me while I did it.

TABLE OF CONTENTS
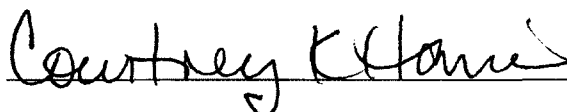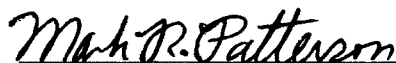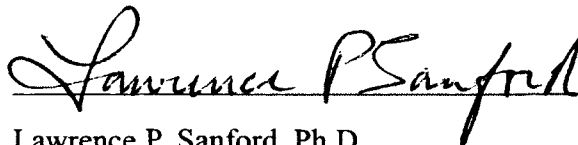
Conclusions and Suggestions for Future Work

ACKNOWLEDGMENTS

It's funny how in life when one door closes and it seems like it can't get any worse, we find that it really did happen for a reason. I would like to thank David Evans, John Boon, and Carl Hershner for their encouraging advice 17 years ago at a time I thought the world was about to end. I also want to thank John Milliman for his belief in my ability as a student (even though he thought I was a "late bloomer" and his Airedale was better looking than my Aussies). But most of all I would like to thank Carl Friedrichs for stepping up and offering me a full time position that would not only allow me to support myself and my daughter, but would also allow me to continue to grow in ways that I never thought would be possible on that fateful day way back when! Carl's belief in family and his ability to give credit to those that do the work has made it possible for me to blossom. Improvements in my scientific reasoning were made possible by him allowing me to run with a project with only slight nudges now and then to keep me on track. My writing skills improved with many a "great job" even though the paper was full of red ink as he polished my rough edges. Of course, knowing he would do the "Happy Dance" for accomplishments both big and small made me strive to continue to do my best. And now I can add this dissertation as one more accomplishment to the list of many I have been able to complete while working with Carl. So Carl, Thank you again for all you have done for me!

Family, Friends, Science, Motorcycles and Aussies... Life doesn't get any better than this!

LIST OF TABLES

LIST OF FIGURES

Chapter 3

Chapter 4

Chapter 5

Chapter 6

ABSTRACT

As part of this dissertation work, a long term observing station at Clay Bank on the York River in Virginia has been established and maintained since 2006, and was used to gain a better understanding of sediment processes in a muddy estuary and in muddy coastal environments in general. While data from this NSF-funded Multi-Disciplinary Benthic Exchange Dynamic (MUDBED) observing system has and will be used by other students for this general purpose, this dissertation focuses specifically on better understanding and interpretation of the data collected by key instrumentation regularly deployed at the observing station, especially the acoustic Doppler velocimeter (ADV).

Chapter 1, the introduction to this dissertation, provides an overview of the setting for the MUDBED observing system, namely the York River Estuary, Virginia, and briefly discusses some of the scientific and societal issues that motivate the ongoing study of this environment. Background is provided into the history of the MUDBED observing system and into the properties and operation of the ADV and other key instruments applied in this dissertation, including the Laser *In Situ* Scattering Transmissometer (LISST) and two particle cameras. In the context of describing these instruments, the science papers associated with the dissertation (Chapters 2 through 6) are introduced.

Chapter 2 describes use of SonTek ADVs within the real-time components of the MUDBED observing system and findings based on ADV observations through 2009. ADVs deployed at Clay Bank, and also at a more biologically-dominated down-river site, provided long-term estimates of water velocity, bottom stress, suspended sediment concentration, sediment settling velocity (w_s), and bed stress under spatially and seasonally variable conditions. Bed erodibility and w_s were found to be inversely correlated in both time and space, but both tended to remain more consistent in time at the biological site. At the physical site the erodibility increased and w_s decreased following seasonal increases in river discharge.

Chapter 3 reports on dual use of a mixing tank for calibrating SonTek ADV acoustic backscatter (ABS) and for direct Doppler measurement of w_s. This study utilized the fact that, absent net vertical volume flux, the average vertical velocity registered by an ADV across a horizontal plane is equal to the sediment's mean w_s. A series of calibrations were run for sand sizes between 63 and 150 µm . A grid of ADV measurements revealed that the mean vertical velocity registered by the ADV was indeed consistent with each grain size's w_s as independently measured in a settling tube. Also, a systematic increase in the proportionality between sand concentration and ABS was observed with increasing grain size.

Chapter 4 compares ABS from five 6-MHz Nortek ADVs versus five 5-MHz SonTek ADVs to examine the relative roles played by inter-vendor, intra-vendor, and sediment variability in determining their ABS response. Significant ABS offsets were found for both vendors' ADVs. Before offset correction, ABS was more consistent among Nortek

or SonTek units which had consecutive serial numbers. Sand calibrations indicated that the higher frequency Norteks were more susceptible to attenuation. For well-mixed silty-mud in the lab, calibration slopes for both vendors were close to the theoretical value for a constant grain-size suspension. In the field, however, a clearly different slope suggests a change in the acoustic properties of suspended particles with concentration.

Chapter 5 characterizes suspended sediment at Clay Bank in the presence of both muddy flocs and pellets through use of an ADV for bulk w_s, pump samples for mass concentration, and a LISST plus a high definition (non-video) particle camera for size distribution. Mass concentration, bulk w_s and an abundant ~90 mm size class were found to be in phase with velocity and stress, consistent with the suspension of relatively dense, rapidly settling and resilient pellets. Volume concentration of an abundant ~300 mm class peaked well after stress and velocity began to decrease, consistent with the formation of lower density, slowly settling and fragile flocs.

Chapter 6 builds on Chapter 3 by utilizing two separate ADV methods to measure w_s and comparing both to observations from settling tubes. As well as direct Doppler measurement of sand, w_s for mud was measured by assuming a Rouse balance between upward Reynolds flux and downward settling. Rouse-balance ADV estimates of w_s were collected at Clay Bank for muddy flocs and confirmed *in situ* by a high-definition video settling column. Observations suggested that, in the absence of significant particle aggregation/disaggregation, (i) measurement of w_s and (ii) w_s itself are both relatively insensitive to the local intensity of fluid turbulence for w_s up to several cm/s.

Application of Acoustics and Optics for the Characterization of Suspended Particulate Matter within an Estuarine Observing System

CHAPTER 1

INTRODUCTION

1.1 Observing Systems

Observing systems allow for almost continuous collection of data records, some reported in real-time, which enable scientists to better understand long-term and short-term processes, many of which directly affect the quality of human life. Observing systems that allow for detection of short term changes that affect human lives include (for example): the National Oceanic and Atmospheric Administration's (NOAA) National Data Buoy Center's DART buoy system for tsunami detection in both the Pacific and Atlantic Oceans as well as the Gulf of Mexico and the U.S. Geological Survey nationwide real-time Streamflow program to monitor river discharge for the prediction of floods. The models to forecast the tsunamis and floods save lives but would be much less reliable without the good quality data from these observing stations.

Probably one of the best-known networks of observing systems is the around 1500 weather stations reporting to the NOAA National Weather Service (NWS). Forecasts based on past and present observations from these weather stations are used on a daily basis for things as mundane as deciding to take a sweater to wear because the temperature is expected to drop this afternoon, to lifesaving decisions such as ordering the evacuation of areas in New York and New Jersey when Category 1 Hurricane Sandy was predicted to make landfall in that area. The decision turned out to be a sound one since the eye of the nearly 1000-mile wind-field named Sandy made landfall near Atlantic City, NJ on

3
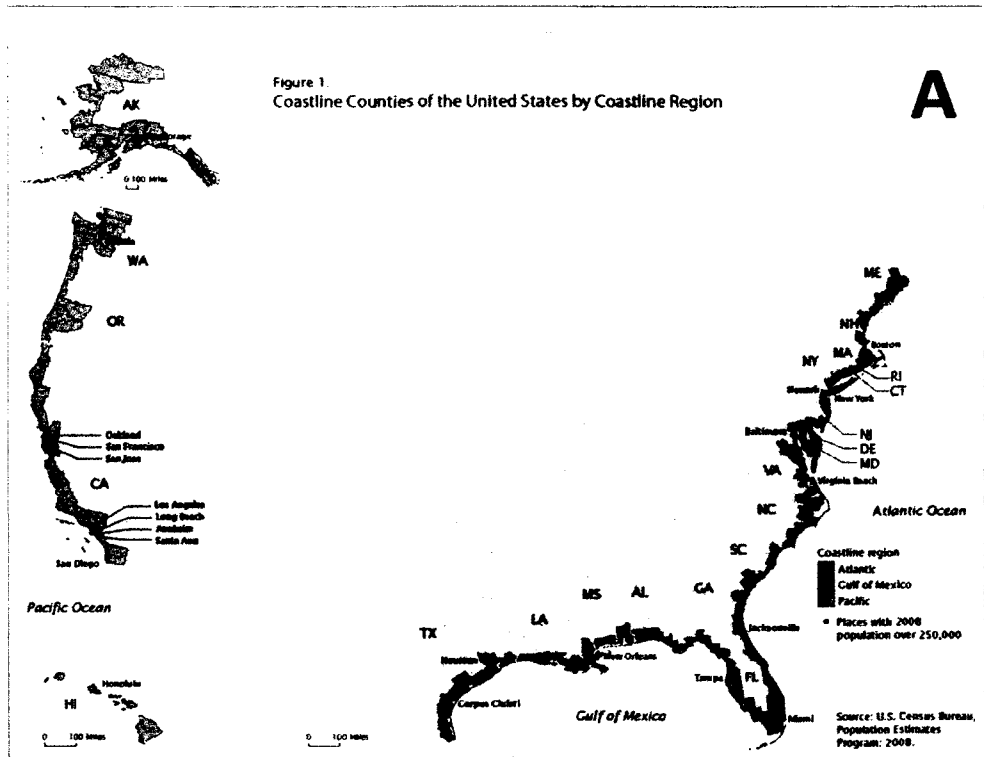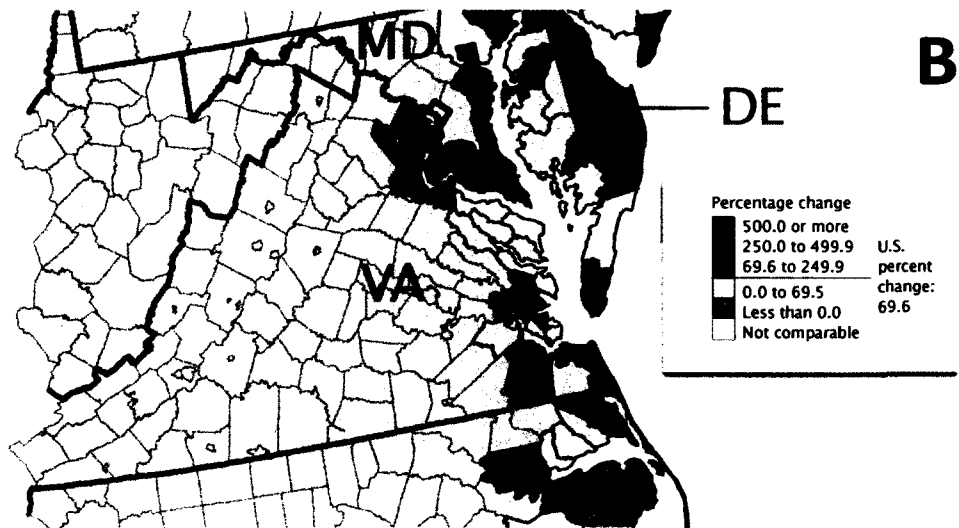
Figure 1.1. A) Coastline counties along the East Coast marked in green. Cities with populations over 250,000 are labeled. B) Percentage change in population density (number of people per square mile) between 1960-2008 along the Chesapeake Bay. (Wilson and Fischetti, 2010)

October 29, 2012, where it joined a Nor'Easter to become a superstorm. Sandy ultimately affected 23 states causing snowstorms, widespread power outages and flooding across some of the most densely populated areas of the United States, including New York City, causing an estimated $50 billion in damages, making it one of the most costly in US history (Washington Post, 2012; San Francisco Chronicle, 2012; Wilson and Fischetti, 2010).

Twenty-nine percent of the United State's population resides in 254 coastline counties located along the country's saltwater edges identified in Figure 1.1A. Almost 50 percent of the population in the 23 coastal states resides within the coastline counties of those states. Most of the populations along the coast in 1960 were in the metropolitan areas but since then the areas between have filled in leaving very little area along the coast without human impact (Wilson and Fischetti, 2010). The high density of the population along our coasts, especially areas along the East Coast with its gently sloping topography and the highest population densities of the nation, are very vulnerable. With sea-level rise and a more intense storm pattern expected in the future it is more important than ever to have good quality data from observing systems to protect our people. But observation stations can also be used to understand natural processes and recognize changes occurring within our ecosystems due to our changing environment. These changes impact not only people's lives and property but our nation's natural resources as well (for example: land use for food sources, natural habitat and recreation, energy sources, fisheries).

1.1.1 Why an observing station in the York River, Virginia?

An observing station set up in an estuary allows for the study of present day hydrodynamic and sediment dynamics processes during the most energetic periods of episodic events when most of the erosion and transport processes are likely occurring. The conditions during these events are prohibitive for the use of vessels and personnel to collect the information. Without an observing station the cost of regularly repeated data collections, necessary to understanding the long and short term changes in the dynamics, using vessels and personnel is also prohibitive and biased toward more quiescent periods. The York River Estuary is an ideal choice among the Chesapeake Bay estuaries as the Virginia Institute of Marine Science is located near the mouth of the York making deployment and maintenance of equipment on the observing system more cost effective than other estuaries of the Chesapeake Bay.

Effective management recognizes that climate change and sea-level rise are affecting our natural resources. Change in ecosystems is inevitable, yet often unpredictable; therefore it is important to rigorously monitor the environment and living resources (Duffy, 2008). Significant research that ties in well with a hydrodynamic and sediment dynamic observing station has been and continues to be conducted on the Chesapeake Bay and its tributaries including, but are not limited to the following:

Local Sea-level Research

A sea-level curve, using only Chesapeake Bay area sea-level data, estimates the relative sea level (RSL) at the beginning of the Holocene to be about 60 meters below present sea level. This is about the depth of the deepest parts of the Susquehanna River palaeo-channel beneath the present Chesapeake Bay. The curve shows a relatively rapid rise in sea-level in the period from the beginning of the Holocene to approximately 6000 years ago of ~12.5 mm/year. The present rate of relative sea level rise (RSL) for the lower York River area is 3.95 ± 0.27 mm/year. While this is less than seen in the early Holocene, the lower York is expected to see sea-level rise of 0.7 ± 0.21 meters above present day levels by 2050, among the highest experienced along the US East coast (Colman et al, 1992; Boon et al, 2010; Boon, 2012; Sallenger et al., 2012).

The absolute sea level rise (ASL) measured at Gloucester Point on the York is estimated to be 1.37 ± 1.19 mm/year. Over fifty percent of the relative sea level in the Mid-Atlantic States is due to subsidence (subsidence = RSL − ASL). A large portion has been attributed to the collapse of a last glacial forebulge. As the glacial ice receded it caused a post-glacial rebound of the previously underlying crust and subsequent subsidence of the forebulge (Gornitz and Seeber, 1990; Engehart et al., 2009; Hobbs et al., 2010). Anthropogenic subsidence, compaction of the sedimentary layer when groundwater is removed, has also been attributed to further lowering the elevation near the confluence of the Pamunkey and Mattaponi rivers where they flow into the York River Estuary.

Groundwater pumped for cooling water at the pulp plant caused subsidence (between 1940 and 1971) of up to 4.8 mm/year, or more than twice the rate of the surrounding watershed (Davis, 1987; Holzer and Galloway, 2005; Boon et al., 2010). Ongoing compaction of disturbed sediment along the rim and outer edge of the Chesapeake Bay comet or meteor strike crater and megablock faulting just inside the crater also likely enhances local subsidence of the lower York River (Powars & Bruce 1999; Boon et al. 2010).

Population

Study of the effects of sea level rise must not be limited to just the states bordering the sea but should also include those areas inland affected by the sea's tidal range. The inland Chesapeake Bay and its tributaries (including the York River in Virginia) have counties along the tidal excursion which account for over 14% of the coastline counties identified by Wilson and Fischetti (2010). Of the 36 counties along the coasts of the Chesapeake Bay, six in 2008 were found to be within the top 20 coastline counties, of 254, with the highest population density including: the city of Baltimore in Maryland; and the Virginia cities of Norfolk, Portsmouth, Hampton, Newport News; and the county of Fairfax. The population densities for four of these counties have increased more than 500 percent since 1960. Thirteen others have grown by more than the 70 percent increase seen in the rest of the United States, over half of those more than 250 percent. (Figure 1.1B). This increase in the population density means that more people than ever before along the

8

shores of the Chesapeake Bay are vulnerable to sea level rise and the associated changing weather patterns causing more intense storms and tidal flooding. Not only their lives, their homes, and their livelihoods will be affected, but also the natural resources of the bay and its tributaries that many depend on to survive or, at the very least, to provide a better quality of life. The Gloucester, York and James City Counties bordering the York River are representative of the above average population density increases seen in other coastal counties (Wilson and Fischetti, 2010).

Geologic History

In order to better plan for sea level rise it is necessary to understand hydrodynamic and sediment dynamics processes involved. The geologic record of the coastal plain around the Chesapeake Bay shows that during the Pleistocene (~2.6 MY to ~11,700 years ago) there were large oscillations in global sea level due to the repeated advance and retreat of the northern hemisphere ice sheets. Every time the sea level rose, marine terraces and scarps were cut into the earlier formations and the sediment eroded was moved around and eventually deposited. Because of the terraces and scarps we can make good estimates of how high the sea level rose for each successively lower stand. However, because the same sedimentary material was reworked during each high stand it is difficult to guess exactly how it was moved around and deposited unless we apply the Law of Uniformitarianism and assume the processes that are working on the sediment today are

9

the same as those that were present during the previous high stands (Mixon et al., 1989; Johnson and Hobbs, 1990; Hobbs 2010).

Local Storm Inundation Research and Land Loss Projections

Impacts of rising sea-level are increased erosion or up-land conversion, resulting in less usable land and an influx of suspended sediment into the water column. Shoreline studies using photo rectification and shoreline digitizing found the average long-term, since 1937, erosion rate to be -0.24 meters/year for the shorelines along the York River Estuary. Man-made accretion occurred, up to 1 meters/year, in locations where breakwaters were installed while the shorelines along the Catlett Islands experienced erosion rates of almost -2 meters/year. Whether the shore will respond by erosion or upland conversion depends on elevation, sediment type and supply, wave energy, tidal range, and rate of sea-level rise (Leatherman et al, 1995; Milligan et al, 2010a-c).

Even with the effects of sea-level to date, waterfront property owners have had little reason to be concerned until water levels exceed the vertical limits of the astronomical tide and become "extratidal". The level that separates "normal" from "above normal" water levels varies because tidal range varies from place to place. Therefore a true measure of the flooding potential is when the water level exceeds the highest astronomical tide (HAT) for a specific location. Tidewatch and Chesapeake Inundation

Prediction System (CIPS) are two programs dedicated to real-time observations and modeling to forecast flooding. Repeated flooding will affect not only homeowners, but all levels of Virginia's coastal resources, including transportation, infrastructure, military installations, marine ecosystems, agriculture, human health, and recreation. (Boon et al., 2008).

Local Wetlands Research

Mixon et al. (1989) identifies the sedimentary units deposited during the Holocene along the York River estuary system and exposed sub-aerially as consisting of two main units. The first unit is up to 3 meters of soft coastal mud captured by salt marshes, usually medium to dark gray with grayish-brown peat. These muddy deposits are found mostly near the mouth in salt marshes fringing the edges of Goodwin Islands, Plum Tree Island and Mobjack Bay. The second unit is alluvial deposits of light to medium gray and yellowish gray, fine to coarse gravelly sand and sand gravel, silt and clay. These deposits are found mostly in the brackish to fresh water marshes along the upper York and along the Mattaponi and Pamunkey, and are also found in narrow beaches, in flood plain environments, and on point bars along the estuary.

These tidal marshes are important to the estuarine system as they provide high primary productivity, have important habitat and nursery value, provide erosion buffering and

filtering capacity useful for trapping sediment, pollutants and nutrients. There are four Chesapeake Bay Virginia National Estuarine Research Reserve sites with wetland marshes along the York River. There is one each in the polyhaline, mesohaline, oligohaline and freshwater salinity regimes with largely pristine vegetation communities documented to have abundant fauna characteristic of their individual community types. Over time, changes in the vegetation communities have been documented for each site. These changes have been attributed to relative sea level rise since salt tolerant perennial species (for example: *Spartina alternifolia* and *S. cynosuroides*) have become more prominent (Perry and Hershner, 1999; Davies, 2004; Perry and Atkinson, 2009).

Local Fisheries Research

Eelgrass (*Zostera marina*), growing at the most southern limit of its range, is an important nursery habitat for many species of fish and shellfish. It is also home to many small animals that provide food for commercially and recreationally important fish. Record warm temperatures in the summer of 2005, combined with nutrient pollution, caused large beds of the grass to die off. In some areas the buried seeds and rhizomes have allowed the beds to become reestablished but in most other areas the sediment is mixed up into the water column and reduces light and interferes with re-establishment of the grasses. This results in a continuing loss of nursery area potentially affecting future recruitment. (Scheffer et al, 2001; Duffy, 2008). Increasing temperatures could cause loss from the Chesapeake Bay of cold-water species such as soft-shell clams and winter

flounder. Deterioration of habitat quality and increasing diseases due to rising temperatures could also cause declines of economically important species such as the blue crab, menhaden and rockfish (Glick et al., 2007; Duffy, 2008).

Additional Monitoring Project

The Chesapeake Bay monitoring program, a bay-wide cooperative effort since 1984, involves Maryland, Pennsylvania, Virginia, the District of Columbia, several federal agencies (including National Estuarine Research Reserve System and US Geological Service), 10 academic institutions and over 30 scientists. Twenty times a year, nineteen physical, chemical and biological characteristics are monitored in the Bay's mainstem and many tributaries. These include: freshwater inputs, nutrients and sediment, chemical contaminants, plankton, benthos, finfish and shellfish, underwater bay grasses, water temperature, salinity and dissolved oxygen. The datasets collected can be found at http://www.chesapeakebay.net/data

1.1.2 *Introduction to Chapter 2 – York River Observing System*

Chapter 2 describes the observing system maintained as part of the National Science Foundation MUDBED (Multi-Disciplinary Benthic Exchange Dynamics) project. From December 2006 until March 2009, tripod-mounted 5 MHz ADVs were deployed within 50 cm above the seabed at two muddy sites along the York River Estuary. The project

identifies the down-river Gloucester Point site as more biologically dominated and the up-river Clay Bank site as more physically dominated. The ADVs used provide long-term estimates of water velocity, bottom stress, suspended sediment concentration, sediment settling velocity, and bed stress under spatially and seasonally variable conditions. The results from this time period, described in this chapter, indicate that settling velocity tends to be higher at the biological site. Suspended sediment concentration and seabed erodibility tend to be higher at the physical site. Sediment settling velocity and bed erodibility were found to be inversely correlated in both time and space, but both tended to remain more consistent in time at the biological site. At the physical site the erodibility increases and settling velocity decreases following the winter and spring increases in river water discharge. (Cartwright et. al, 2009).

Changes in the Observing System since March 2009

After March, 2009 the monitoring of the biological site was discontinued, as the results from this site were not as variable in time. Effort and resources were instead concentrated at Clay Bank, the more dynamic, more physically dominated site. Like the more physically dominated site where the ADV continues to be maintained, the configuration of the deployments have been dynamic in an effort to provide additional information to address scientific questions that have arose. For example: two ADVs were deployed on separate tripods (allowing for future work to look at collocated spatial variability to be estimated for the parameters calculated from the ADV burst data), two ADVs were

deployed on the same tripod (allowing for future work looking at seasonal variability in the log layer) and additional optical instruments were deployed, such as the LISST and RIPScam – both described later in section 1.3 (allowing for the study of the variability in the suspended particle size distribution to describe the variation in the temporally changing concentration and settling velocity – see Chapter 5). The timeline of the deployment and retrieval of the tripods and their associated instrumentation areprovided in section 1.1.3. The burst-averaged ADV data are provided in CHSD data report CHSD2013-01.

The methods section of chapter 2 describes the effort needed to collect real-time data from the ADV, an instrument not designed to collect both internally and send real-time results. The program developed by Franktronics, Inc., has proven to be very robust in handling this procedure, especially in times when the communications link was broken. The serial-to-Ethernet (S2E) convertor deployed on the tripod proved had problems because it required a lot of power, and quit converting data for transmission before retrieval of the tripod was scheduled. Another weak link was the power supply to the FreeWave radio on the surface buoy attached to the tripod. During extended cloudy periods the solar panel was not able to keep the FreeWave radio battery charged and communication lapsed. The use of the surface buoy with a freeWave radio and a repeater on the piling was eliminated, and the communications problems solved, by moving the S2E to the crows-nest piling with the tripod wired directly to it.

Future changes to the observing system, to be used in Kelsey Fall's PhD work, include the addition of a 3-D anemometer mounted on the crow's nest to measure local wind turbulence, a string of 6 HOBO conductivity and temperature sensors to capture changes in water column stratification and a tower of 4 Nortek (6 MHz) Vector ADVs to measure changes in velocity, concentration, bulk settling velocity and stress in the water column.

Calibration Cruises

Cruises using a profiler equipped with at least an ADV and submersible pump were performed each time a tripod was deployed in an effort to provide *in situ* measurements of concentration of burst averaged acoustic backscatter and SPM from pump samples. This calibration procedure is described in Chapter 2. Section 1.1.4 is a timeline of when the cruises occurred, the instruments used, and the number of "bursts" and pump samples collected. CHSD data report CHSD2013-01 contains the burst average calibration cruise data.

Ancillary Data Sets

Bottom characterization cruises have been conducted in the general vicinity of the Clay Bank tripod since May 2011 on about a monthly basis (twice monthly in some cases), generally corresponding with either a Spring (within 3 days of new or full moon) or Neap tide (within 3 days of halfway between the new and full moons). The plan is to continue

these cruises into the foreseeable future. For each of these cruises, sub-cores are collected for X-ray and core logger analysis as well as % moisture and grain-size distributions at 1 cm intervals through the depth of the core. Two cores are also measured for surface erodibility using a Gust microcosm developed based on Gust and Mueller, 1997 and modified by The University of Maryland Center of Environmental Sciences (UMCES). Previous bottom characterization cruises have also been conducted in the Clay Bank area during the time the observing station has been established and used by several VIMS students for their Master's and PhD work (Dickhudt, 2008; Rodríguez-Calderón, 2010; Kraatz, in prep.). These cruises are only mentioned in the interest of completeness. Data from them will not be used in this dissertation.

1.1.3 *Timeline of Tripod Data Collected 2006-2012*

Appendix 1 contains information (metadata) such as of when the tripods were deployed, retrieved, including what instruments were used. Data are available in Data Report CHSD2013-01.

1.1.4 *Timeline of Calibration Cruise Data collected 2006-2012*

Appendix 2 contains information (metadata) such as of when the calibration cruises occurred, instruments used, number of "bursts" from which instruments, and number of pump samples collected. Data are available in Data Report CHSD2013-01.

1.2   Acoustic Instruments

As recently as 2002 optical sensors were more commonly used than acoustic sensors for suspended sediment measurements (Thorne and Hanes, 2002). Studies such as Ogston and Sternberg (1995) paired optical backscatter sensor water velocity instruments, with corrected electromagnetic current meters such as the intrusive Marsh-McBirney model to study sediment transport. Acoustic sensors were mostly used in the study of non-cohesive sediment concentrations in the coastal zone (Crawford and Hay, 1993; Harris et al., 2003; VanderWerf, 2007; Thorne et al., 2009). The Acoustic Doppler Velocitimeter (ADV), first sold by SonTek in 1993, however, is proving to be an excellent instrument for the measure of currents, wave and turbulent flow parameters, because of its rapid stable response and zero offset, as well as measurement of suspended sediment concentration using its acoustic backscatter (Voulgaris and Trowbridge, 1998; SonTek, 2001). These instruments are now more commonly being used to measure concentrations in rivers and in mixed sediment regimes (Gray and Gartner, 2009; Cartwright et al., 2009; Hanes, 2011). Thorne and Hay (2012) however states "The use of acoustics for estimating sediment concentration in flocculating (cohesive) suspensions is still problematic and requires fundamental studies on the interaction of sound with aggregated fine-grained particles, before quantitative inversions can be formulated.". More study is also needed on acoustic response to natural mixed grain-size suspensions.

1.2.1 Acoustic Doppler Velocimeter (ADV) Background
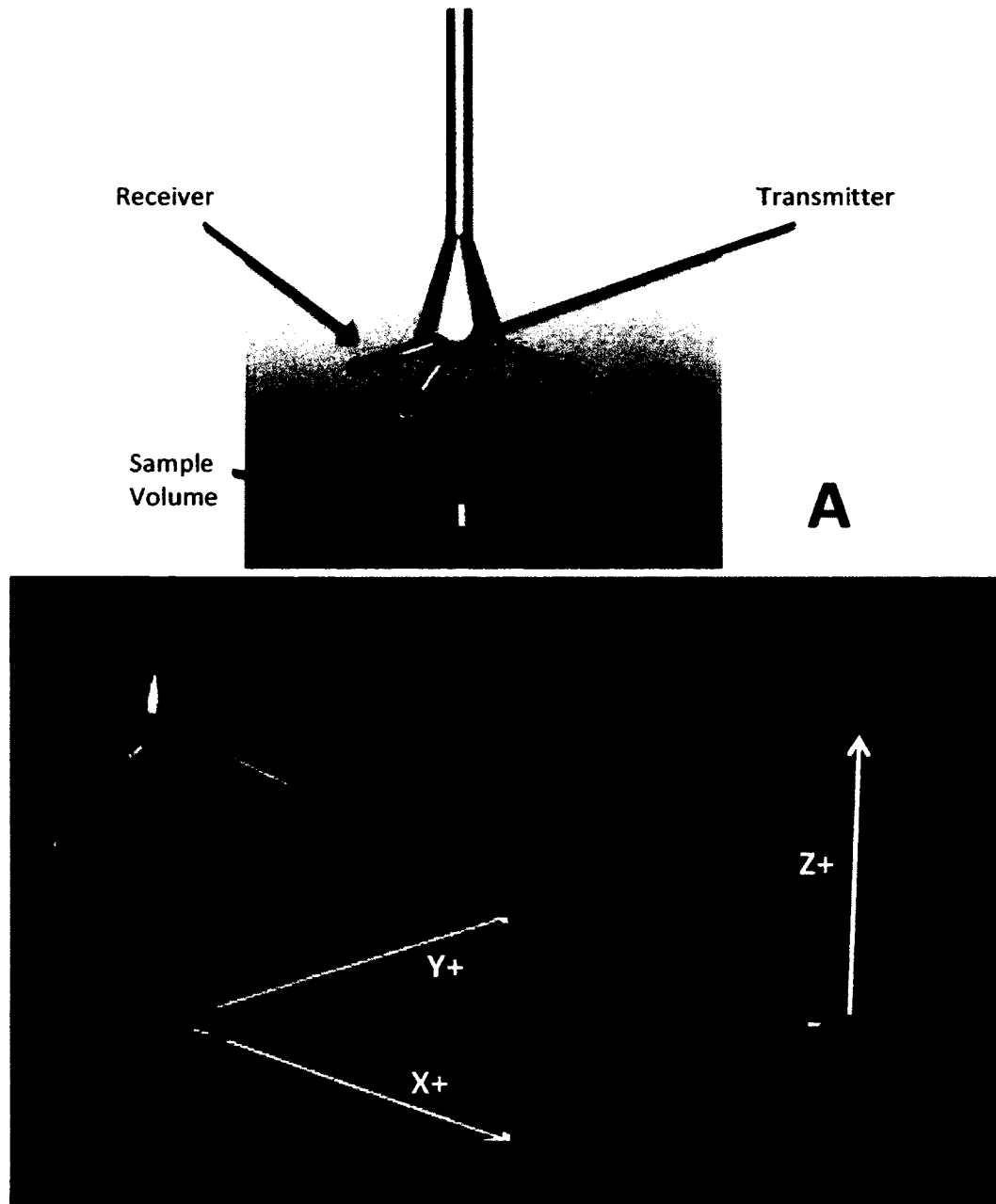
Figure 1.2. A) Acoustic Doppler Velocimeter showing the acoustic pulses being sent from transmitter to the sample volume and the acoustic reflect off deflector (suspended particles) transported by the water (acoustic backscatter) measured by 3 receivers. B) Depending on the changes in frequency received by the three receivers, because of the movement of the suspended particles, a 3-dimensional velocity is calculated. (Modified from Nortek, 2005; Nortek, 2010)

How the ADV Works

Two commercially available ADVs used in this dissertation are the Nortek Vector (6 MHz) and the SonTek ADVOcean (5 MHz). They both utilize a bistatic design, i.e., separate acoustic transducers to transmit and receive sound waves. The geometry of three receivers in relation to the transmitter creates a fixed remote sample volume (Figure 1.2A), which allows for the study of single-point, high-resolution 3D velocity fields with little or no flow obstruction. The ADV cannot measure the velocity of water unless it has scatterers (suspended particulate matter) to reflect the sound back to the receiver. The echo (reflected sound) is called acoustic backscatter. By definition, acoustic backscatter is the echo of the acoustic wave reflected back along the same axis as the transmitter. However, since the ADV is bistatic, the acoustic backscatter as mentioned in this dissertation, is the reflected sound wave measured by each of the three receivers.

The ADV current meter measures the velocity of the water by a principle called the Doppler effect. The Doppler effect can be perceived as the change in the frequency of the sound as an object passes by (for example, a passing motorcycle). For the ADVs in this project, the frequency of the sound sent by the transmitter, f_0, is related to the new frequency of the echo returned to the receiver, f, by the velocity of the source (what the sound is reflected off of), v_s, in relation to the stationary receiver and the speed of sound for water, C, as seen in equation 1.1 (Rosen and Gothard, 2009):

$$f = \left(\frac{C}{C+v_s}\right) f_0 \qquad (1.1)$$

The speed of sound in water is affected by the temperature and density (including salinity) (SonTek, 2001; Nortek, 2005).

The Doppler technology utilizes the backscatter to determine the speed and direction of the particle, and thus the flow of the water carrying it (providing the scatterer is not swimming itself), at the sample volume. If the particle is moving perpendicular to the line connecting the sample volume (reflected transmitted sound) and the receiver then there is no Doppler shift and no velocity registered in that direction. If the distance is increasing between the particle and receiver, the frequency of the sound received decreases (positive velocity of the particle) and if the distance is decreasing, the frequency increases (negative velocity of the particle).

With three receivers focused on the same sample volume, the velocity (the particle movement) is measured in 3-dimensional space and later rotated to Cartesian (XYZ) vectors (Figure 1.2B). The X-axis is defined as positive from the sample volume out in the direction of receiver 1 and negative from the sample volume in the opposite direction. The Y-axis is the perpendicular horizontal axis and is positive in the direction between receivers 1 and 2. The Z-axis is the perpendicular vertical axis with the positive direction being up from the sample volume. The ADV is more sensitive to the Z-velocity (the component parallel to the transmit beam) than it is to the X- or Y-velocity because of the geometry of the transmit/receive beam pair. This means the Z-velocity yields a lower

measurement uncertainty (SonTek 2001; Nortek, 2005).

Acoustic Backscatter

The signal strength is a measure of the power of the reflected acoustic signal (also called the acoustic backscatter strength), and is recorded by internal components for each receiver. This component outputs a signal referred to as the RSSI (Received Signal Strength Indicator) in decibels (dB) that is proportional to the logarithm of the echo strength. This signal is recorded in the unit of counts. One count is equal to about 0.43 dB (with a variation of 0.40 to 0.47) (Lohmann, 2001). Lohmann (2001) suggests using the following relation to "range normalize" the echo level (EL) in dB:

$$EL = AMP * 0.43 + 20log_{10}(R) + 2\alpha_w * R + 20R \int \alpha_p * dr \qquad (1.2)$$

$$ \text{(a)} \text{(b)} \text{(c)}$$

where AMP is the stored counts, R is the range along the acoustic beam in m, α_w is the water absorption in dB/m, and α_p is particle attenuation in dB/m. The terms (a), (b) and (c) account for the loss of the of the returned echo strength due to (a) acoustic spreading with distance from the transmitter, (b) water absorption, and (c) particle attenuation. Term (a) is really not necessary when using an ADV since the sample volume is or can/should be set to be a fixed distance from the transducer when the ADV is being used to estimate sediment concentration (described below). This means the only variables are α_w and α_p. At frequencies of 5 and 6 MHz, the change in α_w due to salinity is

negligible, and even though a 10° C change in temperature can almost double α_w, it will contribute less than 1 dB to the normalized echo level (Ainslie and McColm, 1998). According to Lohmann (2001), the final term (c) can be ignored when the SPM concentrations are low as α_p will be small. In general, using an ADV makes "range normalizing" the echo unnecessary. The range is set by the geometry of the sensor.

For a given particle type and size distribution, acoustic backscattering strength within the sample volume is expected to be proportional to the $\log_{10}$ of the particle concentration. Theoretically if suspended sediment concentration, C, increases from C_1 to C_2 by a factor of 2 (i.e., $C_2/C_1 = 2$), then, in the absence of attenuation, the power of the return signal, P, will also increase by a factor of 2 (i.e., $P_2/P_1 = 2$), meaning the volume scattering strength will increase by about 3 dB (i.e., $10*\log_{10} (P_2/P_1)$) (Lohrmann, 2001). Then the ADV acoustic backscatter in counts is expected to increase by (3 dB)/(0.43) $\approx$ 7 counts. The findings of Cartwright et al. (2012) indicate that the acoustic backscatter from ADVs does generally increase linearly with $\log_{10}$ of the concentration. In the field, however, ADV counts do not precisely increase by 7 for every factor of two in concentration. This is because particles in suspension in estuarine and coastal environments are a mixture of sizes and types that change in time as total concentration changes. Also, the dB to counts conversion factor of ~0.43 may vary somewhat from ADV to ADV. Variations in the conversion factor among 10 sensors is investigated in Chapter 4. In addition, if concentrations become high enough, at some point attenuation will begin to overwhelm

backscatter (e.g., Traykovski et al., 2000). At that point, the rate of increase in backscatter with increased concentration will slow and eventually reverse, such that backscatter will then decrease with greater concentration.
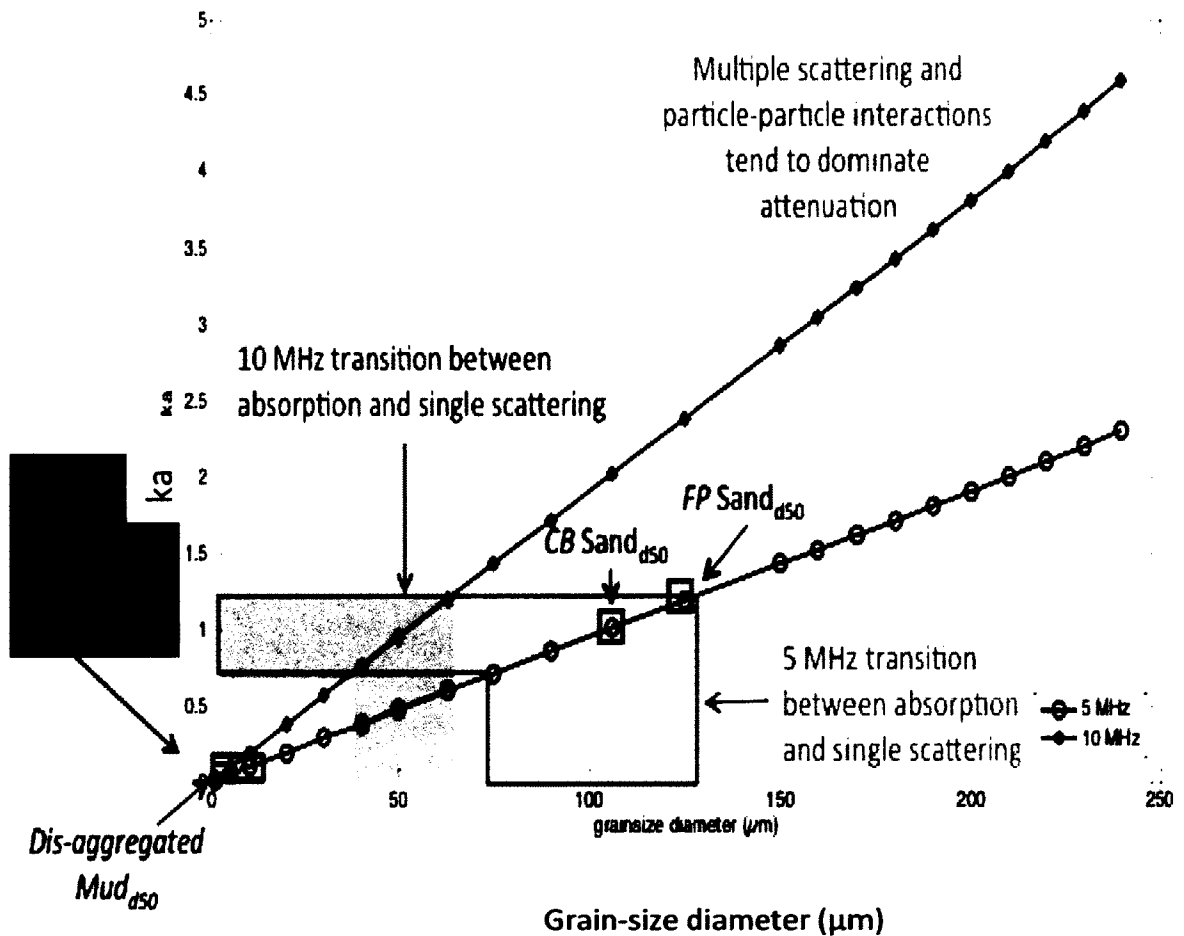
Figure 1.3. Schematic relationship between grain-size and attenuation contributions, highlighting the role of frequency. The black squares show where the Clay Bank and Ferry Pier dis-aggregated component sand and mud grain-sizes fall along the 5 MHz frequency regression line (from Cartwright et al., 2012)

Roll of Frequency and Grain-size in the Strength of the Acoustic Backscatter

Each acoustic frequency has a different particle size sensitivity (e.g., Flammer, 1962; Thorne and Campbell, 1992; Lohmann, 2001; Thorne and Hanes, 2002; Gartner, 2004; Topping et al., 2006). Sensitivity is the acoustic volume scattering strength for a given concentration. The peak sensitivity occurs at a value of approximately $ka=1$ (Figure 4.2) where k is the acoustic wave number ($2\pi/\lambda$, where λ is acoustic wavelength in cm) and a is the particle radius in μm (assuming a sphere of uniform density). Below the transition zone where is $ka \ll 1$, absorption of sound due to viscous losses tends to dominate attenuation (Figure 4.2), and, for a given frequency, the volume scattering strength becomes proportional to a^4, i.e., the radius of the particle to the fourth power. This means that as particle size decreases further below $ka=1$, the strength of the scattering for a given concentration dramatically decreases. The qualitative effects of this sensitivity are seen in Figure 1.3, where the acoustic response for the mud-dominated cases (which have $ka \ll 1$) are dramatically lower than the acoustic response of the sand cases (which have ka on the order of ~ 1) (Jackson and Richardson, 2007; Wright et al., 2010; Ainslie and McColm, 1998)

For particles larger than $ka \gg 1$, multiple scattering and particle interactions tend to dominate the attenuation (Figure 1.3), and the volume scattering strength becomes linearly proportional to a (i.e., radius to the first power). As the frequency increases, the sediment size within the transition zone ($ka \approx 1$) decreases (e.g. ~ 100 μm for 5 MHz and ~ 50 μm for 10 MHz). For a given frequency, with $ka \geq \sim 1$, the strength of scattering still

increases with particle radius, but not as markedly. The qualitative effects of this $ka \geq \sim 1$ sensitivity are also seen in Figure 1.3, where the acoustic response for the sand cases still increases with a, but not nearly as dramatically as the difference in backscatter between the mud alone and sand alone cases. Although not within the range shown in Figure 1.3, the concentration at which the proportionality between backscatter and concentration eventually reverses is also a function of ka, with the reversal occurring at lower concentrations for smaller ka (i.e., at lower concentrations in response to higher frequencies or in response to smaller grain sizes) (Jackson and Richardson, 2007; Wright et al., 2010; Ainslie and McColm, 1998)

Most of the work on acoustic response has been performed on individual grain-sizes, mostly of coarse-grain non-cohesive material. ADVs are now more commonly being used to measure concentrations in muddy rivers and in mixed sediment regimes (Gray and Gartner, 2009; Cartwright et al., 2009; Hanes, 2011). More study is also needed on acoustic response to natural mixed grain-size suspensions. Thorne and Hay (2012) state "The use of acoustics for estimating sediment concentration in flocculating (cohesive) suspensions is still problematic and requires fundamental studies on the interaction of sound with aggregated fine-grained particles, before quantitative inversions can be formulated."

Differences between Nortek and SonTek ADVs

The transmit frequency of the SonTek ADVOcean and the Nortek Vector is 5 MHz and 6 MHz, respectively. Each instrument has a set of fixed velocity ranges. The acoustic frequency and the velocity range used determine the ping rate (nominally 80-500 Hz for the SonTek and 100-250 Hz for the Nortek). The user set "sample rate" determines how often the pings are averaged together, with the instrument pinging as fast as possible, for an outputted sample. Decreasing the sample rate increases the number of pings averaged, thereby decreasing the error in the average. (SonTek 2001; Nortek, 2008).

The geometry of the round transmitter and three rectangular receivers sets the distance from the transmitter to the center of the roughly cylindrical sample volume for the SonTek to 18 cm and the Nortek to 15.7 cm. The diameter of the sample volume cylinder is determined by the intersection of the transmit and receive beams and is roughly the diameter of the transmit ceramic, 12 and 15 mm for the SonTek and Nortek, respectively. The SonTek sample volume height is controlled by software to be 18±1 mm giving a sample volume of approximately 2 cm^3. The Nortek allows the user to specify the sample volume height between 5 to 20 mm resulting in sample volume of approximately 0.8 to 35 cm^3, respectively. Increasing the sample volume increases the number of pings averaged per sample and decreases the error in the average (SonTek, 2001; Nortek, 2005).

27
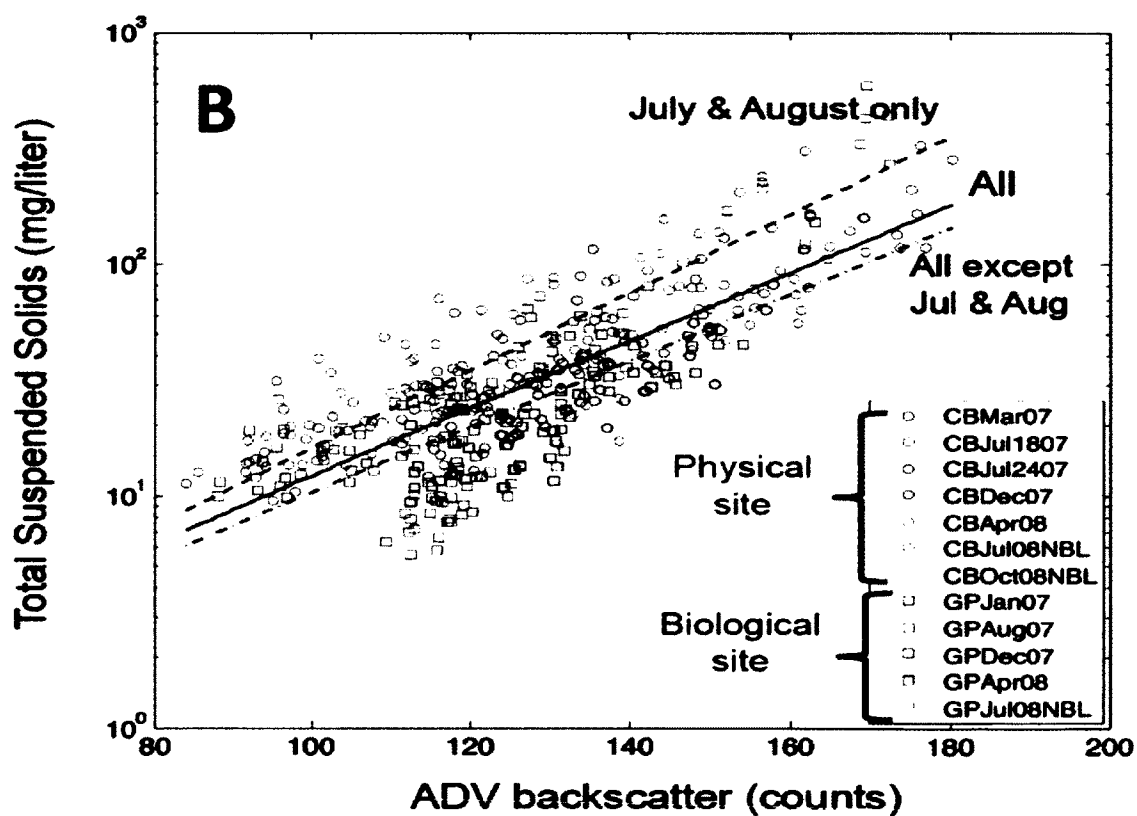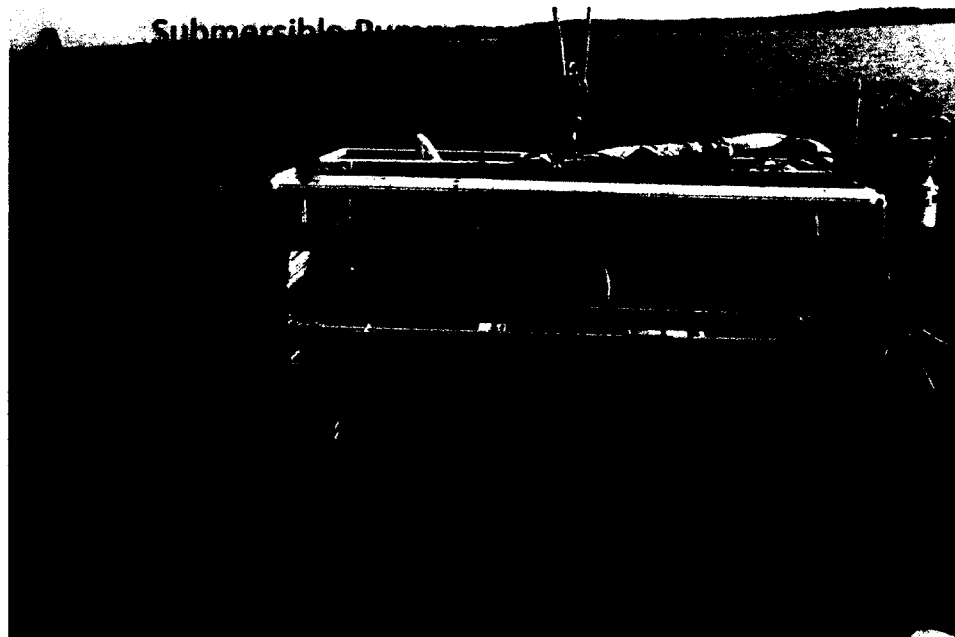
Figure 1.4. A) Profiler with ADV and submersible pump used for acoustic backscatter calibration cruises. B) Regression curve using MUDBED 2007-2008 calibration cruises (Cartwright et al. 2009).

28

1.2.2 Use of the ADV to measure suspended particulate matter (SPM) concentration and settling velocity

The use of the ADV for velocity and turbulence measurements is well understood (SonTek, 2001; Nortek, 2005; Voulgaris and Trowbridge, 1998). Chapter 2 shows that ADV derived bed stress, τ_b, plotted against ADV derived eroded mass, M, agrees well with the independent measure of M versus stresses applied in a Gust microcosm. More work however needs to be done to better understand how the concentration, C, and the settling velocity, w_s, (derived from the ADV turbulence and backscatter parameters) used in the calculation of M is affected by the acoustic response to cohesive and mixed sediment suspensions. The goal of this dissertation is to look at the use of the ADV to measure both SPM concentration and settling velocity.

Concentration

Using the profiler shown in Figure 1.4A pump samples were collected, during 2007-2008 MUDBED calibration cruises, concurrently at the same water depth as ADV backscatter. The pump samples were analyzed using gravimetric methods. Figure 1.4B displays best-fit linear regressions between ADV backscatter in count and the log of the SPM concentrations used to convert ADV backscatter to concentration in Chapter 2. The regression curves, and those from more than 30 cruises between 2006-2012, are used to convert backscatter from benthic mounted ADVs to concentration. There is, however,

abundant scatter in the data. There has been a good deal of research on the response of acoustics to non-cohesive sediment, recently, for example, by Hamilton and Hall (2012) and Moate and Thorne (2012). In contrast, there has been comparatively little done on cohesive sediments that form flocs or are formed into fecal pellets by benthic organisms.

Chapter 4 explores the acoustic response to natural sediment in the laboratory and Chapter 5 studies the change in acoustic response to changes in suspended sediment throughout a tidal cycle.
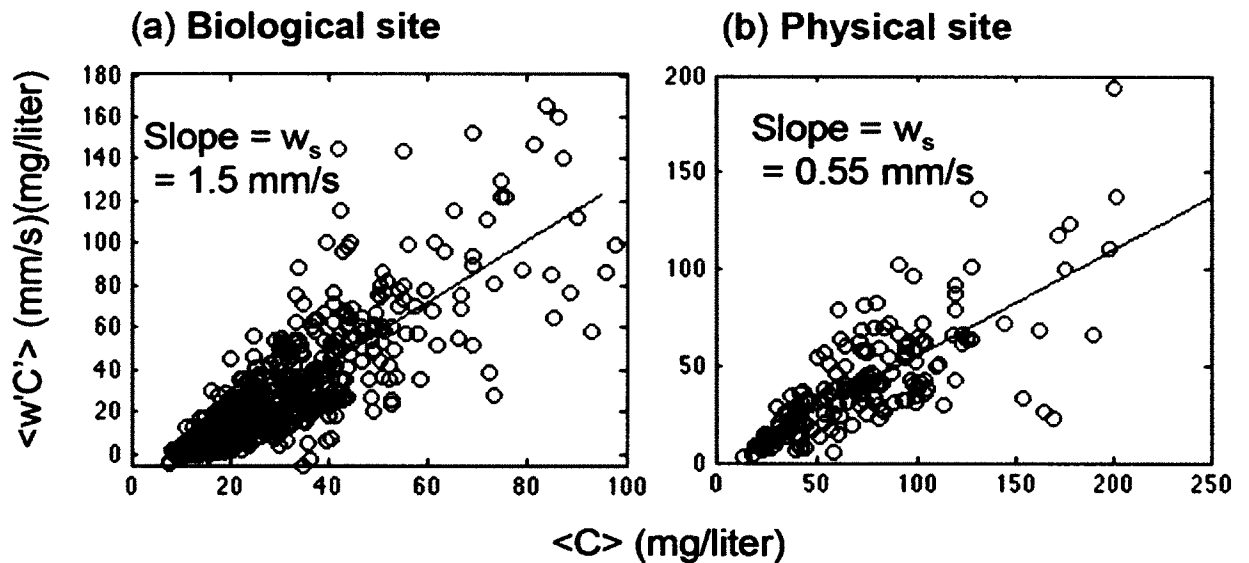
Figure 1.5. Example estimates of settling velocity (w_s) from ADV data collected on benthic tripods deployed in the York River Estuary, Virginia. (Cartwright et al., 2009)

Settling Velocity

Also in Chapter 2 it is shown that since the ADV can measure both suspended sediment mass concentration, C, and vertical water velocity, w, within the same sampling volume,

including turbulent fluctuations, the ADV can be used to estimate the settling velocity, w_s, for the sediment in suspension. Example estimates of settling velocity from a series of bursts collected using an ADV can be seen in Figure 1.5. (A burst is a series of rapid samples collected over a relatively short, specified period of time. Bursts are normally collected during a set time interval, for example: one burst of 900 samples collected at 10 Hz for a duration of 90 seconds every fifteen minutes). The settling velocities in Figure 1.5 were calculated following Fugate and Friedrichs (2002), assuming a local balance within the water column between upward turbulent transport by turbulent Reynolds flux and downward settling by gravity. However, concentration due to washload, $C_{background}$, doesn't contribute to the population settling out of the water column so it should be subtracted from the mean burst concentration. The $C_{background}$, can be estimated by finding the lowest burst average concentration during a given period of interest. A logical candidate is during a slack water during Neap tide. Modifying the following formula fromChapter 2 by subtracting the $C_{background}$, the formula for obtaining the settling velocity can be written:

$$W_{s(bulk)} = \frac{<C> - C_{background}}{<w'C'>} \qquad (1.3)$$

where primes indicate turbulent fluctuations from the mean, and angle brackets indicate a burst average. $W_{s(bulk)}$ is considered the bulk sediment settling velocity for a burst since the sediment in suspension isn't of only one size class, but is an average of all the "non-background" sediment in suspension, A less variable $W_{s(bulk)}$ can found by plotting the $< C > - C_{background}$ vs. $< w'C' >$ for a series of bursts. The slope equals $W_{s(bulk)}$

(Fugate and Friedrichs, 2002; Cartwright et al., 2009).

While the settling velocities calculated using this ADV method were found to be reasonable in Chapter 2, verification of the methodology needs to be obtained. Chapter 3 addresses the ability of the ADV to measure settling velocity in a calibration chamber in a laboratory setting, and Chapter 6 takes it a step further to provide verification *in situ* using independent video settling chamber methodology, the Particle Imaging Camera System (PICS).

Chapters 3 and 4 explore the use of the ADV to measure settling velocity and concentration.

1.2.3 *Introduction to Chapter 3*

While the ADV is designed to determine the fluid velocity, it is important to recognize that it is actually the velocities of the scatterers themselves that are measured. Thus in a calibration tank designed to relate sediment-induced backscatter to sediment concentration, the vertical velocity registered by an ADV at a given point is actually the true fluid velocity plus the sediment's settling velocity. And absent net vertical volume flux of the fluid, the average vertical velocity registered by an ADV across a horizontal plane is equal to the mean sediment settling velocity. For this study described in Chapter 3, a series of ADV calibrations were run in a 118-liter re-circulating tank for six sand

sizes between 63 and 150 μm. A grid of ADV measurements distributed in a horizontal plane across the tank revealed that the mean vertical velocity registered by the ADV in each case was indeed consistent with each grain size's settling velocity as independently measured by a "rapid sand analyzer" laboratory settling tube (Cartwright et al., 2012).

In a series of acoustic calibration experiments, a systematic increase in the proportionality between sand concentration and backscatter was observed with increasing grain size. These were an expected increase from the proportionality between mud concentrations and backscatter. For naturally occurring mud and sand solutions, the backscattering was intermediate between the mud and sand, rather than reaching a level that was the sum of the two backscattering amplitudes. This may be explained by the interrelationship between the acoustic backscattering, attenuation, and the particle size-frequency range (Cartwright et al., 2012).

1.2.4 *Introduction to Chapter 4*

This chapter compared acoustic backscatter (ABS) response to sand, mud, and mixed sediment in the lab and *in situ* among ten relatively similar acoustic Doppler velocimeter (ADV) units: five 6-MHz Nortek Vector ADVs and five 5-MHz SonTek ADVOcean-Hydras. This approach allowed for an examination of the relative roles played by inter-vendor, intra-vendor, and sediment variability in determining their ABS response. As

well as consistently responding more strongly to sand than to mud, ABS in counts (a logarithmic unit proportional to decibels) revealed clear offsets apparent among the various instruments within both vendors. One of the ADVs from each vendor was defined as a reference unit, and the offsets in counts of the other four ADVs from each vendor were adjusted to become consistent with the reference unit. For either vendor, pre-correction ABS response was more similar if the vendor's units had been purchased together with consecutive manufacturer's serial numbers and subsequently had not had electronic components replaced. After adjustment, ABS counts for all the SonTek vs. Nortek ADVs largely lay along a single curve. The SonTek vs. Nortek ABS curve began with a slope of ~1:1 at low backscatter; but at higher ABS, the response of the 5-MHz SonTek ADVs increased more rapidly than that of the 6-MHz Norteks, suggesting that the backscatter registered by the higher frequency Norteks was more susceptible to attenuation. Plots of the $\log_{10}$ of sand concentration ($\log_{10} C$) vs. ABS for concentrations from ~ 10 to 600 mg/L was significantly quadratic for both the Nortek and SonTek ADV although more strongly so for the Nortek. In contrast, mud calibrations of $\log_{10} C$ vs. ABS (for ~20 to 700 mg/L) were not quadratic for either vendor, providing less clear evidence of ABS attenuation. For well-mixed silty mud in the lab, the slope of the calibration of $\log_{10} C$ vs. ABS for both vendors was close to the theoretical value expected for a single, constant grain-size suspension. In the field, however, the calibration slope of $\log_{10} C$ vs. ABS was significantly smaller, which suggested a change in the acoustic properties of the suspended particles with increasing C. When calculating predicted ABS in counts in response to varying proportions of different grain sizes,

results showed that transforming logarithmic counts back to linear units of acoustic power before adding them together allowed successful prediction of the expected acoustic response.

1.3 Optical Instruments

Optical instruments are often used for measuring SPM concentration, size distributions and settling velocity (Ahn, 2012; Fettweis, 2012; Mikkelsen, 2012; Cross, 2012; Garcia, 2012; Sherwood et al., 2012, Todd et al., 2012). Optical instruments, however, are highly susceptible to biofouling because the windows have to be clear for the laser, or light source, to pass through. So it is not feasible to paint them with antifouling paint like the type that is used on the transducers of the ADV, as described in Chapter 2, to discourage growth. Also, moderate biologic growth that entirely blocks optics can still be relatively transparent to acoustics. Wipers have been used on optical instruments, but they typically consume a lot of power, so the length of time the optical instrument can be deployed is still usually significantly shorter than for an acoustic instrument. The deployment time for optical instruments in the York River Estuary can be as little as one week in the warm summer months in shallow water, to no more than a couple of months in the colder winter months. Acoustic instruments, however, can be deployed for several months in the summer and practically all winter long if there is enough battery life and file storage.

Two of the most commonly used, commercially available, optical instruments for measuring suspended sediment concentration and size distribution, respectively, are the Seapoint Optical Backscatter Sensor (OBS) and the Sequoia Laser *In situ* Scattering Transmissometer (LISST-100X). The OBS is a very simple instrument that uses light reflected back from the surface of the particles in suspension to infer the SPM concentration. The amount of backscattered light is directly related to the concentration of particles in suspension, but the amount of light reflected changes with the size of the particles. Clay size particles will scatter back much more light relative to the same concentration of sand size particles (Battisto, 2000). OBS sensors were deployed in the MUDBED observing system as an auxiliary sensor with the LISST-100X. The LISST-100X uses forward scattering from a laser to measure the particle size distribution from 2.5 - 500 μm. A detailed described of the LISST-100X follows in Section 1.3.1, as it is used extensively in Chapter 5.

Several specialized optical instruments are being used today for measuring size distributions and settling velocities that employ either a digital still or video camera (Davies, 2011; Mikkelson et al., 2012; Smith and Friedrichs, 2012; Cartwright et al., 2011). Two of these instruments, the RIPScam and the PICS, were used in Chapters 5 and 6 and are described below in Sections 1.3.2 and 1.3.3.
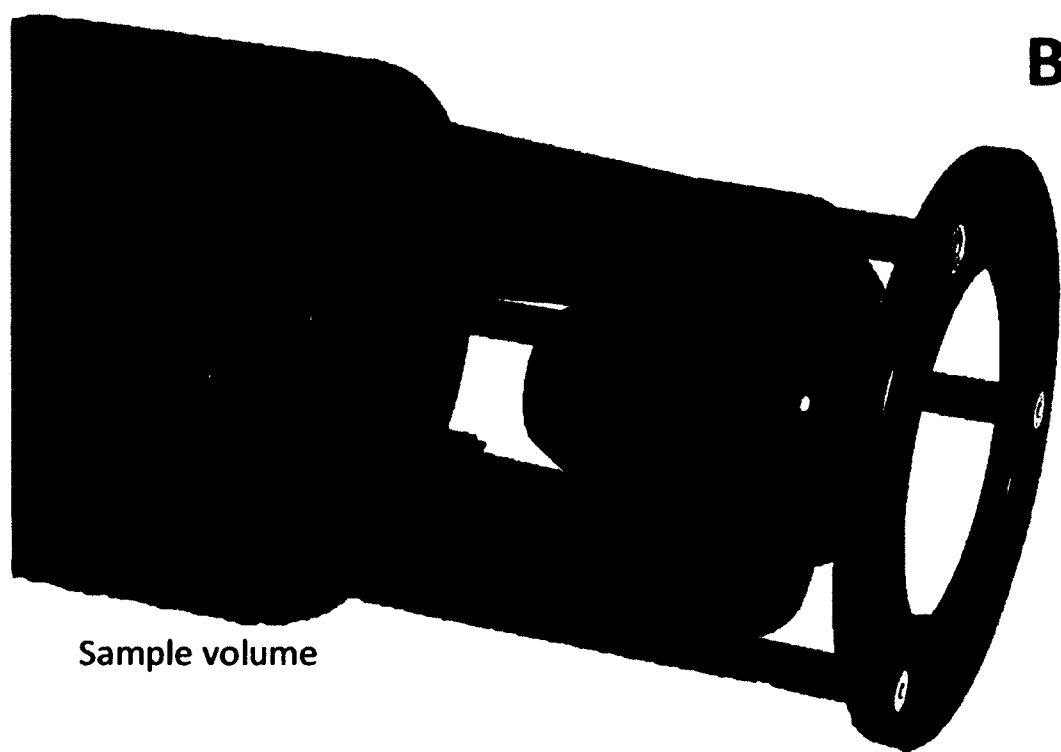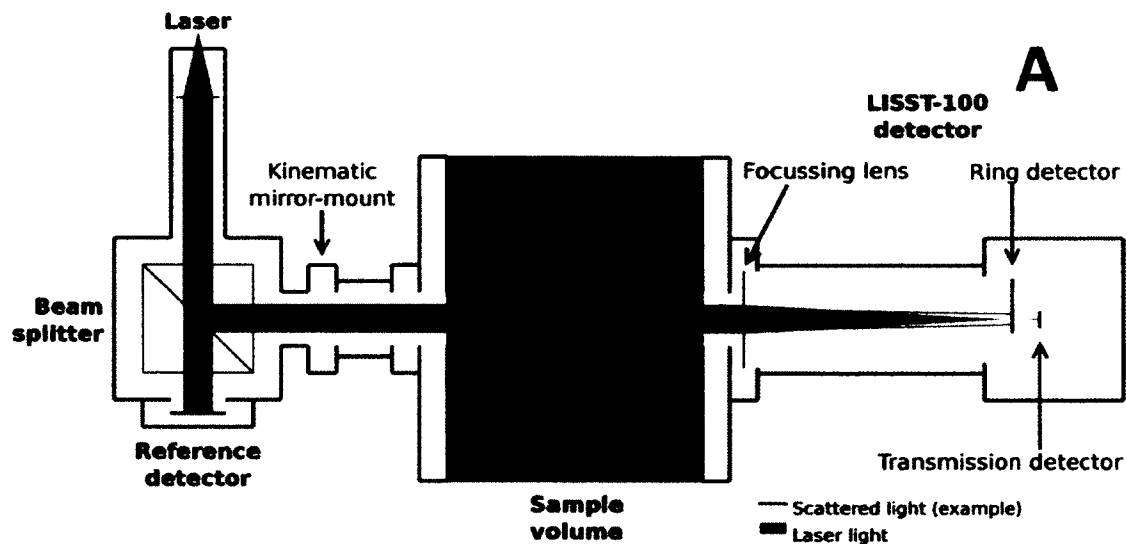
Figure 1.6. A) Schematic of Laser path through sample volume to logarithmically space ring detector B) LISST 100X 5 cm sample volume. Acrylic spacers can be installed to reduce the sample volume (Smith, 2011; LISST-100 User's Guide)

1.3.1 LISST background

The Sequoia Laser *In Situ* Scattering Transmissometer (LISST-100X) uses laser diffraction to measure the suspended particle size distribution in 32 logarithmically spaced size classes over the range 2.5 to 500 µm. Light is emitted by a laser diode with a wavelength of 670 nm and passes through a focusing lens, then through the 5 cm length sampling volume (Figure 1.6). After passing through another focusing lens, the scattered light is collected by a set of concentric ring detectors. Particles in the sampling volume refract the beam, forming a diffraction pattern. For simple particle geometries (spheres), the diffraction pattern can be predicted theoretically (Agrawal and Pottsmith, 2000). The measured diffraction pattern, as sampled by the ring detectors, is then inverted based the theoretical result, giving an estimate of the actual particle size distribution. The nature of forward scattering by spheres is such that the scattering angle is inversely proportional to particle diameter. The inner rings detect the largest particles, and the outer rings detect the smallest. The LISST does not use pumps, so that physical disturbances to the water column, which might breakup aggregates or flocs, are minimized. Traykovski et al. (1999) conducted a series of laboratory tests using natural particles ranging in size from coarse sand (710 µm) to silt (<5 µm). They demonstrated that the LISST was able to accurately resolve unimodal size distributions within the measurement range. Uncertainties using LISST-100 detectors may arise when particles are non-spherical or exceed the instrument range, or when SPM concentration or stratification of the water column is large (Styles, 2006; Fettweis, 2008). Styles (2006) showed that small scale

salinity fluctuations can cause small angle scattering patterns that are indistinguishable from particle scattering. In the absence of the above confounding effects, LISST-100 instruments have been shown to be well suited for measuring floc sizes, because the diffraction patterns induced by flocculated mud are formed by the flocs and aggregates themselves, and not by the primary grains composing the aggregates. Multiple diffraction can become a problem when total transmission is lower than about 20-30% and results in a shift in the derived size distribution towards smaller size classes (Agrawal and Pottsmith, 2000).

1.3.2 RIPScam background

The Remote *In situ* Particle Settling Camera (RIPSCam), developed specifically for the MUDBED project, contains a Canon EOS XSi 12 MP digital SLR camera with a pair of red LED line lights connected to a strobe controller to provide a focused, controllably flashed light sheet (Figure 1.7A). The light sheet illuminates the center of a clear acrylic 7 cm ID vertical tube, approximately 50 cm below the tube opening at the top of the bottom frame, which is deployed approximately 0.9 mab. A pneumatic knife valve opens and closes across the top of the tube to admit external particles (Figure 1.7B). The camera, the strobes, and the knife valve are controlled by an internal micro-computer running Windows XP. The computer also collects and stores the particle images, communicates with the surface buoy, and controls sampling and remote communications. Sampling can be initiated at any interval. The knife valve is opened for several minutes
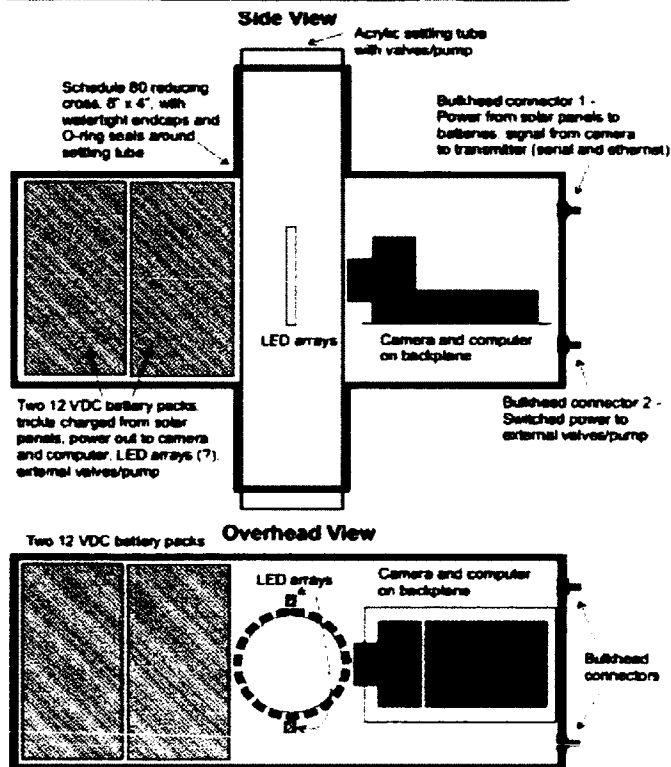
Figure 1.7. A) RIPSCam bottom frame ready for deployment on March 19, 2009. B)
Side and overhead schematic views of the central section of the RIPSCam (right).
(Cartwright et al., 2011)

before sampling and then closed just prior to sampling to limit internal motion in the tube. During sampling, a 2-sec time exposure image is first collected with the strobes flashed at 0.35-sec intervals. This is then followed by a sequence of 5 flash exposures at 1-sec intervals. Each image frame is 21 mm high, 31.5 mm wide, and the depth of focus is approximately 1 mm. Calcium hypochlorite hydrated pellets in a mesh bag is normally added to the bottom of the settling tube (approximately 0.25 m below the sample section) to limit biofouling (Cartwright, 2011).

1.3.3 PICScamera background

The Particle Imaging Camera System (PICS) developed by Smith and Friedrichs (2011, 2012) is a high definition video camera system that is used to measure particle size distribution and settling velocity of the component particles (Figure 1.8A). It has been designed to have a single chamber whereby the current is allowed to flow through until the sample is captured by closing ball valves at each end. After sampling, the 5-cm (inside diameter) chamber is mechanically turned to a vertical position to become a settling column (Figure 1.8B). During periods of weak currents, less than 15 cm/s, the ball valves are closed to collect the sample with the column already in the vertical position as soon as the profiler reaches the desired sample depth. The camera and laser diode light, providing a uniformly thin, ~1 mm, strobed sheet of light, are located on the bottom half of the column (Figure 1.8C). The turbulence is allowed to dissipate for approximately 15-30 sec, and a 30 second image is collected. The video camera utilized by the PICS is a Prosilica/AVT GC1380 with 1024x1380 pixel resolution at up to 20 fps,

with a resolution of a particle sizes distributed between 30 and ~1000 μm. The length of the settling column above the imaging plane and strobe duration permits resolution of settling velocities between 0 and 15 mm/s (Smith and Friedrichs, 2011; Cartwright et al., 2012).

Particles large enough to be accurately characterized in terms of both settling velocity and size (diameter, d>30 μm) are tracked by Particle Tracking Velocimetry (PTV) methods described by Smith and Friedrichs (2012). The automated process of tracking the particles makes collection of relatively long sampling records possible and allows for a large number of particles to be tracked. This provides better statistical characterization of size, settling velocity and density of particle populations, especially of relatively low abundance large macroflocs (d> 150 μm), which can account for a large percentage of the total volume concentration in suspension (Smith and Friedrichs, 2012; Cartwright et al., 2012)

Turbulence introduced during sample capture, thermally induced circulation, volume displacement of settling particles, and motion of the settling column all create fluid motion within the sampling tube and interfere with the measurement of settling velocity of the particles. Smith and Friedrichs (2012) describe the automated Particle Image Velocimetry (PIV) method used by PICS to estimate the space- and time-variant fluid
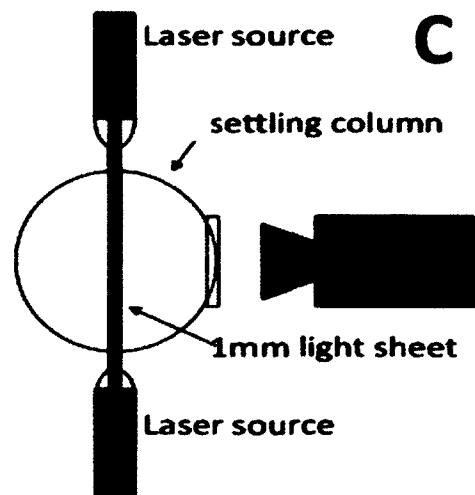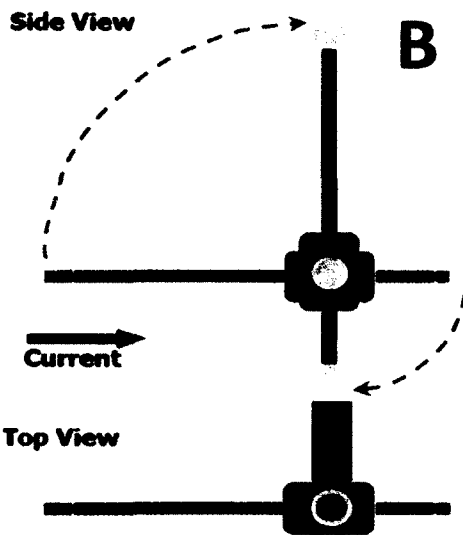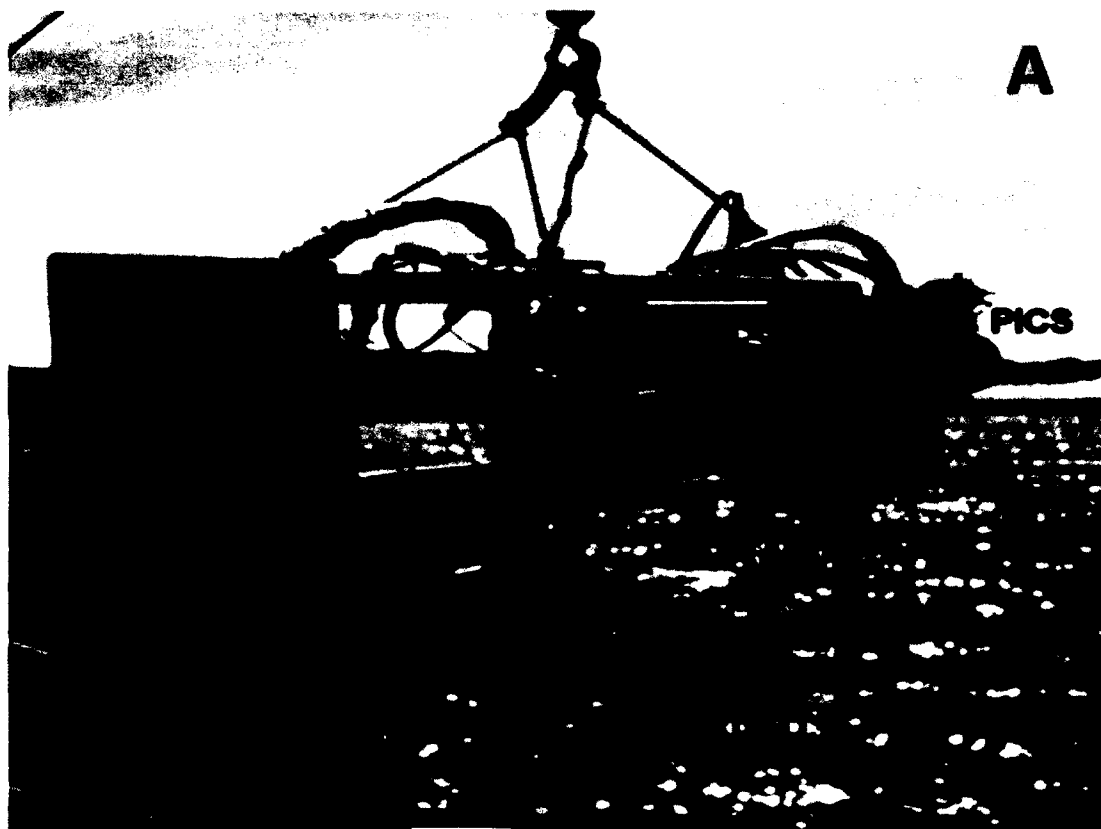
Figure 1.8. A) First generation PICS camera mounted on profiling frame with ADV, LISST 100X, CTD and submersible pump with inlet at instrument's sampling height. B) Settling column schematic indicating sample collection and image analysis positions and C) schematic of camera, settling column cross section and LED lighting (Smith and Friedrichs, 2010; Cartwright et al, 2012_PiE)

Thread Number: 3533 (82): d=200 μm; X= 9.2 mm; $w_{s,mean}$ = 0.57 mm/s
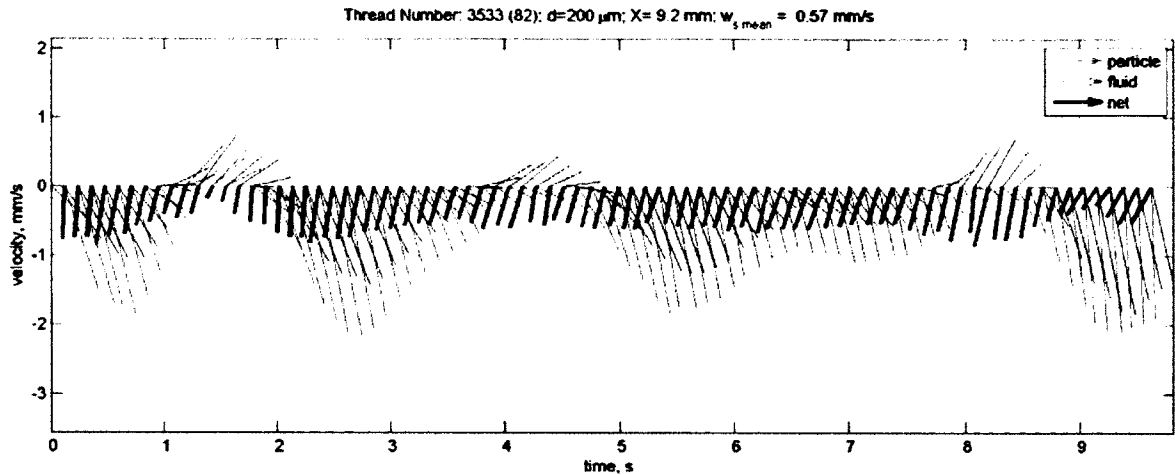
Figure 1.9. Time-series velocities for the 200 μm particle size class of a sample series. Vectors indicate particle velocity (red), local fluid velocity (blue), and net (settling) velocity (black) (Smith and Friedrichs, 2012).

velocity fields through which the larger particles settle. The smallest detected particles (d<30 μm) are used as natural tracers to estimate the local fluid velocity (Figure 1.9). The local fluid velocity is subtracted from the velocity of each larger detected particle (d>30 μm) to determine the net settling velocity of each larger particle. The PTV-PIV automated image processing frees the PICS from needing a stable platform as required by most settling velocity systems and allows sample collection throughout the whole water column. (Cartwright et al., 2012).

Chapters 5 and 6 couple optical instruments with the ADV to better understand the settling velocity measured by the ADV

1.3.4 Introduction to Chapter 5

Settling velocity (w_s) of a mud particle of known diameter (D) and density (ρ) in the York estuary can be theoretically predicted based on well-established relationships between the force of gravity and the opposing fluid resistance to be $w_s \sim D \times \rho$ (Dyer, 1984). Disaggregated mud in the York, based on the D and ρ of its component mineral grain size, ~5-10 μm, would be expected to have w_s < to << 0.1 mm/s. However, w_s for mud in the York under relatively turbid (concentration > ~ O(50) mg/L) has been found to be on the order of 0.2 to 2 mm/s (Cartwright et al., 2009). These larger settling velocities are due to the packaging of the principle mineral grains into flocculants or into fecal pellets created by benthic organisms. Data collected, for Chapter 5, in the Clay Bank region of the York River during a 25 hour period in July 2009 using a LISST 100X (range of 2.5- 500 μm) and RIPScam video images (range of 20 μm to 20mm) show evidence for both muddy flocs and pellets in the lower 1 m of the water column (Cartwright et al., 2011).

The results from the tidal anchor station sampling at Clay Bank (Cartwright et al., 2011) indicate the dominate floc size at slack tide reached ~300 μm. Larger, much more scarce flocs, of ~1 mm were also observed during periods of decreasing stress. As the stress increased to between 0.2-0.3 Pa the dominant floc size was reduced to ~ 200 μm. During this time, a second population of more resilient, denser particles (~ 95 μm) was also present in suspension. This second population particle size is consistent with pellets identified for this region in the seabed by Rodríguez-Calderón (2010) and Kraatz (2012).

The settling velocity calculated during high stress, when the floc size was at its minimum and the pellet population was present, was measured using an ADV to be over 1 mm/sec. As the stress decreased and the larger flocs formed, the w_s dropped to around 0.8 mm/sec. The size of the flocculants and composition of the suspended concentration, and the resultant settling velocity, would be expected to vary (tidally, spring/neap, seasonally and longer term) due to the changing stresses present as well as the varying constituent particles and SPM concentration (Cartwright et al., 2011).

1.3.5 Introduction to Chapter 6

Acoustic Doppler Velocimeters (ADVs) can be used to measure (i) relatively large ($\leq \sim$ 0.5 cm/s) sediment settling velocities (w_s) by direct Doppler measurement of sediment motion relative to the surrounding fluid and (ii) relatively small w_s ($\leq \sim 0.2$ mm/s) by assuming a Rouse balance between upward Reynolds flux and downward settling. Advantages of ADV-based w_s estimates include their non-intrusive nature, their resilience to high energy and biofouling and, for these two specific methods, their relative insensitivity to precise calibration of acoustic backscatter for sediment concentration. In the past, however, these ADV-based estimates of w_s had not been confirmed by independent measurements of w_s using other instruments observing the same particle populations. Here, independent observations of w_s utilizing gravimetric and video settling tubes are shown to be consistent with these two types of ADV-based w_s measurements for large and for small w_s, respectively. Direct Doppler-based ADV estimates of w_s were

collected for sand in a laboratory mixing tank and confirmed by a Rapid Sediment Analyzer gravimetric settling tube. Rouse-balance ADV estimates were collected in the York River estuary for muddy flocs and confirmed *in situ* by a particle tracking/particle image velocimetry settling tube. These lab and field-based observations in this chapter both suggest that, in the absence of significant particle aggregation/disaggregation, (i) measurement of w_s and (ii) w_s itself are both relatively insensitive to the local intensity of fluid turbulence.

1.4 References

Agrawal, Y.C. and Pottsmith H.C., 2000. Instruments for particle size and settling velocity observations in sediment transport. Marine Geology, 168, 89-114.

Ahn, J.H., 2012. Size distribution and settling velocities of suspended particles in a tidal embayment, Water Research, vol 46, pp.3219-3228.

Ainslie, M. A., and McColm, J. G., 1998. A simplified formula for viscous and chemical absorption in sea water, Journal of the Acoustical Society of America, 103(3), 1671-1672.

Baeye, M., Fettweis M., Boulgaris G., and Van Lanker, V., 2012. Sediment mobility in response to tidal and wind-driven flows along the Belgain shelf, southern North Sea. Ocean Dynamics (Springer). 33-50

Battisto, G.M., 2000. Field measurement of mixed grain size suspension in the near-shore under waves. MS Thesis, School of Marine Science, College of William and Mary, Gloucester Point, VA, 87 p.

Boon J.D., Wang H.V., Shen J., 2008. Planning for Sea Level Rise and Coastal Flooding. 4p. White Paper available online at http://www.virginiaclimatechange.vims.edu

Boon, J.D.; Brubaker, J.M., and Forrest, D.R., 2010. Chesapeake Bay Land Subsidence and Sea Level Change: An Evaluation of Past and Present Trends and Future Outlook. Special Report No. 425 in Applied Marine Science and Ocean Engineering. Gloucester

Point, Virginia: Virginia Institute of Marine Science, 42p

Boon, J.D., 2012. Evidence of sea level acceleration at U.S. and Canadian tide stations, Atlantic Coast, North America. Journal of Coastal Research, 28(6), 1437–1445. Coconut Creek (Florida), ISSN 0749-0208.

Cartwright, G.M, Friedrichs, C.T., Dickhudt, P.J., Gass, T. and Farmer, F.H., 2009. Using the Acoustic Doppler Velocimeter (ADV) in the MUDBED Realtime Observing System. Proceedings, Oceans '09, MTS/IEEE, Biloxi, MS, 26-29 Oct , 9 p.

Cartwright, G.M, Friedrichs, C.T. and Sanford, L.P., 2011. *In situ* characterization of estuarine suspended sediment in the presence of muddy flocs and pellets. In: N.C. Kraus and J.D. Rosati (eds.), Coastal Sediments 2011, American Society of Civil Engineers, 14 p.

Cartwright, G.M, Friedrichs, C.T. and Panetta, P.D., 2012. Dual Use of a Sediment Mixing Tank for Calibrating Acoustic Backscatter and Direct Doppler Measurement of Settling Velocity. Proceedings, Oceans '12, MTS/IEEE, Hampton Roads, VA, 14-19 Oct,7 p.

Colman S.M., Halka, J.P. and Hobbs, C.H., 1992. Patterns and rates of sediment accumulation in the Chesapeake Bay during the Holocene rise in sea level. Quaternary Coasts of the United States: Marine and Lacustrine Systems, SEPM Special Publication 48, p. 101-111

Crawford, A.M., Hay, A.E., 1993. Determining suspended sand size and concentration from multifrequency acoustic backscatter. Journal of the Acoustic Society of America 94 (6), 3312–3324.

Cross, J., Nimmo Smith, W.A.M., Torres, R. and Hosegood, P.J., 2012. Dispersal of phytoplankton populations in response to enhanced turbulent mixing in a shelf sea. Abstract, Particles in Europe, ICM, Barcelona, Spain, 17-19 Oct., 3 p.

Davies, S. B., 2004. Vegetation Dynamics of a Tidal Freshwater Marsh: Long-term and Inter-annual Variability and Their Relation to Salinity. M.S. Thesis. College of William and Mary, Virginia Institute of Marine Science. Gloucester Point, VA. USA, 75p.

Davies, E.J., Nimmo-Smith, W.A.M., Agrawal, Y.C., Souza, A.J., 2011. Scattering signatures of suspended particles: an integrated system for combining digital holography and laser diffraction. Optics Express 19, 25488–25499.

Dickhudt, P.J. 2008. Controls on erodibility in a partially mixed estuary, York River, Virginia. M.S. Thesis, College of William & Mary, Gloucester Point, VA. 230p.

Duffy, J.E. 2008. Vanishing and emerging ecosystems of coastal Virginia: Climate change impacts and adaptation. 4p. White Paper available online at: http://www.virginiaclimatechange.vims.edu

Engelhart and Horton., 2009. Holocene sea level database for the Atlantic coast of the United States. Quaternary Science Reviews. Article in press: 1-14.

Fall, K.A., 2012, Relationships among fine sediment settling and suspension, bed erodibility, and particle type in the York River estuary Virginia. M.S. Thesis, College of William & Mary, Gloucester Point, VA. 144p.

Fettweis, M., 2008. Uncertainty of excess density and settling velocity of mud and flocs derived from *in situ* measurements. Estuarine, Coastal and Shelf Science 78, 426-436

Flammer, G. H., 1962. Ultrasonic Measurement of suspended sediment. Geological Survey bulletin 1141-A. United States Government Printing Office, Washington. 56 p.

Friedrichs, C.T., Cartwright, G.M. and Dickhudt, P.J., 2008. Quantifying benthic exchange of fine sediment via continuous, non-invasive measurements of settling velocity and bed erodibility," Oceanography, vol. 21(4), pp. 168-172.

Fugate, D.C. and Friedrichs, C.T., 2002. "Determining concentration and fall velocity of estuarine particle populations using ADV, OBS and LISST," Continental Shelf Research, vol. 22, pp. 1867-1886.

Garcia, V., Garcia, M., Sospedra, J., Grifoll, M., Caceres, I., Sanchez, J.F. and Sanchez-Arcilla, A. 2012, Suspended sediment fluxes near the break zone under moderate energy conditions. Abstract, Particles in Europe, ICM, Barcelona, Spain, 17-19 Oct., 3 p

Gartner, J.W. 2004. Estimating suspended solids concentrations from backscatter intensity measured by acoustic Doppler current profiler in San Francisco Bay. Marine Geology, 211 (2004): 169–187.

Gray, J.R, and Gartner, J.W., 2009. Technological advances in suspended-sediment surrogate monitoring. Water Resources Research, 45. Doi:10.1029/2008WR007063.

Gust, G., and Mueller, V., 1997. Interfacial hydrodynamics and entrainment functions of currently used erosion devices, in: Burt, N., Parker, W.R., Watts, J. (Eds.), Cohesive Sediments. John Wiley and Sons, New York, pp. 149-174.

Hamilton, L.J. and Hall, M.V., 2012. Direct solution of the backscatter equation for ABS instruments through a Riccati reformulation. Continental Shelf Research, 46: 83-86.

Hanes, D.M., 2011. On the possibility of single-frequency acoustic measurement of sand and clay concentrations in uniform suspensions. Continental Shelf Research, doi:10.1016/j.csr.2011.10.008.

Harris, C.K., Butman, B., and Traykovski, P., 2003. Winter-time circulation and sediment transport in the Hudson Shelf Valley. Continental Shelf Research, 23 (8): 801–820

Hobbs, C.H. III, D.E. Krantz, G.L. Wikel (submitted 2010). Coastal Processes and Offshore Geology. In: C. Bailey (ed.), The Geology of Virginia.

Holzer, T.L. and Galloway, D.L., 2005. Impacts of land subsidence caused by withdrawal of underground fluids in the United States. In: Ehlen J, Haneberg WC, Larson RA (eds) Humans as geologic agents. Rev Eng Geol 16:87–99

Jackson, D.R. and Richardson, M.D., 2007. High-Frequency Seafloor Acoustics, Springer ISBN 978-0-387-34154-5. 616 p.

Johnson G.H. and Hobbs, C.H. III 1990. Pliocene and Pleistocene Depositional Environments on the York-James Peninsula, VA: A Field Guide. American Society of Limnology and Oceanography meeting June 1990. College of William and Mary, Virginia Institute of Marine Science.

Kraatz, L.M., In Prep (2013). Deposition, erosion and biological reworking within the York River estuary: An acoustic investigation of bio-physio-geological parameters influencing seabed erodibility in a tidally energetic, fine grained environment. Ph.D. Dissertation, College of William & Mary, Gloucester Point, VA.

Leatherman. S.P., Chalfont, R., Pendleton, E.C., McCandless, T.L. and Funderburk, S., 1995. Vanishing land: Sea level, society and Chesapeake Bay. 47 p.

Lohmann, A., 2001. Monitoring sediment concentration with acoustic backscattering instruments. Nortek Technical note no 3. www.nortek-as.com. 5 p.

Mikkelsen. O., 2012. Grain size distribution and sediment flux structure in a river profile, measured with a LISST-SL instrument. Abstract, Particles in Europe, ICM, Barcelona, Spain, 17-19 Oct., 4 p

Milligan D.A., O'Brien., K.P., Wilcox, C. and Hardaway, C.S., 2010(a). Shoreline Evolution: Gloucester County, Virginia: York River, Mobjack Bay, and Piankatank River

Shorelines. Data Report. Shorelines Studies Program, Department of Physical Sciences, Virginia Institute of Marine Sciences. 14p.

Milligan D.A., O'Brien., K.P., Wilcox, C. and Hardaway, C.S., 2010(b). Shoreline Evolution: James City County, Virginia: James, York and Chickahominy River Shorelines. Data Report. Shorelines Studies Program, Department of Physical Sciences, Virginia Institute of Marine Sciences. 14p.

Milligan D.A., O'Brien., K.P., Wilcox, C. and Hardaway, C.S., 2010(c). Shoreline Evolution: York County, Virginia: York River, Chesapeake Bay and Poquoson River Shorelines. Data Report. Shorelines Studies Program, Department of Physical Sciences, Virginia Institute of Marine Sciences. 14p.

Mixon et al., 1989. Geologic Map and generalized cross sections of the coastal plain and adjacent parts of the Piedmont, Virginia. USGS Miscellaneous Investigations Series, Map I-2033

Moate, B.D. and Thorne, P.D., 2012. Interpreting acoustic backscatter from suspended sediments of different and mixed mineralogical composition. Continental Shelf Research, 46: 67-82

Nortek, 2005. Vector current meter user manual. Doc No N300-100. www.nortek-as.com.

Nortek, 2010. Datasheet_Vector-1. Document TS-050-en-06.2010. www.nortek-as.com

Perry, J.E. and Atkinson, R.B., 2009. York River Tidal Marshes. Journal of Coastal Research, SI (57), 40-49.

Perry, J.E. and C. Hershner, 1999. Temporal changes in the vegetation pattern in a tidal freshwater marsh. Wetlands, 19 (1), 90-99.

Powars, D.S., and Bruce, T.S., 1999. The effects of the Chesapeake Bay impact crater on the geological framework and correlation of hydrogeologic units of the lower York-James Peninsula, Virginia: U.S. Geological Survey Professional Paper 1612, 82 p., 7 pl.

Rodríguez-Calderón, C. (2010). Spatial and temporal patterns in erosional and depositional processes: physical and biological controls in the York River, Chesapeake Bay, Virginia. M.S. Thesis, School

Rosen, Joe and Gothard, Lisa Quinn, 2009. Encyclopedia of Physical Science. Infobase Publishing. P. 155. ISBN 0-8160-7011-3.

Sallenger A. H., Doran, K.S, and Howd, P.A., 2012. Hotspot of accelerated sea-level rise on the Atlantic coast of North America. Nature Climate Change doi:10..1038/nclimate1597, 13p.

San Francisco Chronicle, 2012. Sand becomes largest Atlantic storm on path to northeast. Retrieved 12-10-30.

Scheffer, M., Carpenter, S., Foley, J.A., Folke, C., and Walker, B., 2001. Catastrophic shifts in ecosystems. Nature, 413: 591-596.

Sherwood, C. R., Dickhudt, P.J., and Boss, E.S., 2012. Abstract, Particles in Europe, ICM, Barcelona, Spain, 17-19 Oct., 3 p

Smith, S.J. and Friedrichs, C.T., 2011. Size and settling velocities of cohesive flocs and suspended sediment aggregates in a trailing suction hopper dredge plume, Continental Shelf Research, 31: 500-553.

Smith, S.J. and Friedrichs, C.T., 2012. Image processing methods for *in situ* estimation of cohesive sediment floc size, settling velocity, and density. Limnology and Oceanography: Methods. In press.

SonTek, 2001, Getting started with the ADVField/Hydra system. San Diego, CA. www.sontek.com.

Styles, R., 2006. Laboratory evaluation of the LISST in a stratified fluid. Marine Geology 227, 151-162.

Thorne, P.D. and Campbell, S.C., 1992. Backscattering by suspension of spheres. Journal of the Acoustical Society of America. 92: 978-986.

Thorne, P.D., and Hanes, D.M., 2002. A review of acoustic measurement of small-scale sediment processes. Continental Shelf Research, 22: 603-632.

Thorne, P.D. and Hay, A.E., 2012. Introduction to the Special Issue of Continental Shelf Research on 'The application of acoustic to sediment transport processes'. Continental Shelf Research, 46:1.

Thorne, P.D., Davies, J.S., Bell, P.S., 2009. Observations and analysis of sediment diffusivity profiles over sandy rippled beds under waves. J. Geophys. Res. 114, C02023, doi:10.1029/2008JC004944.

Todd, D., Souza, A. J. and Jago, C., 2012. Seasonally varying flocculation in a macrotidal estuary. Abstract, Particles in Europe, ICM, Barcelona, Spain, 17-19 Oct., 3 p

Traykovski, P., Geyer, W.R., Irish, J.D. and Lynch, J.F., 2000. The role of wave-induced density-driven fluid mud flows for cross-shelf transport on the Eel River continental shelf. Continental Shelf Research 20: 2113-2140.

VanderWerf, J.J., Doucette, J.S., O'Donoghue, T., Ribberink, J.S., 2007. Detailed measurements of velocities and suspended sand concentrations over full-scale ripples in regular oscillatory flow. J. Geophys. Res. 112, F02012.

Voulgaris, G. and Trowbridge, J.H., 1998. Evaluation of the Acoustic Doppler Velocimeter (ADV) for Turbulence Measurements. Journal of Atmospheric and Oceanic Technology. 15(1): 272-289.

Washington Post, 2012. Sandy brings hurricane-force gusts after New Jersey landfall. Retrieved 2012-10-30.

Wilson S.G. and Fischetti T.R. (2010). Coastline Population Trends in the United States: 1960–2008. US Census Bureau. Report P25-1139 available online at http://www.census.gov/prod/2010pubs/p25-1139

Wright, S.A., Topping, D.T., Williams, C.A., 2010. Discriminating silt-and clay from suspended-sand in rivers using side-looking profilers. In:Proceedings of the 2nd Joint Federal Interagency Sedimentation Conference. June 2010, Las Vegas, NV.

CHAPTER 2

Using the Acoustic Doppler Velocimeter (ADV) in the MUDBED Real-Time Observing System*

By Cartwright, G.M., C.T. Friedrichs, P.J. Dickhudt, T. Gass, and F.H. Farmer

2.1. Abstract

As Part of the National Science Foundation MUDBED (Multi-Disciplinary Benthic Exchange Dynamics) project, we have deployed 5 MHz SonTek ADVs at two muddy sites along the York River estuary for the last 3 years. One of the two MUDBED Observing System sites is more biologically dominated, whereas the other is more physically dominated. At both sites, internally recorded ADV data have proven invaluable in allowing reliable long-term estimates of water velocity, bottom stress, suspended sediment concentration, sediment settling velocity, and bed erodibility under spatially and seasonally variable conditions. Nonetheless, it has been challenging to reliably collect these ADV data in a real-time mode. Working with Franktronics, Inc., an automated terminal emulator has been developed to allow ADV data to be logged internally and burst data to be automatically transferred off the internal logger every 15 minutes in near real-time. To facilitate wireless data transmission, we have placed a serial-to-Ethernet converter in an underwater housing on our benthic tripod. This allows us to transmit near-bed ADV data via an Ethernet cable up to a relatively small surface buoy, wirelessly transmit the signal via an Ethernet radio and omni-directional antenna on the buoy to a nearby stationary platform, and relay the ADV data via a second Ethernet radio and a uni-directional antenna back to VIMS. At VIMS, the data stream is received into a local intranet, which isolates the wireless Ethernet links from general internet traffic. To date, the results of ADV deployments at the MUDBED observing system sites indicate that settling velocity tends to be higher at the biological site, whereas suspended sediment concentration and seabed erodibility tend to be higher at the physical site. In addition, sediment settling velocity and bed erodibility are inversely correlated in both time and space. Finally, settling velocity and erodibility remain more consistent in time at the biological site, whereas erodibility increases and settling velocity decreases at the physical site following winter/spring increases in river water discharge.

2.2. Introduction

Deployments of turbulence-resolving Acoustic Doppler Velocimeters (ADVs) are providing insights into fine erodibility and settling as part of the National Science Foundation Mult-Disciplinary Benthic Exchange Dynamics (MUDBED) project (Friedrichs et al., 2008). Bed erodibility and settling velocity are among the most sensitive, yet poorly constrained, parameters in fine sediment transport models (Harris et al., 2005). Although ADVs were originally designed for velocity measurement only, the

backscatter associated with the acoustic returns can be successfully calibrated for suspended sediment concentration (Fugate and Friedrichs, 2002). In addition, acoustic returns registered by ADVs can be used to track local seabed elevation, highlighting periods of erosion or deposition. Furthermore, ADVs are noninvasive, their acoustic signal is resistant to biofouling, and acoustic backscatter measurements are temporally and spatially collocated with turbulent velocity measurements.

However, a limitation of the ADV system's off-the-shelf commercial logger has been the inability to both log the burst data internally and display the data in a real-time format simultaneously. It is important to have both capabilities so that real-time data are not lost in case communications between the instrument and the shore-based real-time data server are interrupted. A second limitation with regards to ADV communication has been the need to transmit a "hard-break" in order to communicate directly with the ADV. While this is not problematic when communicating directly through a serial communication cable to the instrument, it is difficult to transmit a hard break over a wireless serial radio modem.

A successful and sustained real-time observing system incorporating ADVs on benthic tripods in the York River estuary allows rapid response benthic sampling of additional environmental parameters to be targeted to key events and locations where suspended sediment concentration, bed elevation, seabed erodibility, and/or suspended particle

properties are evolving most rapidly. The practical advantages of real-time communications with ADVs are also significant in that potential interruptions in data collection and possible equipment failures can be identified immediately and repaired far earlier than was the case when we were dependent solely on periodic, pre-scheduled instrument turnarounds.

The MUDBED observing system's two benthic arrays (locations indicated by "B" symbols in Fig. 2.1) benefit from being situated within the larger VIMS/CBNERR (Virginia Institute of Marine Science/Chesapeake Bay National Estuarine Research Reserve) network. The VIMS/CBNERR observing system (Moore and Reay, 2009) consists of continually recording water quality and sea level recorders, wind sensors, and wave and current sensors concentrated along the York River estuary (Fig. 2.1). The VIMS/CBNERR observing system also monitors portions of neighboring estuaries.

Scientifically, the MUBED sites further benefit from the presence of a strong gradient in biological vs. physical control of seabed properties (Schaffner et al., 2001), as illustrated by the X-radiographs displayed as part of Fig. 2.1. The two MUDBED sites are similar in that they are both dominated by mud and are both moderately energetic. However, bioturbation is more prevalent within the seabed in the vicinity of the down-estuary "biological" site, and physically-induced layering is more commonly seen near the up-estuary "physical" site (Dickhudt et al., 2009). This trend is illustrated in Fig. 2.1 by the
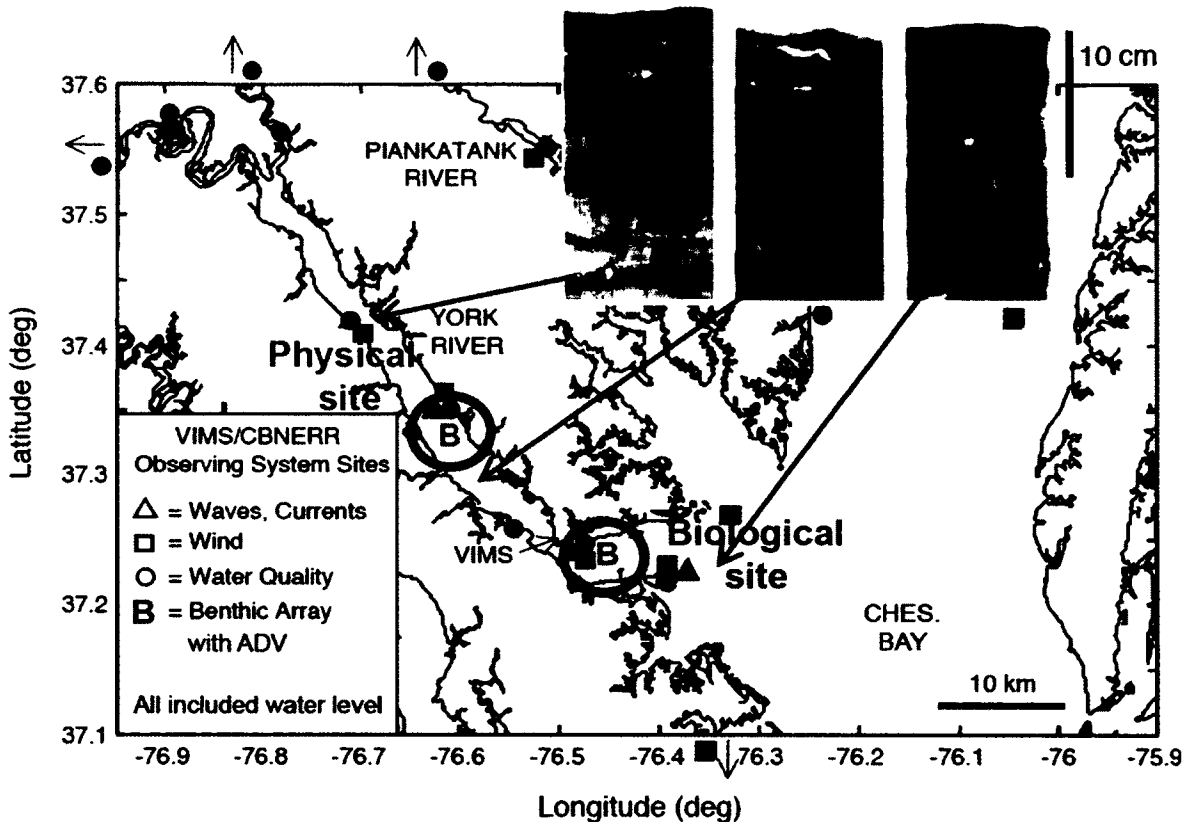
Figure 2.1. Location of MUDBED benthic ADV tripods (indicated by "B") within the VIMS/CBNERR Observing system. X-radiograph images from cores collected along the York River estuary are courtesy of L. Schaffner.

distinct patterns seen in X-radiographs at locations bracketing the MUDBED sites. In the upper York River estuary, disturbance by sediment transport reduces macrobenthic activity and sediment layering is commonly preserved. In the lower York layering is typically destroyed by bioturbation (Schaffener et al., 2001). This gradient provides a natural laboratory for investigating the relative roles of biological vs. physical processes in affecting sediment resuspension and subsequent settlement.

The remainder of this paper consists of two main parts: first a "Methods" section which describes the physical, electronic and communications structure of the ADV-based MUDBED observing system and, second, a "Results" section which provides a significant example application of MUDBED ADV data, namely better understanding of seasonal variation in fine sediment erosion and settling.

Figure 2.2. SonTek 5 MHz ADVOcean sensor mounted in a downward looking position on a MUDBED tripod.

2.3. Methods

ADV Description

The ADVs used in the MUDBED observing system are SonTek 5MHz ADVOcean Probes. The ADV sensor (Fig. 2.2) is a heavy-duty stainless steel assembly consisting of one acoustic transmitter and three acoustic receivers. The ADV's 2-cm^3 sampling volume is located approximately 18 cm below the center transmitter. The probe's x-axis is defined by the orientation of the ADV's number 1 receiver, which is marked by a small indentation on the sensor head. The acoustic sensor is mounted on a signal-conditioning module with internal receiver electronics. Included in the module used for this paper are the following optional sensors: compass, 2-axis tilt sensor, strain gauge pressure sensor and temperature sensor. The ADVOcean Probe with optional sensors has a total length of 39 cm (SonTek, 1997).

Underwater mate-able connectors are used to connect the module via a high frequency cable to the processor housing, called the "Hydra". The Hydra (a watertight cylinder 75 cm long with a 16-cm diameter) houses the ADV's internal recorder with a memory card and battery packs for autonomous deployment. The ADV can be deployed in either a continuous real-time mode or an autonomous burst mode. In the real-time mode, the data streams continuously out of the instrument via a cable connected to the Hydra using an underwater mate-able connector and a DB9 connector to plug into a RS-232 serial port on a computer. In the autonomous mode, the burst data is stored in binary format on the

memory card. A burst is a set number of samples, (1200 samples/burst, in our application) taken at a set interval (15 minutes in our case). The sampling rate we have chosen is 10 Hz. At the start of each burst, the ADV outputs the burst header, in ASCII format, over the serial port. The header contains the serial number, burst number, date and time of the burst, the probe and sampling volume distances to the seabed, the battery voltage and system diagnostic data.

In order to communicate with the data logger in the Hydra, a "hard-break" needs to be sent via the RS232 serial communication cable to "wake up" the instrument. A hard-break is a serial communication signal that causes a reset in the logger electronics and returns the system to command mode from deploy mode. A hard-break requires holding the transmit serial communication lines high for a period of 300 ms.

Tripod Preparation

The ADV, cable and Hydra are all wrapped with Saran Wrap and electrical tape to help protect their surfaces from biological growth and are then mounted on a tripod that stands approximately 1 meter tall. The aluminum tripod is painted with a primer followed with Interlux Trilux 33 Antifouling Paint. The ADV's transducer and receiver faces are painted with a thin coat of Interlux MicronCSC Antifouling Paint. Fig. 2.3 shows a tripod ready for deployment on the back of the R/V Elis Olsson and one in the foreground

covered with three months worth of biofouling. The housings, sensors and the tripod are each equipped with zinc anodes for corrosion protection. The ADV probe is mounted in a downward looking position on a center post and secured with 316 stainless steel band clamps and heavy-duty cable ties. The metal of the band clamps and instruments are insulated from each other and from the tripod using pieces of plastic shelf liner. All band clamps are then wrapped with electrical tape to facilitate later removal of biological growth.

A Sequoia Scientific Instruments Laser *In Situ* Scattering Transmissometer (LISST), which measures suspended particle size distribution between 2.5 and 500 microns, is the second of three instruments mounted on the tripod. A YSI 6600 Conductivity, Temperature and Depth sensor (CTD), equipped with a turbidity probe, is the third. The #1 receiver on the ADV probe faces in the same direction as the front end of the LISST. A Seapoint Optical Backscatter Sensor (OBS) is cabled to the LISST's auxiliary input and mounted on one of the tripod legs at the same height above the bottom as the ADV sampling volume.

Underwater mate-able plugs allow all three instruments output their data in real-time mode via RS232 serial communication cables. Serial communication, however, is slow and hard to transmit wirelessly via serial radio modems. Several different serial radio

Figure 2.3. Fully equipped tripod ready for deployment on board the R/V Elis Olsson (background). The tripod in the foreground had been deployed at least three months.

modems were tried with minimal success. The hard-break needed to communicate with the ADV is particularly difficult to transmit over wireless serial communication. Ethernet protocol, on the other hand, was found to be quick to transmit, and it does allow a hard-break to be sent to the ADV, allowing for 2-way communication between the instrument and the computer collecting the real-time data.

An underwater serial-to-Ethernet converter instrument (S2E) was developed using an empty Hydra housing provided by SonTek. A StarTech 4-port RS-232 Serial-to-Ethernet
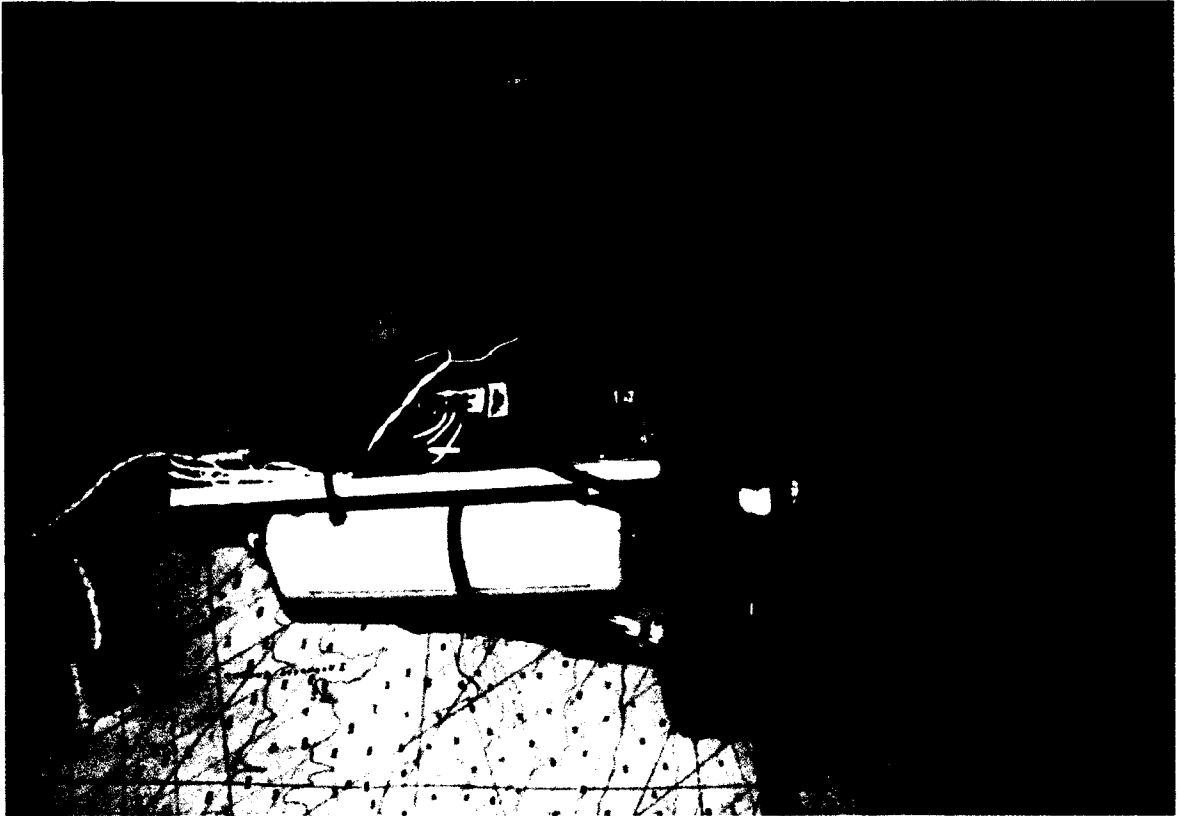
Figure 2.4. SonTek housing (yellow) retrofitted with a 4-port serial-to-Ethernet converter (white housing on endcap) and an A-to-D converter to monitor battery usage (red housing on endcap).

over IP Adapter Device Server (Manufacture's part number NETRS232_4) was mounted inside (Fig. 2.4). The StarTech interface converter allows for four serial devices to be connected and serial output converted to Ethernet with a TCP/IP network transport protocol and a data transfer rate of up to 115.2 Kbps. The three serial wet-pluggable connector pigtails that connect to the LISST, CTD and ADV serial ouput ports were molded to a single wet-pluggable connector to be plugged into the S2E serial input port. The output port of the S2E is connected via a wet-pluggable connector to an Ethernet

On piling: Freewave radio repeater,
directional antenna, solar panel,
batteries, navigation light

On buoy: Freewave radio, rechargable
battery pack, solar panels, omni-
directional antenna, navigation light

Ethernet cable
connecting buoy
and tripod

On Andrews Hall rooftop:
router, Freewave radio,
directional antenna

On tripod: Sontek ADV, S2E
converter, LISST, CTD

Fiber optic cable
to VIMS internet

Computers in lab for collecting real-time data

Figure 2.5. Flowchart of Ethernet communication between instruments mounted on tripod and computers in the lab collecting real-time data.

cable. The S2E is powered by the same type of SonTek battery packs used in the Hydra to power the ADV. A SuperLogic A-to-D convertor was mounted inside the S2E and connected to the battery packs and the fourth serial port to allow the voltage of the battery packs to be monitored. The S2E is wrapped and mounted on the tripod along with the other instruments.

Communications Data Flow

Fig. 2.5 shows the path of travel of the Ethernet communications between the instruments and the computers collecting the real-time data. Fifty meters of Falmat Extreme Net underwater network data/power cable is used to transmit the information via Ethernet between the S2E and the top-hat buoy on the surface (Fig. 2.5 top right.). Two-thirds of the cable is attached to a 3/16" mooring chain to act as a ground line that can be grappled to retrieve the tripod if the surface float above it is lost. The chain is connected at one end to the tripod and at the other end to a 100-kg concrete clump that acts as an anchor for the top-hat buoy. A heavier 3/8" mooring chain is connected between the concrete clump and the buoy, and the last one third of the cable is attached to it. Care must be taken to make sure the chain is shorter than the cable to prevent unnecessary strain on the cable and connectors.

The top-hat buoy to which the chain is connected is a yellow Rolyan lighted float collar can buoy, model B1428L (Fig. 2.6). The buoy was modified by the manufacturer to have

Figure 2.6. The Roylan top-hat buoy modified for PVC pipe insert to house FreeWave radio and battery pack.

a 5" open tube at the top. A water-tight PVC pipe canister was made to fit in the top of the buoy (Fig. 2.6 insert). This canister houses a rechargeable battery pack produced specifically for this application by Battery Barn consisting of twelve Enersys Cyclon

0860-0004 E-cell 2-volt/4.5-Amp-Hr sealed lead acid batteries and an HTplus FreeWave radio modem. The battery pack is recharged with four flexible Discover Power solar panels (11 watt, 12 volt, 7 amp). Over charge of the batteries is prevented by the Morningstar SunSaver-10 Solar controller housed in the buoy insert with the radio and batteries. The Ethernet cable connected to the tripod is connected to the radio using wet-pluggable connectors. The length of cable that is part of the connector pigtail was kept as short as possible when molded to the Ethernet cable to reduce the interference introduced by using non-Ethernet cable in the communications system. The signal is broadcast through an omni-directional fiberglass radome-enclosed base antenna. At the top of the canister, for navigation purposes, is a Sealite SL-60 Marine Light Amber (set for a 1 second flash length every 4 seconds). This light has a self-contained rechargeable battery and solar panel.

The Ethernet signal travels from the FreeWave radio in the buoy to another HTplus FreeWave radio mounted on the piling (Fig. 5 top left). The piling is a three-pole dolphin sunk 5 meters into the bottom, with height above water of 4 meters at mean low tide. A crows-nest platform was erected approx 1 meter from the top end of the piling and has approximately a 1-meter radius. The piling is marked for navigation with another Sealite SL-60 (whose flash pattern is the same as the buoy's) and a yellow day marker labeled "VIMS CB" (Fig. 7). The buoy is deployed within 100 meters of the piling. Power on the piling is provided by three 12-volt, 63-amp-hour rechargeable batteries (8A22NF) housed in a large battery box (Port Supply 3669942). The batteries are kept charged by
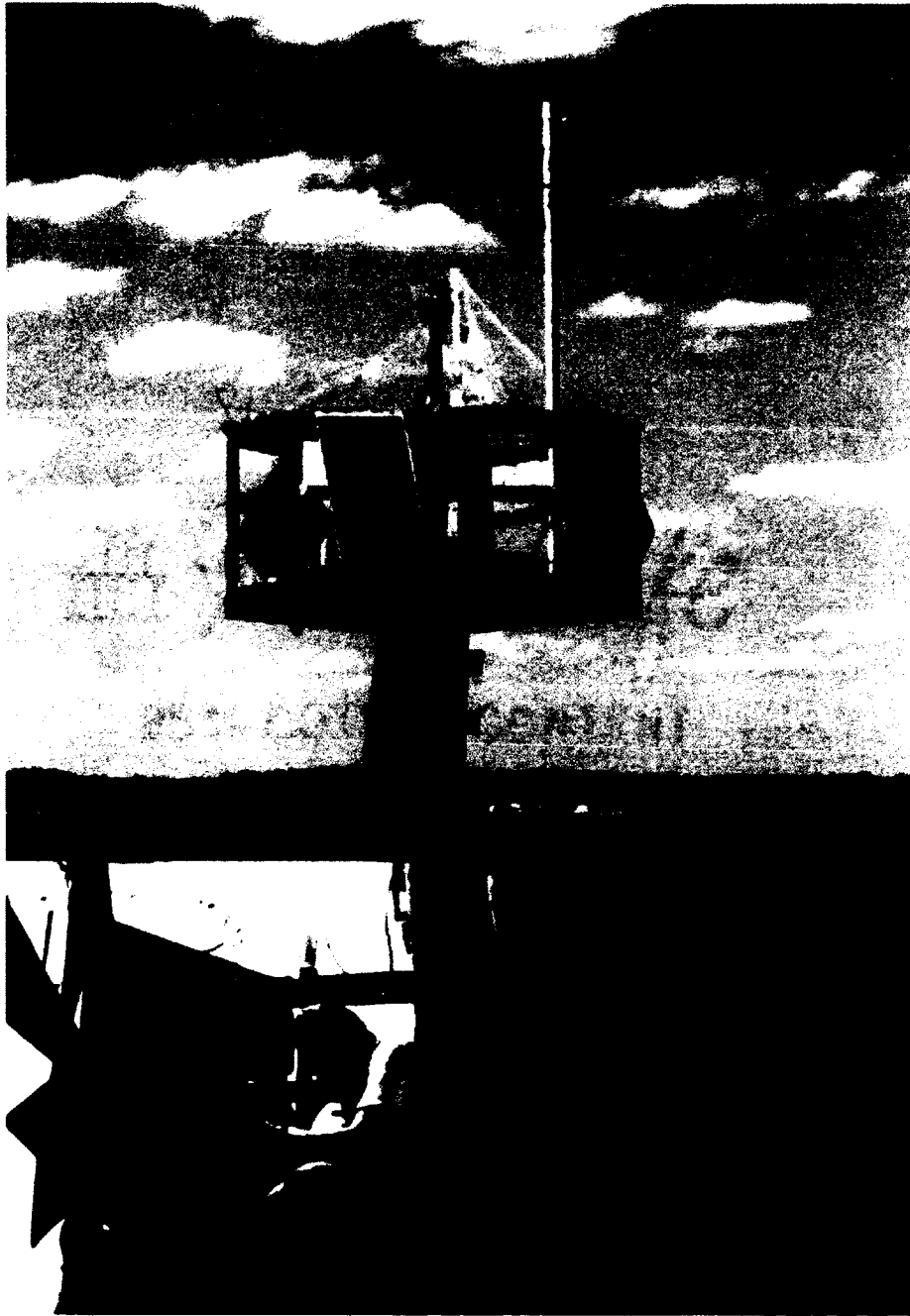
Figure 2.7. "VIMS CB" piling (photo by T. Gass). Insert photo of FreeWave radio installation on piling (photo by L. Kraatz).

an 80-watt Solar Panel (sharp 80) from PowerUp. In the near future, a 400-watt wind turbine (Air-MX-1), also from PowerUp, will be installed to charge the batteries during times that the solar panel cannot. A PowerUp 30-Amp Charge Controller (PS30) for the solar panel and the FreeWave Radio are housed in Pelican 1400 cases mounted on the railing of the crows-nest (Fig. 2.7 insert). A fishing throw-net is placed over the top of the crows-nest to discourage osprey from nesting on it.

The radio mounted on the piling acts as repeater between the radio in the buoy and one mounted in a Pelican 1400 case on the roof of Andrews Hall on the VIMS campus in Gloucester Point, VA (Fig. 2.5, middle left). These FreeWave HTplus radios broadcast between the range of 902 and 928 MHz. Over the wireless Ethernet connection, data is transmitted at a rate of up to 867 kbps. Use of a repeater can slow the transmit rate to approximately half that. The antennas on both the piling and the rooftop of Andrews Hall are FreeWave 890-960 MHz 10-dB 7-element welded Yagi directional units. Directional antennas are use to facilitate more reliable higher rates of data transfer.

Data Collection

All transmissions among the radios are on an isolated intranet kept separate from the VIMS-wide intranet by a DLINK wired router (model number EBR2310), mounted in a Pelican 1400 case on the roof of Andrews Hall (Fig. 2.5 middle left). The router is physically connected to the VIMS intranet via a fiber optic cable. Fiber optic cable was chosen because the buildings at VIMS are susceptible to lightning strikes.

In our VIMS lab, system control laptops are set up with Startech.com IP-Extender Manager. This software works with the serial-to-Ethernet converter and allows virtual communication ports to be set up on computers to collect the data coming from the instruments. A single laptop can be used to collect data from the ADV, LISST, CTD and the A-D converter, the last of which is used to monitor the battery power in the S2E. Two-way communications are possible with each of the instruments, the S2E and all the radios. With the use of Window Remote Desktop Connection, the data laptops can be accessed from anywhere within the VIMS intranet, and, with VPN Client, communication with the ADVs and other instruments is accessible from anywhere the internet is available.

Most oceanographic field instruments are designed to be used in either a real-time mode or to be deployed autonomously. Because we are interested in collecting a burst of data every 15 minutes from the ADV, and we want to have the data available as soon as the burst is collected, software had to be developed to allow us to do repeatedly switch between modes. Franktronics, Inc., developed a software GUI called the "VIMS ADV Binary Downloader" (Fig. 2.8). This GUI is composed of three panels. The first is the "Terminal" panel. In this panel we can connect directly to the ADV data logger and talk to it as though we were connected directly with a serial cable. We are able to send a hard-break to wake the instrument and send commands such as "show system" to get a

list of the system parameters and "show deploy" to show a list of the Deployment parameters, as well as any other command recognized by the ADV.

The second section of the GUI is the "Schedule" panel. In this panel the Instrument time, Burst Interval, Sample Rate and the number of Samples/Burst to be collected can be set. The start time for the first scheduled burst can also be set. Once the "Deploy button" is clicked, the "Start Time" is sent to the ADV which will collect a burst at the scheduled time. The file name, limited to five characters, is automatically set to the day plus one number for the year. For example, Au309, for August 30, 2009, has a prefix of two letters for the month and three numbers for the day/year. The ADV data-logger appends three more digits starting with 001 and increases by 1 for each burst collected throughout the day.

Following a pre-determined delay after the scheduled burst start time, the Downloader sends the instrument a hard-break and requests a File List from the instrument recorder. The list is then displayed in the "Download" panel. The most current file is downloaded from the device and any other files not stored in the Download Directory on the data collection computer are also downloaded. The ADV data logger can store only 255 files, so at midnight the memory card is reformatted to erase all the files for the day (96 files each day when files are restarted every 15 minutes). Nothing is deleted if all the files have not been verified as having been downloaded to the download directory. The
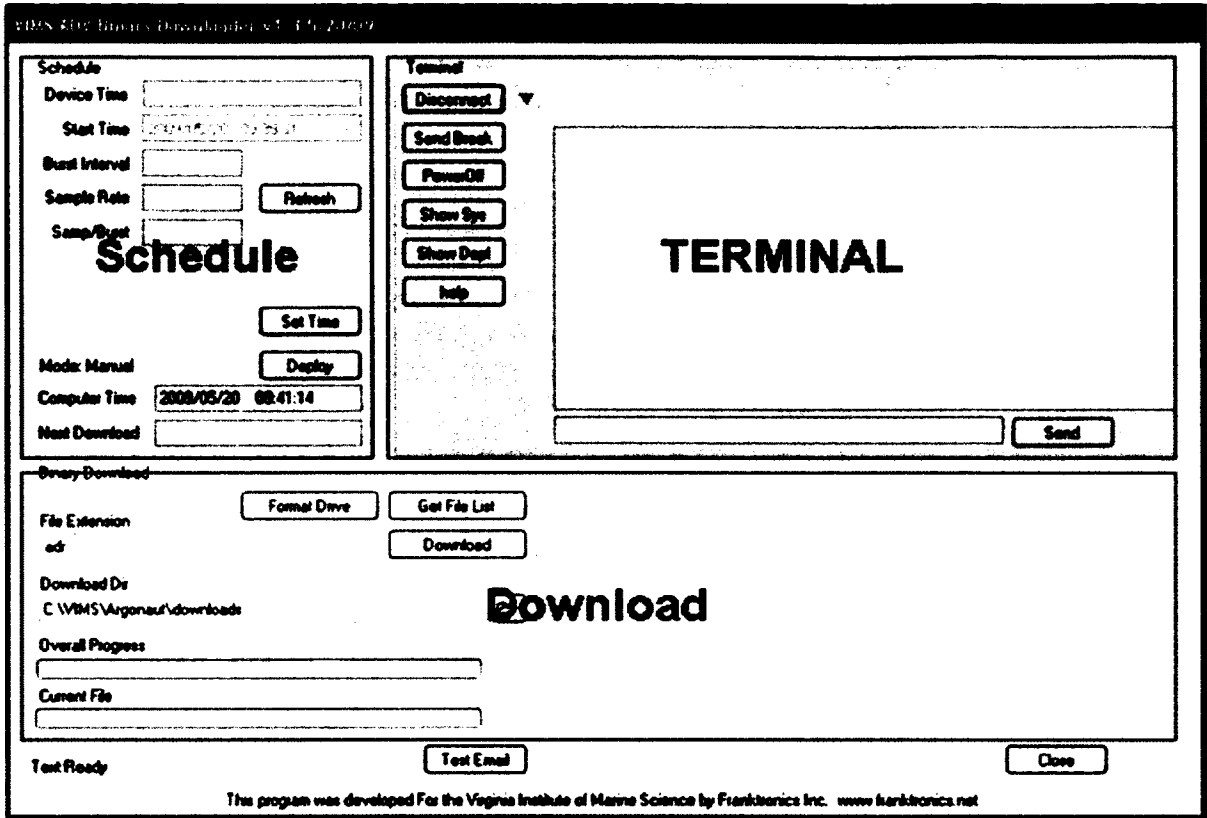
Figure 2.8. VIMS ADV Binary Downloader developed by Franktronics, Inc., for collection of ADV real-time bursts.

download directory and the file extension can be changed in this panel before the program is started by clicking the "Deploy" button in the "Schedule" panel.

The program adds the "Burst Interval" (15 minutes) to the last "Start Time" for a new "Start Time" and redeploys the instrument. Fig. 2.9 shows a schematic of the download schedule. The new start time is displayed in the "Schedule" panel along with the "Next
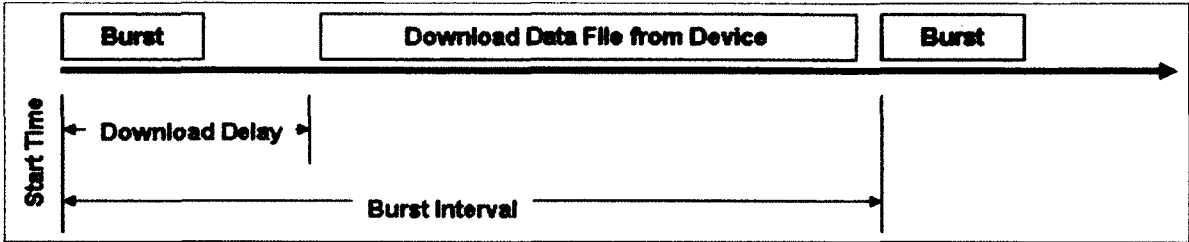
Figure 2.9. Schematic of the download schedule for ADV Binary.

Download" time. The advantage of this program is the ability to download each burst within minutes of completion of the burst. The burst is also stored on a memory card in the instrument in case there is a problem with the communications and it is not downloaded properly. If this happens, the program sends a cell phone text and/or an email to preset phone numbers or email addresses to let the administrator know a problem exists. If a problem occurs while the instrument is deployed, the instrument appends each subsequent burst to the end of the file until taken out of deploy mode. The files that are downloaded to the download directory are automatically backed up to the CHSD Linux server for archival using cwRsync, a program that is able to bridge PC and Linux platforms.

The next step in developing seamless data delivery will be is to take the binary data that is being archived on the CHSD Linux server and convert it to ASCII format. In ASCII format MATLAB will be used to calculate burst average statistics. Burst-average

velocity, suspended sediment concentration, and bottom stress will be calculated, as well as the settling velocity and bed erodibility corresponding to each burst. These values will then be stored in a relational database.

A publically viewable website and interactive exhibit is also being developed to display the real-time data. A touch-screen monitor will be mounted in the main hall of our building to allow visitors to query the site and navigate between the different instruments and the corresponding data. Both the external website and local interactive display will allow the user to choose the timeframe of the data to be displayed -- anywhere from hours, to days, to months.

2.4. Results

In this section we provide an example application of ADV data from the MUDBED observing system. In this case the ADV data are being used to better understand the nature of seasonal variations in fine sediment erosion and settling.

Calibration of ADV and Example Time-Series

When properly calibrated, ADV backscatter can provide a useful estimate of suspended sediment concentration (Fugate and Friedrichs, 2002). Fig. 2.10 displays best-fit linear regressions between ADV backscatter in counts and the log of total suspended solids (TSS). The ADV measurements are from a 5MHz SonTek ADV Ocean Probe deployed
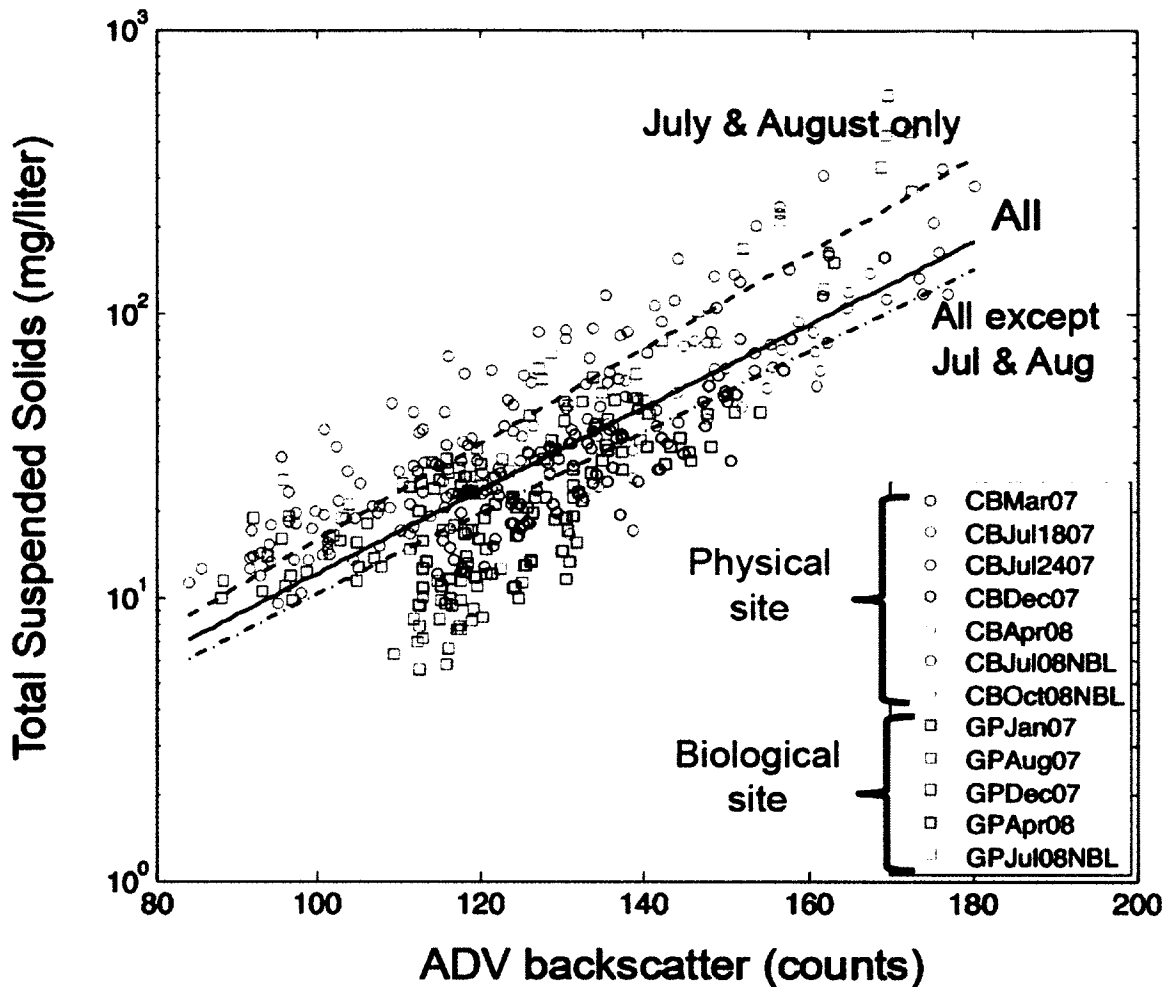
Figure 2.10. *In situ* calibration of ADV backscatter for total suspended solids based on filtered pump samples collected at MUDBED observation system sites.

on a profiler within ~100 m of our identical model benthic tripod-mounted ADV. Also on the profiler is a high capacity submersible pump used to collect water samples for TSS analysis. Pump samples collected in the field were stored in the dark on ice during transit back to the lab. At VIMS the samples were then passed through pre-weighed ~0.7 micron pore-size glass fiber filters, dried at 100 deg C, and reweighed.

For individual cruises, the regressions between backscatter and the log(TSS) were strongly linear. But notable shifts in shifts in the calibration curves were seen between calibration cruises (Fig. 2.10). Attempts were made to use distinct calibration curves for different times of year. However, the most consistent and sensible results from the benthic tripods were found when a single calibration based on all pump samples together was used. It may be that the acoustic properties of sediment at ~35 cmab (the tripod ADV sampling height) vary somewhat less than properties higher in the water column where pump samples were more commonly collected.

Fig. 2.11 displays example data for burst-averaged current speed, burst-averaged suspended sediment concentration and elevation of the seabed. Although the strength of the tidal current, the seabed grain size and the seabed percent mud were similar at both locations, there was a tendency for higher sediment concentrations and greater amplitude changes in seabed elevation at the physical site. This difference has been interpreted to be due ultimately to a tendency for an along-channel transition in water column mixing to occur seasonally in the vicinity of the physical site (Dickhudt et al.., 2009; Lin and Kuo, 2001). The seasonal front at the physical site ephemerally traps sediment, leading to temporarily high sediment concentrations, rapid deposition, and subsequent rapid erosion of easily resuspended sediment (Dickhudt et al., 2009).
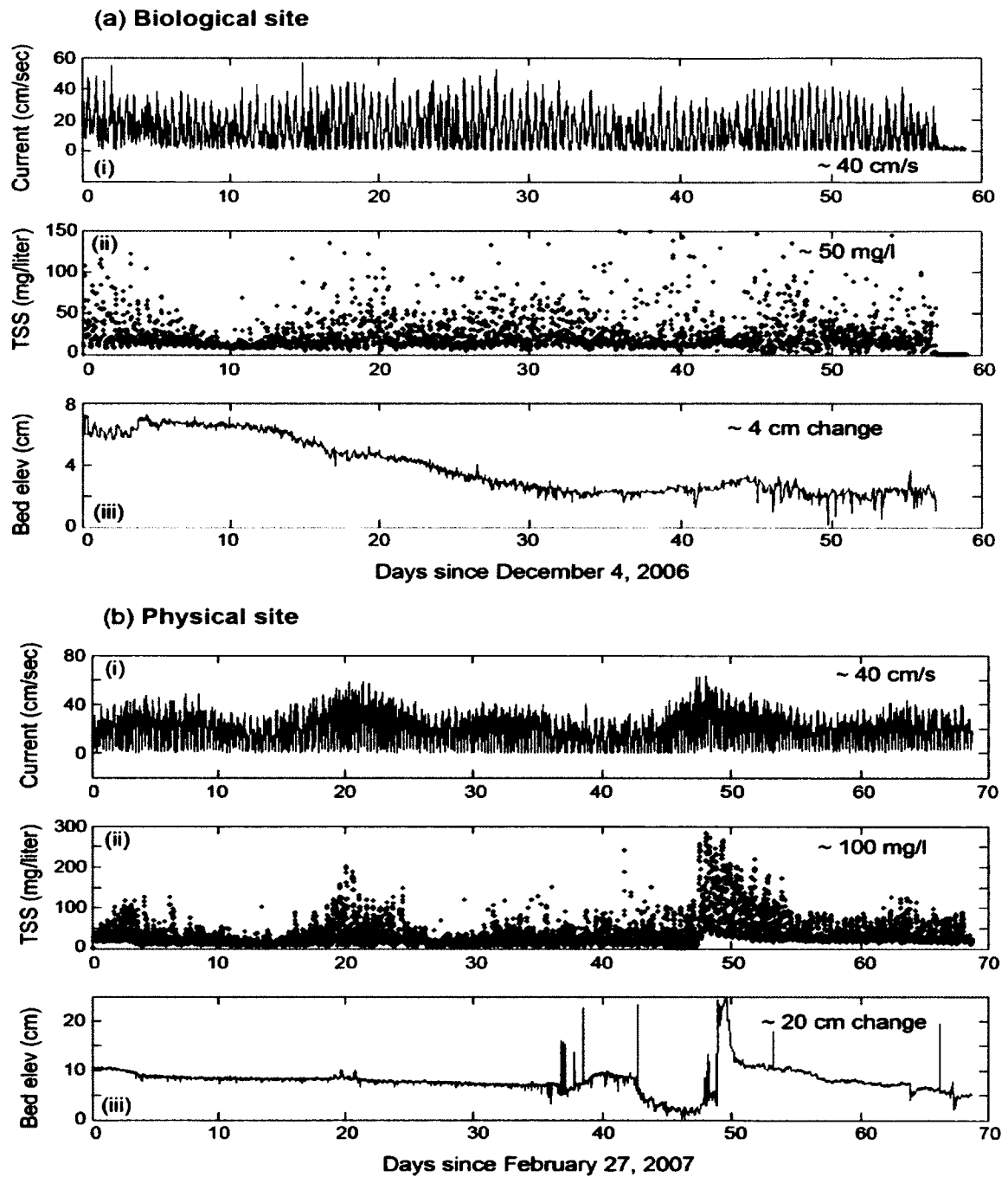
Figure 2.11. Example time-series based on ADV output collected ~35 cm above the bed at the MUDBED sites. (a) The more biologically-influenced ("biological") site and (b) the more physically-influenced ("physical") site: (i) burst-averaged current speed, (ii) burst-averaged total suspended solids concentration, (iii) seabed elevation.
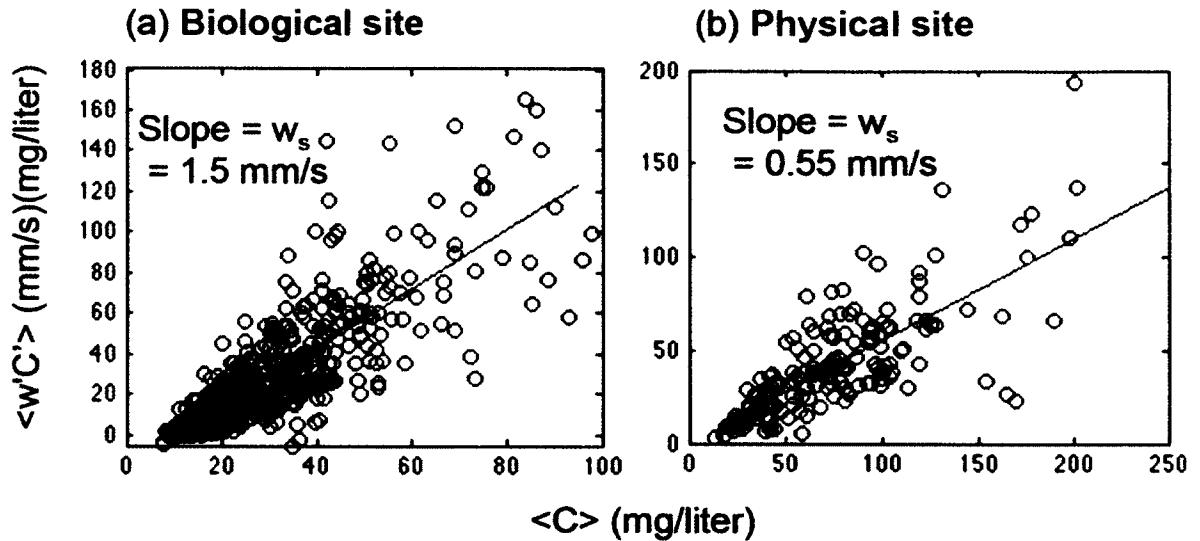
Figure 2.12. Example estimates of sediment settling velocity (ws) from ADV data displayed in Fig. 2.11(a) for the biological MUDBED site and from data displayed in Fig. 2.11(b) for the physical MUDBED site.

Settling Velocity and Bed Erodibility

Assuming a local balance within the water column between upward turbulent transport by turbulent Reynolds flux and downward settling by gravity yields:

$$< w'C'> = w_s <C>$$ (2.1)

where w is vertical water velocity, C is suspended sediment mass concentration, w_s is sediment settling velocity, primes indicate turbulent fluctuations, and angle brackets indicate a burst average. Within a few tens of centimeters of the bed, this balance

commonly holds to with 1-10% at temporal scales as short as a few minutes (Fugate and Friedrichs, 2002). Because the ADV can measure both C and w within the same 2-cm^3 sampling volume, including turbulent fluctuations, one can use the slope of $<w'C'>$ vs. $<C>$ to estimate w_s (Fig. 2.12). Applying this ADV-based method, settling velocity was found to be generally higher at the biological MUDBED site relative to the physical MUDBED site.

Output from ADVs at the MUDBED sites can also be used to provide an indirect estimate of bed erodibility (Friedrichs et al., 2008). Traditionally, bed erodibility is determined by applying controlled stresses to the bed, either *in situ* or on seabed cores in a lab setting, and then recording the amount of material suspended as stress is increased. The result is a graph of total eroded mass as a function of bed stress. Such direct measurements were collected periodically by at the MUDBED sites in 2006-2008 by (Dickhudt et al., 2009) using a Gust microcosm. Because the ADV documents both bottom stress (t_b) and suspended sediment concentration (C), similar data can also be derived from *in situ* ADV time-series. Although the ADV cannot control stress, a bottom-mounted ADV still documents time-varying bed stress via $t_b = - r <u'w'>$, where r is fluid density, and u' and w' are turbulent fluctuations in horizontal and vertical velocity. Estimating the vertical integral of C during a period of slowly increasing current speed then gives an estimate of eroded mass as a continuous function of t_b.
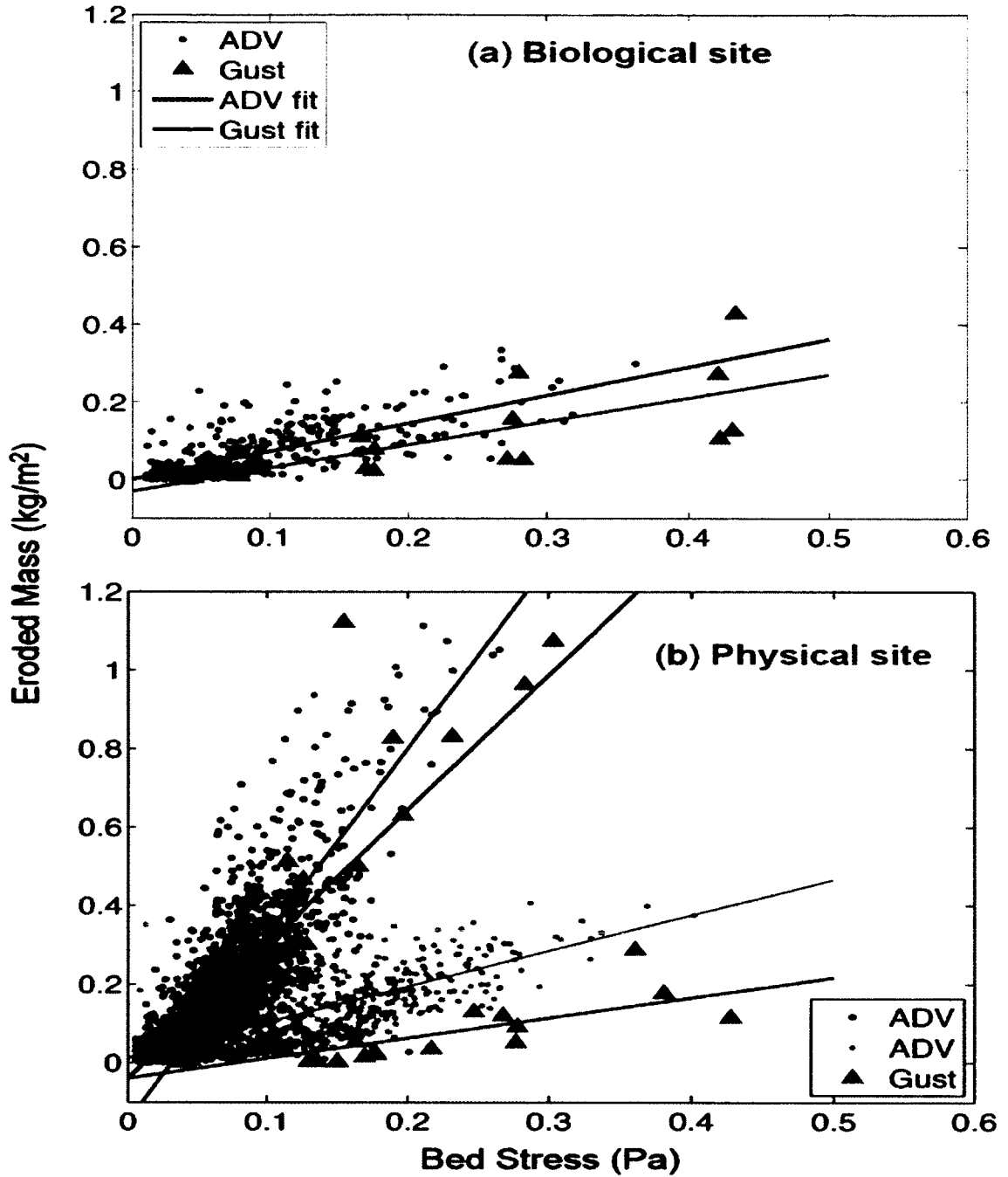
Figure 2.13. Comparison of ADV-based estimates of eroded mass as a function of bottom stress to data measured by a Gust microcosm (microcosm data from Dickhudt et al., 2009).

Close to the bed, a reasonable approximation for the vertical variation in suspended sediment concentration below and above an ADV sampling at height z_o is given by the Rouse profile in the form of a power law (Friedrichs et al., 2008):

$$C = C_o \, (z/z_o)^{-P} \tag{2.2}$$

Where C_o is observed C within the ADV sampling volume, and the Rouse Parameter $P = 2.5 \, w_s \, (t_b/r)^{-1/2}$. Although there are several simplifying assumptions inherent in (2.2), including nearly steady flow, settling velocity independent of z, no sediment-induced stratification, and the presence of a logarithmic velocity layer, a simple vertical integration of (2.2) can still provide a rough estimate of eroded mass, M (Friedrichs et al., 2008):

$$M = z_o C_o \, (1-P)^{-1} \, (h/z_o)^{1-P} \tag{2.3}$$

where h is the height of the integration.

Fig. 2.13 compares the results of ADV-based eroded mass vs. stress as inferred from ADV data with eroded mass vs. stress measured directly at the same sites using a Gust microcosm. Both the Gust microcosm and the ADV-based estimates of eroded mass suggest that the response of the seabed to stress at the physical site tends to be bimodal (Fig. 2.13b). Some of the time, the mass eroded by a given stress at the physical site is
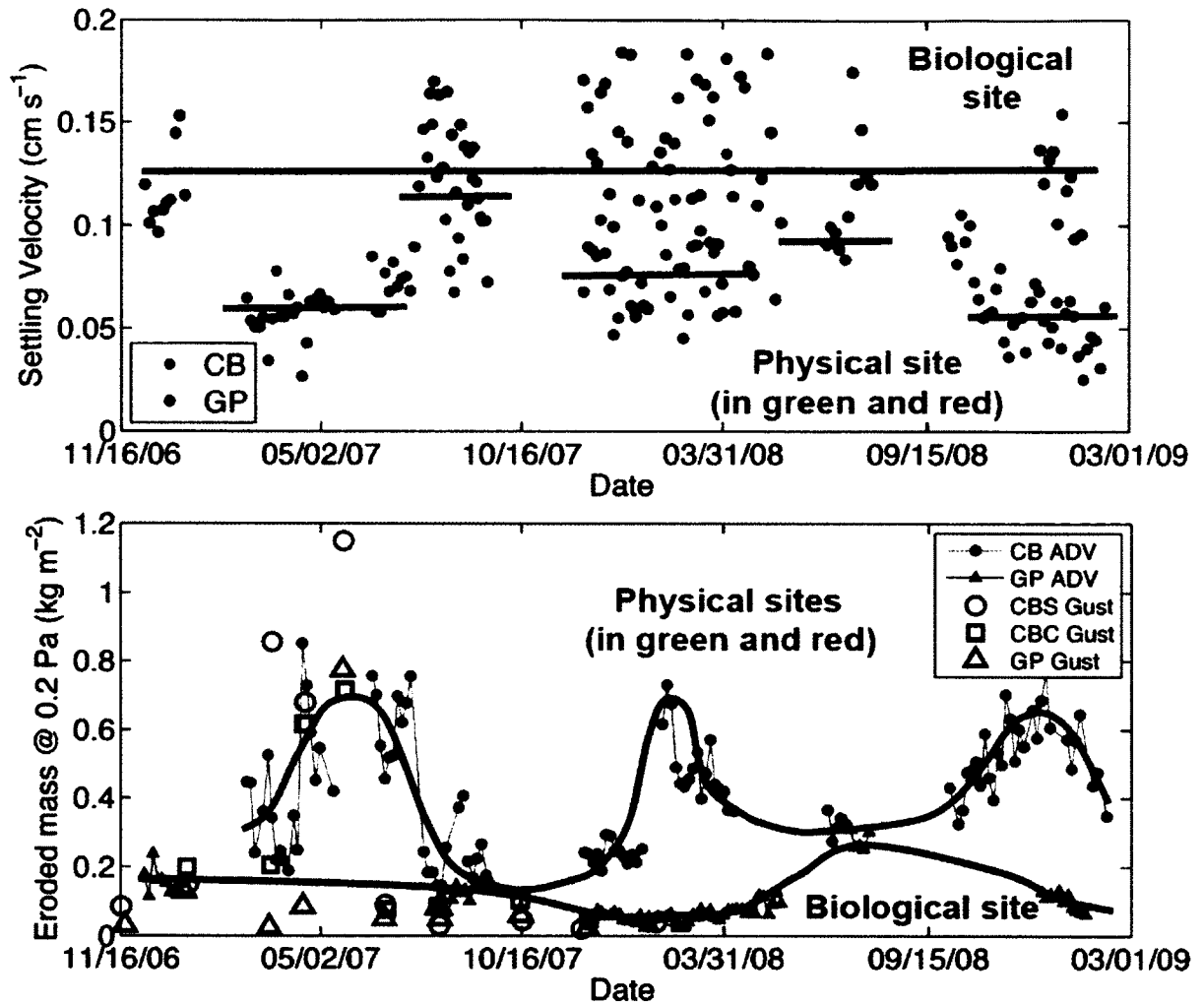
Figure 2.14. (a) ADV-based estimates of sediment settling velocity. (b) ADV-based estimates of eroded mass at 0.2 Pa along with analogous eroded mass data measured by a Gust microcosm (microcosm data from Dickhudt et al., 2009)

similar to the trend seen at the biological site, and some of the time much more sediment is eroded at the physical site. In either case, the general trends document by ADV-based estimate and the more direct microcosm measurement are remarkably consistent.

To examine seasonal trends in characteristic settling velocity and seabed erodibility at the biological and physical sites, the ADV data analysis methods shown in Figs. 2.12 and 2.13 were performed on for all available ADV time-series at the two MUDBED Observatory sites (Fig. 2.14). The MUDBED ADV time-series, which extend back to late 2006 at the biological site and early 2007 at the physical site, were first divided into discrete 3.5-day segments. Linear regressions were then used to produce an independent estimate of W_s and eroded mass twice-a-week during each week for which ADVs were operating. Each linear regression performed on eroded mass vs. bed stress was used to define a best-fit estimate of eroded mass at 0.2 Pascals of stress. The results of this ADV analysis as displayed in Fig 2.14 show the following: (1) Suspended sediment settling velocity tends to be higher at the biological site, whereas seabed erodibility tends to be higher at the physical site (ii) Sediment settling velocity and bed erodibility are inversely correlated in both time and space, such that settling velocity tends to increase as erodibility decreases. (iii) Settling velocity and erodibility remain more consistent in time at the biological site, whereas erodibility increases and settling velocity decreases in the winter/spring at the physical site. The results of the seasonal ADV data analysis confirm and clarify the findings of Dickhudt et al. (2009), which were based Gust microcosm measurements. Together, Friedrichs et al. (2008) and Dickhudt et al. (2009) concluded that lower erodibility and higher settling velocity is consistent with "equilibrium" biological processing, whereas high erodibility and lower settling velocity is characteristic of episodic winter/springtime deposition following high river discharge (Fig. 2.15).

After period of high river flow

20 ‰   15 ‰   10 ‰   5 ‰   0 ‰

Gloucester Point   Clay Bank   West Point
Biological site   Physical site

After period of low river flow   Near bed sediment flux

Salinity isohalines   20 ‰   15 ‰   10 ‰   5 ‰   0 ‰

Low suspended sediment
concentrations

High suspended sedimen
concentrations

Pelletized sediment

Fines and/or flocs

Laminated seabed

Mottled seabed

Equilibrium case:
- Lower erodibility
- Higher settling velocity

Depositional case:
- Higher erodibility
- Lower settling velocity

Figure 2.15. Conceptual model for sediment transport in the York River estuary, including changes in seabed structure and patterns of concentration, seabed erodibility and suspended sediment settling velocity (Dickhudt et al., 2009).

2.5. Acknowledgement

2.6. References

Dickhudt, P.J., Friedrichs, C.T., Schaffner, L.C., and Sanford, L.P. , 2009. Spatial and temporal variation in cohesive sediment erodibility in the York River estuary: a biologically-influenced equilibrium modified by seasonal deposition, *Marine Geology*, vol. 267(3-4), pp. 128-140.

Friedrichs, C.T., Cartwright, G.M. and Dickhudt, P.J. , 2008. Quantifying. benthic exchange of fine sediment via continuous, non-invasive measurements of settling velocity and bed erodibility, *Oceanography*, vol. 21(4), pp. 168-172.

Fugate, D.C. and Friedrichs, C.T. , 2002. Determining concentration and fall velocity of estuarine particle populations using ADV, OBS and LISST, *Continental Shelf Res.*, vol. 22, pp. 1867-1886.

Harris, C.K., Traykovski, P. and Geyer, W.R., 2005. Flood dispersal and deposition by near-bed gravitational sediment flows and oceanographic transport: A numerical modeling study of the Eel River shelf, northern California, *J. Geophys. Res.*, vol. 110(C09025), doi:10.0129/ 2004JC002727.

Lin, J., and Kuo, A.Y. , 2001. Secondary turbidity maximum in a partially mixed microtidal estuary, *Estuaries*, vol. 24, pp. 707-720.

Moore, K.A. and Reay, W.G. (eds.), 2009. A Site Profile of the Chesapeake Bay National Estuarine Research Reserve, *J. Coastal Res.*, Spec. Iss. No. 57.

Schaffner, L.C., Hinchey, E.K., Dellapenna, T.M., Friedrichs, C.T., Thompson Neubauer, M., Smith, M.E., and Kuehl, S.A., 2001. Physical energy regimes, sea-bed dynamics and organism-sediment interactions along an estuarine gradient, In: J.Y Aller, S.A. Woodin and R.C. Aller (eds.), *Organism-Sediment Interactions*, Univ. South Carolina Press, Columbia, SC. pp. 161-182.

SonTek, 1997. ADV Operation Manual – Firmware Version 4.0, SonTek, San Diego, CA. October.

CHAPTER 3

Dual Use of a Sediment Mixing Tank for Calibrating Acoustic Backscatter and Direct Doppler Measurement of Settling Velocity*

By Grace M. Cartwright, Carl T. Friedrichs, and Paul D. Panetta

3.1. Abstract

While the Acoustic Doppler Velocimeter (ADV) is designed to determine fluid velocity, it is important to recognize that it is actually the velocity of the scatterers themselves that is measured. Thus in a calibration tank designed to relate sediment-induced backscatter to sediment concentration, the vertical velocity registered by an ADV at a given point is actually the true fluid velocity plus the sediment's settling velocity. And absent net vertical volume flux, the average vertical velocity registered by an ADV across a horizontal plane is equal to the mean sediment settling velocity. For this study, a series of ADV calibrations were run in a 118-liter re-circulating tank for six sand sizes between 63 and 150 microns. A grid of ADV measurements distributed in a horizontal plane across the tank revealed that the mean vertical velocity registered by the ADV in each case was indeed consistent with each grain size's settling velocity as independently measured by a "rapid sand analyzer" laboratory settling tube. In addition, a systematic increase in the proportionality between sand concentration and backscatter was observed with increasing grain size.
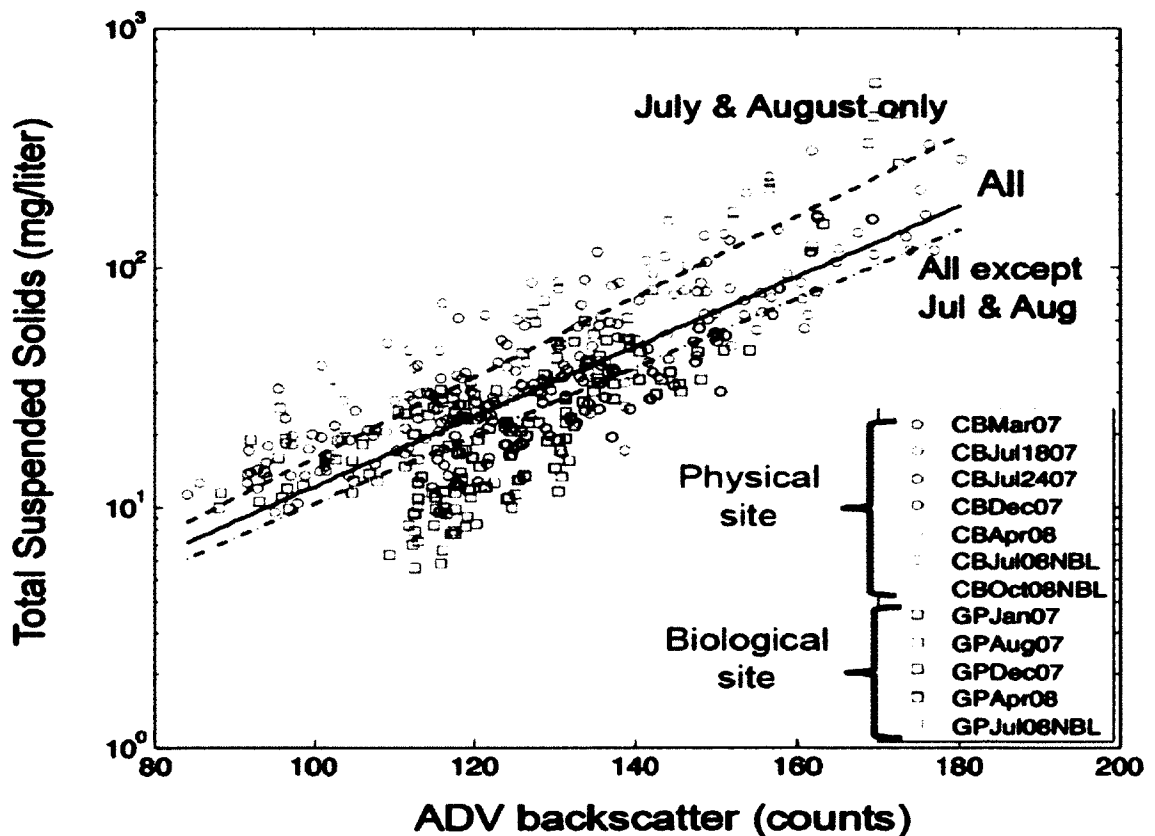
Figure 3.1. *In situ* pump samples from the York River estuary, Virginia, analyzed for total suspended solids. Concentrations are used to calibrate the acoustic backscatter from ADVs deployed on nearby benthic tripods. (Cartwright et al., 2009)
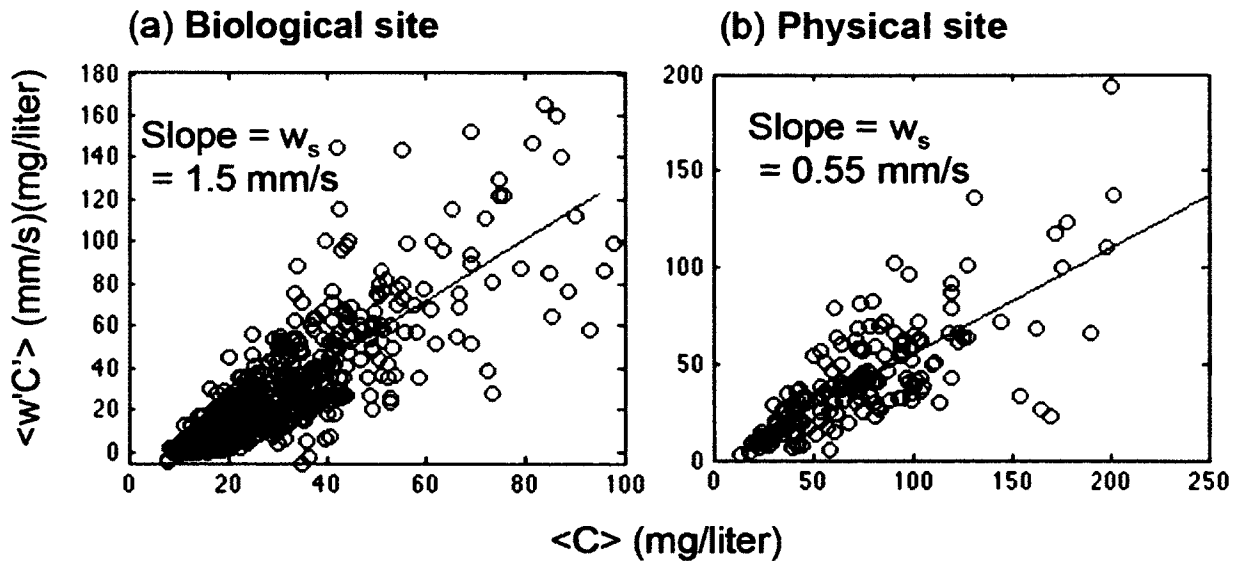
Figure 3.2. Example estimates of settling velocity (ws) from ADV data collected on benthic tripods deployed in the York River Estuary, Virginia. (Cartwright et al, 2009)

3.2. Introduction

Size distribution and settling velocities are features of suspended sediment particle populations that affect nearly every aspect of particle fate and transport, including physiochemical (re-suspension, deposition and flocculation) and biological (production, mineralization and repackaging) processes (Dyer and Manning, 1999; Hill et al., 2001; Van Leussen, 1999). Optical instruments are commonly used to determine *in situ* and bench top suspended size concentration and settling velocity, including such example instruments as the PICcamera, the LISST-ST, and the DIGIHOLOCAM (Smith and Friedrichs, 2011; Ahn, 2012; Davies, 2010). In estuarine and coastal waters, these instruments are generally limited to short-term field deployments due to their

susceptibility to bio-fouling. The Acoustic Doppler Velocimeter (ADV), however, is an instrument that is able to withstand the bio-fouling associated with field deployments lasting several months and has been found to provide reasonable estimates of *in situ* suspended sediment concentrations (C) and particle settling velocity (w_s) when calibrated with pumped suspended sediment concentrations collected at the study site (Fugate and Friedrichs, 2002; Voulgaris and Meyers, 2004). But *in situ* estimates of C and w_s such as those illustrated in Figures 3.1 and 3.2 tend to exhibit significant scatter, largely because of changing particle size and density, and the simultaneous presence of multiple particle types (Cartwright et al., 2009; Cartwright et al., 2011).

To ultimately facilitate better interpretation of *in situ* observations, this study used a laboratory sediment mixing tank to simultaneously measure sediment solids concentration, acoustic backscatter, and particle settling velocity under more highly controlled conditions than are possible in the field. We utilized an ADV along with various single grain-size sand suspensions as well as sand-mud mixtures over a range of concentrations. In the next sections of this paper we describe the VIMS acoustic calibration chamber and the ADV's properties, our approaches in measuring sediment concentration, size and settling velocity, and the results of our experiments. Our main findings include the well constrained proportionality between acoustic backscatter and mass concentration for a given particle type at moderate concentrations, the clear proportionality between acoustic backscatter and grain size for a particles of a given
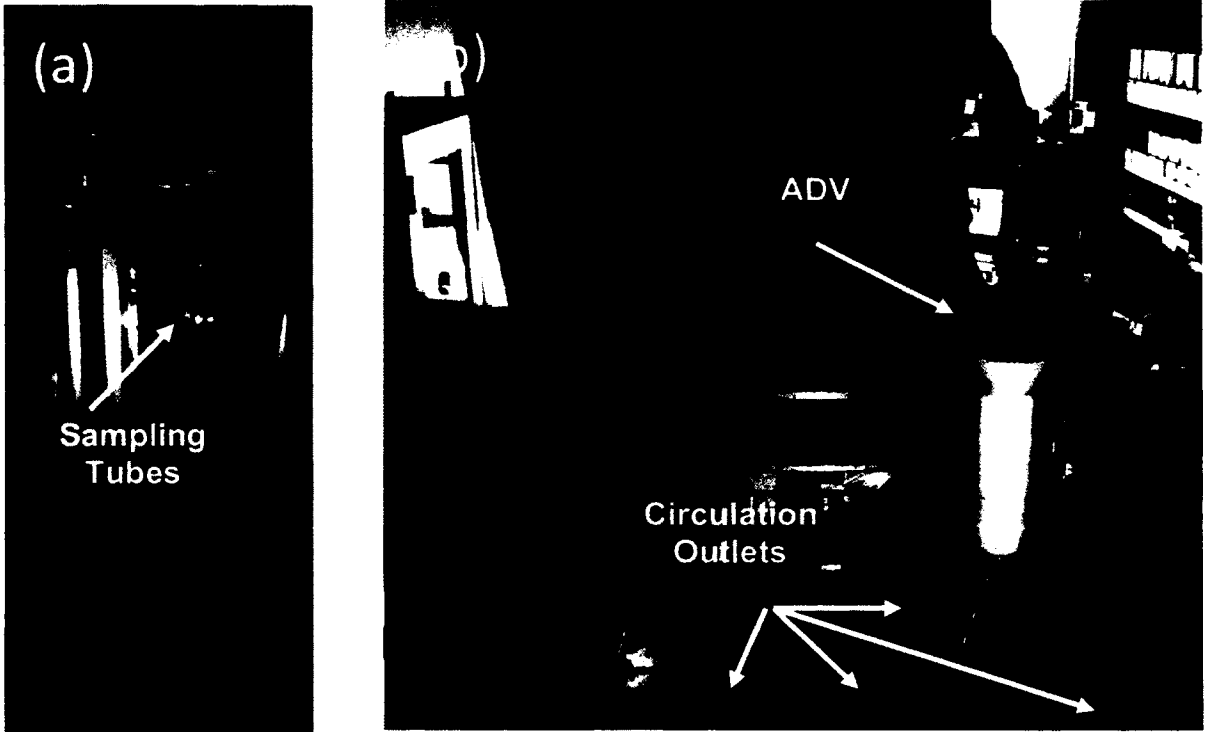
Figure 3.3. a) VIMS sediment mixing tank, with suspended sediment sampling tubes highlighted, b) example placement of ADV in chamber, with pump circulation outlets highlighted.

density, and the novel use of direct Doppler velocity measurements to measure sediment settling velocity within a multi-use sediment mixing tank.

3.3 Methods

Acoustic Calibration Chamber

The design of the VIMS sediment mixing tank that we utilized for acoustic calibration is based on similar chambers the lead author has used at NIWA in Hamilton, NZ, and at the University of East Anglia in Norwich, UK. The VIMS chamber, built by the

Physics Department machine shop at the College of William and Mary (Figure 3.3), has inside dimensions, which measure 31.6 cm square at the top and 1.5 meters tall down the center. The top meter of the chamber is square and the bottom 0.5 meter tapers to facilitate the collection of sediment to be pumped back to the surface. At the bottom of the taper is an insert which minimizes sediment trapping corners and helps return all of the sediment back into the pump inlet.

A Cal Pump MS900 marine pump powers the circulation of the water in the tank, which according to the manufacture's performance curve, pumps at a rate of 44.2 liters/minute with a head of approximately 2 meters. The pump is kept cool by placement in a water bath with tap water running through a submersed coiled copper tube. After passing through the pump, the chamber water is re-circulated through a four-way splitter to four jet outlets, one centered on each wall of the chamber 25 cm below the top. The water jets meet forcefully in the center of the chamber, level with the outlets. Once the jets converge, the dominant flow of the chamber is downward toward the pump inlet, but some of the sediment is carried above the level of the outlet tubes by a component of upward flow also produced at the jet convergence point.

The chamber has several sliding sampling tubes situated along one side that can be pushed in to the center of chamber to allow the collection of water samples. The flow rate out of one of the sampling 1.27 cm (I.D.) tubes has been measured to be on the

order of 1 m/s (1970 cm^3 in 16.4 sec). This is sufficient to capture a representative

portion of the suspended sediment given the chamber circulation rate (Battisto, 2000).

The water can later be analyzed for suspended solids concentrations to be paired with

ADV backscatter collected at that same location in the chamber.

Acoustic Doppler Velocimeter

The ADV used in this study is a SonTek ADVocean sensor (Figure 3.3b). The sensor is

mounted in a downward looking position on a plate that is clamped to a second plate

attached to the top of the calibration chamber. Each plate can be moved to change the

position of the ADV in relation to the top of the chamber. The ADV is a bi-static sonar,

which means it uses separate transmit and receive beams. The location of the ADV

sample volume is determined by the geometry of the three acoustic receivers around the

centrally located 5-MHz acoustic transmitter. These receivers, encased in stainless steel,

radiate out at 120° azimuth intervals and angle away from the transmitter. A ~2 cm^3

sample volume is created ~18 cm below the transmitter, corresponding to where beams

projected out from the receivers would intersect the transmit beam (SonTek, 1997). The

transmitter emits a short pulse, and the receivers listen to an echo that is range gated to

correspond to travel time from the sample volume to the receiver. At 10 Hz, the ADV

records the velocity of scatters in three directions (x, y and z), the amplitude of the

signal strength of the "echo" received by each of the receivers (beams 1, 2 and 3), and

the percent correlation between the transmit and receive signals for each beam. The units for

Figure 3.4. (a) sand captured on 63 micron sieve showing some impurities, (b) sand captured on 106 micron sieve with no visible impurities.

the amplitude of the return "echo" are in "counts", a unit proportional to decibels, i.e., a logarithmic scaling of the amplitude of the backscatter. The ADV also records water pressure and temperature, as well as compass direction, tilt, and roll of the sensor.

Sediment Sample Preparation

To isolate constant density, relatively simple-shaped particles of known sizes, a sample of clean quartz sand was sorted into 6 size classes from 4 phi (63μm) to 2.5 phi (150 μm) using 0.25 phi graduations. The size classes in this study are identified by the size of the sieve the sand was captured on. Sub-samples of the sand were placed on the 2.5 phi sieve and mechanically shaken through the 6 sieves with a Ro-tap for 30 minutes. The literature suggests that there was no significant difference in the distributions obtained from a Ro-Tap after shaking durations ranging from 10 to 30 minutes, but we

opted for the longer time since we were sieving more than 20 grams at a time (Sanford and Swift, 1971). The sand captured on each sieve from the different subsamples was then combined together by size class. Next, the sand from each size class was individually shaken through all the sieves a second time for an additional 45 minutes in an effort to make sure what was captured on each sieve was only sand from that sieve size to a quarter phi size larger. Figure 3.4 shows the sand collected on the 4.0 phi (63 μm) sieve and the 3.0 phi (106 μm) sieve. Most of the impurities (i.e., non-quartz particles) were concentrated on the two smallest sieve sizes.

Acoustic Response to Grain-size Experiments

A separate regression was determined for each of the sand size classes described in Section C. The ADV in Figure 3.3 is mounted for the experiments described below in Section E. For the grain-size experiments described in this Section, the ADV was lowered until the ADV sample volume was level with the sampling tube marked by an arrow in Figure 3a. For each grain-size experiment, a series of the aliquots of processed sand was added to the chamber to bring the expected concentration to approximately 25, 50, 75, 100, 150, 200, 250 mg/L, respectively. Although the chamber was designed to have as few places as possible for the sand to settle out of suspension, it was noticed that the exposed edges of the tubes designed to allow for sampling of the water actually became sediment traps, and there were also spots along the taper at the bottom of the chamber where the sediment "stuck" and wasn't re-circulated. (Later experiments have

shown that even though all the sand isn't kept in suspension, the center of the chamber stays homogeneous if it is allowed some time to reach equilibrium.) A 10-minute ADV backscatter burst, sampled at 10 Hz, was collected for each sand concentration. Before the addition of the next sand aliquot, the sample tube, inserted into location of the ADV sample volume, was flushed with water as the chamber continued to circulate. An approximately 2-liter water sample was collected from the appropriate sampling tube and analyzed for suspended solids concentration.

ADV Settling Velocity Measurements

Six separate settling velocity experiments were conducted, one for each size class of the sand described in Section C. The experiments were conducted in the winter when the water coming from the tap was only 12-14 °C. As the water warmed, air bubbles were released. Since bubbles are a strong reflector of acoustic sound, it was imperative to verify that the bubbles were completely dissipated, so the chamber was left to sit overnight with the pump running. The next day, a series of 10 minute ADV bursts were taken and analyzed until the backscatter and mean velocity in the vertical direction for that location stabilized. A decrease likely would be seen from the previous burst if a significant number of bubbles were still present. Tap water was used so that passive reflectors inherent to non-purified water were still available for the acoustic signal for the zero sand concentration conditions. Note that the backscatter from passive reflectors in tap water is strong enough to provide a reliable Doppler velocity measurement, but

weak enough that backscatter from added sand entirely overwhelms the passive reflector signal.

Once it was verified that any remaining bubbles were not going to interfere, for each ADV settling velocity experiment enough sand was added to the 118 liters of water in the chamber to bring the concentration to approximately 200 mg/L (except for the 75 micron size class -- there was only enough sand available for that size class to bring the concentration to 123 mg/L). The chamber was filled to the maximum capacity of 118L in order to bring the ADV sample volume above the circulation outlets (see Figure 3.3b). A grid (see * symbols in Figure 3.7) was created across the top of the chamber, with 6 locations (3 cm apart) along the x-axis and 6 locations (3 cm apart) along the y-axis, for a total of 36 positions. A 10-minute "burst" with a sampling rate of 10Hz was collected at each of these positions. The mean velocity in the z direction ($<w>$) and the standard deviation about the mean (w') was calculated for each burst.

Rapid Sand Analyzer Settling Velocity Measurements

The Rapid Sand Analyzer (RSA) is a 12-cm inside-diameter column filled with tap water (Figure 3.5). Sediment to be analyzed is placed on the drop pan. When the pan is released, a computer records a time series of the change in weight of sediment collected on the weight dish suspended by a wire a fixed distance below the balance mounted at

the top of the column. The known distance between the drop pan and the weight dish is divided by time to give the settling velocity for each time period of the time series. The
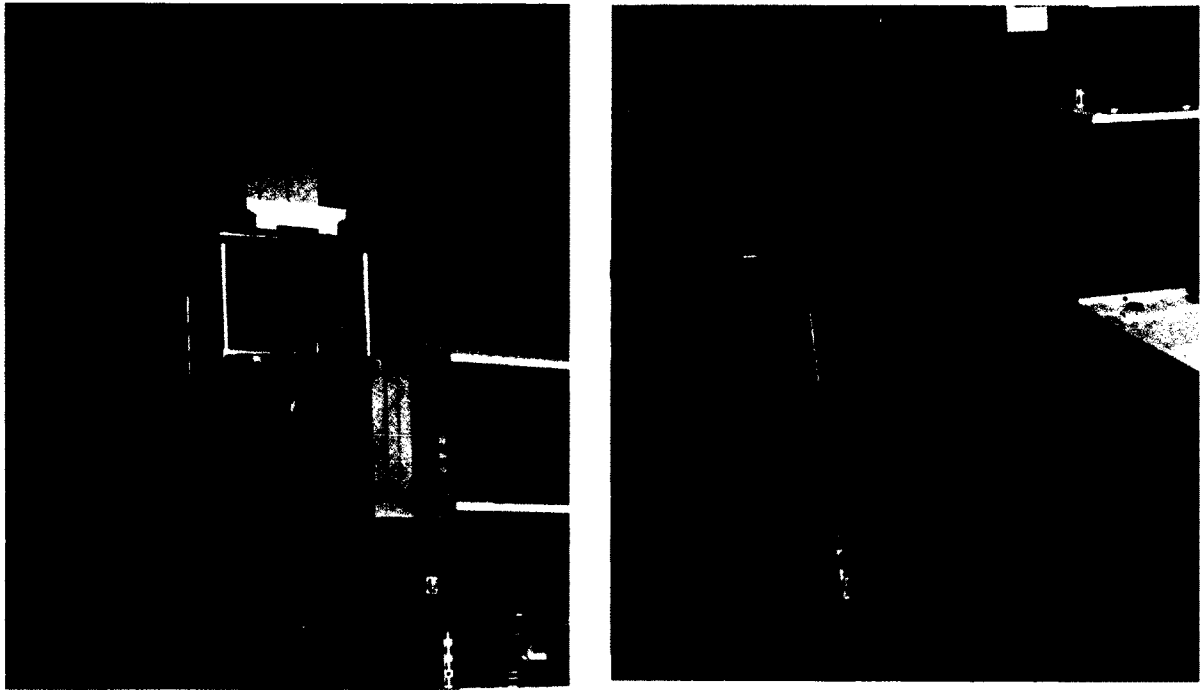
Figure 3.5. Rapid Sand Analyzer housed at the Army Corps of Engineers Field Research Facility (FRF) in Duck, NC

temperature of the water is recorded so that the density and viscosity of the water can be calculated. The settling velocity is then associated with a theoretical sediment grain size, assuming the sediment is composed of typical quartz sand particles with a constant density of 2.65 g/cm^3. The percentage of sand, by weight, is determined for each settling velocity, thus providing a grain- size distribution for the sample. Removing sediment with slow settling velocities (<63 μm) prior to analysis ensures that the column can clear in less than 10 minutes, reducing the amount of time between samples.
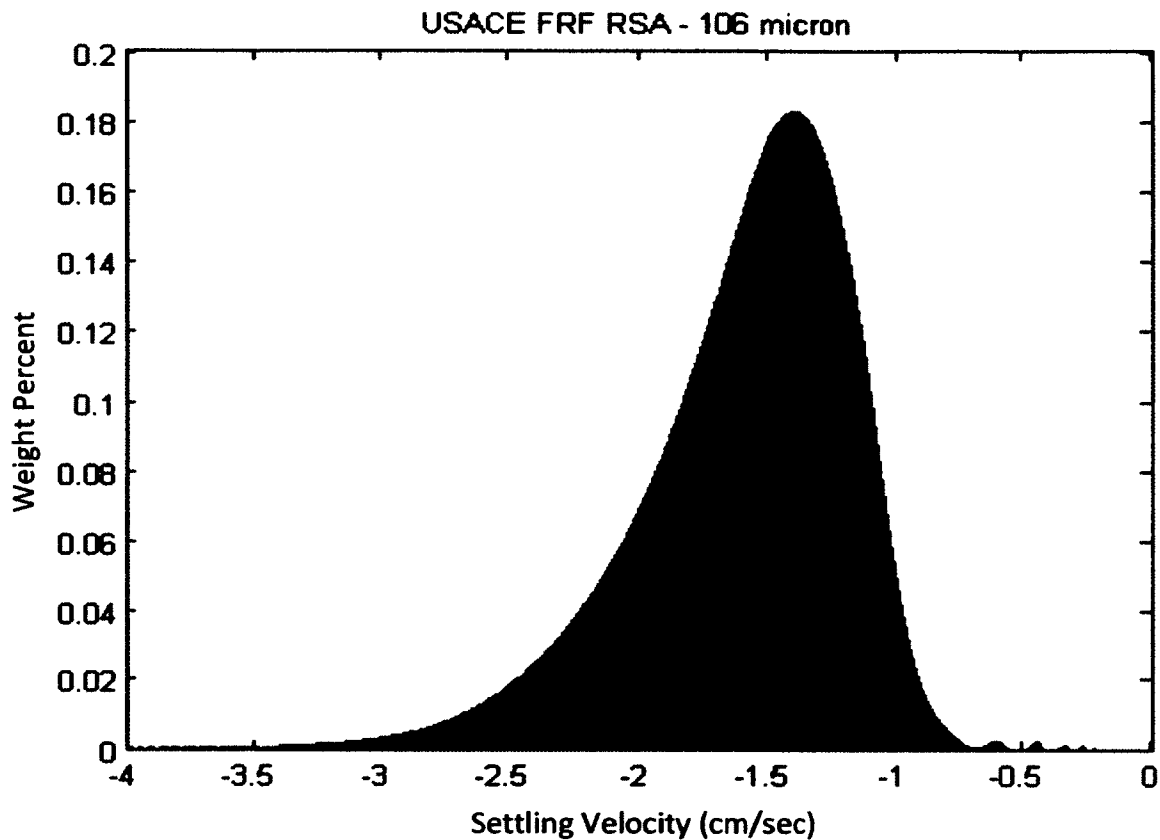
Figure 3.6. Rapid Sand Analyzer results for sand collected on the 106 μm sieve. For this size sieve, the RSA effective bulk settling velocity was calculated to be 1.31 ± 0.06 cm/sec. (mean and standard deviation calculated from sample replicates)

Each size class prepared as described in Section C was passed through the FRF RSA in duplicate or triplicate. For each sample, approximately 0.3 grams of sand was placed on the drop pan. Using less than 0.5 g sample permits grains to settle at distances in excess of two grain diameters from each other so they settle without the acceleration or deceleration due to grain interactions (Sanford and Swift, 1971). The balance was tared

software was started at the same time a button was pushed to mechanically release the drop pan to disperse the sand. This step introduces the greatest chance for error since both the start button and the disperse button have to be pushed at exactly the same time for the best possible fall velocity measurements. The timing software then records the weight of the sediment settling on the weight tray at a sampling rate of 10 Hz. The time-series distribution of settling velocities for a given RSA run is integrated to derive a single effective bulk settling velocity for that drop pan release.

3.4. Results

Settling Velocity Experiments

Figure 3.6 is an example of the settling velocity results measured for each of the sieve sizes using the FRF RSA. The effective bulk settling velocity was calculated for each replicate of each sieve sample. The mean and standard deviation about the mean of the replicates were then calculated and are listed in Table 3.1.

Figure 3.7a shows the flow pattern in the z-direction as interpolated from the grid of burst-averaged ADV velocity measurements collected 18 cm from the top of the chamber. The jets from the four circulation outlets (see outlets identified in Figure 3.3b) meet in the center of the chamber 25 cm from the top and cause an upward flow of up to 5 cm/sec. This upward flux returns to the lower section of the chamber along the edges
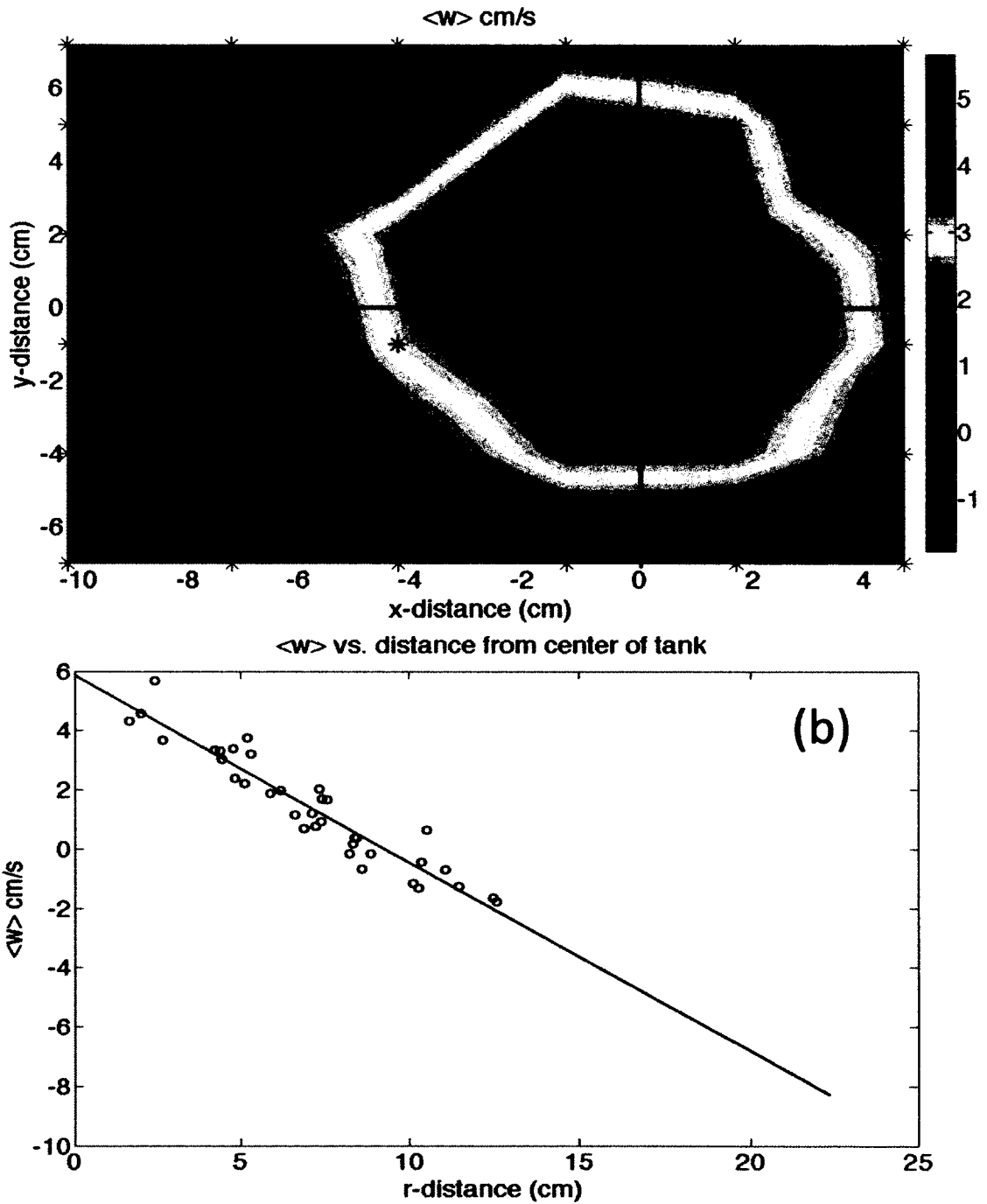
Figure 3.7. a) Mean vertical velocity recorded by the ADV <w>, within the sample grid measured 18 cm from the top of the chamber for the 125 mm sieve case. Each location in the sample grid is marked with an *. b) Regression of mean vertical ADV velocity versus distance from the center of the tank.
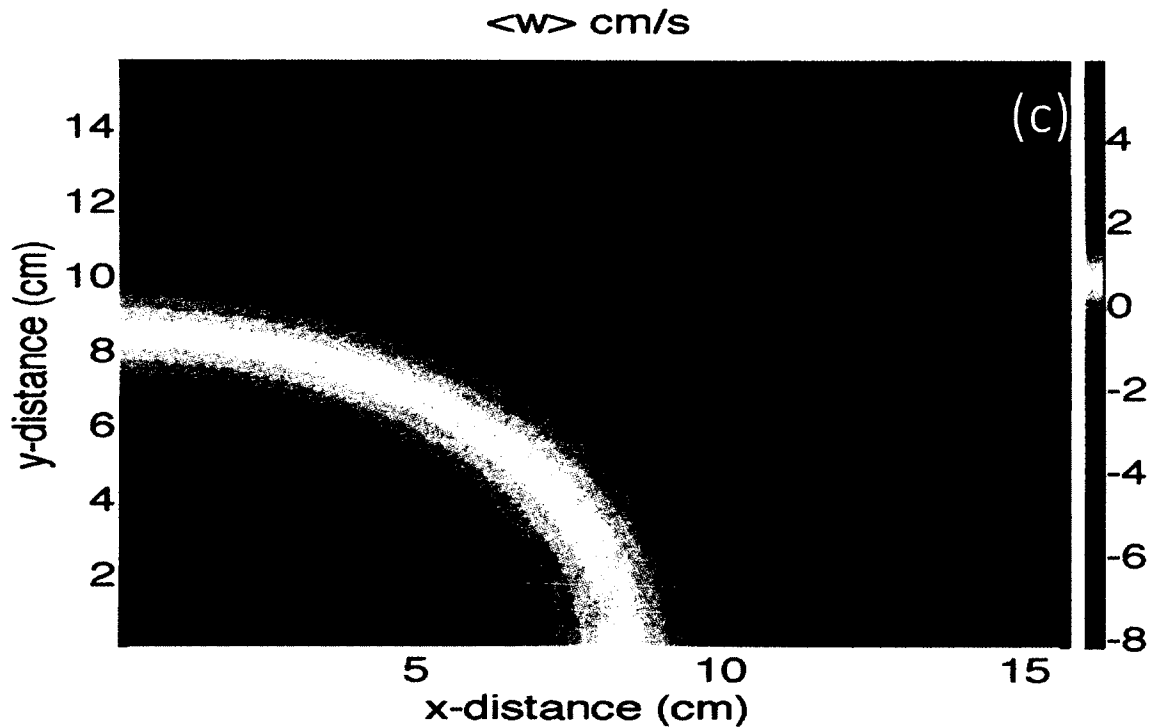
Figure 3.7. c) Circular fit of regression to allow for estimate of <w> for areas not directly measured for.

of the tank (as indicated by the negative numbers and blue color in Figure 3.7a). By collecting the grid of ADV measurements 5 cm above the jet outlets, we know that the horizontally integrated vertical volume flux of water through the total horizontal cross-section of the tank must be zero. Because of the geometry of the ADV, it was impossible to directly measure vertical velocities all the way to the far edges of the chamber. When the ADV burst-averaged z-velocities are plotted versus the distance of each grid point from the center of the tank, however, a clear linear relation is seen (Figure 3.7b). A linear regression fitted through the points was therefore used to estimate the ADV vertical velocities out to the far edges of the tank (Figure 3.7b). It

was then possible to horizontally integrate the inferred burst-averaged ADV vertical velocities over the entire horizontal tank cross-section.

Absent a net vertical volume flux of water, it follows that the average vertical velocity registered by an ADV across a horizontal plane is equal to the mean vertical velocity of the dominant scatterers relative to the water, i.e., the mean sediment settling velocity. This may seem counter-intuitive, since the horizontally-integrated net vertical flux of sediment at the height of the ADV grid must also be zero (since C is not increasing or decreasing). Nonetheless, the mean velocity of the sediment is still negative, because the Doppler calculation measures only the velocity of the scatters, not their mass flux. The downward flux of sediment associated with settling has a non-zero mean velocity defined as W_s. In contrast, the balancing upward flux of sediment associated with vertical circulation cells of water has, by definition, a zero mean water velocity. This concept is analogous to the balance between upward Reynolds flux of sediment and downward settling often seen in benthic boundary layers.

The grid of ADV measurements distributed in a horizontal plane across the tank revealed that the mean vertical velocity registered by the ADV for each sieve case was indeed consistent with each grain size's settling velocity as separately measured by the FRF RSA settling tube. Figure 8a displays these extrapolated and then horizontally-averaged ADV velocities, each calculated individually for a single sieve size, plotted
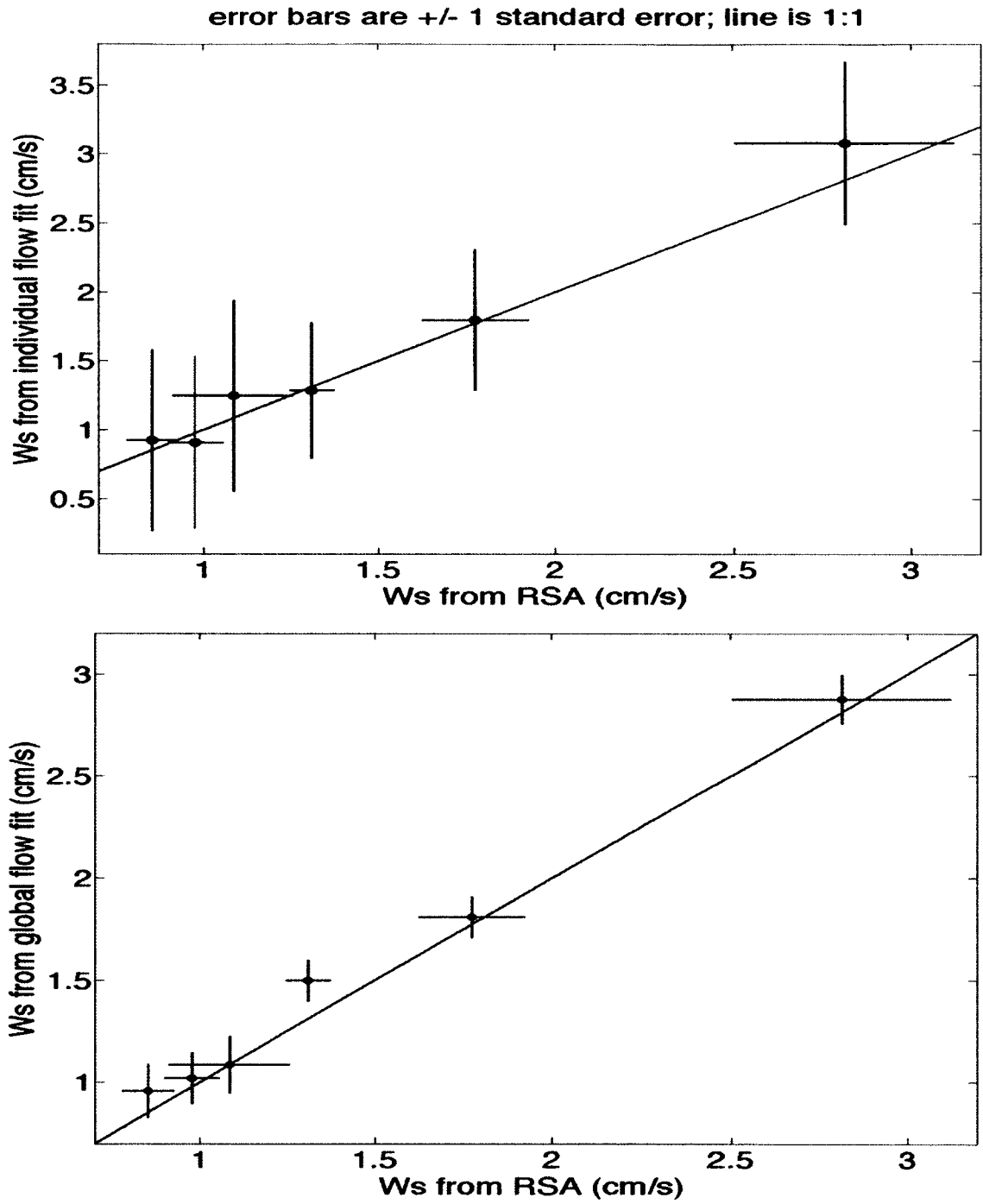
Figure 3.8. a) RSA Ws and Individual Flow Fit Ws comparison b) RSA Ws and Global Flow Fit Ws comparison

against Ws as measured by the RSA. The green line is the 1:1 ratio line. Each circle represents the mean settling velocity by both methods for one of the 6 grain-sizes tested and the lines are the standard deviations about that mean. Table 3.1 lists these mean ADV-inferred settling velocities and standard errors for these "individual flow fit" cases.

In theory, the slope of the regression in Figure 3.7b should be identical for each settling velocity case, since the settling velocity only contributes to the vertical offset of the curve. The circulation pattern of the water itself controls the slope. Thus the scatter in Figure 3.8a can be reduced by using all of the observations to calculate a single best-fit slope for use in every ADV spatial velocity extrapolation. Doing so yields slightly different ADV means and reduced standard error bars as displayed in Figure 9b and Table 3.1 for the "global flow fit" case.

Table 3.1

Effective Settling Velocity

| Sieve Size | | FRF RSA | | Individual Flow Fit | | Global Flow fit | | Ws-circular Regression | |
PHI	Micron	Mean cm/s	Std Dev cm/s	Mean (cm/s)	Std dev (cm/s)	Mean (cm/s)	Std dev (cm/s)	(m)	(b)
4.00	63	0.85	0.07	0.93	0.66	0.96	0.13	-0.63	6.68
3.75	75	0.98	0.08	0.91	0.63	1.02	0.13	-0.61	6.52
3.50	90	1.08	0.17	1.25	0.70	1.09	0.14	-0.67	6.83
3.25	106	1.31	0.06	1.29	0.49	1.50	0.10	-0.59	5.89
3.00	125	1.77	0.15	1.80	0.51	1.81	0.10	-0.63	5.86
2.75	150	2.81	0.31	3.08	0.59	2.88	0.12	-0.68	5.10
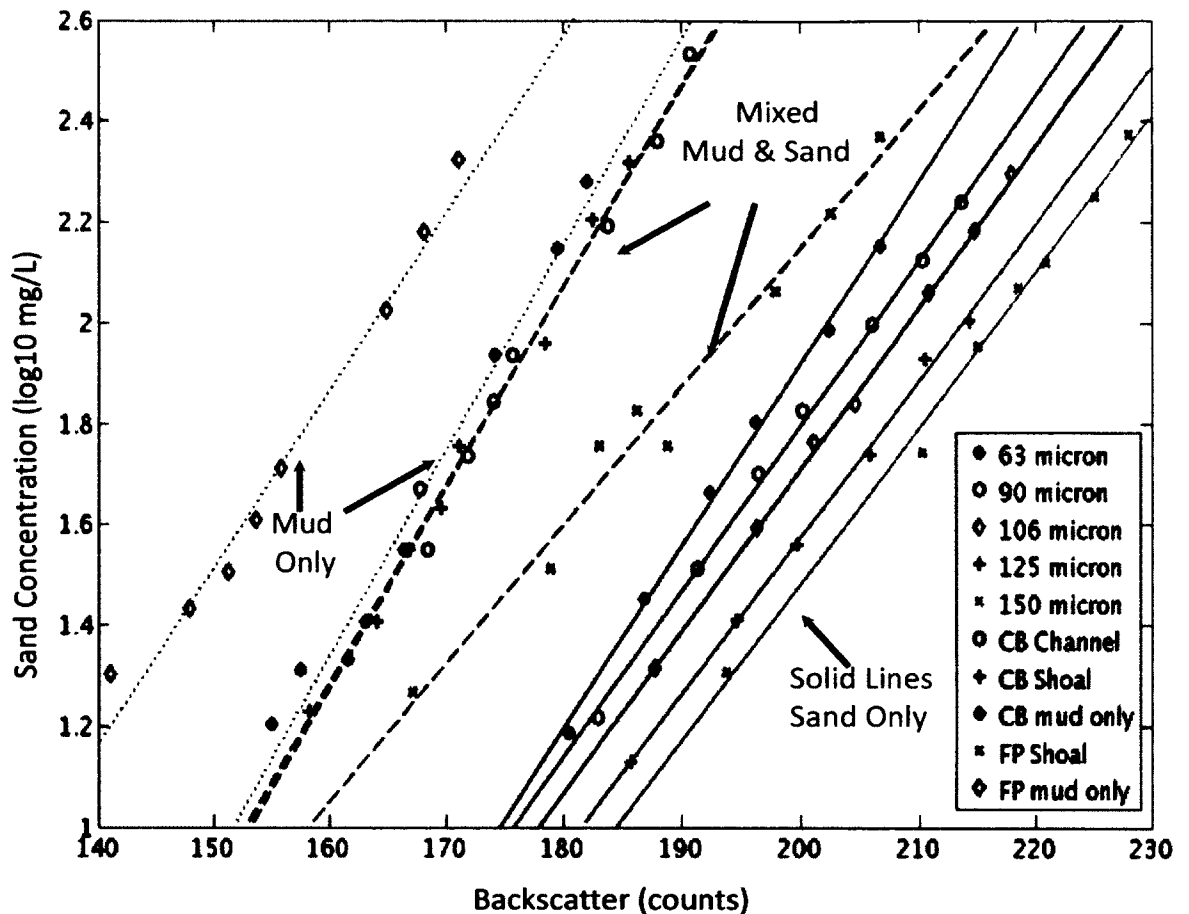
Figure 3.9. The solid lines are the regression curve of the acoustic backscatter and the log10 concentrations for each sand size distribution. The dashed lines are the mixed mud and sand regressions curves, and the dotted lines are the mud only regression curves from Newbill, 2010.

Acoustic Response to Grain-size Experiments

ADV backscatter in counts was plotted against the log10 of the measured suspended sediment concentration for each of the acoustic response to grain-size experiments (Solid lines in Figure 3.9). The relationship was linear up to the highest concentration measured for all sand distributions (nominally 250 mg/L). A systematic increase in the

proportionality between sand concentration and backscatter was observed with increasing grain size.

Also included in Figure 3.9 are regression curves from previous experiments) using natural bottom sediment collected from the bed of the York River estuary at sites known as Clay Bank (CB) Channel, CB Shoal, and Ferry Pier (FP) (Newbill, 2010). The CB Channel sample was 80% mud and 20% sand, the CB Shoal sample was 99% mud and 1% sand, and the FP sample was 90% mud and 10% sand. The grain-size of the dis-aggregated mud measured by pipet analysis was <5 μm and the sand D50 grain-sizes for the CB and FP sites were 106 μm and 125 μm, respectively (Newbill, 2010). The dashed lines in Figure 3.9 represent the naturally mixed sediment regressions and the dotted lines are regression curves from mud only samples from the Clay Bank and Ferry Point Shoals.

3.5 Discussion

Settling Velocity Experiments

In Figure 3.7 it can be seen that the area where the settling velocity of the sediment was estimated in the tank was not a simple flow field. The discharge from the circulation pump was divided into four outlet jets that met in the middle of the chamber. Above the level of the outlets this caused an upward flow of water in the center of the chamber and

a downward flow along the far edges of the tank. Because of the size and shape of the ADV, it was impossible to measure velocity close to the edges of the calibration chamber. Therefore a regression of the velocity in the w direction vs. distance from the center of the tank was used to estimate what the flow would be in the areas where it could not be measured. When the flow was integrated over the whole area, the circulatory flow of the water cancelled out, and the spatially-averaged apparent residual velocity measured by the ADV was consistent with the sand settling velocity as measured independently using a Rapid Sand Analyzer for all six size classes measured.

Acoustic Response to Grain-size

For the second portion of the experiment, a systematic increase in the proportionality between sediment concentration and backscatter amplitude was observed with increasing grain size. In Figure 3.9, using a 5 MHz ADV, a decrease in acoustic backscatter response was seen as the grain size of the sand decreased. Theoretically this behavior is expected in the range of particle sizes where scattering and particle-particle interactions dominate attenuation (Jackson and Richarson, 2007; Topping et al., 2007). The acoustic backscattered amplitude in the mud was much lower than the sand as is expected for these particle sizes (<63 micron) and these frequencies used, where the backscattering is low and the absorption tends to dominate the attenuation.

Interestingly, when the mud and sand were mixed, the backscattering was intermediate between the mud and sand, rather than reaching a level that was the sum of the two backscattering amplitudes. This may be explained by the interrelationship between the acoustic backscattering, attenuation, and the particle size-frequency range.
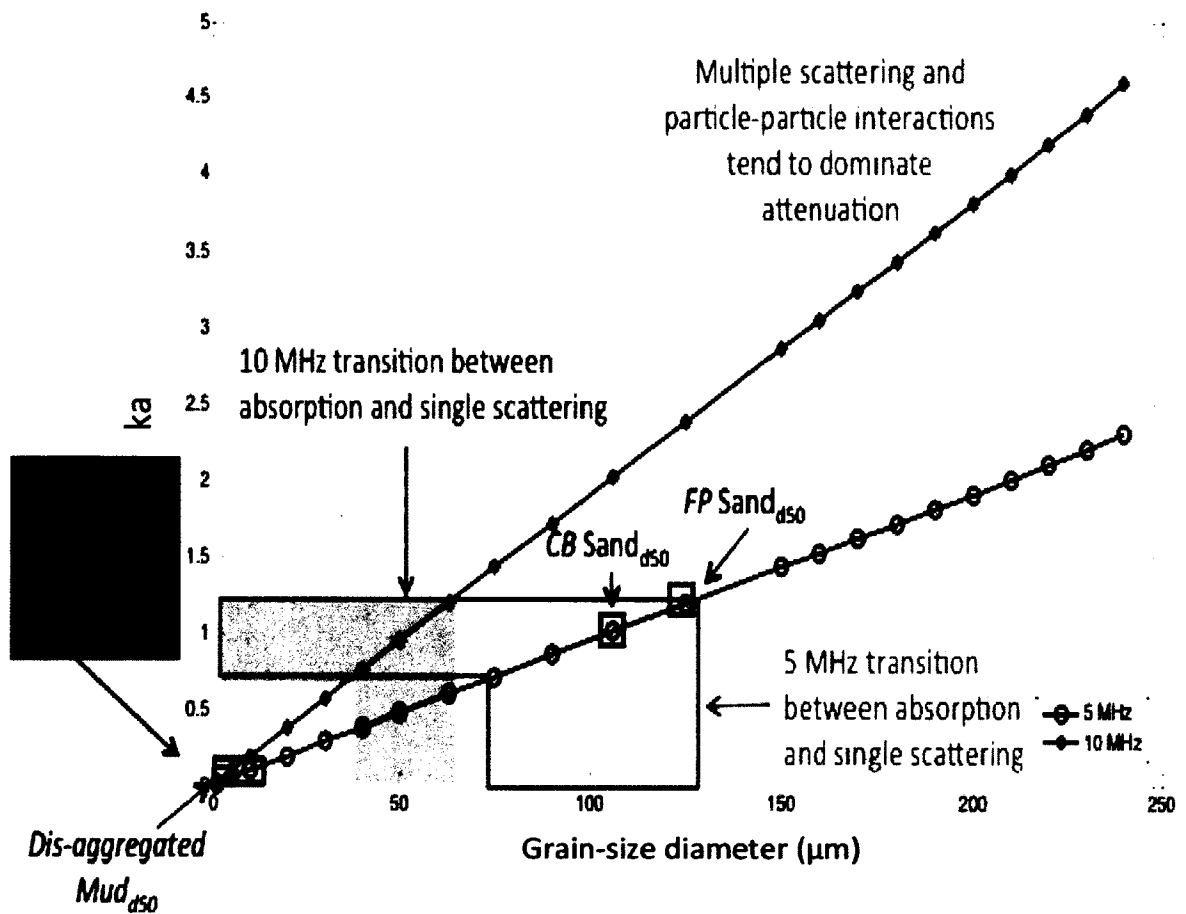
Figure 3.10. Schematic relationship between grain-size and attenuation contributions, highlighting the role of frequency. The black squares show where the Clay Bank and Ferry Pier dis-aggregated component sand and mud grain-sizes fall along the 5 MHz frequency regression line.

What was not expected was the nearly identical response of the natural samples from the Clay Bank channel and shoal containing 1% and 20% sand, respectively. Figure 10 shows a schematic relationship between grain-size and attenuation contributions, highlighting the role of the acoustic frequency. Acoustic attenuation is a measure of the energy loss of sound propagation in media. Acoustic absorption is that property of any material that changes the acoustic energy of sound waves into another form, often heat, which it to some extent retains, as opposed to that sound energy that material reflects or scatters. The acoustic wavelength (l) is related to the frequency by

$$\lambda = v\frac{1}{f} \tag{3.3}$$

where v is the speed of sound (0.165 cm/µs) and f is the frequency of the ADV (5 or 10 MHz). ka is calculated as

$$ka = \frac{2\pi}{\lambda}a \tag{3.4}$$

where a is the radius of the grain particle, and k is the acoustic wavenumber.

Figure 3.10 displays the diameter of the grain-size plotted against ka for two frequencies. The red line represents the SonTek ADV used in this paper's experiments at 5 MHz frequency, and the blue line is a frequency of 10 MHz (the frequency of the Nortek ADV to be added in future work). When $ka \gg 1$, multiple scattering and particle-particle interactions tend to dominate attenuation. When $ka \ll 1$ absorption

tends to dominate attenuation. When $ka \approx 1$ there is a transition between these two end-members. The Clay Bank sand for both the channel and shoal has a D50 grain-size of 106 µm that falls right in the center of the transition zone for 5 MHz. It is possible that the acoustic response to the sand in the mud sample for Clay Bank samples was more absorption dominated rather than scattering dominated. This may explain why the same concentrations of both samples gave similar acoustic responses even though the channel contained almost 20% more sand than the shoal.

3.6 Future Work

Future work will further explore these interrelationships by systematically studying the frequency response of the backscattering and attenuation independently. This will include exploration of the response of acoustic backscatter and attenuation of various mud/sand mixtures as a function of frequency and concentration using SonTek and Nortek ADVs (5 and 6 MHz, respectively) as well as UTEX Scientific Instruments INSPECTIONWARE program with a series of acoustic transducers from 0.5 to 10 MHz

.

3.7 Acknowledgments

3.8 References

Ahn, J.H. , 2012. Size distribution and settling velocities of suspended particles in a tidal embayment, *Water Research*, vol 46, pp.3219-3228.

Battisto, G.M. , 2000. Field measurement of mixed grain size suspension in the near-shore under waves, MS Thesis, School of Marine Science, College of William and Mary, Gloucester Point, VA, 87 p.

Cartwright, G.M., C.T. Friedrichs, P.J. Dickhudt, T. Gass, and F.H. Farmer, 2009. Using the acoustic Doppler velocimeter (ADV) in the MUDBED real-time observing system. Proceedings, OCEANS 2009, Institute of Electrical and Electronics Engineers, ISBN 978-1-4244-4960-6, p. 1428-1436.

Cartwright, G.M., C.T. Friedrichs, and L.P. Sanford, 2011. *In situ* characterization of estuarine suspended sediment in the presence of muddy flocs and pellets. In: P. Wang, J.D. Rosati, and T.M. Roberts (eds.), Coastal Sediments 2011, World Scientific, ISBN 978-981-4355-52-0, p. 642-655.

Davies, E., 2010. Dynamics of Suspended Particulate Matter in the Lower Tamar Estuary, *The Plymouth Student Scientist*, vol 3, pp. 63-108.

Dyer, K.R. and Manning, A.J. , 1999. Observation of the size, settling velocity and effective density of flocs, and their fractal dimensions, *Journal of Sea Research*, vol 41, pp.87-95.

Fugate, D.C. and Friedrichs, C.T., 2002. Determining concentration and fall velocity of estuarine particle populations using ADV, OBS and LISST, *Continental Shelf Res.*, vol. 22, pp. 1867-1886.

Hill, P.S, Voulgaris, G., and Trowbridge, J.H. , 2001. Controls on floc size in a continental shelf bottom boundary layer, *Journal of Geophysical Research*, vol 106, pp.9543-9549.

Jackson, D.R. and Richardson, M.D. , 2007. High-Frequency Seafloor Acoustics, Springer ISBN 978-0-387-34154-5, 616 p.

Newbill, D.D., 2010. How Accurate is Your ADV? An Investigative Analysis on the Effect of Grain Size on Acoustic Doppler Velocimeter Backscatter, William and Mary Senior Thesis, 24 p, 2010.

Sanford, R.B. and Swift, D.J.P., 1971. Comparison of sieving and settling techniques for size analysis, using a benthos rapid sediment analyzer, *Sedimentology*, vol 17, pp.257-264.

Smith, S.J., and Friedrichs, C.T., 2011. Size and settling velocities of cohesive flocs and suspended sediment aggregates in a trailing suction hopper dredge plume, *Continental Shelf Research*, vol 31, pp 500-553.

SonTek, 1997. ADV Operation Manual – Firmware Version 4.0, SonTek, San Diego, CA.

Topping, D.J., Wright, S.A., Melis, T.A., and Rubin, D.M., 2007. High-Resolution Monitoring of Suspended-sediment Concentration and Grain Size in the Colorado River Using Laser Diffraction Instruments and a Three-Frequency Acoustic System, USGS report, 8 p.

Van Leussen, W., 1999. The variability of settling velocities of suspended fine-grained sediment in the Ems estuary, *Journal of Sea Research*, vol 41, pp.109-111.

Voulgaris, G. and Meyers, S.T., 2004. Temporal Variability of Hydrodynamics, Sediment Concentration and Sediment Settling Velocity in a Tidal Creek, *Continental Shelf Research*, vol 24, pp 1659-1693.

CHAPTER 4

Comparison of SonTek ADVOcean-Hydras and Nortek ADV Vectors for measuring suspended sediment concentration via acoustic backscatter

By Grace M. Cartwright and Carl T. Friedrichs

.

4.1 Abstract

This study compared acoustic backscatter (ABS) response to sand, mud, and mixed sediment in the lab and *in situ* among ten relatively similar acoustic Doppler velocimeter (ADV) units: five 6-MHz Nortek Vector ADVs and five 5-MHz SonTek ADVOcean-Hydras. This approach allowed for an examination of the relative roles played by inter-vendor, intra-vendor, and sediment variability in determining their ABS response. As well as consistently responding more strongly to sand than to mud, ABS in counts (a logarithmic unit proportional to decibels) revealed clear offsets apparent among the various instruments within both vendors. One of the ADVs from each vendor was defined as a reference unit, and the offsets in counts of the other four ADVs from each vendor were adjusted to become consistent with the reference unit. For either vendor, pre-correction ABS response was more similar if the vendor's units had been purchased together with consecutive manufacturer's serial numbers and subsequently had not had electronic components replaced. After adjustment, ABS counts for all the SonTek vs. Nortek ADVs largely lay along a single curve. The SonTek vs. Nortek ABS curve began with a slope of ~1:1 at low backscatter; but at higher ABS, the response of the 5-MHz SonTek ADVs increased more rapidly than that of the 6-MHz Norteks, suggesting that the backscatter registered by the higher frequency Nortek units were more susceptible to attenuation. Plots of the $\log_{10}$ of sand concentration ($\log_{10} C$) vs. ABS for concentrations from ~ 10 to 600 mg/L was significantly quadratic for both the Nortek and SonTek ADV although more strongly so for the Nortek. In contrast, mud calibrations of $\log_{10} C$ vs. ABS (for ~20 to 700 mg/L) were not quadratic for either vendor, providing less clear evidence of ABS attenuation. For well-mixed silty mud in the lab, the slope of the calibration of $\log_{10} C$ vs. ABS for both vendors was close to the theoretical value expected for a single, constant grain-size suspension. In the field, however, the calibration slope of $\log_{10} C$ vs. ABS was significantly smaller, which suggested a change in the acoustic properties of the suspended particles with increasing C. When calculating predicted ABS in counts in response to varying proportions of different grain sizes, results showed that transforming logarithmic counts back to linear units of acoustic power before adding them added together allowed successful prediction of the expected acoustic response.

4.2 Introduction

Sediment transport is an important process that greatly affects the geomorphology of coastal environments such as estuaries (Dalrymple et al., 1992). Yet sediment movement has implications beyond physical changes. Because particles can be a source of both nutrients and toxic material like pollutants, suspended sediment transport can redistribute these, thus exerting major control on estuarine water quality (Friedrichs et al., 2008; MacDonald et al., 2012). In limiting light transmission, suspended sediment can also influence photosynthesis, and sediment deposition can interfere with shipping channels navigation (Gartner, 2004). In tidally energetic estuaries, the suspended sediment field constantly changes; over hourly, the spring-neap cycle, and seasonal timescales. Aggregate sizes, suspended sediment concentration and settling velocities can often shift on multiple time scales, making it difficult to study the condition of these highly variable systems (Fugate and Friedrichs, 2003; Gartne, 2004; Vousdoukas et al., 2011). A crucial part of sediment transport that needs to be better understood and measured is the concentration of suspended solids.

Although originally designed to measure velocities, the acoustic Doppler velocimeter (ADV) is now widely used to determine suspended sediment concentration in coastal and estuarine systems (Fugate and Friedrichs, 2002; Voulgaris and Meyers, 2004; Cartwright et al., 2012; Baeye et al., 2012). Advantages of ADVs include non-intrusive

measurements, resistance to biofouling and high energy conditions, relative simplicity of operation, and simultaneous measurement of velocity and turbulence, as well as acoustic backscatter. Specifically, ADV receiver components measure the power of the acoustic echo off of suspended particles. An estimate of suspended sediment concentration can then made by applying an empirical relationship to the measured acoustic backscatter recorded by the ADV in "counts". Empirical relationships between acoustic backscatter intensity and suspended sediment concentration in general have often been derived via by laboratory calibrations (Rehman and Vincent, 1990, Thorne et al., 1993, Voulgaris and Meyers, 2004, Cartwright et al., 2009, MacDonald et al., 2012, Moate and Thorne, 2012).

Backscatter in counts registered by both SonTek and Nortek ADVs is defined such that one count equals 0.43 dB (with a variation of about 0.40 to 0.47) (Lohrmann, 2001; SonTek, 2001). For acoustic backscatter sensors in general, decibels are defined by 1 dB = 10 $\log_{10}(P/P_0)$, where P is the power of the backscatter registered at the receiver relative to an instrument-specific reference power, P_0 (e.g., Hodges). That is why ADV backscatter in counts is typically found to be proportional to the logarithm of sediment concentration, rather than being linearly proportional. For a given particle type with a single grain size, if concentration, C, increases from time 1 to time 2 by a factor of two (i.e., $C_2/C_1 = 2$), then, in the absence of attenuation, the power of the return signal, P, will also increase by a factor of two (i.e., $P_2/P_1 = 2$), meaning the volume scattering

strength will increase by $10*\log_{10}(P_2/P_1) \approx 3$ dB (e.g., Lohrmann, 2001; Hodges, 2010). The ADV acoustic backscatter in counts is then expected to increase by $(3$ dB$)/(0.43) \approx$ 7 counts, varying linearly with the $\log_{10}$ of C. In the field, however, ADV backscatter does not increase by precisely 7 counts for every factor of two in $\log_{10}$ concentration. This is because particles in suspension in estuarine and coastal environments are a mixture of sizes and types who proportions and properties may change as the total concentration changes. Also, the dB to counts conversion factor of ~0.43 may vary somewhat from for different ADVs due in part to the efficiency of the transducer to convert electrical voltage to an acoustical wave. In addition, if concentrations become high enough, at some point attenuation will begin to decrease the backscatter (e.g., Traykovski et al., 2000). At that point, the rate of increase in backscatter with increased concentration will slow and eventually reverse, such that backscatter will then decrease with greater concentration.

Most of the previous work on the acoustic response of suspended sediment has been performed on well-sorted, narrow distribution grain-sizes, mostly of coarse-grain non-cohesive material (Hanes et al. 1988, Vincent, 2007, VanderWerf et al., 2007, Green et al., 2004). Recently, acoustic backscatter, including backscatter from ADVs, has increasingly been used to measure concentrations in muddy rivers and in mixed sediment regimes (Gray and Gartner, 2009; Cartwright et al., 2009; Hanes, 2011). Even in strictly non-cohesive regimes, the presence of multiple grain sizes add additional
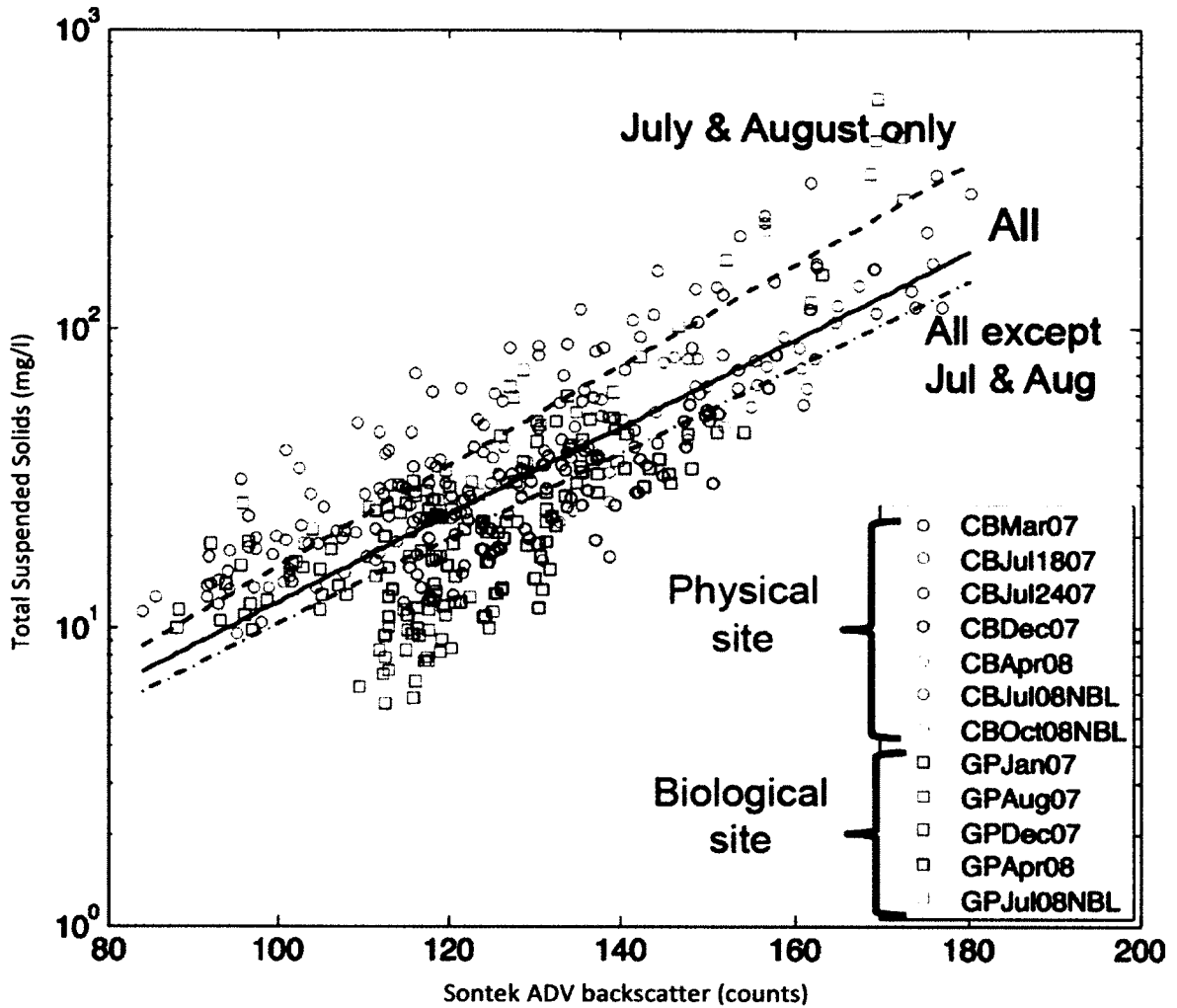
Figure 4.1 . *In situ* calibration of backscatter from VIMS SonTek ADVOcean-Hydras for total suspended solids based on filtered pump samples collected at MUDBED observation system sites in the York River estuary (from Cartwright et al., 2009).

complexities because each acoustic frequency is most sensitive to specific particle sizes that, in turn, is related to the size of the particles relative to the acoustic wavelength (e.g., Flammer, 1962; Thorne and Campbell, 1992; Lohrmann, 2001; Thorne and Hanes, 2002; Gartner, 2004; Topping et al., 2006). Muddy aggregates and flocs add further complications because they do not acoustically behave like the solid mineral

grains for which existing theory has been developed. As stated recently by Thorne and Hay (2012), "The use of acoustics for estimating sediment concentrationin flocculating (cohesive) suspensions is still problematic and requires fundamental studies on the interaction of sound with aggregated fine-grained particles, before quantitative inversions can be formulated".

The MUDBED observing site in the York River estuary, USA, represents the world's longest, nearly continual deployment of ADVs for the purpose of documenting sediment concentration in a muddy, mixed grain-size environment (Friedrichs et al., 2008). Maintaining this long-term observing system has necessitated rotation of several SonTek ADVOceans sensors in the field over time (Cartwright et al., 2009). Field calibrations of these multiple ADVs has documented substantial scatter in the relationship between mass concentration and ADV backscatter among various cruises (Figure 4.1). In order to improve observations of the sediment dynamics in mixed sediment environments like the York, it would be beneficial to determine what part of the scatter in Figure 4.1 is due to changing sediment properties and what part is due to variability in the responses of the various SonTek ADVs themselves. Furthermore, the MUDBED observing system has recently acquired several additional ADVs from a second vendor, namely Nortek ADV Vectors at 6 MHz, to add to its long-term observing system. Addition of this second set of ADVs, with a slightly higher frequency

121

Table 4.1. Summary of ADVs used in various comparisons along with their serial numbers, acquisition/repair year and acoustic backscatter offset shift (see text for additional explanation).

ADV serial number		NORTEK					SONTEK				
		VCH 4844	VEH 4493	VCH 4854	VCH 4856	VCH 4921	B336	B337	B338	B339	B3084
VIMS acquisition year		2005	2006	2011	2011	2011	2006	2006	2006	2006	2006
repair year			2011				2011				
Run 1: Inter-/intra-vendor,paint/no-paint	21 Jun '12	X	X	X	X		X	X		X	X
Run 2: Inter-/intra-vendor, no-paint	18 Jul '12		X	X		X			X	X	X
Run 3: Method Reproducabilty	22 Jun '12			X							X
Run 4: Mud (silty-clay) calibration	24 Jan '13					X	X				
Run 5: Sand calibration	11 Jul '12, 20 Jul'12			X			X				
Run 6: Mixed (sandy mud) calibration	28 Jan '13, 1 Feb '13					X	X				
In-situ calibration Muddy flocs	24 Jul '12			X							X
Offset in counts needed to match reference ADV		-3.97	3.38	0	-0.82	4.96	-32.75	-1.21	-6.8	0	-9.14

122

and a different electronic package, argues for a systematic comparison of the acoustic backscatter response of the sensors from these two vendors.

The following sections of this chapter first describe the SonTek ADVOcean-Hydra and Nortek Vector ADV models in more detail, along with the specific ADV arrangement and settings applied in this study. Sediment preparation and pump sampling for the mixing tank and field experiments are explained next, together with the procedures for collecting ABS data during the various experimental runs. In the results and discussion section, general trends in ABS response are discussed in terms of the relative roles played by inter-vendor, intra-vendor and sediment variability. Inter- and intra vendor response of ABS to a single concentration of mud is used to test the effects of anti-fouling paint, test method repeatability, and, most importantly, to assign offset corrections to make all the ABS readings more consistent with either a SonTek or a Nortek reference unit. ABS comparisons incorporating adjusted offsets are then used to explore consistencies between the SonTek and Nortek models (such as their similar ABS response to changes in grain size) and differences between the two models (such as their varying sensitivity to attenuation of backscatter). Finally, ADV response to mixed sediments is discussed in the context of how to sum ABS responses due to sand plus mud.
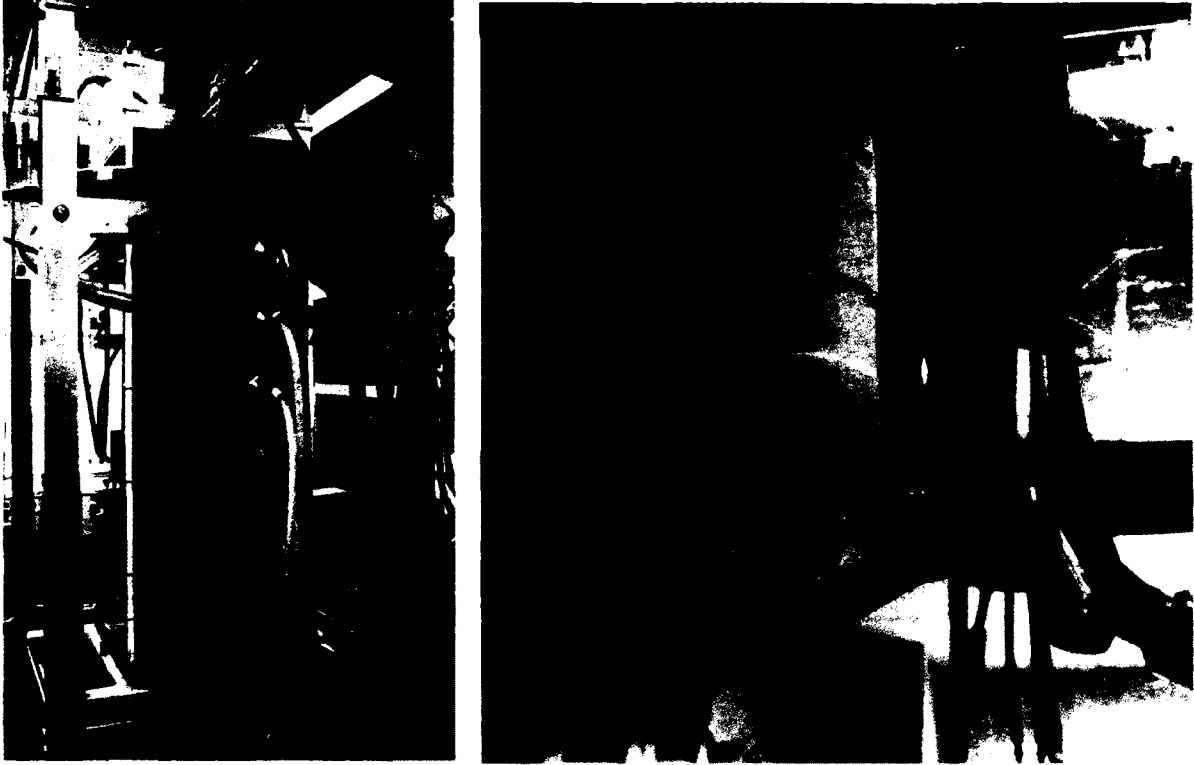
Figure 4.2. A) 110-liter mixing tank containing ~700 mg/L silty-clay solution used for mud calibration (Table 4.1, Run 4). The height of the ADV sampling volume and associated sample tube are marked by green tape. B) SonTek ADVOcean-Hydra (with wide white stem) and Nortek Vector ADV (with narrow black stem) set up for sand calibration (Table 4.1, Run 5). Also in the tank are a cluster of five other acoustic transducers, results from which are not discussed here.

4.3 Methods

4.3.1. ADV Sensors and Settings

The response of acoustic backscatter (ABS) from multiple ADVs to suspended

sediment was investigated via series of laboratory mixing tank experiments carried out

at VIMS between June 2012 and January 2013, along with an *in situ* ADV calibration

cruise in the York River estuary in July 2012. A total of ten ADVs from two vendors

were inter-compared, namely five Nortek 6-MHz ADV Vector units and five SonTek 5-

MHz ADVOcean-Hydra units (Table 4.1). The Norteks were acquired by VIMS in

2005, 2006 and 2012, and only two were from a common production run. In contrast,

all five SonTeks were acquired by VIMS in 2006, and four were from a single

production run. Over the years, the electronics of one of the Norteks and one of the

SonTeks were replaced by the manufacturer, which may have altered their individual

ABS response somewhat.

In terms of other ADV properties that affect ABS response, the sampling volumes for

the Nortek Vector and the SonTek ADVOcean-Hydra units were fixed by their

manufacturers to be 15 cm and 18 cm below their central transmitters, respectively. The

size of the sampling volume for all the measurements in this study was kept at each

manufacturer's default value of approximately 2 cm^3. Additional settings which do not

affect the systems' ABS response were set in this study as follows: All of the Norteks

recorded data at a sampling rate of 8 Hz and a velocity range of ± 1 m/s, while all the

SonTeks recorded at 10 Hz with a velocity range ± 2 m/s. In both the lab and the field,

all ADV bursts lasted 5 minutes.

4.3.2. Laboratory and Field Arrangement of ADVs

All the laboratory ADV experiments utilized the 110-liter VIMS sediment mixing tank (Figure 4.2), which is 1.5-m tall, square in cross-section, with an inside width of 31.6 cm, and tapers at its base to facilitate the return of sediment to be pumped back to its upper section (Cartwright et al., 2013). A 44-liter/minute Cal Pump MS900 powers the circulation of water in the tank. After passing through the pump, tank water is re-circulated through a four-way splitter to four jet outlets, one centered on each tank wall, 25 cm below the top of the tank. Sliding sampling tubes situated along one side of the tank can be pushed in to the center of the chamber to allow the collection of ground-truth water samples. In all the tank experiments, the Nortek and SonTek ADVs were always mounted such that their sampling volumes coincided with the height of the sample tube located 57 cm below the top of the mixing tank (Figure 4.2). Pairs of Nortek and SonTek ADVs were rotated through for use in the various tank experiments. The high capacity circulating pump incorporated into the design of the tank aims to keep the chamber well mixed over the course of any given lab experiment. Our experience has shown that mud is largely well-mixed throughout the tank. But for sand-sized sediment, there still exists a notable vertical gradient in concentration at steady state, decreasing toward the top of the tank. Collection of water samples at the height of the ADV sampling volume avoided problems from this vertical gradient in tank sand concentration.

126

An *in situ* comparison of Nortek versus SonTek ABS response in the York River estuary was conducted on 24 July 2012 using the R/V Elis Olsson, anchored at 37 deg 20.52 min N, 76 deg 37.51 min W, in the vicinity of the Clay Bank study site described in Chapter 2 (Cartwright et al., 2009). One Nortek ADV and one SonTek ADV (Table 4.1) were mounted on the front of the ROSE (Real-time Oceanographic Sensing Equipment) profiler (Figure 4.3A) such that a fin on the back of ROSE turned the ADVs into the oncoming tidal current. The ADV sensors were mounted such that their sampling volumes were each 37 cm above the feet of the profiler, which also corresponded to elevation of the intake hose leading to a ~20 liter/minute Dayton Model 1P809 submersible pump. The anchor station was maintained for just over six hours on 24 July 2012, encompassing an entire flood tide. ROSE was lowered once each hour for a downward profile. On the way back up, ROSE was stopped at three levels, one within the bottom third of the column, one within the middle third, and one within the top third (Figure 4.3B). ROSE was kept at each sample height for at least 5 minutes while a sample burst was collected by each ADV. A water sample was pumped during each burst and collected on deck in 0.5-liter bottles.
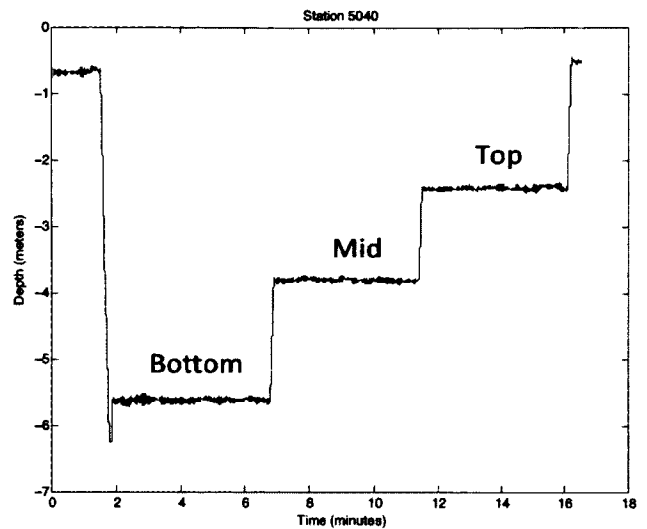
Figure 4.3. A) ROSE profiler with SonTek ADVOcean-Hydra (with wide white stem) and Nortek Vector ADV (with narrow black stem) from October 2012, but set up as used for this study's July 2012 *in situ* ADV calibration. Also mounted on ROSE in July 2012 were a pump with an inlet at the ADVs' sampling height, a LISST and a CTD. The tall instrument to the left is a video settling column which was not used in July 2012. B) Example CTD profile showing typical depths of top, middle and bottom ADV sample bursts.

4.3.3. Sediment Processing

Suspended sediment mass concentrations in both the lab and field were determined by filtering of water samples for total suspended solids (TSS). Based on the sample pump rates and the inside diameter of the water intake tubes, the velocity at the sample intakes in the field and in the lab were each more than 1 m/s. High intake speeds were designed

128

specifically to prevent possible sorting of grains at the intake associated with the inertia of more massive particles (Battisto et al., 1999). The goal of pump sampling was simply to calibrate for TSS; thus particle break up within the sampling hoses was not an issue. Between collection and filtering, water sample bottles were kept in dark cold storage. Water samples were then passed through 47-mm diameter, pre-weighed 0.7 mm glass fiber filters and dried for overnight at 103°C. The next day the individual filters were repeatedly weighed as they continue to dry until consecutive weights agreed to within 0.5 mg.

Sediment was prepared for use in mixing tank experiments as follows. Mud "stock solutions" were created from bottom sediment samples collected near the Clay Bank study site in the York River estuary using a GOMEX boxcore. One stock solution was made from bottom sediment collected on 12 July 2012 at CHSD lab stations BC5022 to BC5024, and a second was made from sediment collected on 8 January 2013 at CHSD stations BC5078-BC5080. In each case, the top centimeter from subsamples of several boxcores were combined and wet-sieved through a 63-mm screen size. These filtrates were each allowed to settle for one week, and a large portion of the surface liquid was decanted off. After homogenizing the remaining portion, filtering (as described in the previous paragraph) was used to determine each solution's mass concentration. The concentration of the 2012 and 2013 stock solutions were determined to be 27.3 ± 3.6 g/L and 74.9 ± 0.2 g/L, respectively, where ± are standard errors. Based on pipette

analysis, the 2013 stock solution was determined to be $78.9 \pm 0.3\%$ clay and $21.1 \pm 0.3\%$ silt, respectively. The percent clay and silt of the 2012 stock solution was not determined. Sand-sized material was prepared for mixing tank experiments by passing commercial quartz sand though a stack of sieves and collecting that which passed through a 180-mm screen but was retained a 150-mm screen.

4.3.4. Individual Mixing Tank Experiments

In 2012 and 2013, several mixing tank experiments were performed to inter-compare ABS response among Nortek and SonTek ADVs (identified as Runs 1 through 6, with specific dates and ADV serial numbers indicated in Table 4.1). Runs 1 and 2 each compared multiple ADVs, whereas Runs 3 through 6 each compared a single Nortek to a single SonTek. It was never possible to intercompare all ten ADVs at once because the MUDBED long-term observing site (Cartwright et al., 2009) always required some instruments to be dedicated to field work.

Inter-/intra-vendor variability, paint/no-paint (Runs 1 and 2):

As part of Run 1, the sensors of several ADVs were painted with a thin coat of antifouling paint (Trilux 33) in the same manner as they are painted for tripod deployments at the MUDBED observing site (Cartwright et al., 2009). The thickness of the paint was the thinnest layer possible which did not expose the color of the

underlying transducer. After the coating had dried, a "painted" sample burst was collected for each ADV. All paint was then removed from the sensors, and each ADV was re-inserted one at a time into the chamber, and a "non-painted" sample burst was collected. Run 2 which included two ADVs unavailable for Run 1, used only unpainted sensors. (None of the other lab or field measurements utilized painted ADVs.) Runs 1 and 2 each utilized the 2012 stock solution, diluted by additional tank water. Runs 1 and 2 occurred a month apart, so the mixing tank was drained in between, and the sediment concentrations for the two runs were not identical. For each run, the concentration (reported under results) was measured via the sampling tube at the height of the ADV sampling volume.

Method repeatability limit (Run 3):

To determine the repeatability of the ADV sampling procedure in the calibration chamber, one Nortek ADV was inserted and removed from the calibration chamber ten times. Care was taken to place the instrument each time such that its sample volume would be in the same location, and a 5-minute data burst was recorded for each insertion. The procedure was then repeated ten times for one SonTek ADV. Approximately 400 mL of the 2012 stock solution was added to the calibration chamber for Run 3 to bring the calibration chamber to approximately 100 mg/L. Unfortunately, error occurred in the processing of the pump samples collected during Run 3, so the TSS concentration in the chamber was not ground-truthed by filtering.

Mud calibration (Run 4):

An incremental ABS calibration for one SonTek and one Nortek ADV was performed using multiple additions of the 2013 stock solution to the mixing tank. Aliquots of the stock solution were chosen to sequentially bring the sediment mass concentration of the tank as a whole to approximately 25, 50, 75, 100, 150, 200, 250, 300, 400, 600 and 700 mg/L ("added concentration" in Table 4.2 Run 4). A 5-minute data burst was collected with each sensor after each aliquot had been given time to equilibrate. For each concentration, a water sample was collected from the interior of the chamber at the height of the ADV sampling volume and filtered for TSS ("measured concentration" in Table 4.2 Run 4). The average ratio of "measured conc."/"added conc." (equal to 0.945) was then used to scale the "added concentration" to produce a "calculated concentration" (see Table 4.2 Run 4). By accounting for imperfect tank mixing, the calculated concentration reflected the theoretically expected concentration better than the added concentration did.

Sand calibration (Run 5):

An incremental ABS calibration was similarly performed using multiple additions of the 150-to-180-μm sieved quartz sand. Aliquots of sand were added to the chamber to bring the mass concentration for the tank as a whole to approximately 25, 50, 100, 150,

132

200, 300, 400, 600, 800, 1000, 1200 and 1600 mg/L ("added concentration" in Table 4.2 Run 5). Before addition of the next sand aliquot, a 5-minute data burst was collected with one SonTek and one Nortek sensor, and a water sample was collected at the height of the ADV sampling volume and filtered for TSS. After completing the ADV data collection, systematic problems with initial filtering analysis were discovered for the lower concentration water samples, and the experiment was repeated for the 25 to 400 mg/L cases. Final "measured" and "calculated" sand concentrations, determined by the method described above for Run 4, are displayed in Table 4.2 Run 5. For sand, the average ratio of "measured conc."/"added conc." was 0.579, reflecting the less efficient mixing of suspended sand concentration in the mixing tank relative to that for mud.

Mixed sand-mud calibration (Run 6):

Finally, a progressive amount of 150-to-180-μm sand was added to each of two mud suspensions. On separate days, samples of the 2013 mud stock solution were diluted to produce mixing tank concentrations of approximately 100 mg/L and 200 mg/L and pump samples were collected for TSS ground-truthing. In each case, aliquots of sand were then added to the mixing tank to bring the percentage of sand in the tank as a whole to ~25% sand via steps of 1 to 3% at a time (a table of more precise values is presented in Section 4.4). Before addition of each subsequent sand aliquot, a 5-minute data burst was collected with both a SonTek and a Nortek ADV. Because of difficulties

in accurately pumping of sand at low concentrations, pump samples were not collected at each sand percent. Instead, total TSS at each step at was calculated based on the mass of sand added to the tank, adjusted by the factor of 0.579 for "measured conc."/"added conc." as determined during Run 5.
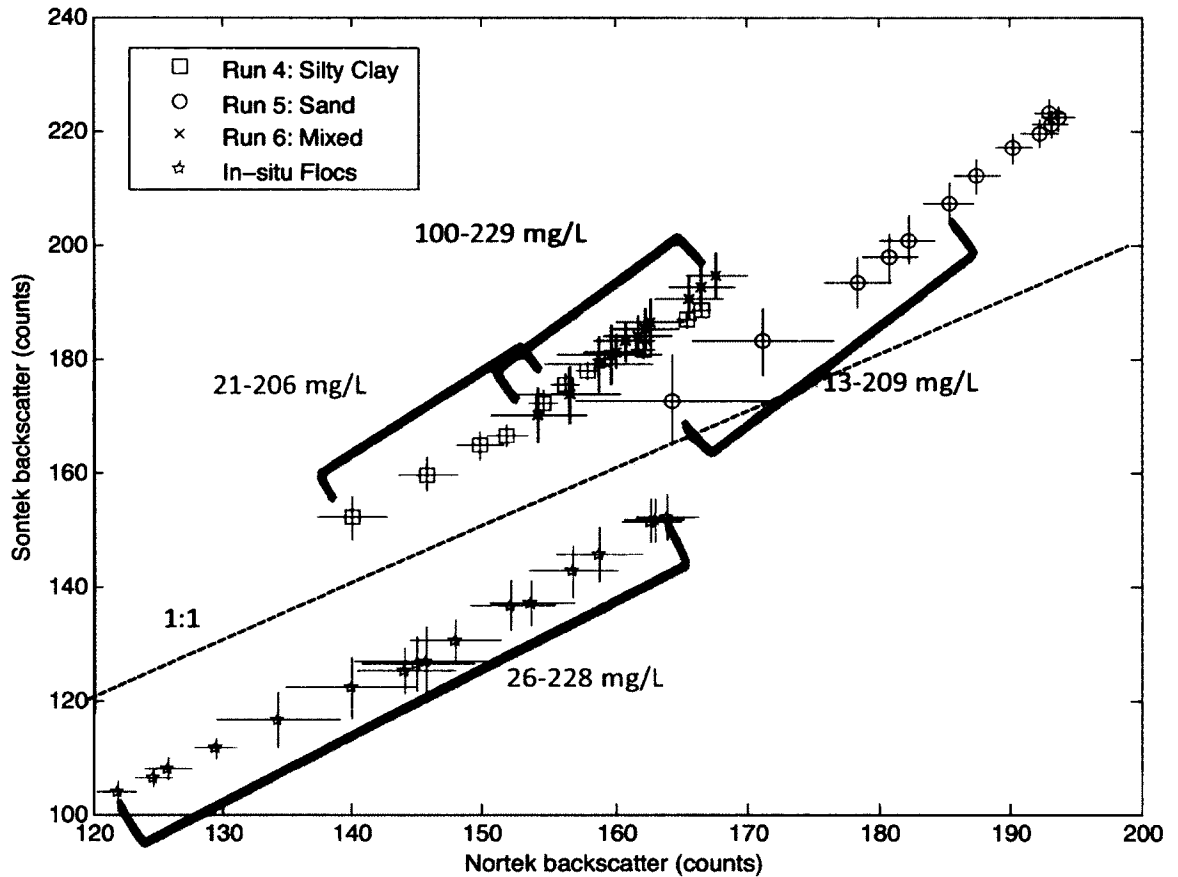
Figure 4.4. Comparison of acoustic backscatter burst response from Nortek Vector ADV and SonTek ADVOcean sensor pairs during lab calibrations for silty-clay (red squares), sand (blue circles), and mixed sandy mud (black x's) as well as an *in situ* calibration with muddy flocs (green stars). Brackets provide an indication of the mass concentration ranges relative to the ADV responses in counts. The "error" bars are ± one standard deviation about each burst mean. With thousands of observations per burst, each standard error (i.e., the uncertainty in each mean) is much smaller than the symbols themselves.

4.4 Results and Discussion

4.4.1. General Trends in ABS Response – Sediment vs. ADV Properties

The laboratory and field calibration runs demonstrate that the response of ADV backscatter to suspended sediment is a function of both sediment properties and the physical properties of the ADVs themselves. Figure 4.4 and Table 4.1 display ABS responses for a pair of SonTek and Nortek ADVs for the three lab calibration series (Runs 4 through 6) plus the York River estuary *in situ* calibration. Runs 4 and 6 used the same pair of instruments. Despite shifts associated with specific ADV serial numbers, it is clear that the sediment type systematically impacts the ABS response for both the SonTeks and the Norteks. For both vendors, the ABS response to overlapping concentrations is strongest for sand, then mixed sand and mud, then silty clay, and finally weakest for *in situ* muddy flocs. Although the overall trend in response to changing sediment type is similar, the ABS response is also instrument dependent. If the response of all the instruments were identical, all of the ABS data would lay along a single 1:1 line in terms of ABS response. The four SonTek vs. Nortek calibrations plainly do not lie along a 1:1 line or even along a single line of any kind.

Independent of sediment type, differences in ABS response in Figure 4.4 between the various SonTek and Nortek ADVs can be further divided into inter- and intra-vendor

135

variability. Two trends are suggested by Figure R1 regarding systematic differences between SonTeks and Norteks (i.e., inter-vendor variability). First, the ABS range in counts registered by the SonTeks is greater in all three cases: 1.1:1 for the *in situ* flocs, 1.4:1 for silty clay and sandy mud, and 1.7:1 for sand. Second, the greater ABS range registered by the SonTeks becomes more pronounced as ABS magnitude increases. However, inter-vendor variability cannot explain all the trends seen in Figure 4.4. If the SonTeks systematically differed from the Norteks, but ABS response was still consistent within a single vendor, all the ABS data still would lay along a single curve other than a 1:1 line. This is not the case, however, so some of the variability must be due to intra-vendor variability, i.e., differences among individual SonTeks and/or individual Norteks. The lab experiments whose results are described in the next section were specifically designed to help explore this inter- vs. intra-vendor variability.

4.4.2. Inter-vendor, intra-vendor Response of ABS to Single Sediment Concentrations

Results from systematic inter-comparisons of multiple ADVs provide an assessment of the general variability in ABS response for cases with fixed sediment concentration, both between vendor models, i.e., Nortek versus SonTek, and also among multiple examples of individual Nortek or SonTek models (Figure 4.5, Table 4.2A). For example, for the four unpainted Norteks plus four unpainted SonTeks compared during Run 1 at 130 ± 7 mg/L, the largest difference in mean ABS response was 8 counts among Nortek units and 33 counts among SonTek units. For the three Norteks and three

Table 4.2. A) Burst average acoustic backscatter for mud, sand and *in situ* calibrations

RUN 4: Mud (silty-clay) Calibration (January 24, 2013)

			NORTEK VCH4921			SONTEK B336		
			Burst		Record	Burst		Record
Added conc (mg/L)	Measured conc (mg/L)	Calculated conc (mg/L)	Mean (counts)	Std Dev (counts)	Std Dev (counts)	Mean (counts)	Std Dev (counts)	Std Dev (counts)
25	21.0	23.62	139.97	2.71	2.19	151.85	3.94	3.38
50	40.8	47.24	145.79	2.31	2.23	159.56	3.00	3.23
75	67.9	70.87	149.77	1.93	2.09	164.58	2.55	3.18
100	94.2	94.49	151.85	1.55	1.97	166.38	2.02	3.11
150	123.5	141.73	154.58	1.14	1.93	172.24	2.06	2.79
200	206.5	188.98	156.28	1.08	1.94	175.37	1.83	2.65
250	252.5	236.22	157.95	0.94	1.84	177.81	1.67	2.56
300	331.1	283.47	159.19	0.90	1.81	179.75	1.65	2.48
400	408.4	377.96	162.08	0.90	1.53	181.31	1.58	2.39
600	543.8	566.94	165.39	0.74	1.38	186.61	1.54	2.41
700	695.5	661.43	166.58	0.71	1.35	188.52	1.54	2.48

Run 5: Sand Calibration (July 11 and 20, 2012)

			NORTEK VCH4854			SONTEK B336		
			Burst		Record	Burst		Record
Added conc (mg/L)	Measured conc (mg/L)	Calculated conc (mg/L)	Mean (counts)	Std Dev (counts)	Std Dev (counts)	Mean (counts)	Std Dev (counts)	Std Dev (counts)
25	13	14.47	164.41	7.52	4.79	172.55	8.04	4.83
50	24	28.95	171.18	5.29	3.91	182.89	5.82	4.17
100	67	57.90	178.36	2.52	3.15	193.2	4.51	3.94
150	75	86.85	180.76	2.13	3.12	197.68	4.31	3.98
200	85	115.79	182.15	2.06	3.06	200.81	4.1	3.85
300	170	173.69	185.26	1.87	3.3	207.08	3.58	3.94
400	209	231.59	187.44	1.77	3.6	211.87	3.16	3.8
600	467	347.38	190.23	1.45	3.76	216.83	2.71	3.64
800	480	463.18	192.1	1.48	3.89	219.32	2.49	3.4
1000	587	578.97	193.04	1.4	4.02	221.17	2.47	3.27
1200	834	694.76	193.59	1.31	4.3	222.16	2.26	3.15
1600	965	926.35	192.97	1.17	4.17	223.14	2.19	3.03

In-situ Muddy Flocs Calibration (July 24, 2012)

	NORTEK VCH4854			SONTEK B3084		
	Burst		Record	Burst		Record
TSS (mg/l)	Mean (counts)	Std Dev (counts)	Std Dev (counts)	Mean (counts)	Std Dev (counts)	Std Dev (counts)
57.10	144.10	3.81	2.57	125.00	4.16	3.28
44.10	153.72	3.22	2.01	136.97	4.15	3.37
94.80	147.90	3.45	2.22	130.23	4.05	3.12
24.50	125.85	1.87	2.02	107.88	2.06	2.38
27.60	124.72	1.48	1.99	106.34	1.76	2.46
228.40	162.76	2.36	1.54	151.34	3.82	3.08
88.20	152.24	3.20	1.80	136.38	4.50	2.99
26.40	121.85	1.63	1.67	103.80	2.13	2.26
146.80	163.00	2.28	1.51	151.44	3.72	3.04
116.80	158.83	3.29	1.61	145.52	4.78	3.07
37.10	129.49	1.70	1.69	111.47	1.98	2.19
156.20	163.98	2.46	1.43	152.04	3.91	3.07
86.60	145.67	5.45	1.84	126.90	6.09	2.85
59.00	145.06	4.39	1.94	126.33	4.94	2.82
114.00	156.85	3.43	1.87	142.55	4.70	3.27
40.30	139.96	5.08	2.14	122.17	5.48	2.92
47.60	134.23	4.79	2.13	116.45	4.84	2.67

Table 4.2. B) Burst average acoustic backscatter for mixed sediment calibrations

95 mg/l Mud (Jan 28, 2013)

		NORTEK VCH4921			SONTEK B336		
Sand Added Conc (mg/L)	Calculated conc (mg/L)	Backscatter Burst Mean (counts)	Std Dev (counts)	Record Std Dev (counts)	Backscatter Burst Mean (counts)	Std Dev (counts)	Record Std Dev (counts)
0	0.0	152.86	1.96	2.00	169.28	2.45	3.42
2.1	1.3		No Data		169.20	3.61	4.17
3.1	2.0		No Data		168.96	3.78	4.56
4.1	2.6	154.54	3.01	2.24		No Data	
5.1	3.2	154.54	3.00	2.24		No Data	
6.2	3.9	153.71	3.29	2.30	171.29	4.23	3.67
7.3	4.6	154.47	3.24	2.26	170.99	4.59	4.10
8.3	5.2	154.48	3.43	2.28	170.57	4.57	4.44
9.3	5.9	154.54	3.58	2.31	170.80	5.08	5.20
10.5	6.6	154.28	3.53	2.40	169.94	4.95	5.72
15.5	9.8	156.61	3.87	2.39	173.53	5.12	6.13
20.5	12.9		No Data		176.94	5.21	5.46
25.7	16.2	158.87	4.05	2.41	179.03	5.03	5.32
30.7	19.3	159.64	3.98	2.37	180.58	5.34	5.54

190 mg/l Mud (Feb 1, 2013)

		NORTEK VCH4921			SONTEK B336		
Sand Added Conc (mg/L)	Calculated conc (mg/L)	Backscatter Burst Mean (counts)	Std Dev (counts)	Record Std Dev (counts)	Backscatter Burst Mean (counts)	Std Dev (counts)	Record Std Dev (counts)
0.0	0.0	159.11	1.28	1.66	179.28	1.78	3.06
2.2	1.4	158.47	1.73	1.70	179.71	2.62	3.23
4.3	2.7	158.90	2.01	1.76	179.51	2.85	3.32
8.3	5.2	160.01	2.24	1.85	181.22	3.23	3.48
12.4	7.8	160.76	2.34	1.84	182.86	3.48	3.44
16.6	10.5	161.75	2.55	1.79	183.96	3.64	3.55
20.8	13.1	162.26	2.55	1.83	185.16	3.74	3.50
24.8	15.6	162.75	2.57	1.81	186.30	4.10	3.58
30.9	19.5		No Data		187.52	3.97	3.54
41.4	26.1	165.63	2.58	1.72	190.49	3.87	3.56
51.9	32.7	166.58	2.51	1.68	192.30	3.77	3.54
62.4	39.3	167.69	2.33	1.62	194.36	4.03	3.68

For Tables 4.2 A and B:

AverageABS = mean of acoustic backscatter (ABS) for three beams for each record
Record Std Dev= mean of all the records of standard deviation about the AverageABS for each record.
Burst mean = mean AverageABS in the burst
Burst Std Dev=standard deviation about the Burst mean.
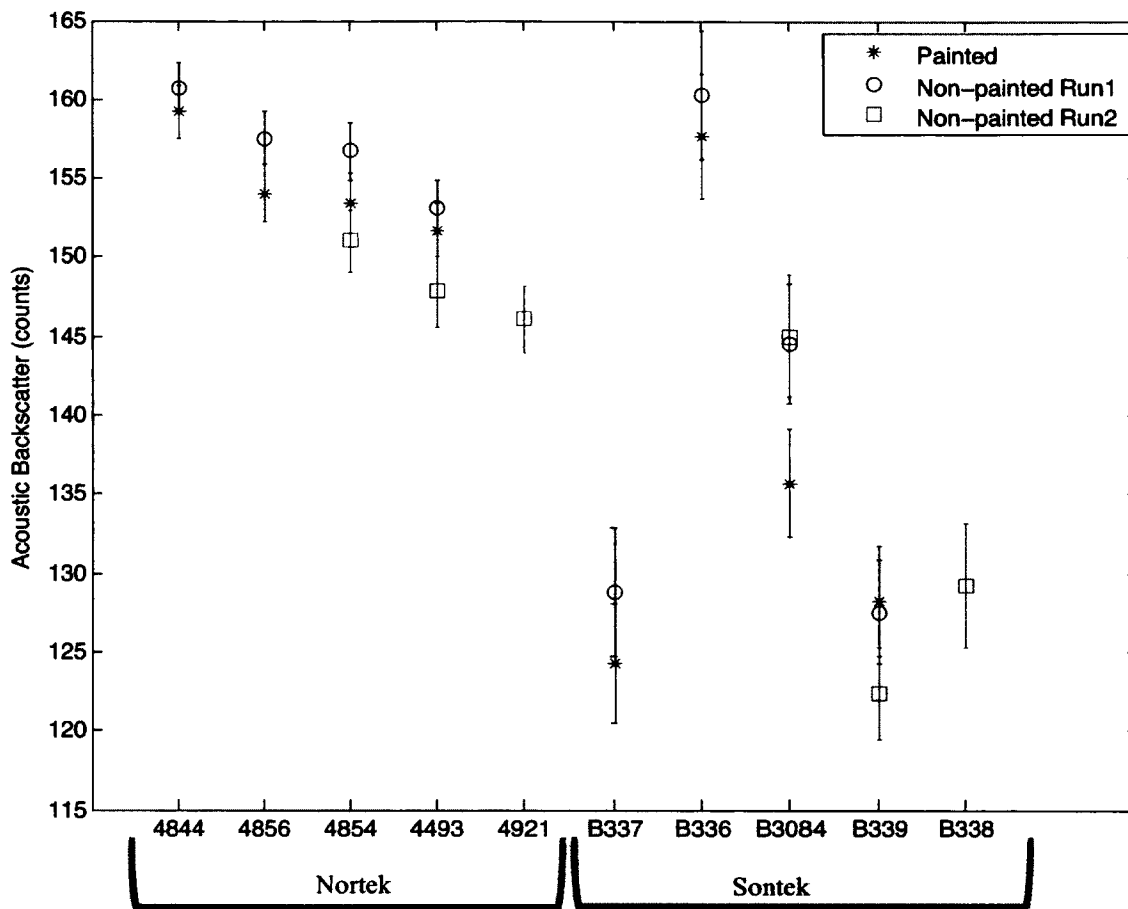
Figure 4.5. Inter-comparison of acoustic backscatter burst response for multiple Nortek Vector ADVs and SonTek ADVOceans. Blue circles and green squares indicate non-painted sensors from Runs 1 and 2, respectively. Red stars are sensors from Run 1 coated with Trilux 33 anti-fouling paint. The serial numbers for the individual Nortek and SonTek ADVs appear along the x-axis. "Error" bars are ± one standard deviation about each burst mean.

SonTeks compared in Run 2 at 80 ± 4 mg/L, the largest difference in mean response was 5 counts and 23 counts, respectively. The history of the SonTek ADVOcean-Hydras and Nortek ADV Vectors used in this study are relatively similar, in that they each include units purchased and/or repaired over a 5 to 6 year time frame. Thus these

results suggest that in general, Nortek ADV Vectors may have a more consistent ABS response among units of the same model than is the case for SonTek ADVOcean-Hydras.

The manufacturing production run and repair history for ADVs may also play a role in determining differences in intra-vendor ABS response. For both the SonTek and Nortek units, the smallest mean ABS differences were for pairs of instruments that were part of the same production run. During Run 1, the unpainted SonTek B337 and B339 (bought together in 2006) differed by only 1.2 counts, and the unpainted Nortek VCH4854 and VCH4856 (bought together in 2011) differed by only 0.8 counts. In contrast, the largest difference in mean ABS for a given unit relative to the others from its vendor was for SonTek B336, which was bought in 2006 but had several of its components replaced in 2011. The consistency in response of SonTek B337 and B339, which are each 7 years old and have been in a field deployment rotation ever since, suggests, that in the absence of repair, the ABS response of ADVs can be remarkably stable. Although a repair may alter an ADV's ABS response, it is likely that the ADV's altered ABS response would then remain stable at its new level following the repair.

4.4.3. Inter-vendor, Intra-vendor Response of ABS to Anti-fouling Paint

The inter-/intra-vendor mixing tank experiments also provided an opportunity to test for possible biases associated with application of anti-fouling paint onto the transducers of the ADVs. A thin coating of anti-fouling paint is helpful in extending the duration for field deployments such as those associated with maintain the long-term MUDBED observation station in the York River estuary (Cartwright et al., 2009). However, anti-fouling paint is not typically used in short-term ADV deployments, such as tidal profiling at anchor utilizing ROSE. Thus it is important to quantify any acoustic effect of a thin coat of Trilux 33 (the thinnest possible coat which hides the color of the underlying transducer). As seen in Table 4.2A and Figure 4.5, the effect of anti-fouling paint is small but detectable. On average, a thin coating of Trilux 33 reduced the backscatter recorded by the Nortek ADV Vectors and SonTek ADVOcean-Hydras tested by 2.4 ± 0.6 and 3.8 ± 2.0 counts, respectively. In contrast, there was no systematic effect of anti-fouling paint on the standard deviation of the ABS time-series.

4.4.4. Method repeatability limit for each vendor

The Nortek ADV Vector and SonTek ADVOcean-Hydra both demonstrated a consistent ABS response as determined by testing the repeatability of the ADV sampling procedure in the sediment mixing tank (Figure 4.6, Table 4.3). This was not surprising, given the remarkably consistent ABS response up to six years after delivery to VIMS for pairs of ADVs from the same factory production run. The burst means for

141
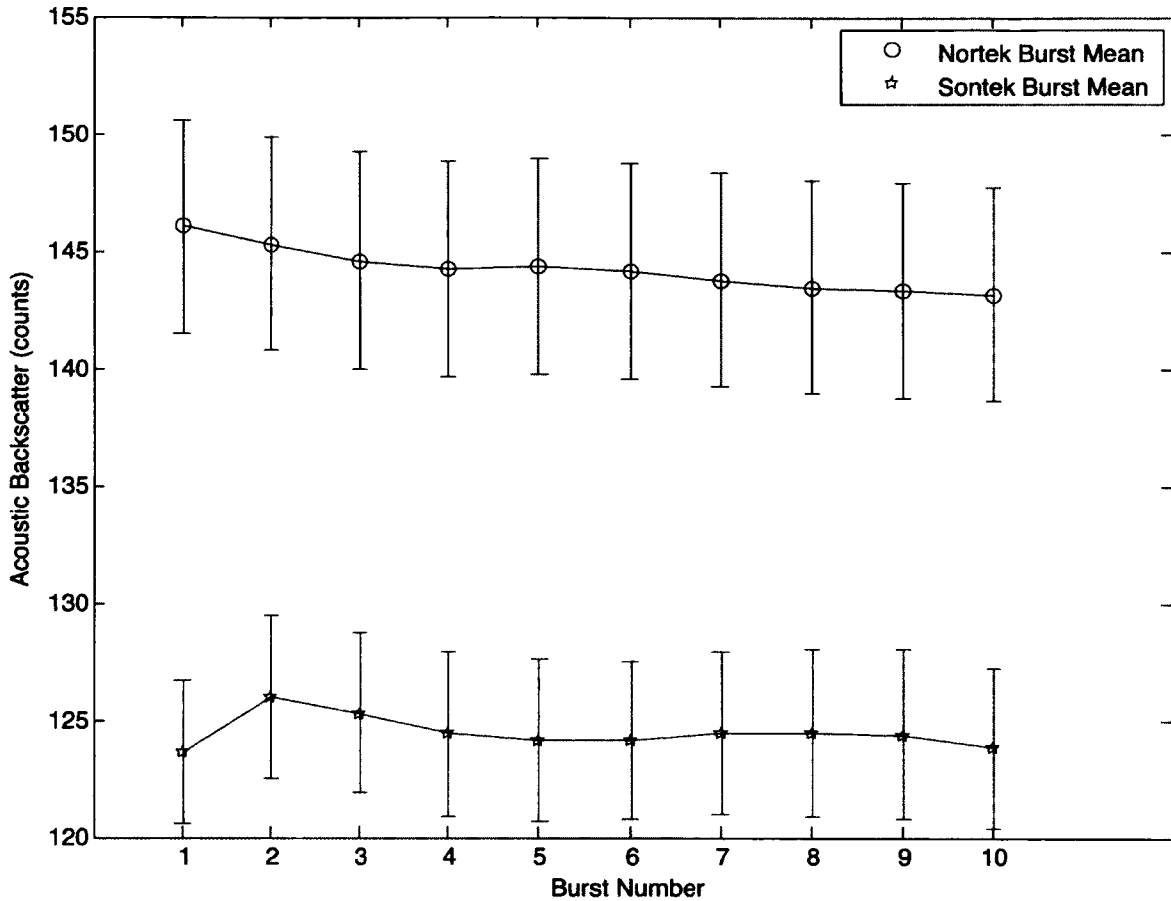
Figure 4.6. Acoustic backscatter burst response of Nortek Vector sensor VCH4854 (blue circles) and SonTek ADVOcean sensor B3084 (red stars) for 10 bursts in a single mud concentration as a measure of method reproducibility. "Error" bars are ± one standard deviation about each burst mean.

the 10 repetitions for the Nortek and SonTek ranged from 143.1 to 146.1 counts and

123.6 to 126.0 counts, respectively. In each case the standard deviation for the time-

series of these 10 burst means was less than 1 count. It should be kept in mind that the

method repeatability test is for the entire method, not just the ability of the ADV to

register repeatedly similar ABS values. Sediment mixing in the tank is not perfect, and

it is possible that concentration field evolved and/or oscillated slightly in time. So the

Table 4.3. Method repeatability burst averaged acoustic backscatter

	NORTEK VCH4854				SONTEK B3084		
	Backscatter				Backscatter		
	Burst		Record		Burst		Record
Burst No.	mean	Std Dev	Std Dev	Burst No.	mean	Std Dev	Std Dev
	(counts)	(counts)	(counts)		(counts)	(counts)	(counts)
1	146.06	1.91	4.55	1	123.61	3.99	3.08
2	145.30	1.88	4.57	2	125.96	5.37	3.43
3	144.56	1.96	4.66	3	125.30	4.50	3.46
4	144.24	1.90	4.61	4	124.42	4.12	3.53
5	144.32	1.96	4.60	5	124.14	4.28	3.48
6	144.13	2.05	4.58	6	124.11	4.08	3.35
7	143.76	1.94	4.57	7	124.43	5.22	3.45
8	143.43	2.07	4.55	8	124.44	4.53	3.54
9	143.34	2.03	4.61	9	124.37	4.48	3.61
10	143.13	2.00	4.54	10	123.78	4.19	3.45

For Table 4.3:
AverageABS = mean of acoustic backscatter (ABS) for three beams for each record
Record Std Dev= mean of all the records of standard deviation about the AverageABS for each record.
Burst mean = mean AverageABS in the burst
Burst Std Dev=standard deviation about the Burst mean

variability of the ABS burst averages in Figure 4.6 and Table 4.33 may somewhat

overestimate the contribution of the ADVs themselves to the limit of repeatability.

143

4.4.5. Assignment of Offset Correction to Match ABS of Reference ADVs

The mean responses for multiple ADV units determined in Runs 1 through 3, all using muds derived from the 2012 stock solution, and all using concentrations on the order of ~100 mg/L, provide an opportunity to define reasonable correction values in units of counts to help compensate for intra-vendor variability in ABS response. Experience with the SonTek ADVOcean-Hydra (Cartwright et al., 2009) has shown that variability among ADV calibrations (plotted as log(C) vs. ADV counts) tends to exhibit itself more strongly

in terms of shifts in calibration curve offsets as opposed to changes in calibration curve slope (see Figure 4.1). Recall that ADV counts are proportional to $\log 10(P/P_0)$, where P is the received power relative to an instrument-specific reference power, P_0. Thus changing the calibration offset for a given instrument is equivalent to redefining its reference power, P_0. Once a change in P_0 is log-transformed, what was a division by P_0 in power "space" becomes a subtraction (or addition) in count "space" (depending on whether P_0 is made larger or smaller). In other words, one of the SonTek and one Nortek units in Table 4.2 can each be assigned to be a reference unit (with a fixed P_0), and the ABS values recorded by each of the other units can be each be shifted by a constant offset in counts relative to the reference unit. Each reference unit must be a serial number present during multiple runs, and it also makes sense for each to be one of the units that has a production run "sibling" also at VIMS. By default, then, the Nortek reference unit is VCH4856, and the SonTek reference unit is B339.

For those units that were used multiple times over the course of Runs 1 through 3, their relative behavior from one run to the next provides a double check on data quality. For example, three of the four units used in both Run 1 (130 ± 7 mg/L) and Run 2 (80 ± 4 mg/L) show a sensible decrease in backscatter between these two runs. However, mean backscatter from unit B3084 inexplicably increased between Runs 1 and 2; and it is not clear which (or both) of these measurements may be in error. Fortunately, B3084 was also used as part of the method repeatability test (Run 3, Figure 4.6, Table 4.3), where it provided ten consistent ABS measurements at a constant sediment concentration. Thus the repeatedly stable difference between B3084 and VCH4856 counts during Run 3, along with the average (and stable) difference in between VCH4856 and B339 counts found in Runs 1 and 2, were used to set the offset for B3084 relative to B339. In summary, the bottom row in Table 4.1 then contains the number of counts that should be added to each other ADV to make their (unpainted) means consistent with the counts recorded by the reference unit.

4.4.6. Results of SonTek-Nortek ABS comparisons incorporating adjusted offsets

The adjusted ABS counts for all the ADVs now largely lay along a single curve in Figure 4.7, which highlights some consistent aspects of their acoustic responses. For example, counts from the SonTek ADVOcean-Hydra and the Nortek ADV Vector are consistently and monotonically related across multiple particle types for the full range

of backscatter considered in Figure 4.7. In other words, if various (progressively increasing) concentrations of sand, sandy mud, silty clay, and flocculated mud each produced a response of about 160 counts from a reference-adjusted SonTek ADVOcean-Hydra, then those same concentrations of sand, sandy mud, silty clay, and flocculated mud would each consistently produce about 140 counts from a reference adjusted Nortek ADV Vector. It is reassuring to note that the individual instrument offset corrections were derived entirely using the 2012 mud stock solution, yet the chosen offset corrections do reasonably well for the separately acquired and diverse group of sediments displayed in Figure 4.7.

There are also systematic differences between the response of the two ADV models which are clarified by Figure 4.7. Most notably, the best-fit curve in Figure 4.7 is quadratic, such that at least one of the ADVs must not have a purely log-linear response to sediment concentration across the range of concentrations and sediment types considered in this study. At low backscatter, the ABS response by the SonTek and Nortek initially grow together at a roughly equal rate (parallel to the 1:1 line), suggesting that both instruments initially respond similarly to the log of concentration. But as ABS strength continues to increase, SonTek counts start to grow more quickly. Fluctuations in ABS within individual bursts (i.e., the +/- one standard deviation "error" bars in Figure 4.7) also systematically vary between the SonTeks vs. the Norteks. Figure 4.8 compares the ratio of ABS standard deviation for the SonTeks vs. the

146

Norteks as a function of burst-averaged ABS. In close analogy with the quadratic curve

in Figure 4.7, the ratio of standard deviations displayed in Figure 4.8 is about 1:1 at

lower ABS values, but increases towards 2:1 at higher ABS values.
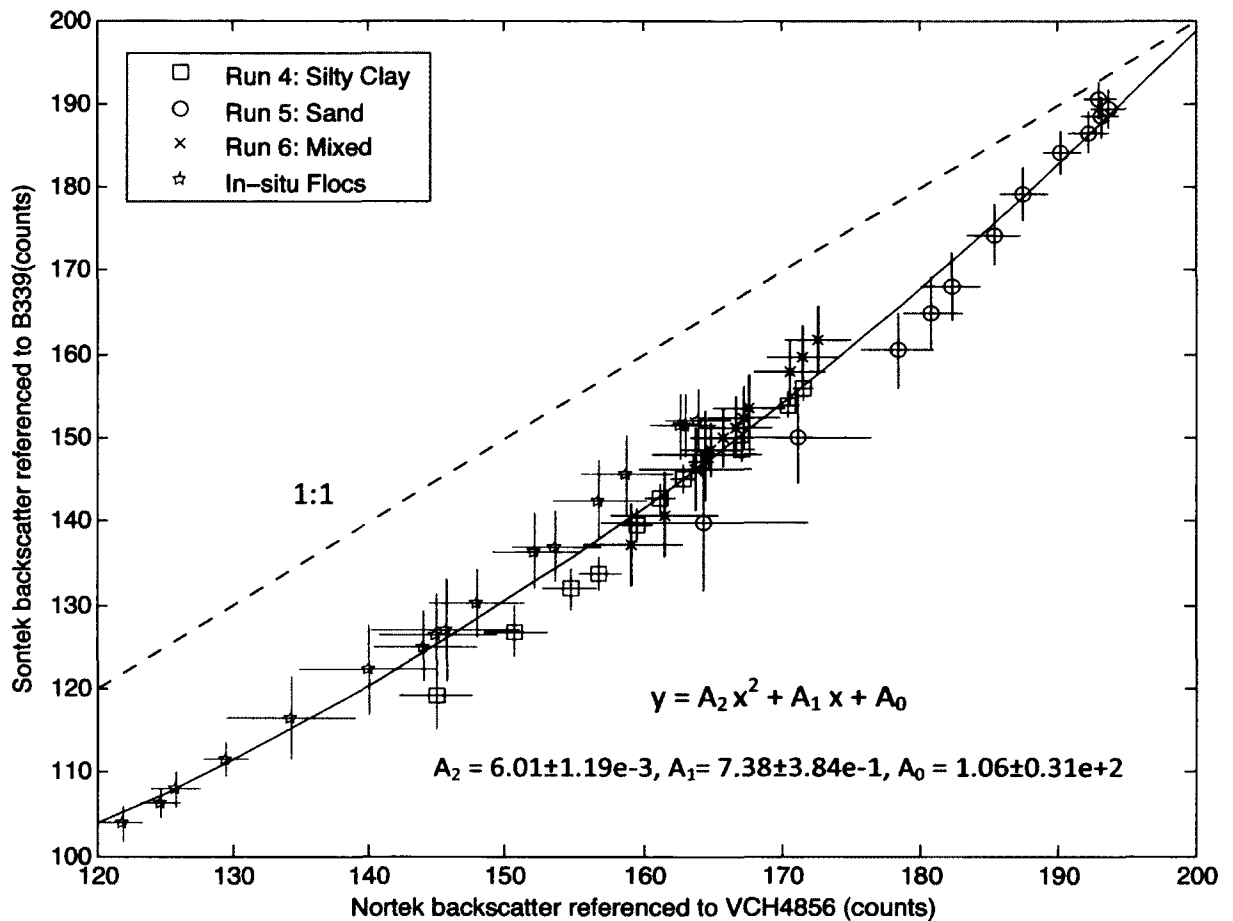
Figure 4.7. Comparison of acoustic backscatter burst response adjusted to a reference sensor (see table 4.1) from Nortek Vector ADV and SonTek ADVOcean sensor pairs during lab calibrations for silty-clay (red squares), sand (blue circles), and mixed sandy mud (black x's) as well as an *in situ* calibration with muddy flocs (green stars). Dotted line represents the 1:1 ratio between the two. The solid black line is the least-squares quadratic fit for all the data.

All else being equal, one would expect the Nortek's higher frequency (6 MHz vs. 5

MHz) to cause the backscattering to decrease more rapidly due to a higher attenuation at

6 MHz vs 5 MHz at higher sediment concentrations. Both the quadratic relationship in
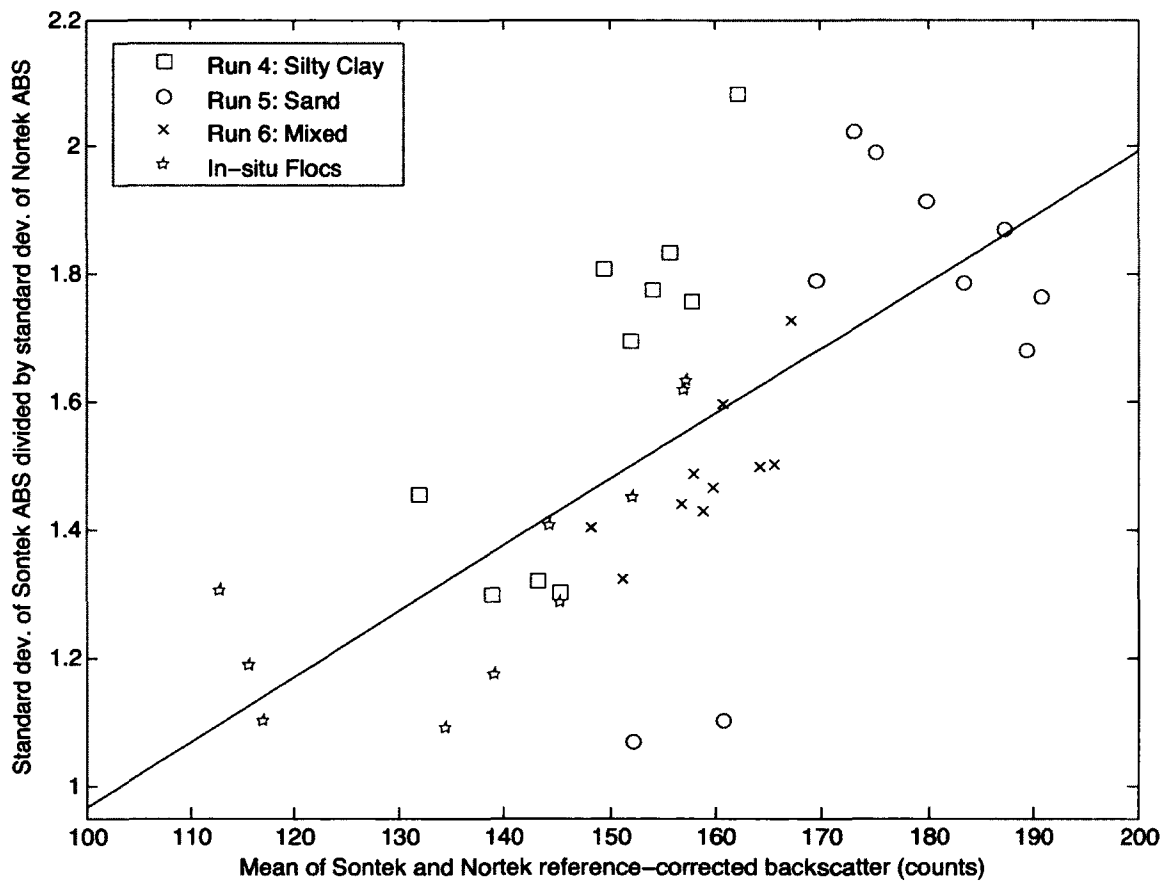
Figure 4.8. Ratio of SonTek/Nortek standard deviations of acoustic backscatter for each burst as a function of the mean of the SonTek and Nortek reference corrected response for silty-clay (red squares), sand (blue circles), mixed sandy mud (black x's), and muddy flocs (green stars). The solid line is the best-fit linear regression.

Figure 4.7 and the trend in standard deviations in Figure 4.8 are consistent with this explanation. At sufficiently low levels of ABS, neither instrument's counts are expected to be notably affected by attenuation, since the backscattered acoustic energy would be expected travel back to both instruments with little energy loss. The similar response of the two instruments would then result in a 1:1 relationship. But as concentration increased, loss of backscattered energy through attenuation would eventually become more apparent in the higher frequency Nortek. Counts would then grow more quickly for the SonTek relative to the Nortek, and the slope of the SonTek vs. Nortek ABS curve would increase along with their ratio of standard deviations.

4.4.7. Acoustic response to well-sorted sand – clear evidence of attenuation

A closer examination of the acoustic response of the Nortek ADV Vector versus the SonTek ADVOcean-Hydra to varying suspended sand concentrations further clarifies patterns of backscatter and attenuation associated with these two instruments. The attenuation associated with the highest two sand concentrations in Table 4.2 Run 5 became particularly clear for both instruments once sand concentration was plotted as a function of backscatter (Figure 4.9). In each case, these highest two concentrations deviated from the trend for the other 10 sand concentrations, and for the Nortek the count level associated with ~950 mg/l was actually lower than that associated with ~750 mg/l. Included on Figure 4.9 are quadratic and linear fits to the log-base-10 of sand

concentration versus ABS counts for the lower 10 concentrations for both instruments

using equations of the form

$$y = A_2 x^2 + A_1 x + A_0 \quad \text{and} \quad y = B_1 x + B_0 \ .$$

Table 4.4 contains coefficients for these least-squares regressions plus the associated

standard errors. For a single grain size in the absence of attenuation, one would expect a

linear relationship between $\log 10$ TSS and ABS counts. In contrast, attenuation would

tend to cause the readings to be above the linear fit, with increasingly more sediment

(beyond even that predicted by the $\log 10$ of TSS) needed to further increase backscatter.

Table 4.4. Results of least squares fits to the calibration curves plotted in Figures 4.9 to 4.11. The fitted equations are of the form: $y = A_2 x^2 + A_1 x + A_0$ and $y = B_1 x + B_0$. The coefficients listed are best-fits $\pm$ one standard error.

		A_2	A_1	A_0	B_1	B_0
Sand	Nortek	7.12 ± 0.93e-4	-1.98 ± 0.33e-1	1.44 ± 0.30e+1	5.80 ± 0.22e-2	-8.50 ± 0.41e+0
	Sontek	1.15 ± 0.37e-4	-4.48 ± 0.33e-3	-4.74 ± 0.37e-5	3.35 ± 0.07e-2	-3.59 ± 0.14e+0
Silty-Clay	Nortek	-0.14 ± 1.66e-4	6.18 ± 0.53e-2	-7.33 ± 4.18e0	5.73 ± 0.14e-2	-6.97 ± 0.26e+0
	Sontek	1.66 ± 7.04e-5	3.63 ± 1.95e-2	-3.21 ± 1.34e0	4.08 ± 0.08e-2	-3.53 ± 0.11e+0
In-situ flocs	Nortek	0.93 ± 1.11e-4	-0.65 ± 3.20e-3	0.81 ± 2.28e0	2.02 ± 0.13e-2	-1.09 ± 0.20e+0
	Sontek	-4.50 ± 8.37e-5	2.81 ± 2.01e-2	-0.87 ± 1.19	1.74 ± 0.16e-2	-2.38 ± 1.40e-1
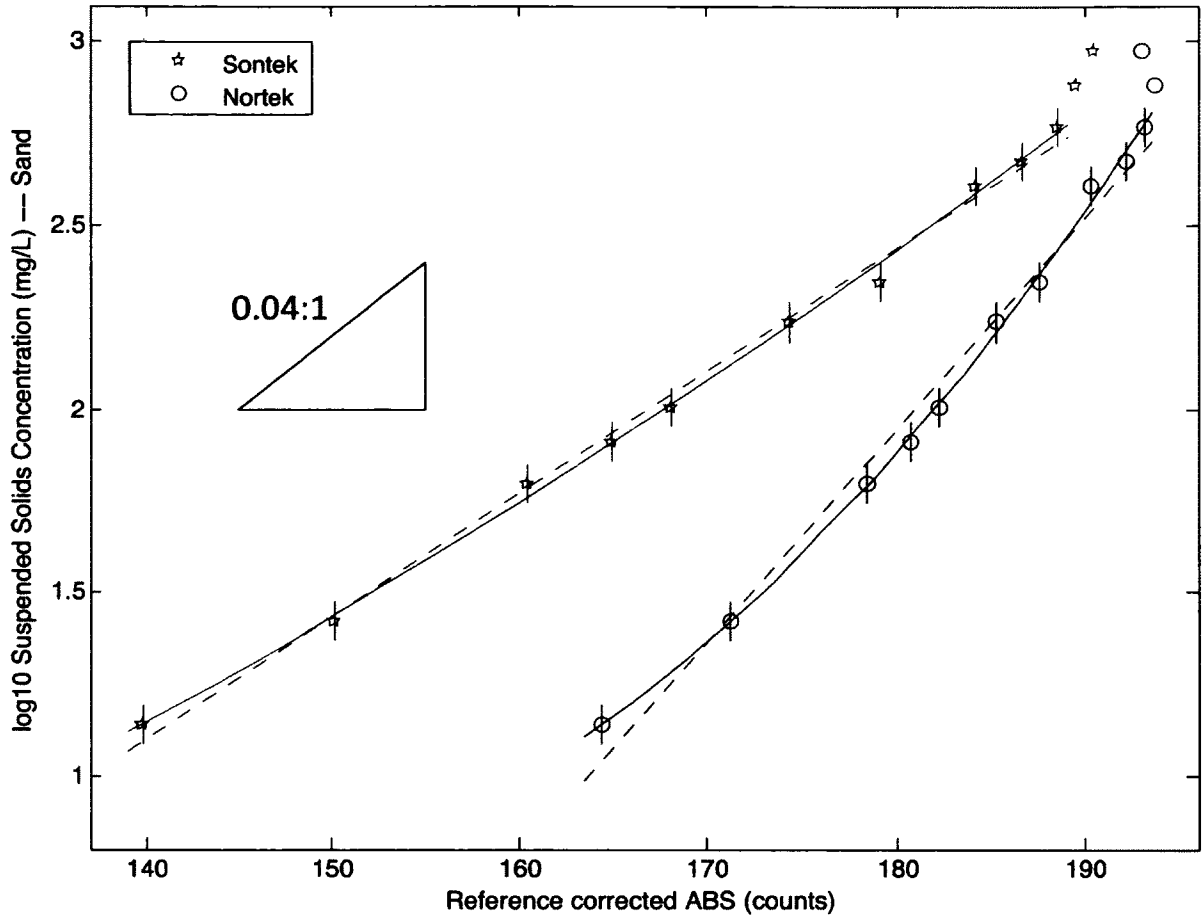
Figure 4.9. Laboratory quartz sand (150-180 μm) calibration regressions for log10 suspended sediment concentration versus reference corrected ABS response for Nortek Vector sensor VCH4854 (blue circles) and SonTek ADVOcean sensor B336 (red stars). The dashed and solid lines are least-squares quadratic and linear fits, respectively. The highest two concentrations are not included in the regressions. The values plotted are the average of the measured and calculated concentrations in Table 4.2 Run 5. Error bars are ± the average percent difference between measured and calculated concentrations in Table 4.2 Run 5.

For a single grain size in the absence of attenuation, ADV backscatter is expected to increase by ~ 7 counts for each doubling of suspended sediment concentration (see

derivation in Section 4.2), which corresponds to a slope of ~ 0.04 on a plot of log10 TSS versus counts (Figure 4.9). For the linear fits in Table 4.4, the least-squares coefficients for the slope, B_1, were relatively close to the expected value of ~ 0.04 for both instruments, with a best-fit value of 0.034 for the SonTek ADVOcean-Hydra and a best- fit value of 0.058 for the Nortek ADV Vector. Despite the sensible slopes for the linear fits, however, the best-fit quadratic curves visually fit the data better, even after removing the two concentrations that were most obviously beyond the instruments' range of linear response. Statistically, the best-fit quadratic coefficient A_2 was significantly greater than zero for sand for both instruments (Table 4.4), supporting the inference that attenuation is systematically affecting the response of both instruments. The quadratic tendency (i.e., the evidence of attenuation) was stronger and more significant for the Nortek unit, which is sensible given the Nortek's higher frequency.

4.4.8. Acoustic response to mud – less attenuation, but size-effects can be correlated to concentration

For the silty-clay laboratory case and the muddy-floc *in situ* case, the evidence for notable attenuation of acoustic energy was somewhat less clear. On the one hand, there was no significant indication of a non-linear relationship between backscatter and the log of concentration for either individual sediment type over the range of concentrations tested (Figures 4.10 and 4.11). For both the Nortek and SonTek units, the best-fit
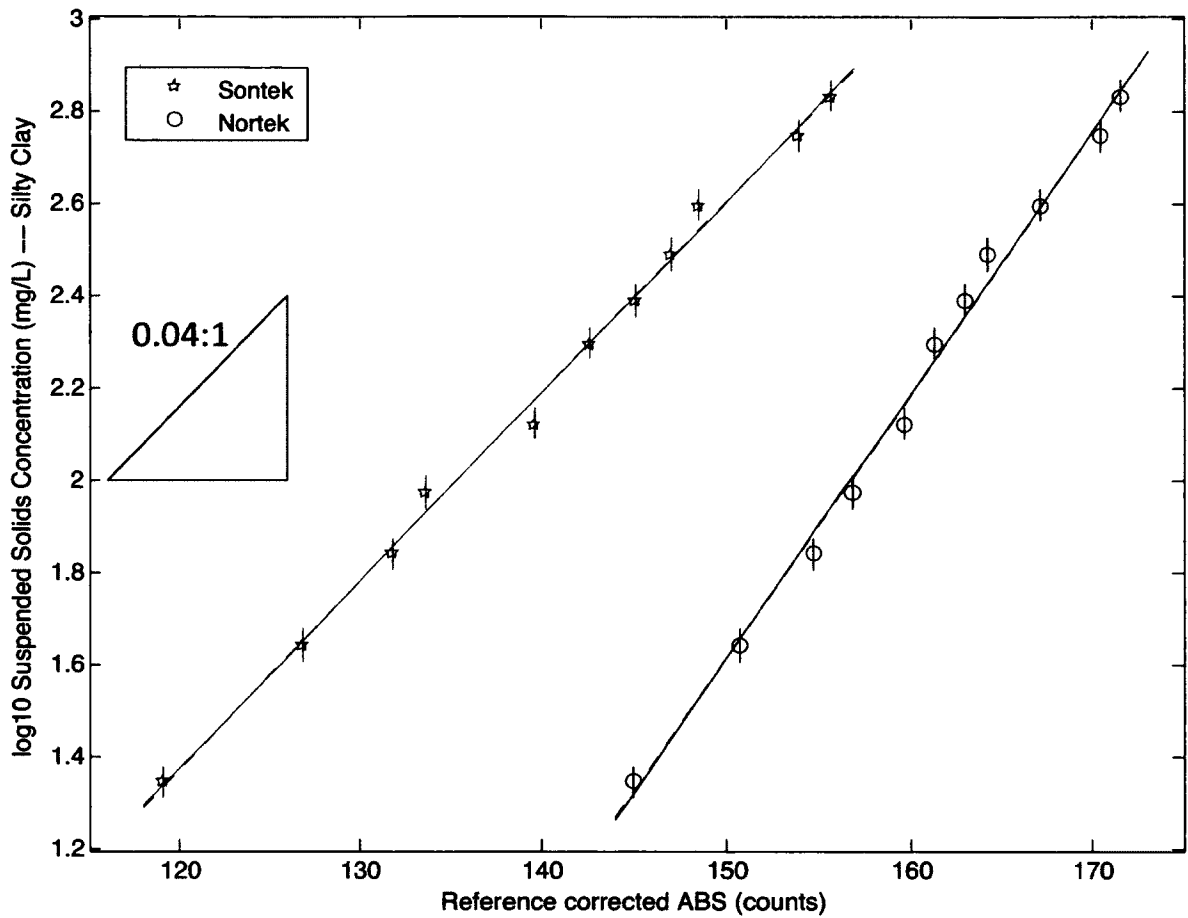
Figure 4.10. Laboratory mud (containing 21.1% silt, 88.9% clay) calibration regressions for log10 suspended sediment concentration versus reference corrected ABS response for Nortek Vector sensor VCH4921 (blue circles) and SonTek ADVOcean sensor B336 (red stars) (see Table 4.2A Run 4). The dashed and solid lines are least-squares quadratic and linear fits, respectively. Error bars are ± the average percent difference between measured and calculated concentrations in Table 4.2 Run 4.

quadratic coefficient A_2 was never significantly different from zero for silty clay or for *in situ* flocs (Table 4.4). Nonetheless, there was still some evidence that differing degrees of attenuation may have been affecting the slopes of the Nortek regressions relative to the slopes of the SonTek regressions as represented by $B_{1\_Nortek}/B_{1\_SonTek}$ for

153
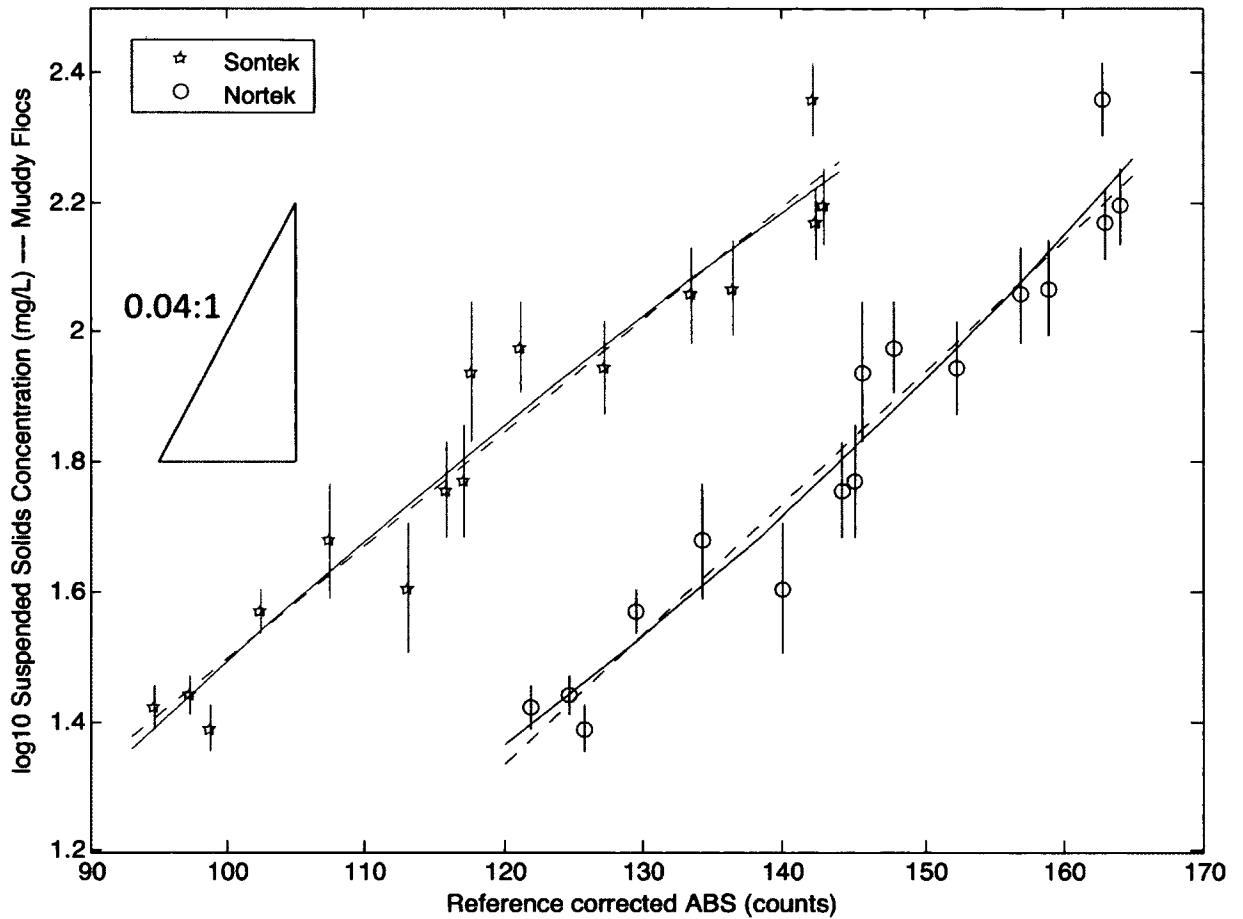
Figure 4.11. *In situ* muddy floc calibration regressions, collected 24 July 2012, for log10 suspended sediment concentration versus reference corrected ABS response for Nortek Vector sensor VCH4854 (blue circles) and SonTek ADVOcean sensor B3084 (red stars) (see Table 4.2A – *In situ*). The dashed and solid lines are least-squares quadratic and linear fits, respectively. Error bars are based on the standard deviation of each ADV burst in counts, translated into TSS using the overall linear fits.

each sediment type (with these B_1 slope values taken from Table 4.4). For *in situ* flocs, $B_{1\_Nortek}/B_{1\_SonTek}$ = 1.16±0.18, while for silty clay and sand flocs, $B_{1\_Nortek}/B_{1\_SonTek}$ = 1.40±0.06 and 1.73±0.10, respectively. This overall trend of the Nortek/SonTek slope

ratio increasing away from 1:1 as the general level of backscatter increases is consistent with the conclusion that at low count values (e.g., relatively low concentrations of floc-like sediment) neither model is significantly affected by attenuation. But at moderate count values, the higher frequency Nortek may be more susceptible to attenuation than the SonTek, even at (reference corrected) Nortek ABS count levels as low as ~160 (corresponding to ~ 100 mg/L of silty clay).

A comparison of the linear-fit slopes (i.e., B_1) for silty-clay versus muddy flocs provides insight into possible variations suspended particle properties during the silty-clay versus muddy floc calibrations. For the silty-clay, laboratory-based calibration, the coefficients for the linear-fit slope, B_1, were still relatively close to the expected value of 0.04, with a

best-fit value of 0.057 for the Nortek Vector ADV and 0.041 for the SonTek ADVOcean Hydra (Table 4.4). This suggests that the size distribution of the silty-clay suspension

remained relatively constant over the course of the entire silty-clay lab calibration. In contrast, for the muddy floc *in situ* calibration, the best-fit values for the slope, B_1 (namely 0.020 for Nortek and 0.017 for SonTek), were only about half that of the value expected for a constant grain size. These anomalous slopes suggest that the *in situ*, floc-like sediment is likely a variable mixture of individual particle sizes and types that change properties and/or proportions in time as the total concentration changes.

155

Furthermore, the fact that B_1 is so much less than 0.04 suggests that particles associated with the higher end of the *in situ* concentration range (~ 150 mg/L) are acoustically more responsive (e.g., larger and/or denser) relative to those associated with the lower end of the *in situ* concentration range (~ 30 mg/L).

4.4.9. Uncertainties associated with lab and field-based estimates of TSS

Error bars associated with the lab-based estimates of total suspended sediment concentration (TSS) (Figures 4.9 and 4.10) are much smaller than those associated with the *in situ* field estimates of TSS (Figure 4.11). In the lab, there were two independent measures of TSS corresponding to each ADV burst (see Methods, Runs 4 and 5): (i) the amount of sediment added to the mixing tank for each burst (corrected for incomplete mixing) and (ii) the corresponding pump sample taken from the tank at the ADV's sampling height. The average absolute percent difference between these two independent estimates of TSS, which was relatively small, was then used to set the size of the error bars in Figures 4.9 and 4.10 (separately for the sand case and for the silty-clay case).

In the field there was only one independent estimate of TSS for each burst, which was the pump sample collected at the height of the ADV sampling volume. Although the filtering process is expected to be about as accurate with field samples as it was with lab samples, the temporal variability of the concentration field itself is much greater for the

in situ case. This is because the physical scale of the dominant turbulent eddies is much larger in the field, and the suspended sediment concentration varies significantly as individual eddies pass the ROSE profiling system. Each ADV burst in the field lasted five minutes (each including thousands of individual count samples), so the standard error on the mean ABS value for each burst is smaller than the symbols on Figure 4.11. However, the corresponding 0.5 liter pump sample lasted only a few seconds. So it represented only a small fraction of the time associated with each ADV burst. The "error" associated with the temporal variability unresolved by pumping is then approximately equal to the relatively large standard deviation of the ADV burst (translated into TSS units via use of the overall regression).

4.4.10. ABS response to mixed sediments – summing sand plus mud

The regressions for the backscatter response to sand and mud individually (Figures 4.9 and 4.10) cannot simply be summed to produce a calibration for the mixed population, because the individual count vs. concentration calibrations are in logspace, not linear space. When adding multiple acoustic sources registered in decibels or ADV counts, the units must first be transformed back to units of acoustic power, added together in (non-logarithmic power units), and then the sum of the acoustic powers must be transformed back to dB or counts. Building from the definition of dB provided in standard acoustic texts (e.g., Hodges, 2010), and utilizing the relation that 1 count = N dB, where N is expected to be about 0.43 (Lohrmann, 2001; SonTek, 2001), it follows that (in the

absence of attenuation) the backscatter in counts due to a mixture of sand plus mud is given by

$$\text{Counts}_{\_\text{sand+mud}} = (10/N)\,\log_{10}\left\{10^{[(N/10)\,\text{Counts\_sand}]} + 10^{[(N/10)\,\text{Counts\_mud}]}\right\}.$$

In the above equation, $\text{Counts}_{\_\text{sand}}$ and $\text{Counts}_{\_\text{mud}}$ are the expected backscatter values in counts for the component concentrations of sand and mud based on their individual calibrations.

The above relation for predicting the total counts expected in backscatter registered from ADVs for varying proportions of sand and mud in mixed sediment is relatively sensitive to the count-to-dB conversion parameter N. The literature value of $N \approx 0.43$ for ADVs is only an approximate value; for example, Lorhmann (2001) suggests that N can vary from 0.40 to 0.47. Fortunately, the available low attenuation calibration plots of $\log_{10}$ TSS versus counts for constant grain size (i.e., the laboratory silty-clay case in Figure 4.10) can be used to derive N directly. Since Counts $\sim (10/N)\,\log_{10}$ P, and the linear regressions in Table 4.4 are fits to $\log_{10}$ TSS $\sim B_1$ Counts, it follows that for constant grain size, relatively low attenuation cases (for which P is proportional to TSS), $N = 10\,B_1$. The laboratory silty-clay case in Table 4.4 then indicates that $N \approx 0.57$ and $N \approx 0.41$ for the Nortek and SonTek models, respectively.

Figure 4.12 displays an application of the above equation and N values to the mixed sediment calibration data (Run 6). The horizontal dashed lines are the count values expected from the mud alone and were set equal to the count values recorded before any sand was added to the tank. The sloping dashed lines indicate the calibration curves used in each case for sand component, initially defined by the lowest two "sand only" concentrations in Figure 4.9 (Run 5). (The other sand concentrations in Figure 4.9 were far higher than the sand concentrations used in the mixed calibration.) This initial choice of sand calibration (based on data from Run 5) worked well for the SonTek unit in Run 6, but not for the Nortek unit in Run 6. This is likely because the same SonTek ADV serial number was used in both Runs 5 and 6 (see Table 4.1), but different Nortek serial numbers were used. It appears that the original offset chosen for reference unit correction (based only on mud from Runs 1 through 3) was not accurate enough to "correct" the sand calibration from Run 5 for use in Run 6. The limitation in the reference adjustment for application to sand can be seen in Figure 4.7, where the two lowest sand calibration points fall an average of 5.1 counts to the right of the best-fit line. An additional offset correction of -5.1 counts was then defined to further correct the Nortek sand calibration for use in above equation for Counts $_{sand+mud}$. This further adjusted calibration worked reasonably well, and the ultimate prediction of ABS for mixed sediment was consistently good to within about 3 counts or less (Figure 4.12).
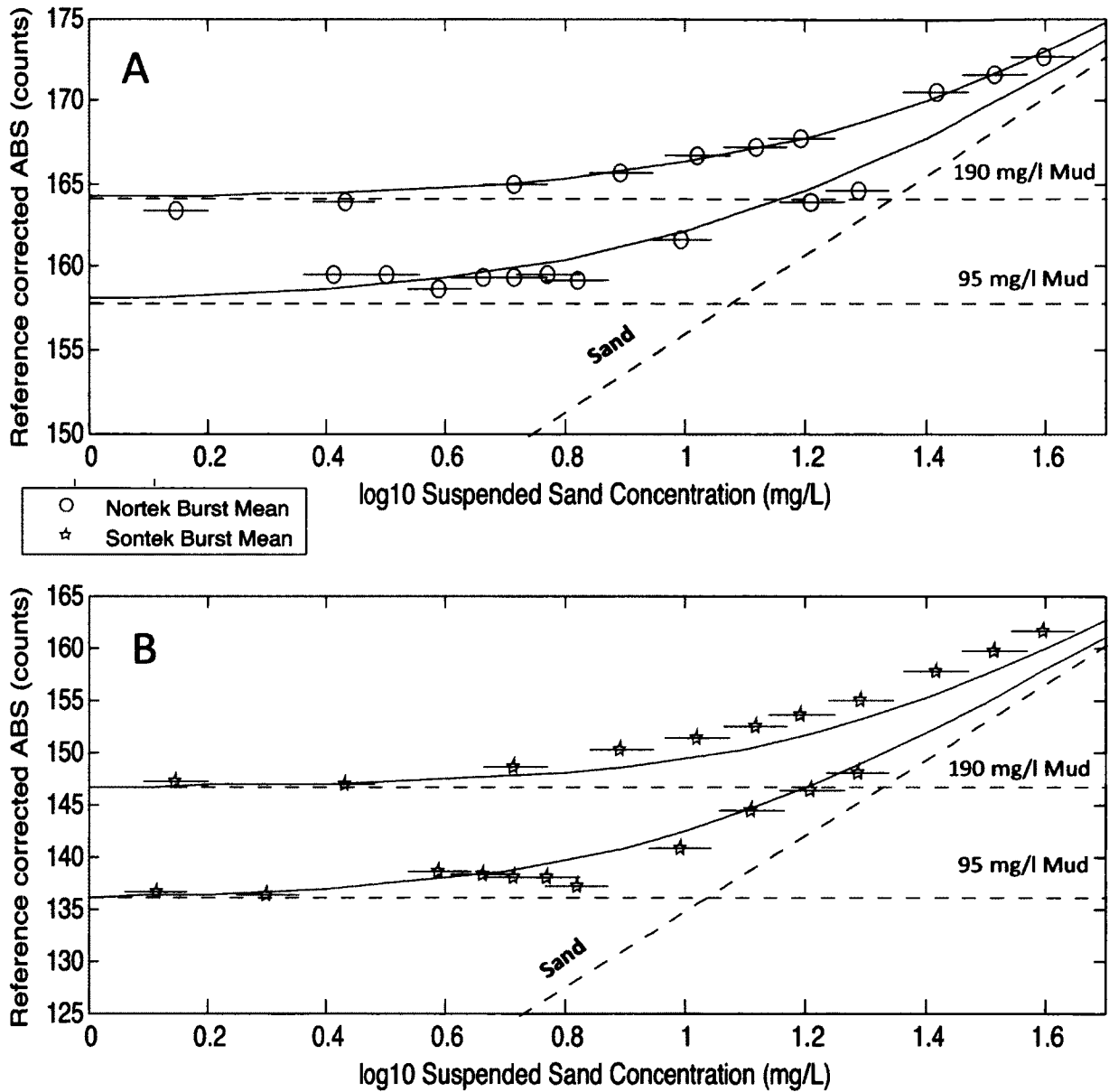
Figure 4.12. Addition of quartz sand (150-180 μm) to two silty clay background concentrations of 95 and 190 mg/l, respectively. Dashed lines represent expected response from mud and sand concentrations alone. Data points represent measured ABS responses to a series of sand concentrations added to mud (see Table 4.2B). Solid lines represent a logarithmic summation of the separate expected mud and sand responses (see text for details). A) Nortek Vector sensor VCH4921 (blue circles). B) SonTek ADVOcean sensor B336 (red stars). In each case, error bars on sand concentration are set equal to the percent uncertainty determined for sand in Figure 4.9.

4.5 Summary and conclusions

The acoustic backscatter (ABS) signal registered by acoustic Doppler velocimeters (ADVs) is often empirically calibrated to represent suspended sediment concentration. However, little work has been done to date to quantify how well a given calibration works if determined for one ADV and applied to another relatively similar ADV. This study compared ABS responses to sand, mud, and mixed sediment in the lab and *in situ* among ten relatively similar ADV units: five 6-MHz Nortek Vector ADVs and five 5-MHz SonTek ADVOcean-Hydras. This approach allowed for an examination of the relative roles played by inter-vendor, intra-vendor, and sediment variability in determining the ABS response of these ADVs.

ABS measurements in counts (a unit proportional to decibels) as registered by the Nortek and SonTek instruments were compared, and sediment type was found to systematically affect ABS response for all of the ADVs tested. ABS response to ~ 100 mg/L of sediment was strongest for sand, then for mixed sand and mud, then for silty clay, and weakest for *in situ* muddy flocs. If the ABS response in count units had been consistent across all of the instruments (i.e., if there had been no intra-vendor variability), then all of the SonTek vs. Nortek ABS data would have fallen on a single 1:1 line. If all the SonTeks and all the Norteks had been separately consistent (i.e., if there had been no intra-vendor variability), then all the ABS data would still have all

followed a single (albeit non-1:1) line. However, the initial count values did not lie along a single line of any kind. Rather, clear offsets were apparent among the various instruments within both vendors. These clear offsets suggested that intra-vendor inconsistency might be significantly reduced by defining a reference unit for each vendor, and then subtracting or adding a constant number of counts to the output of each of the other units to increase consistency with that reference unit.

Before correcting for intra-vendor effects, the Nortek ADV Vectors tended to have a slightly more consistent ABS response among units of the same model than was the case for the SonTek ADVOcean-Hydras. Among either the Nortek or the SonTek units, the pre-correction response was more similar for units that had been purchased together with consecutive manufacturer's serial numbers. In the absence of subsequent incidents requiring significant repair or modification, units manufactured together maintained remarkably consistent offsets (identical to within ~ 1 count) even seven years or longer after purchase. One of the instruments that had been repaired, however, had the most anomalous ABS offset of all, suggesting that different parts manufactured separately can significantly change a single unit's reference power. Anti-fouling paint made a small but notable effect on the count offset for both manufacturers, reducing response on average by about 3 counts. This would cause a 1 to 4% negative bias in the total counts measured, depending on the suspended sediment size distribution and concentration, leading to an underestimation of the SPM concentration.

A stock solution of mud derived from bed samples collected in the York River estuary was used to inter-compare the response of all ten ADVs to similar ~100 mg/L sediment suspensions. One of the ADVs from each vendor was defined as a reference unit, and the offsets in counts of the other four ADVs from each vendor were adjusted (by +5 to − 33 counts) so that the backscatter registered for the stock solution was made consistent. The offset corrections derived from the 2012 mud stock solution were then applied to a separately acquired and diverse group of muddy and sandy sediments, and the offset corrections did reasonably well. The adjusted ABS counts for all the SonTek vs. Nortek ADVs then largely lay along a single curve, within a spread of about ± 5 counts. The common ABS curve did not have a constant 1:1 slope, however. Although the SonTek vs. Nortek ABS curve began with a slope of ~1:1 at low backscatter, at higher ABS, the response of the 5-MHz SonTek ADVs increased more rapidly than that of the 6-MHz Norteks, suggesting that the backscatter registered by the higher frequency Norteks was likely decreased more than the SonTeks due to a higher attenuation at 6 MHz.

Plots of the $\log_{10}$ of concentration ($\log_{10}$ C) vs. ABS clarified overall trends in attenuation and acoustic response to grain size. For both the SonTeks and Norteks, the backscatter registered in response to the two highest concentrations of sand (~ 0.8 to 1 gram/L), clearly deviated from the trend associated with the lower sand concentrations. Even after removing these two highest, obviously attenuated readings, the remaining

163

sand calibration for both instruments (for concentrations from ~10 to 600 mg/L) was still significantly quadratic with values for high concentration mixture registering low relative to trend line obtained for low concentrations. In contrast, mud calibrations between ABS and $\log_{10} C$ (from ~20 to 700 mg/L) were not quadratic, providing less clear evidence of ABS attenuation. For silty mud, the slope of the lab calibration of $\log_{10} C$ vs. ABS was close to the theoretical value of ~0.4 as expected for a single, constant grain-size suspension, suggesting that the effective grain-size in the lab did not change with concentration. In the field, however, the calibration slope of $\log_{10} C$ vs. ABS for *in situ* measurements of muddy flocs was only about ~0.2, which suggested a significant change in particle properties (such as grain size) with increasing C, and that more acoustically responsive particles were suspended at higher concentrations.

When calculating predicted ABS in counts in response to varying proportions of different grain sizes, the counts must first be transformed back to units of acoustic power and added together in non-logarithmic units. Then the sum of the acoustic powers must be transformed back to logarithmic counts. This transformation procedure for combining predicted counts for multiple grain sizes was found to be sensitive to the ADV count-to-dB conversion parameter and also to instrument-specific calibrations for the component grain sizes. Nonetheless, with knowledge of the count-to-dB conversion parameter and access to grain-size specific ABS calibrations, it is indeed possible to use

component calibrations to predict the expected acoustic response of both SonTek and Nortek ADVs to a mixed grain-size population.

4.6 Acknowledgements

4.7 References

Baeye, M., Fettweis M., Voulgaris G., and Van Lanker, V., 2012. Sediment mobility in response to tidal and wind-driven flows along the Belgain shelf, southern North Sea. Ocean Dynamics (Springer). pp.33-50

Battisto, G.M., C.T. Friedrichs, H.C. Miller and D.T. Resio, 1999. Response of OBS to mixed grain-size suspensions during SandyDuck '97. In: N.C. Kraus and W.G. McDougal (eds.), Coastal Sediments 1999, American Society of Civil Engineers, Reston, VA, p. 297-312.

Cartwright, G.M., C.T. Friedrichs, P.J. Dickhudt, T. Gass, and F.H. Farmer. 2009. Using the acoustic Doppler velocimeter (ADV) in the MUDBED real-time observing system. Proceedings, OCEANS 2009 MTS/IEEE, CD ISBN: 978-0-933957-38-1, 9 p.

Cartwright, G.M., C.T. Friedrichs, and P.D. Panetta. 2012. Dual use of a sediment mixing tank for calibrating acoustic backscatter and direct Doppler measurement of settling velocity. Submitted to: Oceans 2012, MTS/IEEE, Virginia Beach, VA, 14-19 Oct.

Cartwright, G.M., C.T. Friedrichs, and S.J. Smith, 2013. Sediment settling velocity from ADVs and settling tubes: agreement over a range of particle types and hydrodynamic conditions. Submitted to Geo-Marine Letters.

Dalrymple, R.W., Zaitlin, B.A., & Boyd, R. (1992). Estuarine facies models: conceptual basis and stratigraphic implications: perspective. Journal of Sedimentary Research, 62(6): 1130-1146.

Flammer, G. H., 1962. Ultrasonic Measurement of suspended sediment. Geological Survey bulletin 1141-A. United States Government Printing Office, Washington. 56 p.

Friedrichs, C.T., G.M. Cartwright, and P.J. Dickhudt. 2008. Quantifying benthic exchange of fine sediment via continuous, non-invasive measurements of settling velocity and bed erodibility. Oceanography, 21(4): 168-172.

Fugate, D.C., and C.T. Friedrichs. 2002. Determining concentration and fall velocity of estuarine particle populations using ADV, OBS and LISST. Continental Shelf Research, 22: 1867-1886.

Fugate, D.C., and C.T. Friedrichs. 2003. Versatility of the SonTek ADV: measurements of sediment fall velocity, sediment concentration, and TKE production from wave contaminated velocity data. In: R.A. Davis et al. (eds.), Coastal Sediments 2003, ASCE, CD ISBN: 978-981-238-422-5, 14 p.

Gartner, J.W. 2004. Estimating suspended solids concentrations from backscatter intensity measured by acoustic Doppler current profiler in San Francisco Bay. Marine Geology, 211 : 169–187.

Gray, J.R, and Gartner, J.W., 2009. Technological advances in suspended-sediment surrogate monitoring. Water Resources Research, 45. Doi:10.1029/2008WR007063.

Green, M.O., Vincent, C.E., Trembanis, A.C., 2004. Suspension of coarse and fine sand on a wae-dominated shoreface, with implications for the development of rippled scour depressions. Continental Sherl Research, 24: 317-335

Hanes, D.M., 2011. On the possibility of single-frequency acoustic measurement of sand and clay concentrations in uniform suspensions. Continental Shelf Research, doi:10.1016/j.csr.2011.10.008.

Hanes, D.M., Vincent, C.E., Huntley, D.A., Clarke, T.L., 1988. Acoustic measurements of suspended sand concentration in the C2S2 experiment at Stanhope Lane, Prince Edward Island. Marine Geology 81, 185–196.

Hodges, R. P., 2010. Underwater Acoustics: Analysis, Design, and Performance of Sonar. Wiley, 353 p.

Lohrmann, A., 2001. Monitoring sediment concentration with acoustic backscattering instruments. Nortek Technical note no 3. www.nortek-as.com. 5 p.

MacDonald, I.T., C.E. Vincent, P.D. Thorne, and B.D. Moate. 2012. Acoustic scattering from a suspension of flocculated sediments. Submitted to: Journal of Geophysical Research.

Moate, B.D. and Thorne, P.D., 2012. Interpreting acoustic backscatter from suspended sediments of different and mixed mineralogical composition. Continental Shelf Research, 46: 67-82

Rehman and Vincent, 1990. Underwater acoustic measurement of suspended sediments: the calibration of a high-frequency acoustic backscatter sensor. Geol. Bull. Univ. Peshawar, 23: 161-173.

SonTek, 2001. Acoustic Doppler Velocimeter principles of operation (September 1, 2001). SonTek/YSI Technical Notes, San Diego, CA. 14 p.

Thorne, P.D. and Campbell, S.C., 1992. Backscattering by suspension of spheres. Journal of the Acoustical Society of America. 92: 978-986.

Thorne, P.D., and Hanes, D.M., 2002. A review of acoustic measurement of small-scale sediment processes. Continental Shelf Research, 22: 603-632.

Thorne, P.D., P.J. Hardcastle, and R.L. Soulsby. 1993. Analysis of Acoustic Measurements of Suspended Sediments. Journal of Geophysical Research, 98, C1: 899-910.

Thorne, P.D. and Hay, A.E., 2012. Introduction to the Special Issue of Continental Shelf Research on 'The application of acoustic to sediment transport processes'. Continental Shelf Research, 46:1.

Topping, D.J, Wright, S.A, Melis, T.S, and Rubin, D.M., 2006. High-resolution monitoring of suspended-sediment concentration and grain size in the Colorado river using laser-diffraction instruments and a three-frequency acoustic system. USGS Grand Canyon Monitoring and Research Center, 442.00 RES-3.20 T675hr7 Downloaded from www.gcmrc.gov/publications/library.aspx

Traykovski, P., Geyer, W.R., Irish, J.D. and Lynch, J.F., 2000. The role of wave-induced density-driven fluid mud flows for cross-shelf transport on the Eel River continental shelf. Continental Shelf Research 20: 2113-2140.

VanderWerf, J.J., Doucette, J.S., O'Donoghue, T., Ribberink, J.S., 2007. Detailed measurements of velocities and suspended sand concentrations over full-scale ripples in regular oscillatory flow. J. Geophys. Res. 112, F02012.

Vincent, C.E., 2007. Measuring suspended sand concentration using acoustic backscatter: a critical look at the errors and uncertainties. Coastal and Shelf Sediment Transport. Geological Society of London, Special Publications, 274: 7-15

Voulgaris, G., and S.T. Meyers. 2004. Temporal Variability of Hydrodynamics, Sediment Concentration and Sediment Settling in a Tidal Creek. Continental Shelf Research, 24: 1659-1683.

Vousdoukas, M.I., S. Aleksiadis, C. Grenz, and R. Verney. 2011. Comparisons of acoustic and optical sensors for suspended sediment concentration measurements under non-homogeneous solutions. Journal of Coastal Research, SI 64 (Proceedings of the 11th International Coastal Symposium): 160-164. Szczecin, Poland.

CHAPTER 5

In Situ Characterization of Estuarine Suspended in the Presence of Muddy Flocs and Pellets.*

By Grace M. Cartwright, Carl T. Friedrichs, and Lawrence P. Sanford

5.1 Abstract

Observations are presented from a benthic observatory in the middle reaches of the York River estuary, VA, USA, that show evidence for both muddy flocs and pellets in the lower 1 m of the water column. This study combines *in situ* time series estimates of (i) volume concentration and particle size distribution from a Laser *In Situ* Scattering Transmisometer (LISST) (for 2.5-500 μm) and a high-definition particle camera (for 20 μm to 20 mm), and (ii) water velocity, turbulent stress, mass concentration and settling velocity derived from an Acoustic Doppler Velocimeter (ADV). Mass concentration, mass settling velocity and the abundant 88 μm size class are in phase with velocity and stress, consistent with suspension of relatively dense, rapidly settling and resilient ~90 μm pellets. Volume concentration of the abundant 280 μm class peaks well after stress and velocity begin to decrease, consistent with the formation of lower density, slowly settling and fragile ~300 μm flocs.

5.2 Introduction

At moderate sediment concentrations (i.e., neglecting sediment-induced convection or hindered settling), the settling velocity of a mud particle of known diameter (D) and density (ρ) can be reasonably predicted based on well-established relationships between the force of gravity acting on the particle and the opposing fluid resistance, such that the fall velocity, $w_s \sim D\rho$ (e.g., Dyer, 1984). The much greater challenge is in predicting D and ρ. If natural mud settled based on the D and ρ of its component mineral grains (typical median mineral grain ~5-10 μm in muddy coastal environments), then we would expect $w_s <$ to $<< 0.1$ mm/s. In fact, w_s for estuarine/coastal mud in relatively turbid ($c \approx O(100)$ mg/liter) but biologically active settings is usually observed to be much higher, on the order of 0.1 to 10 mm/s or more (Andersen, 2001; Sanford et al.,

170

2005). This is a result of the packaging of individual grains into much larger particles, namely flocs and pellets.
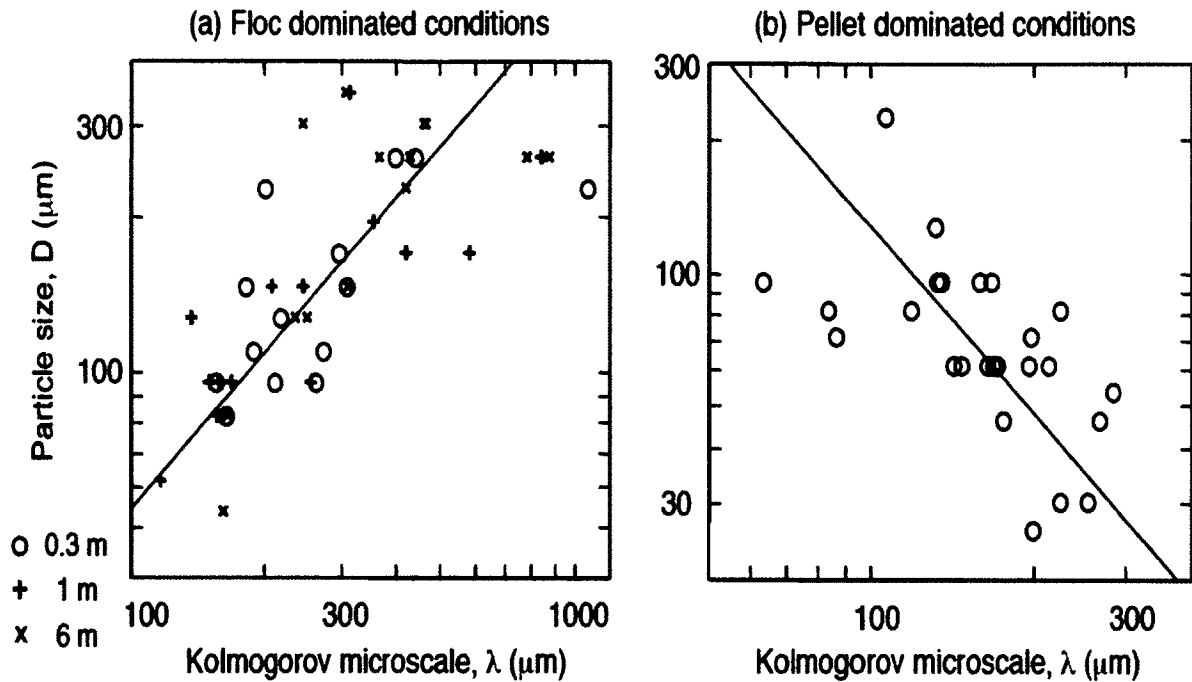
Figure 5.1. As turbulence decreases (i.e., as λ increases) (a) D increases under floc-dominated conditions, but (b) D decreases under pellet-dominated conditions. LISST observations from the York River Estuary and Chesapeake Bay, modified from Fugate & Friedrichs (2003).

Muddy flocs have open structures and form when moderate turbulent shear and/or differential settling brings smaller mud particles close enough together for molecular attraction and/or polymeric binding to create physical adhesion. Significant progress has been made in the last decade in advancing theoretical and conceptual arguments regarding the controls on floc D and ρ, the two quantities which together determine floc settling velocity (e.g., Hill et al., 2001; Fugate & Friedrichs, 2002; Winterwerp, 2002; Son and Hsu, 2008; Pejrup & Mikkelsen, 2010).

For estuarine and coastal environments, recent parameterizations (e.g., Winterwerp et al., 2006) suggest that the median D of muddy flocs should change with time, concentration and velocity shear, adjusting towards an equilibrium size constrained by the smallest turbulence length scale, λ, with λ (the Kolmogorov microscale) inversely related to turbulent intensity (Fig. 5.1a). When turbulence is weak and λ large, floc size may respond instead to self-induced local shear generated by particle settling (Hill et al., 2001). Winterwerp et al. (2006) suggest flocs will tend to be near their equilibrium size of $D \approx O(\lambda)$ only if the floc adjustment time scale, T_f, is less than the amount of time the floc is exposed to a given λ. Otherwise, the median floc D will lag behind changes in λ. Winterwerp et al. (2006) further suggest that T_f is likely to increase (i.e., the sensitivity of D to turbulence decreases) with greater organic content and/or mineral cohesion, and T_f will decrease with greater suspended sediment concentration C and/or turbulence, assuming c isn't large enough to affect λ. Once D is known, ρ as a function of D can be estimated for flocs using fractal theory tuned by observations (Winterwerp et al., 2006). Parameterizations suggest that more porous flocs tend to occur as organic content increases, floc size increases, and/or primary component particle size decreases. As flocs grow, increasing D usually overwhelms decreasing ρ in determining w_s. Thus, (in the absence of very high organic content) w_s for muddy flocs generally increases with floc size, but with a much weaker than quadratic dependence on size.

Muddy pellets, in contrast, are significantly denser than flocs and are formed by mechanical compaction. This compaction commonly occurs during processing by deposit- and suspension-feeding benthic organisms (Taghon et al., 1984; Wheatcroft et al., 2007). Pellets are also formed by zooplankton, though often with higher organic content (and lower density) than benthic pellets. The sediment surface in moderately turbid ($C \approx O(100)$ mg/liter) temperate estuaries and shelves with high organic loadings is commonly 10 to 50% or more biogenetic pellets (Zabawa, 1978; Andersen, 2001; Drake et al., 2002). Biogenic pellets can have D ranging from 10s to 1000s of μm.

Pellet-like muddy aggregates may also be formed abioticly, for example through compaction of the sediment bed during consolidation, followed by exposure and remobilization during energetic events or dredging (Smith & Friedrichs, 2010). Interestingly, recent laboratory experiments (Schieber & Yawar, 2009) and field erosion tests (Debnath et al., 2007) have shown significant bedload transport of cohesive sediments. Such transport is possible only if the settling speed of the transported particles is high and their structure is robust, i.e., if they are relatively tightly packed aggregates. At higher stresses, the fraction transported as bedload in the observations of Debnath et al. (2007) decreased, presumably as the aggregates were suspended. For simplicity, in this paper we combine biogenic pellets and bed aggregates into a single particle class distinguished by its behavior rather than its origin, and refer to them all as pellets.

Although the size distribution of the constituent mineral grains within flocs and pellets may be nearly identical (Andersen, 2001), w_s for muddy pellets is typically much higher than that for similar diameter flocs because of pellets' higher ρ (Edelveng & Austen, 1997). Thus the effective settling velocity of the total suspended mud population can be notably increased by the presence of pellets, even if flocs form the majority of the particle volume in suspension (Wheatcroft & Butman, 1997). Furthermore, the expected relationship between w_s and energetic turbulence may be opposite to that associated with flocs (Fig. 5.1b), since greater bed stress may suspend increasingly larger, robust pellets that readily resist turbulent disruption (Andersen, 2001; Fugate & Friedrichs, 2003).

In this paper, we present observations from a site in the middle reaches of the York River, VA, USA, that has been inferred to seasonally alternate between dominance by muddy flocs or pellets depending on system-scale circulation (Dickhut et al., 2009). In the data presented here, we present evidence for the simultaneous presence of both particle types in the lower 1 m of the water column at this site. Combining time series estimates of volume concentration and particle size distribution from a LISST (2.5-500 µm) and a particle camera (20-20,000 µm), and ADV-derived turbulent stress, mass concentration, and settling velocity, we demonstrate changes in particle properties and behavior that are consistent with the alternating influence of flocs and pellets within individual tidal cycles.
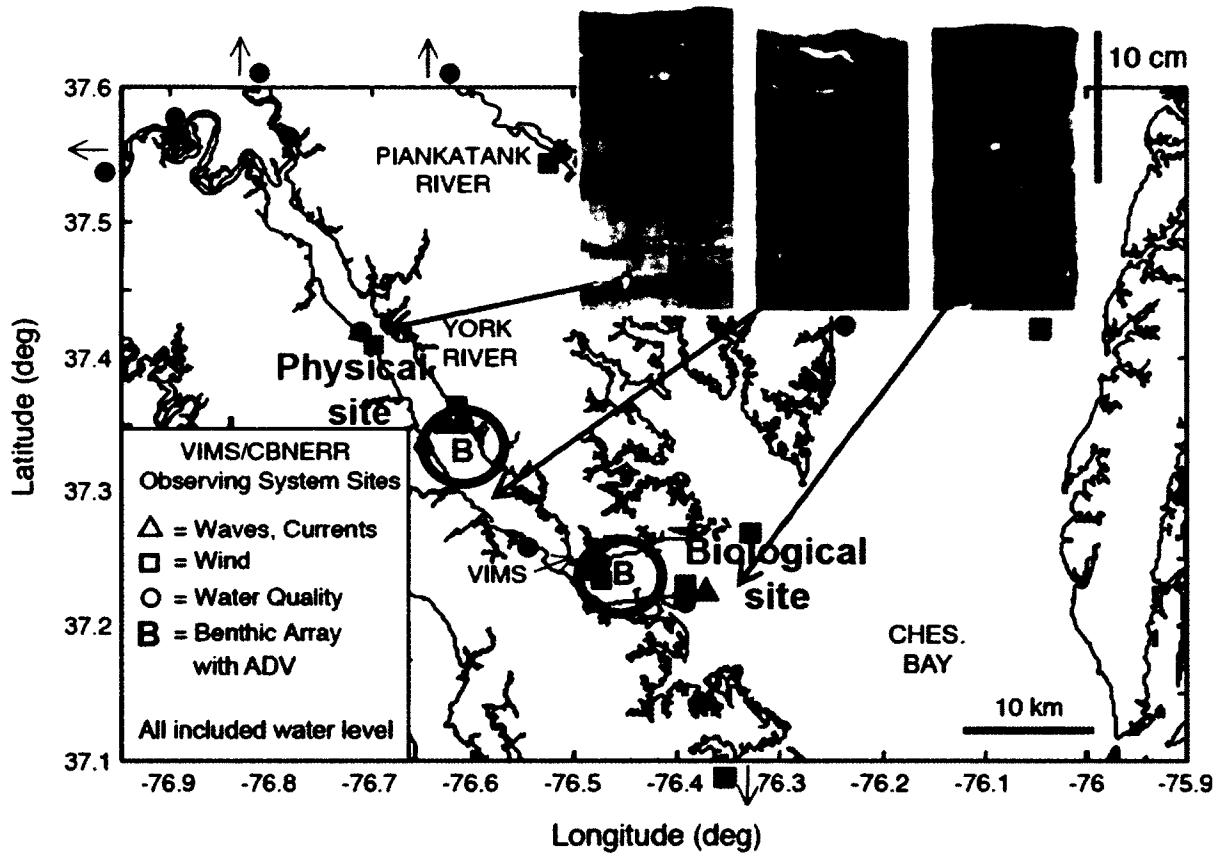
Figure 5.2. Location of MUDBED benthic tripods (indicated by "B") within the VIMS/CBNERR Observing system. X-radiograph images from cores collected along the York River estuary are courtesy of L. Schaffner. The "physical site", in the Clay Bank area, is the study site for this paper.

5.3 Study Area

The study site (Fig. 5.2) is one of two National Science Foundation Multi-Disciplinary

Benthic Exchange Dynamics (MUDBED) array locations (Friedrichs et al., 2008)

nested within the much larger VIMS/CBNERR observing system. It is located in the

Clay Bank region of the York River estuary, a tidal tributary of the Chesapeake Bay.

The tripod was located in the 5-m deep secondary channel of the York where the tidal velocity a meter above the bed is O(50 cm/s), suspended sediment concentration is O(100 mg/L), and the seabed is >75% mud. The intensity of sediment transport in the central York favors abundant pellet-producing deposit feeders and extensive sediment flocculation (Schaffner et al., 2001). Rodriguez-Calderon (2010) documented widespread occurrence of resilient muddy pellets in the study area, seasonally accounting for up to 30% of the upper seabed.
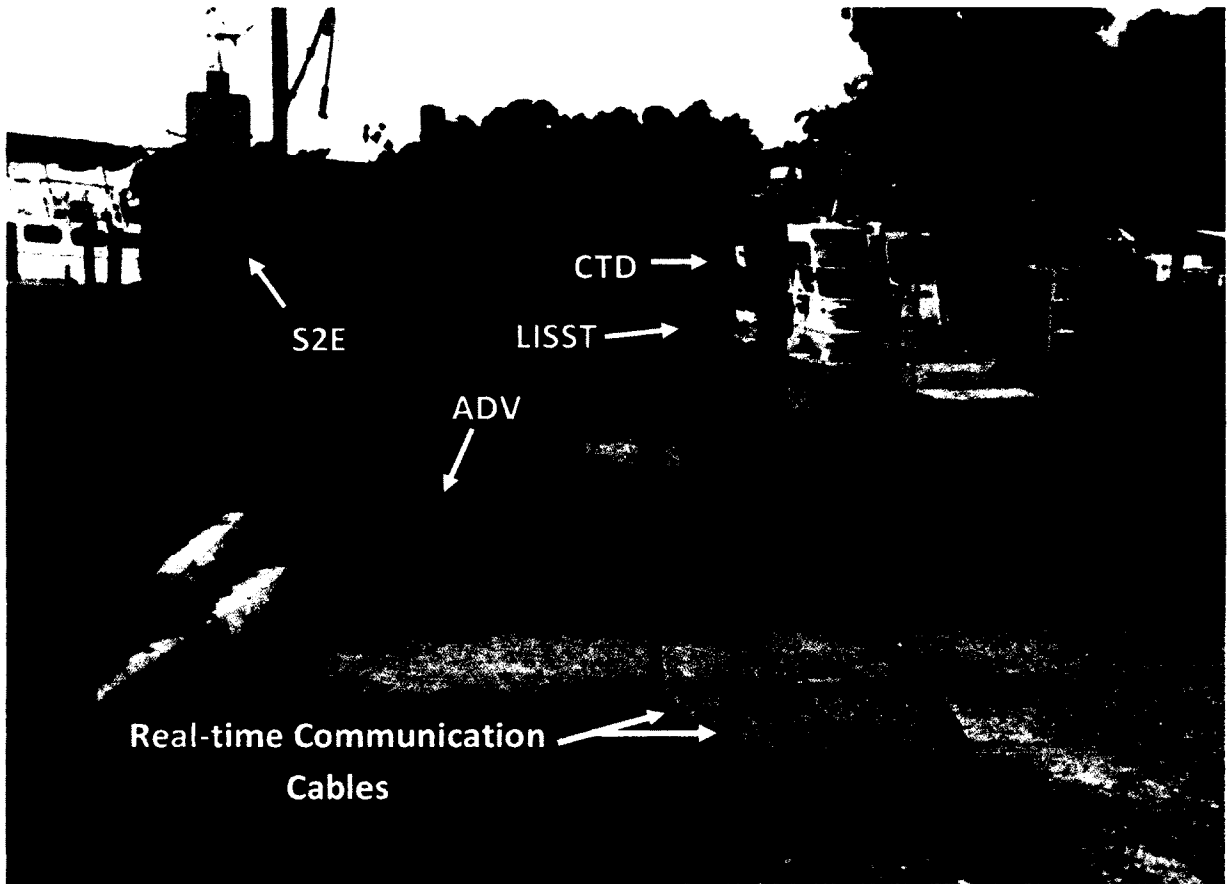
Figure 5.3. The tripod in the foreground shows bio-fouling after having been deployed for 3 months. A cleaned and fully equipped tripod on the R/V Elis Olsson (background) is ready for deployment.

5.4 Methods

ADV, LISST and CTD Benthic Tripod

A 1-m tall tripod equipped with an ADV, a LISST, a Conductivity-Temperature-Depth sensor (CTD) and a Serial to Ethernet convertor (S2E) (Fig. 5.3) was deployed on July 22, 2009 and retrieved on October 21, 2009. The ADV and LISST data were passed through the S2E and transmitted back to VIMS real-time (Cartwright et al., 2009). Communication problems prevented ADV data from being recorded before July 27. A 25-hour period starting July 28, was chosen in an effort to avoid interference by bio-fouling on the LISST (see Fig. 5.3) and to coincide with the deployment of the benthic camera. The ADV (a SonTek 5 MHz Ocean probe) was mounted in a downward looking position such that its sampling volume (18 cm below the sensor) was 35 cm above the seabed (cmab). Two minute bursts of 10 Hz data were collected every 15 min. A Sequoia LISST-100X (2.5 to 500 μm particle size distribution range) was mounted horizontally, 85 cmab. A LISST burst, collected over 100 seconds once every 15 min, consists of 100 records that are each 10 measurement averages (i.e., 1000 total measurements contribute to each burst average).

"Calibration cruises" consisting of 6 hourly profiles (bracketing flood or ebb tide) were conducted along the same isobath, within ~100 m, of almost every tripod deployed over the duration of the MUDBED experiment. The profiler was equipped with an identical model ADV, LISST and CTD along with a high capacity submersible pump. A

regression curve derived from the hundreds of pump samples of total suspended solids (TSS) collected during these calibration cruises was used to convert ADV backscatter to suspended sediment mass concentration (Cartwright et al., 2009).

Settling velocity was estimated from the ADV tripod data by assuming an approximate local balance between downward settling by gravity and upward turbulent transport by Reynolds flux, i.e., $<C>w_s = <C'w'>$, where C is suspended mass concentration, w_s is settling velocity, w is vertical water velocity, primes indicate within burst fluctuations, and $<\ >$ indicates a burst average (Fugate & Friedrichs, 2002). Data were fit to this relation in two ways, one utilizing the slope of a regression between $<C>$ and $<C'w'>$ over 12 or more bursts, and the other by calculating $<C'w'>$ divided by ($<C> - C_{bkgd}$) for each burst, where C_{bkgd} is an estimate of the non-settling background concentration present throughout the entire time series.

RIPSCam Underwater Particle Camera System

A Remote *In situ* Particle Settling Camera (RIPSCam), developed specifically for the MUDBED project (Fig. 5.4), was deployed on a bottom frame ~100 m from the ADV tripod site in June 2009. A surface buoy was anchored nearby to supply solar power to the RIPSCam batteries and to transmit data to and from a land-based ftp server via cell modem. The buoy and camera were connected by an electro-optical underwater Ethernet cable. The on-bottom package contained a Canon EOS XSi 12 MP digital SLR camera with a pair of red LED line lights connected to a strobe controller to provide a

focused, controllably flashed light sheet. The light sheet illuminated the center of a clear acrylic 7-cm ID vertical tube, approximately 50 cm below the tube opening at the top of the bottom frame, which was approximately 0.9 mab. A pneumatic knife valve opened and closed across the top of the tube to admit external particles. The camera, the strobes, and the knife valve were controlled by an internal micro-computer running Windows XP. The computer also collected and stored the particle images, communicated with the surface buoy, and controlled sampling and remote communications. Sampling was initiated at approximately the top of each hour.

During the first 7 weeks of the deployment, the knife valve was opened several minutes before sampling and then closed just prior to sampling to limit internal motion in the tube. During sampling, a 2-sec time exposure image was first collected with the strobes flashed at 0.35-sec intervals. This was followed by a sequence of 5 flash exposures at 1-sec intervals. Each image frame was 21 mm high, 31.5 mm wide, and the depth of focus was approximately 1 mm. Calcium hypochlorite hydrated pellets in a mesh bag were added to the bottom of the settling tube (approximately 0.25 m below the sample section) to limit biofouling. During instrument servicing on July 28, the knife valve was found to be damaged and was left in the open position for the remaining 4 weeks of the deployment.

Side View

Acrylic settling tube
with valves/pump

Schedule 80 reducing
cross, 8" x 4", with
watertight endcaps and
O-ring seals around
settling tube

Bulkhead connector 1 -
Power from solar panels to
batteries, signal from camera
to transmitter (serial and ethernet)

LED arrays

Camera and computer
on backplane

Two 12 VDC battery packs,
trickle charged from solar
panels, power out to camera
and computer, LED arrays (?),
external valves/pump

Bulkhead connector 2 -
Switched power to
external valves/pump

Overhead View

Two 12 VDC battery packs

LED arrays

Camera and computer
on backplane

Bulkhead
connectors

Figure 5.4. Side and overhead schematic views of the central section of the RIPSCam (left). RIPSCam bottom frame ready for deployment on March 19, 2009 (right).

Data presented here are from the first 3 days of the final RIPSCam deployment during MUDBED, immediately following the July 28 servicing. Analysis to date has been limited to particle size distribution and volume concentration estimates using Matlab software shared by O. Mikkelsen and described in Mikkelsen et al. (2004). Settling velocity estimates will require further development of software to remove background fluid motion.

5.5 Results and Discussion

Figure 5.5a displays suspended sediment mass concentration as determined from ADV backscatter, while Fig. 5.5b displays volume concentration as provided by the LISST and as determined from image analysis. The volume concentration as measured by the LISST is a relative value because our unit's factory settings have not been lab tested by our group. The volume concentration measured by the RIPScam is also somewhat uncertain because the exact focal depth of the images is unknown (1 mm was used). In Fig. 6b the RIPScam output for volume concentration was divided by a factor of 10 in order to be easily seen on the same plot with the LISST results. It should also be kept in mind that the LISST misses the larger end of the particle spectrum, while the RIPScam misses the smaller end. Our future work will include lab calibration of our LISST and cross-calibration of the two instruments based on matching of the overlapping portion of
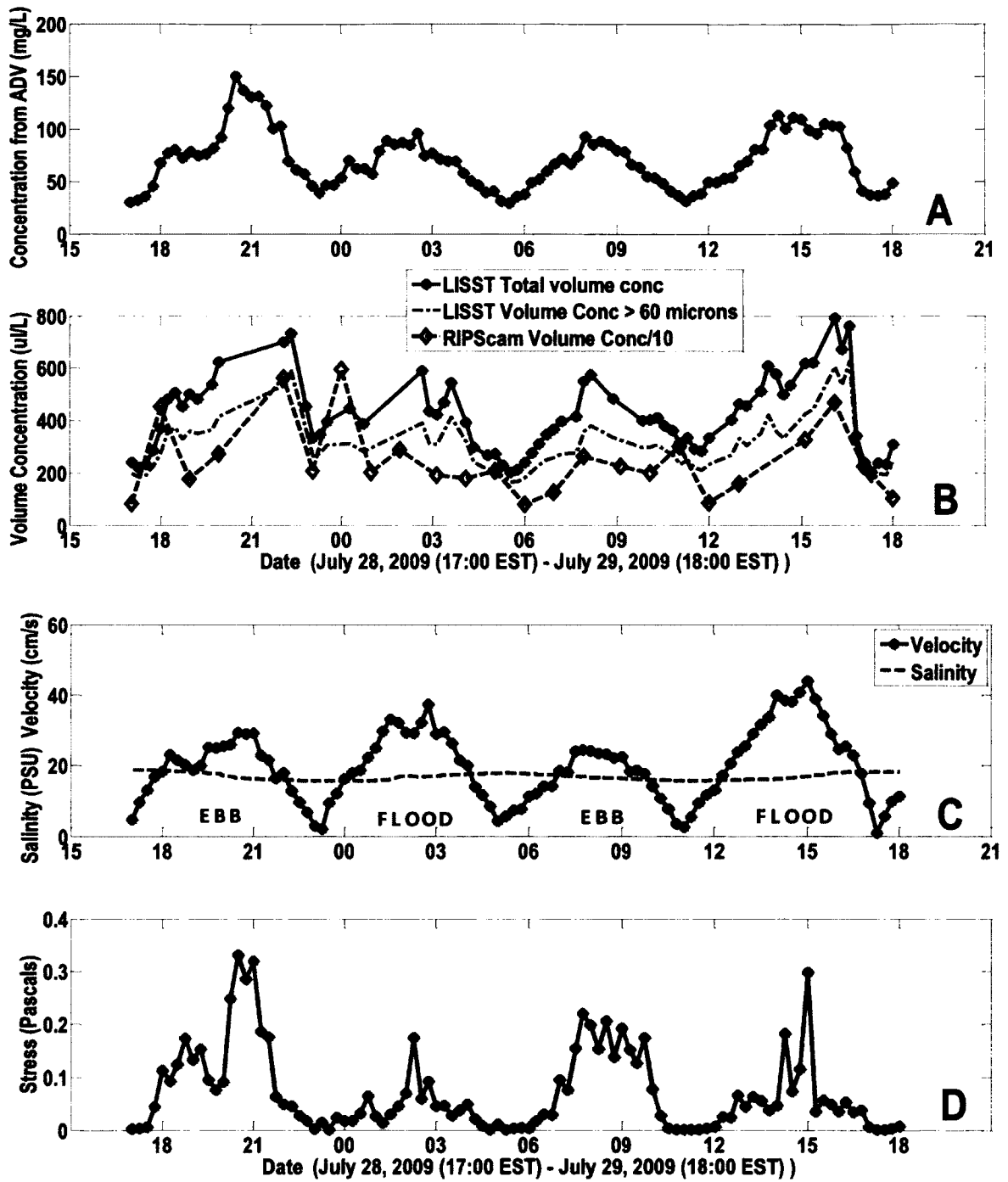
Figure 5.5. July 28-29, 2009, York River time series for (a) mass concentration from ADV backscatter at 45 cmab, (b) uncalibrated volume concentrations from LISST (85 cmab) and RIPScam (90 cmab), (c) ADV current speed (45 cmab) and CTD salinity (85 cmab), (d) ADV Reynolds stress (45 cmab).

182

the size spectrum. A composite size distribution of the entire range of particle sizes can then be derived.

The time series observed for suspended volume concentration is markedly different from that observed for suspended mass concentration. The suspended mass concentration determined from the ADV is generally in phase with the observed current speed and Reynold's stress displayed in Fig. 5.5c,d. This suggests that the total mass in suspension is responding directly to bottom stress. (It should be kept in mind that the stress measurements from the ADV are relatively noisy because the individual 10 Hz ADV bursts were limited to 2 minutes in duration in order to allow transmission back to VIMS between bursts.) During three of the four periods of peak currents, however, the peak volume concentration from the LISST lagged the peak mass concentration in time. These distinct patterns for mass and volume concentration can be explained by the presence of both higher density pellets and lower density flocs.

During each tidal cycle, as stress first began to decrease following peak current speed, the growth of large low-density flocs likely "captured" additional particle volume (i.e., water) more quickly than the smaller, higher density particles settled out. The results of the formation of flocs in concert with the settling of smaller but heavier particles as
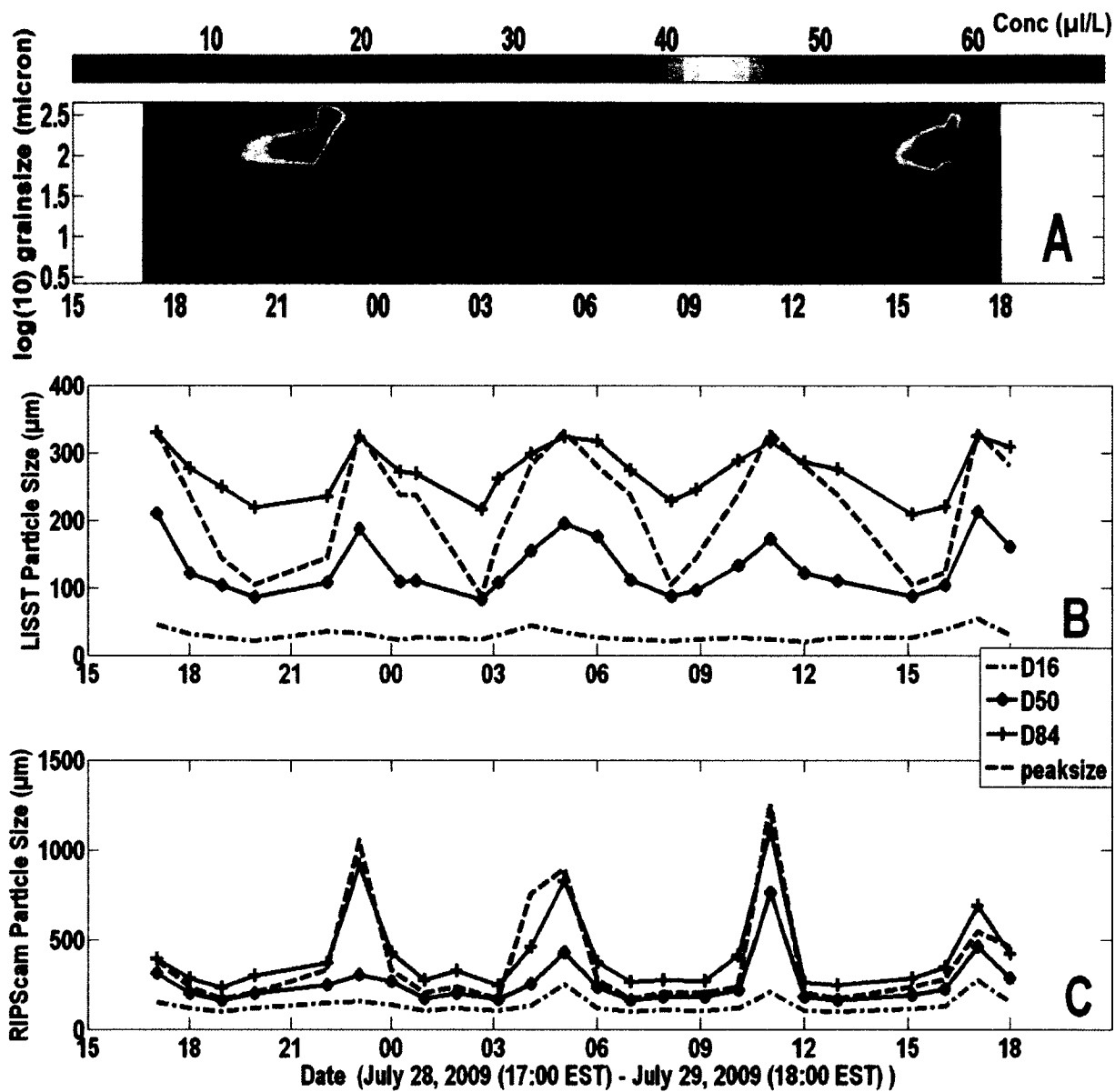
Figure 5.6. (a) Time series of particle size distribution for LISST burst averages. Hotter colors corresponds to higher volume concentrations. D16, D50, D84, and peak particle size time series for (b) LISST and (c) RIPSCam burst averages. LISST data gaps are due to sensor saturation at high C.

184

stress decreased is especially clear in the time series of particle size distribution as recorded by both the LISST and the RIPScam (Fig. 5.6b,c). At each time that the ADV indicates a drop in mass concentration, the peak particle size measured by both the LISST and the RIPscam increases dramatically, rapidly shifting from a peak size corresponding to about D_{50} to a peak size corresponding to about D_{84} (where D_X indicates the diameter with X% of total volume contained in particles smaller than D_X). The combined trend of evolving volume concentration and size distribution is nicely seen in the color shaded time series from the LISST (Fig. 5.6a). The hotter colored (red and yellow), high volume concentration region of the color-contour plot shifts rapidly toward larger particles during each tidal cycle as stress decreases.

Slack tide (lowest stress, lowest concentrations) are when the largest flocs form. Since particle volume goes like D^3, a single very large floc (>1000 µm) accounts for as much volume as >1000 100-µm particles and a single very large floc can account for a large portion of the total volume concentration measured by the camera (Fig. 5.7a). If one examines the lower "peak" in Fig. 5.7b, one sees that the shape better agrees with what the LISST measures (LISST D_{84}, LISST peak, and the RIPScam D_{16} all measure around 300±15 µm. During each slack tide the RIPScam D_{16} agrees best with what the LISST Peak and D_{84} found, suggesting that the majority of flocs in suspension are around this size with occasional larger ones present. During high stress periods when C increases, the LISST distribution broadens (Fig. 5.7b). The RIPScam peak (201 µm) tends to agree with the LISST D_{84} (218 µm), but the LISST peak is now closer to the LISST D_{50}

LISST time = 29-Jul-2009 11:02:24 EST Camera time = 1600 GMT

LISST D16 = 23 µm
LISST D50 = 171 µm
LISST D84 = 315 µm
LISST Peak = 331 µm

RIPScam D16 = 300 µm
RIPScam D50 = 758 µm
RIPScam Peak = 1243 µm

Volume Concentration (µl/L)

(Log10) Particle Size (µm)

A

C

LISST time = 28-Jul-2009 19:55:12 EST Camera time = 100 GMT

LISST D16 = 21 µm
LISST D50 = 85 µm
LISST D84 = 218 µm
LISST Peak = 104 µm

RIPScam D16 = 117 µm
RIPScam D50 = 197 µm
RIPScam Peak = 201 µm

Volume Concentration (µl/L)

(Log10) Particle Size (µm)

B

D

Figure 5.7. LISST and RIPScam Particle size distribution for (a) slack tide after ebb and (b) for higher stress period toward increasing ebb velocity. (c), (d) Corresponding RIPScam photos.

(104 and 85 µm respectively). This could possibly indicate that the flocs present at slack tide (~300 µm) have reduced in size to ~200 µm and a second population of more resilient, denser particles (~95 µm) are now present. The tidally-varying pattern of w_s on the ADV is consistent with the presence of relatively dense pellets in addition to flocs.

186
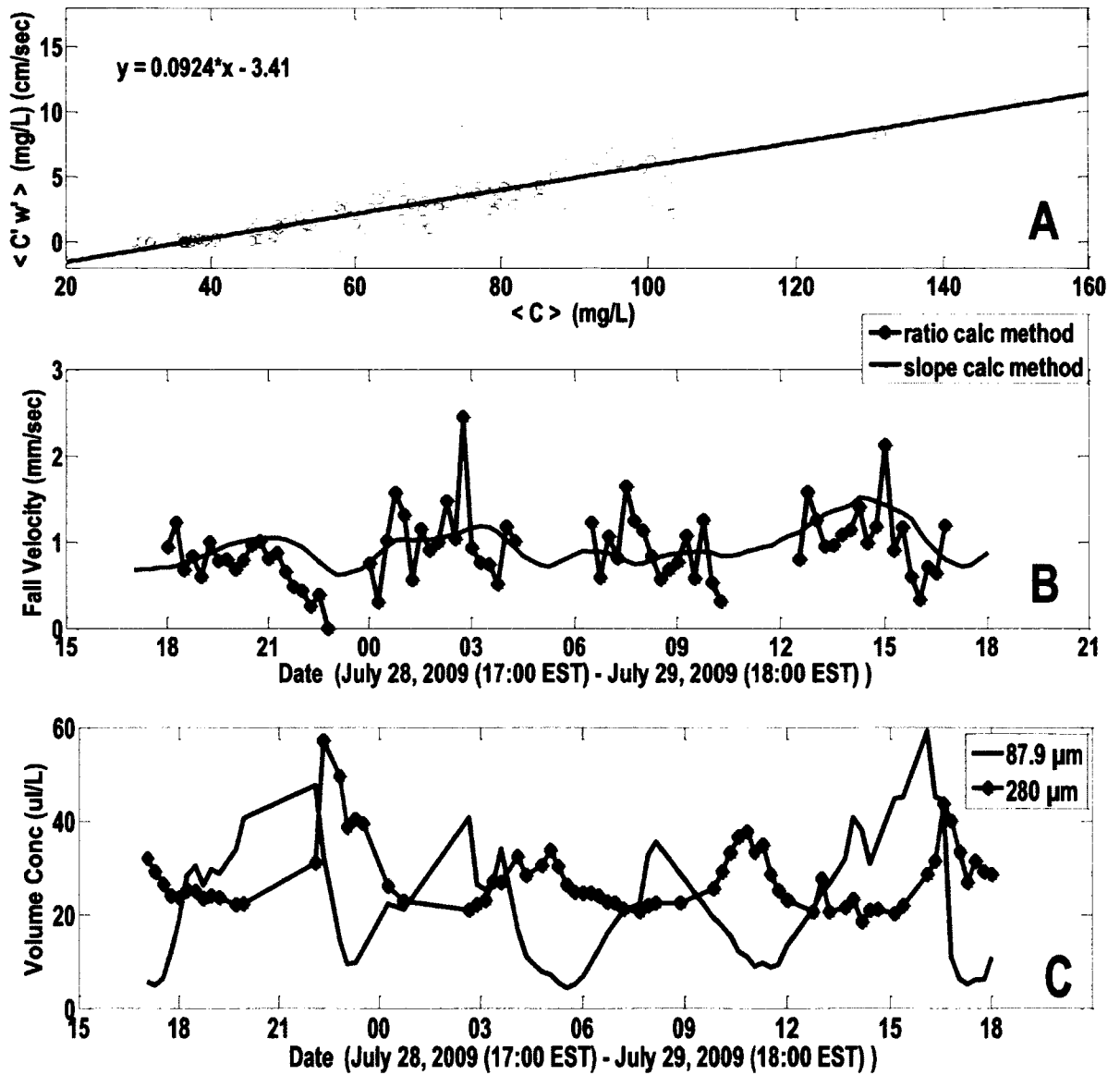
Figure 5.8. (a) Regression of $<C'w'>$ vs. $<C>$, indicating an overall best-fit w_s of 0.09 cm/s = 0.9 mm/s. (b) Fall velocity estimated by instantaneous values of $w_s = < C'w'>/(<C> - C_{bkgd})$ (blue line) and by a running regression of $< C'w'>$ vs. $<C>$ using 12 bursts (red line). (c) Volume concentrations for the LISST bins centered at 88 μm (~ size of pellets) and 280 μm (~ typical flock size approaching slack, excluding "super flocs" seen by RIPScam).

Although the best-fit overall settling velocity for the entire observation period is about 0.9 mm/s (Fig. 5.8a), estimates of time-varying instantaneous settling velocity (Fig. 5.8b) tend to show best-fit w_s based on mass concentration increasing more or less in phase with peak tidal flow. In calculating instantaneous w_s, we have assumed that C_{bkgd} = 36 mg/L, which is the x-intercept in Fig. 5.8. To avoid extreme sensitivity of w_s to small values of ($<C>$ − C_{bkgd}), only bursts with $<C>$ > 50 mg/L were included in the instantaneous w_s calculations. Although the signal is somewhat noisy, settling velocity estimated for individual bursts is positively correlated at 95% confidence with both current speed and Reynolds stress. This pattern is even clearer if one uses a running best-fit slope to estimate time variations in settling velocity (Fig. 5.8b). Having total effective w_s increase with bed stress is consistent with resuspension of relatively dense, resilient pellets with individual settling velocities greater than the flocs. As more and/or heavier pellets are suspended with greater bed stress, the total effective settling velocity of flocs plus pellets will increase. If the suspended sediment population were only composed of flocs, one would expect settling velocity to decrease with sufficiently high bed stress, because higher stress would tend to tear flocs apart.

A closer examination of the volume concentration time series from the LISST for specific size classes further supports the conclusion that both flocs and pellets are present. Fig. 5.8c displays a time series of volume concentration for the LISST bins

188

centered at 88 and 280 μm, the size classes hypothesized from Fig. 5.7 to represent resilient, denser pellets and fragile, less dense flocs, respectively. The volume concentration of the 88 μm bin is in phase with velocity, stress, mass concentration, and effective settling velocity, consistent with the resuspension and rapid settling of pellets. In contrast, the volume of the 280 μm size class becomes largest as velocity and stress first begin to rapidly decrease, consistent with the growth of larger flocs. The volume concentration at 280 μm drops once more around slack because these larger flocs eventually settle out (albeit slowly) as stress drops to zero. The floc concentration does not rise again as stress and velocity first increase because they are ripped apart more quickly than they are resuspended.

5.6 Acknowledgements

5.7 References:

Andersen, T.J., 2001. The role of fecal pellets in sediment settling at an intertidal mudflat, the Danish Wadden Sea. In: W.H. McAnally & A.J. Mehta (eds.), *Coastal and Estuarine Fine Sediment Processes*, Elsevier, p. 387-401.

Cartwright, G.M., Friedrichs, C.T., Dickhudt, P.J., Gass, T., Farmer, F.H., 2009. Using the acoustic Doppler velocimeter (ADV) in the MUDBED real-time observing system. Proceedings, *OCEANS 2009 MTS/IEEE*, 9 p.

Debnath, K., Nikora, V., Aberle, J., Westrich, B., Muste, M., 2007. Erosion of cohesive sediments: resuspension, bed load, and erosion patterns from field experiments. *J. Hydraulic Eng.*, 133: 508-520.

Dickhudt, P.J., Friedrichs, C.T., Schaffner, L.C., Sanford, L.P., 2009. Spatial and temporal variation in cohesive sediment erodibility in the York River estuary: a biologically influenced equilibrium modified by seasonal deposition. *Marine Geol.*, 267: 128-140

Drake, D.E., Eganhouse R., McArthur, W., 2002. Physical and chemical effects of grain aggregates on the Palos Verdes margin, southern California. *Continental Shelf Res.*, 22: 967-986.

Dyer, K.R., 1984. *"Coastal and Estuarine Sediment Dynamics"*. Wiley Interscience, New York, 342 p.

Edelvang, K., Austen, I., 1997. The temporal variation of flocs and fecal pellets in a tidal channel. *Estuarine Coastal Shelf Sci.*, 44: 361-367.

Friedrichs, C.T., Cartwright, G.M., Dickhudt, P.J., 2008. Quantifying benthic exchange of fine sediment via continuous, non-invasive measurements of settling velocity and bed erodibility. *Oceanography*, 21(4): 168-172.

Fugate, D.C., Friedrichs, C.T., 2002. Determining concentration and fall velocity of estuarine particle populations using ADV, OBS and LISST. *Continental Shelf Res.*, 22: 1867-1886.

Fugate, D.C., Friedrichs, C.T., 2003. Controls on suspended aggregate size in partially mixed estuaries. *Estuarine Coastal Shelf Sci.*, 22: 1867-1886.

Harris, C.K., Traykovski, P.A., Geyer, W.R., 2005. Flood dispersal and deposition by near-bed gravitational sediment flows and oceanographic transport: a numerical modeling study of the Eel River shelf, northern California. *J. Geophysical Res.*, 110, C09025, doi: 10.1029/ 2004JC002727.

Hill, P.S., Voulgaris G., Trowbridge, J.H., 2001. Controls on floc size in a continental shelf bottom boundary layer. J. Geophysical Res., 106: 9543-9549.

Mikkelsen, O.A., Milligan, T.G., Hill, P.S., Moffatt, D., 2004. INSSECT - an instrumented platform for investigating floc properties close to the seabed. *Limnology Oceanography-Methods*, 2: 226-236.

Pejrup, M., Mikkelsen, O.A., 2010. Factors controlling the field settling velocity of cohesive sediment in estuaries. *Estuarine Coastal Shelf Sci.*, 87: 177-185.

Rodríguez-Calderón, C., 2010. Spatial and temporal patterns in erosional and depositional processes: physical and biological controls in the York River, Chesapeake Bay, Virginia. *M.S. Thesis, School of Marine Science, College of William & Mary*, Gloucester Point, VA.

Sanford, L.P., P.J. Dickhudt, L. Rubiano-Gomez, M. Yates, S.E. Suttles, C.T. Friedrichs, D.C. Fugate and H. Romine, 2005. Variability of suspended particle concentrations, sizes and settling velocities in the Chesapeake Bay turbidity maximum. In: I.G. Droppo et al. (eds.), *Flocculation in Natural and Engineered Environmental Systems*. CRC Press, p. 211-236.

Schaffner, L.C., Dellapenna, T.M., Hinchey, E.K., Friedrichs, C.T., Thompson, M., Neubauer, S., Smith M.E., Kuehl, S.A., 2001. Physical energy regimes, sea-bed dynamics and organism-sediment interactions along an estuarine gradient. In: J.Y. Aller et al. (eds.), *Organism-Sediment Interactions*. USC Press, p. 161-182.

Schieber, J., Yawar, Z., 2009. A new twist on mud deposition - mud ripples in experiment and rock record. *The Sedimentary Record*, 7(2): 4-8.

Son, M., Hsu, T.J., 2008. Flocculation model of cohesive sediment using variable fractal dimension. *Environmental Fluid Mech.*, 8: 55-71.

Smith, S.J., Friedrichs, C.T., 2010. Size distributions and settling velocities of cohesive flocs and suspended sediment aggregates in a trailing suction hopper dredge plume. *Continental Shelf Res.*, doi:10.1016/ j.crs.2010.04.002

Taghon, G.L., A.R.M. Nowell and P.A. Jumars, 1984. Transport and breakdown of fecal pellets, biological and sedimentological consequences. *Limnology and Oceanography*, 29: 64-72.

Wheatcroft, R.A., and C.A. Butman, 1997. Spatial and temporal variability in aggregated grain-size distributions, with implications for sediment dynamics. *Continental Shelf Research*, 17: 367-390.

Wheatcroft, R.A., P.L. Wiberg, C.R. Alexander, S.J. Bentley, D.E. Drake, C.K. Harris, A.S. Ogston, 2007. Post-depositional alteration and preservation of sedimentary strata. In: C.A. Nittrouer et al. (eds.), *Continental-Margin Sedimentation: From Sediment Transport to Sequence Stratigraphy*, Blackwell, pp. 101-155.

Winterwerp, J.C., 2002. On the flocculation and settling velocity of estuarine mud. *Continental Shelf Res.*, 22: 1339-1360.

Winterwerp, J.C., Manning, A.J., Martens, C., de Mulder, T., Vanlede, J., 2006. A heuristic formula for turbulence-induced flocculation of cohesive sediment. *Estuarine Coastal Shelf Sci.*, 68: 195-207

Zabawa, C.F., 1978. Microstructure of agglomerated suspended sediments in northern Chesapeake Bay estuary. *Science* 202(4363): 49-51.

CHAPTER 6

Sediment settling velocities from Acoustic Doppler Velocimeters and settling tubes: agreement over a range of particle types and hydrodynamic conditions*

By Grace M. Cartwright, Carl T. Friedrichs, and S. Jarrell Smith

6.1 Abstract

Acoustic Doppler Velocimeters (ADVs) can be used to measure (i) relatively large (~cm/s) sediment settling velocities (w_s) by direct Doppler measurement of sediment motion and (ii) relatively small w_s (~mm/s) by assuming a Rouse balance between upward Reynolds flux and downward settling. Advantages of using an ADV to estimate w_s include that the ADV does not impact turbulence in the sampling volume, it isresilient to high energy and biofouling. For the two methods examined here, they are relatively insensitive to precise calibration of acoustic backscatter for sediment concentration. In the past, however, these ADV-based estimates of w_s had not been confirmed by independent measurements of w_s using other instruments observing the same particle populations. Here, independent observations of w_s utilizing gravimetric and video settling tubes are shown to be consistent with these two types of ADV-based w_s measurements for large and for small w_s, respectively. Direct Doppler-based ADV estimates of w_s were collected for sand in a laboratory mixing tank and confirmed by a Rapid Sediment Analyzer gravimetric settling column. Rouse-balance ADV estimates were collected in the York River estuary for muddy flocs and confirmed *in situ* by a particle tracking/particle image velocimetry settling column. These lab and field-based observations both demonstrate that, in the absence of significant particle aggregation/disaggregation, (i) measurement of w_s and (ii) w_s itself are both relatively insensitive to the local magnitude of fluid turbulence for w_s up to several cm/s.

6.2 Introduction

Particle settling velocity, w_s, is defined as the gravity-induced vertical settling speed (treated here as a magnitude such that $w_s > 0$) of a sediment particle relative to the water parcel immediately around it. The nature of suspended sediment transport is extremely sensitive to w_s. Sediment particles with small w_s tend to be well mixed and occur higher in the water column than heavier particles. Along rivers and in coastal environments, sediment is commonly sorted according to w_s (McCave and Hall, 2006), and convergent transport mechanisms, such as estuarine circulation, tend to favor the localized trapping of particles with specific ranges of w_s (Jay et al., 2007). Numerical models of suspended sediment transport are exceedingly sensitive to the specification of w_s, and w_s is often the dominant parameter determining the distance sediment travels in such simulations (Harris et al., 2008).

A key question in the observational and theoretical application of particle settling velocity is whether and to what degree w_s is sensitive to turbulence in the surrounding

194

fluid. When a sediment population remains in suspension, it is generally because non-zero correlations between turbulent velocity and turbulent fluctuations in concentration compensate for the continual downward movement of individual particles relative to local fluid. But the classical method for measuring w_s, namely use of a particle settling column, relies on relatively still water (Mantovanelli and Ridd, 2006). So if w_s itself depends strongly on the intensity of surrounding turbulence, this sensitivity may undermine the assumptions behind its very measurement. Note that here we define w_s as particle settling velocity within a reference frame moving with the local turbulent velocity. So "vortex trapping" and "fast tracking" of individual particles by eddies, considered major affects on w_s by some authors (Kawanisi and Shiozaki 2008), do not necessarily impact w_s by our definition.

The Acoustic Doppler Velocimeter (ADV) provides an attractive tool for estimating w_s *in situ* while fully accounting for the possible effect of turbulent eddies. Unlike sediment settling columns, an ADV makes measurement at the the ambient turbulence of the *in situ* water parcel it measures. Besides providing an opportunity to estimate w_s, ADVs by design provide direct measurements of turbulent velocity (Voulgaris and Trowbridge 1998), and their acoustic backscatter can be calibrated for suspended mass concentration (Voulgaris and Meyers 2004). Unlike some other non-intrusive methods for documenting turbulent conditions, such as Laser Doppler Velocimetry or Particle Imaging Velocimetry, ADVs are highly resistant to biofouling, and can easily be deployed in highly energetic conditions for up to months at a time (Friedrichs et al. 2008).

Although ADV-based methods for determining w_s are theoretically sensible and appear to provide reasonable values, they have not previously been confirmed by independent observations of w_s using other instruments observing the same particle populations. In the present study, independent observations of w_s utilizing settling tubes are compared to estimates of w_s from ADVs based on (i) direct Doppler observations of sediment

velocity (c.f. Kawanisi and Shiozaki 2008) and (ii) assumption of a Rouse balance (c.f. Fugate and Friedrichs 2002). Consistency between the settling column and ADV-based estimates of w_s in our study ultimately suggest that, in the absence of significant particle aggregation/disaggregation, measurement of w_s by both methods are relatively insensitive to the local intensity of fluid turbulence, at least for w_s up to several cm/s.

6.3 Methods

Settling Columns

The classic method for measuring w_s is through use of various types of settling tubes. Settling tubes used in the past for documenting w_s for non-cohesive, disaggregated and/or flocculated sediment particles include simple graduated cylinders used for laboratory pipette analys, Owen tubes on ship decks, to *in situ* settling columns
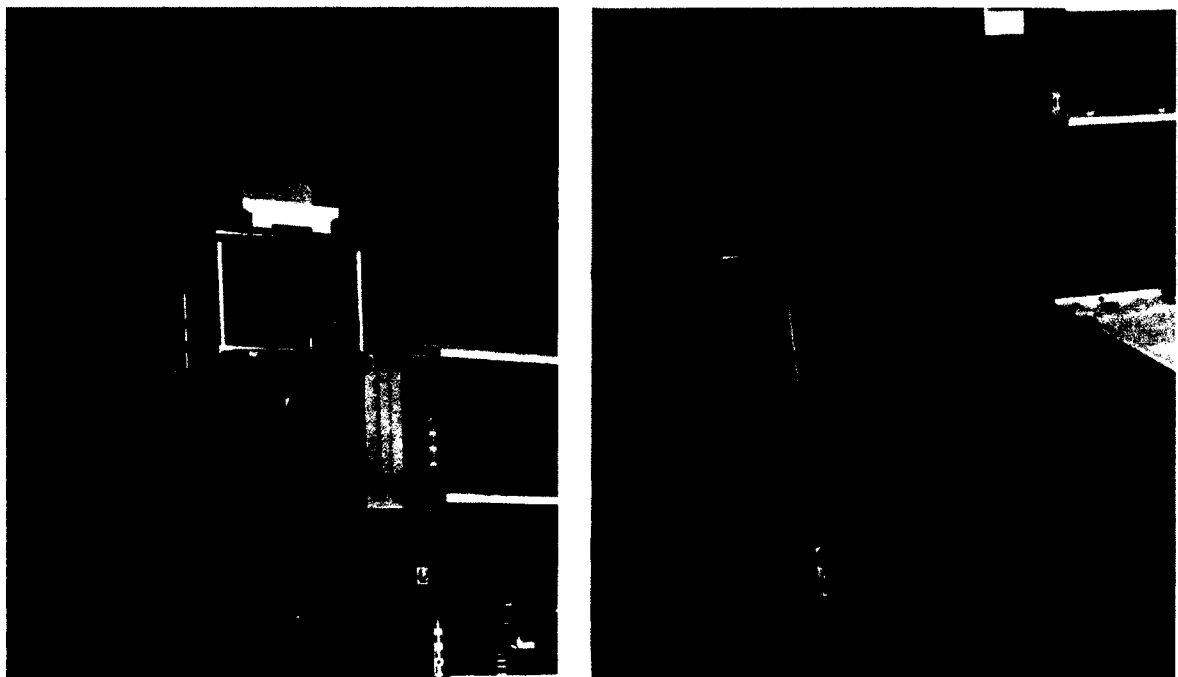
Figure 6.1 Rapid Sand Analyzer housed at the U.S. Army Corps of Engineers Field Research Facility in Duck, NC, USA.

monitored by video, laser diffraction or holography, and columns which directly incorporate a balance for weighing deposited sediment (Mantovanelli and Ridd 2006). Two types of settling columns were employed in this study: for sand, a Rapid Sediment Analyzer incorporating an underwater balance tray, and for mud, a video-based particle tracking/particle imaging velocimetry (PIV) system.

Rapid Sediment Analyzer

The Rapid Sediment Analyzer (RSA) used for this project (Figure 6.1) is housed at the U.S. Army Corps of Engineers Field Research Facility (FRF) in Duck, NC, USA, and is based on the design of Halka et al. (1980). The RSA is a 12-cm inside-diameter acrylic column filled with tap water. When the pan is released, a computer records a time series of the change in weight of sediment collected on the weight dish suspended from the balance by a wire 50 cm below the drop pan. The time-series along with the known distance between the drop pan and the weight dish then provides a distribution of settling velocities for the sample. The median (50th percentile) settling velocity (w_{s50}) within that distribution is then taken to be the characteristic w_s for that sample.

The sediment placed in the RSA for this experiment was derived from commercial quartz sand which was then sorted into 6 size classes using standard laboratory sieves ranging from 4 phi (63μm) to 2.5 phi (150 μm) using 0.25 phi graduations. A Ro-Tap shaker was first applied to the complete stack of sieves for 30 minutes. Next, the sand from each size class was individually shaken through all the sieves a second time for an additional 45 minutes in an effort to make sure what was captured on each sieve was only sand from that sieve size to a quarter phi size larger.

Each sand size class prepared as described above was passed though the FRF RSA in duplicate or triplicate. For each sample, approximately 0.3 g of sand was placed on the drop pan. Using less than a 0.5 g sample permits grains to settle at distances in excess of

197

two grain diameters from each other so they settle without acceleration or deceleration associated with grain-to-grain interactions (Sanford and Swift, 1971). The balance was tared just prior to each release of sand from the drop pan. For the FRF RSA, the timing software was started at the same time a button was pushed to mechanically release the drop pan to disperse the sand.

Particle Tracking/PIV Video Camera

The particle tracking/PIV settling column utilized here (Figure 6.2), known as the Particle Imaging Camera System (PICS), was developed by Smith (2010) and Smith and Friedrichs (2011, 2013). PICS includes a 5-cm inside-diameter chamber that can be rotated horizontally (Figure 6.2b) so that the ambient current flows through until a sample is captured by closing ball valves at each end. After a sample is collected, the chamber is mechanically turned to a vertical position to become a settling column.
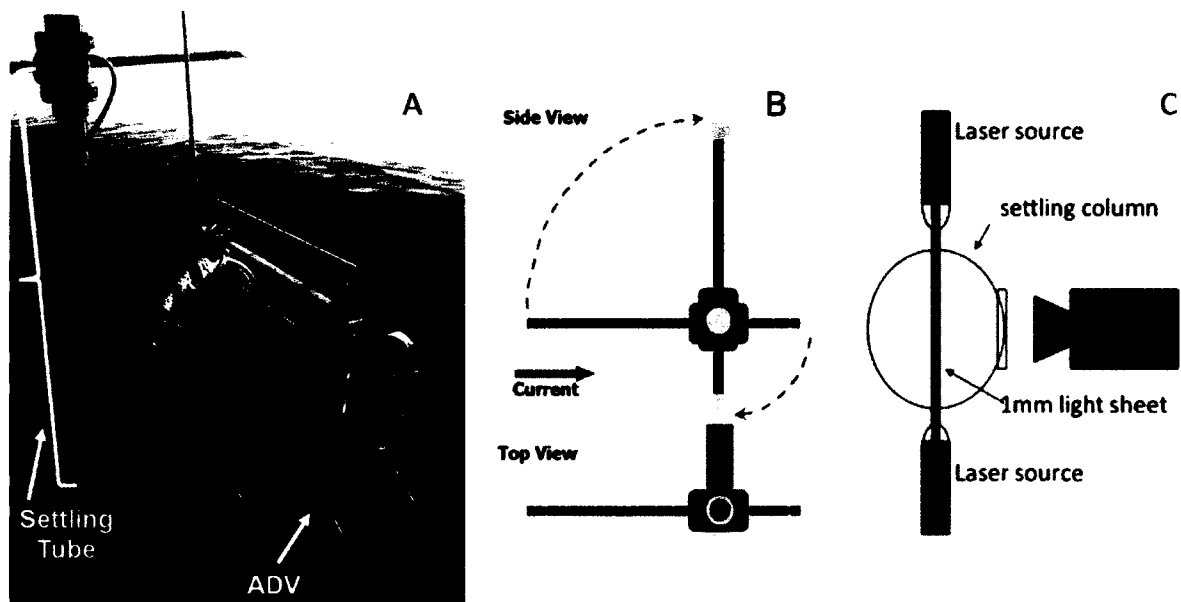
Figure 6.2 A) VIMS profiler indicating the position of the PICS video settling column and the Sontek ADV; **B)** PICS schematic indicating sample collection and image analysis positions; **C)** schematic of camera, settling column cross section, and laser lighting.

During periods of weak currents (< ~ 15 cm/s), the sample is collected by keeping the open column in a vertical position as it is lowered to the desired depth and then closing the ball valves. Once the chamber is closed, a laser diode light passes across the settling column, providing a 1-mm thick sheet of light three-quarters of the way down the 1-m long column (Figure 6.2c). Turbulence within the column is allowed to dissipate for approximately 20 sec, and a 30-sec image sequence is collected at 10 frames per second. The digital video camera within the PICS is a Prosilica/AVT GC1380 with 1024x1380 pixels which images a region 14-mm wide by 10-mm high by 1-mm thick, such that each pixel is 10 μm across. A new water sample can be imaged as often as every two minutes.

Particles large enough to be accurately characterized in terms of both settling velocity and size (diameter, d ≥ 30 μm) are tracked by particle tracking velocimetry (PTV) methods described by Smith and Friedrichs (2013). The automated process of tracking the particles allows w_s to be determined for thousands of particles during each 30-sec image sequence. The smallest detected particles (d < 30 μm) are used as PIV tracers to
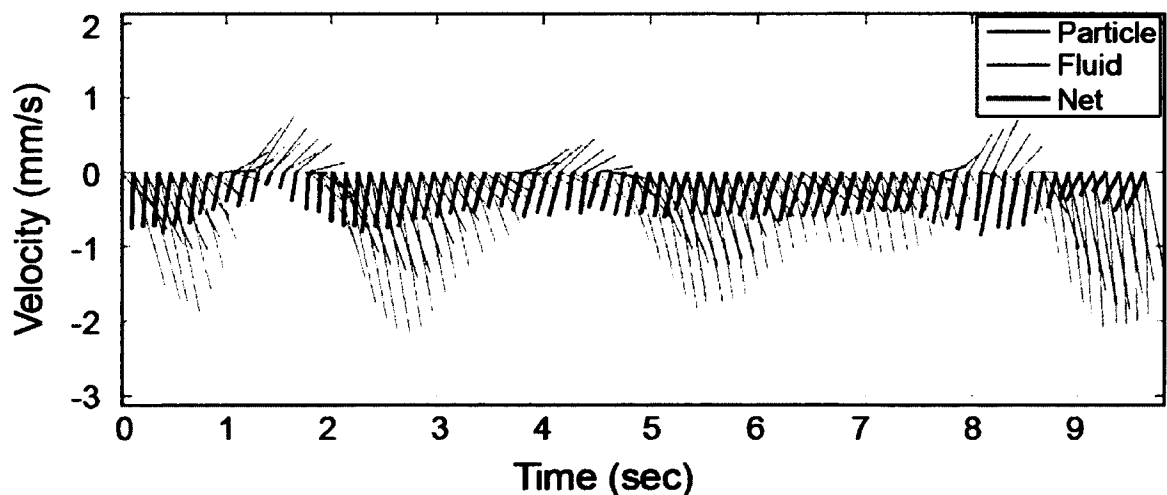
Figure 6.3 Example *in situ* time-series velocities derived from tracking of a 200 μm particle within the video settling column. Vectors indicate particle velocity (red lines), fluid velocity derived from PIV applied to surrounding ~ 20 μm particles (blue lines), and net particle settling velocity (black lines) (modified from Smith, 2010).

estimate the local fluid velocity within the settling tube (Figure 6.3). The local fluid velocity is then subtracted from the PTV motion each larger tracked particle to determine the net w_s of each larger particle (Figure 6.3). The w_{s50} for all the particles with d $\geq$ 30 µm is then taken to be the characteristic w_s for that sample. Note that w_{s50} determined by the PICS thus characterizes an operationally defined "settling component" of the total particle population and neglects the contribution of what here is operationally defined as the non-settling "wash load".
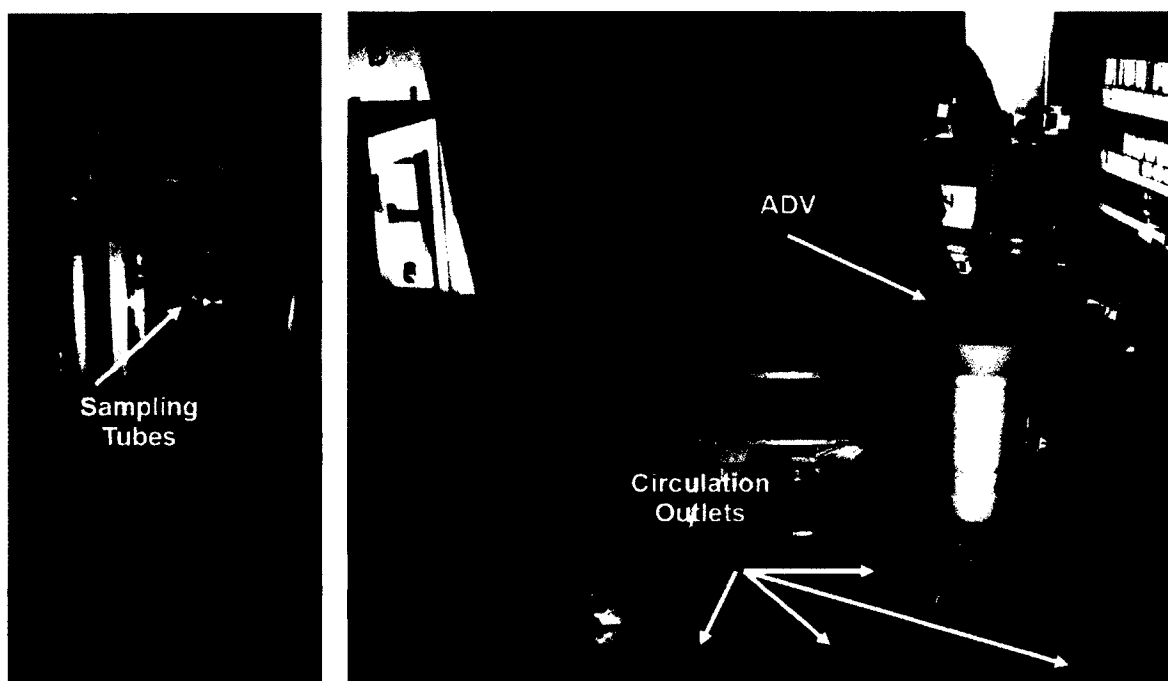
Figure 6.4 A) VIMS sediment mixing tank, with suspended sediment sampling tubes highlighted; **B)** example placement of ADV in chamber, with pump circulation outlets highlighted.

Acoustic Doppler Velocimeter

The type of ADV used for all the measurements presented here was the 5 MHz SonTek ADVOcean-Hydra model (Figures 6.2A and 6.4). Like ADVs in general (Kraus et al. 1994), it utilizes a bistatic design, i.e., separate acoustic transducers to transmit and receive sound waves. The geometry of the central transmitter and three angled receivers results in the sample volume for the ADVOcean-Hydra being 18 cm below the transmitter. The sampling volume is a cylinder with a diameter roughly equal to that of the 15-mm wide transmit ceramic. The cylinder's height is controlled by the SonTek software to be 18 ± 1 mm, giving an overall sample volume of ~ 2 cm^3 (SonTek 2001).

Under typical operating conditions, the noise associated with individual horizontal velocity estimates at a 25 Hz sampling rate is 1% of the horizontal velocity range setting, i.e., ±1 cm/s when using the ±100 cm/s setting (SonTek 2001). Assuming the noise to be random, the standard error on a mean velocity averaged over 1 sec drops to only 2 mm/s. Comparison to independently calibrated currents indicates that errors in longer duration ADV mean velocity drops to less than 0.5 mm/s, and ADV-derived mean Reynolds stress measured in a laboratory flume is accurate to within 1% (Voulgaris and Trowbridge 1998).

Because of the geometry of the ADV, individual vertical velocity measurements (defined as perpendicular to the face of the transmit ceramic), are expected to have 30 times less noise than individual horizontal velocity measurements (Voulgaris and Trowbridge 1998). The especially high accuracy in ADV measurements of vertical velocity is well suited to estimating w_s as described below. Of course, one must remember that it is the velocity of the acoustic scatterers that is actually being measured by the ADV, not simply the water velocity. So for the case of scatterers dominated by negatively buoyant sediment, the vertical velocity recorded by the ADV is actually $w - w_s$, where w is the vertical component of the fluid velocity, and w_s is the settling

velocity of the scatterers. (There is a minus sign in front of w_s here because w_s is defined as being positive downward.)

Direct Doppler Method and Mixing Tank Set-up

If the vertical velocity of the fluid, w, can be independently constrained to within an error smaller than w_s, then the total observation of $w - w_s$ provided by the ADV can be used to estimate w_s. It has long been recognized that where zooplankton are abundant, and the time-averaged value of w is sufficiently small, the vertical component of acoustic Doppler velocity can be used to measure the O(cm/s) vertical migration speed of the zooplankton (Buchholz et al., 1995; Smyth, 2006). More recently, Kawanisi and Shiozaki (2008) used neutrally-buoyant tracer particles to measure w such that ADV response to the occasional passage of clouds of negatively buoyant, settling particles could be accurately determined from the measurement of total $w - w_s$. In this paper we demonstrate a direct Doppler method for measuring sand settling velocity that infers w_s by (i) spatially mapping $w - w_s$ over a horizontal cross-section of a mixing tank and (ii) applying conservation of water mass to subtract out w.

The VIMS sediment mixing tank (Figure 6.4A) is 1.5-m tall, square in cross-section, with an inside width of 31.6 cm, and tapers at its base to facilitate the return of sediment to be pumped back to its upper section. The design of the tank is based on a similar chamber developed at the University of East Anglia, UK (Rehman and Vincent 1990). A 44 liter/minute Cal Pump MS900, which is kept cool in a separate water bath, powers the circulation of water in the tank. After passing through the pump, tank water is re-circulated through a four-way splitter to four jet outlets (Figure 6.4B), one centered on each tank wall, 25 cm below the top of the tank. The water jets meet forcefully in the center of the tank, level with the outlets. Once the jets converge, the dominant flow is downward toward the bottom of the tank, but some of the sediment is carried above the level of the outlet tubes by a component of upward flow also produced at the jet

convergence point. Sliding sampling tubes situated along one side of the tank can be pushed in to the center of the chamber to allow the collection of water samples (Figure 6.4A).

For the laboratory-based, direct Doppler measurements of $w - w_s$, a SonTek ADVOcean-Hydra was mounted in a downward looking position at the top of the VIMS sediment mixing tank (Figure 6.4). The ADV was clamped to a plate that was, in turn, clamped to a second plate such that adjustment of the plates could position the ADV step-by-step through a horizontal grid of measurement positions. A grid was created across the top of the chamber, with six locations (3 cm apart) along the x-axis and six location (3 cm apart) along the y-axis, for a total of 36 positions. Once sand of a given size class had been added to the tank, a 10-minute burst with a sampling rate of 10 Hz was collected at each of these grid points.

This procedure was repeated (with the tank drained and refilled in between) for each of the six sand size classes described above in the RSA section. For all but one size class, enough sand was added to the 118-liter tank in order to bring the tank sand concentration to approximately 200 mg/L. The exception was the 75-mm class, for which there was only enough sand available to bring the concentration to ~120 mg/L. Finally, the spatial pattern of vertical flow observed by the ADV was interpolated over the entire horizontal "slice" of the tank, and conservation of water mass was used to remove w from the measurements of $w - w_s$ (see Results section).

Reynolds Flux Method and Field Experiment

For $w_s < \sim 1$ mm/s, direct Doppler resolution of w_s is problematic, but a representative w_s may still be inferred by assuming a balance between downward settling and upward Reynolds flux, i.e., a Rouse balance. Assuming steady, horizontally homogeneous flow,

with zero mean vertical velocity and a single particle type (size, shape, and density) in suspension, it follows that

$$w_s <C> = <w'C'> , \qquad (6.1)$$

where C is suspended sediment mass concentration, primes indicate turbulent fluctuations, and < > indicates a time average (e.g., McLean 1992). Thanks to it's rapid sampling rate and measurement of both velocity (via Doppler Shift) and concentration (via backscatter intensity), the ADV provides resolution of turbulent fluctuations in both velocity and concentration (Fugate and Friedrichs 2002), so w_s in (6.1) can ideally be solved for immediately. But natural muddy suspensions, even when reasonably steady and homogenous, usually contain a spectrum of particle types, including a significant, non-settling "wash load" that is still caught on filters when using water samples to calibrate acoustic backscatter for *in situ* C.

Assuming that C in (6.1) can be usefully described as being composed of a washload component (C_{wash}) with (effectively) zero settling velocity plus a settling component (C_{sett}) with a characteristic mean settling velocity, w_s, the balance in Eq. (6.1) becomes $w_s C_{sett} = <w'C_{sett}'>$. However, ADV backscatter measures $C = C_{sett} + C_{wash}$, not just C_{sett}. By definition, $C_{wash}' << C_{sett}'$, since C_{wash} is much better mixed vertically in the water column than is C_{sett}. It follows then that $w_s C_{sett} = <w'C_{sett}'>$ can be re-expressed as:

$$w_s (<C> - C_{wash}) = <w'C'> , \qquad (6.2)$$

Two approaches have been developed to use Reynolds Flux ADV observations to solve for w_s in Eq. (6.2): (i) a low-pass, slope-intercept method (Fugate and Friedrichs 2002), and (ii) an instantaneous, prescribed washload method (Cartwright et al. 2011). Method (i) plots $<w'C'>$ versus $<C>$ for a series of consecutive ADV bursts. The resulting best-

fit slope provides an estimate of w_s, and the x-intercept approximates C_{wash}. Changes in w_s as a function of concentration can be accommodated by calculating the slope as a function of $<C>$ from a best-fit curve rather than a best-fit straight line (Maa and Kwon 2007). This is a low-pass estimate because several bursts are needed for a single w_s estimate. Method (ii) first defines a value for C_{wash} based on the intercept from method (i) or from a value of C observed near slack water (Cartwright et al. 2011, Fall 2012). The characteristic settling velocity w_s in Eq. (6.2) can then be determined for each individual burst providing an "instantaneous" estimate.

The SonTek ADVOcean-Hydra used here for applying the Reynolds flux method is shown in Figure 6.2, mounted on the VIMS profiler (along with the PICS). Observations were collected on 6 October 2012 off the 9-m VIMS R/V Eliss Ollson which was anchored in 6 m of water within a few 100 m of the Clay Bank long-term MUDBED benthic tripod site in the secondary channel of the York River estuary, USA (Friedrichs et al. 2008). All samples were collected within an anchor line radius of 37°20.53' N, 76°37.54' W. The ADV sampling volume and the intake to a high-volume submersible pump were both located 37 cm above the feet of the profiler. ADV measurements were collected at 10 Hz in 2 min duration bursts. Most ADV bursts coincided in time with corresponding PICS bursts and collection of 1-liter pump samples (which were then passed through 0.8-mm pore-size glass fiber filters).

Due to logistical constraints, sampling was limited to a single slack-to-slack bracketing of flood tide (~ 6 hrs), two days before neap tide The goals were to both (i) collect samples with the profiler sitting on the bed where ADV measurements would not be contaminated by rocking motion, and (ii) also collect samples throughout the water column in order sample a large variety of particles. This, along with some initial problems with operating the PICS, resulted in irregular time intervals between sample collections at any one depth.
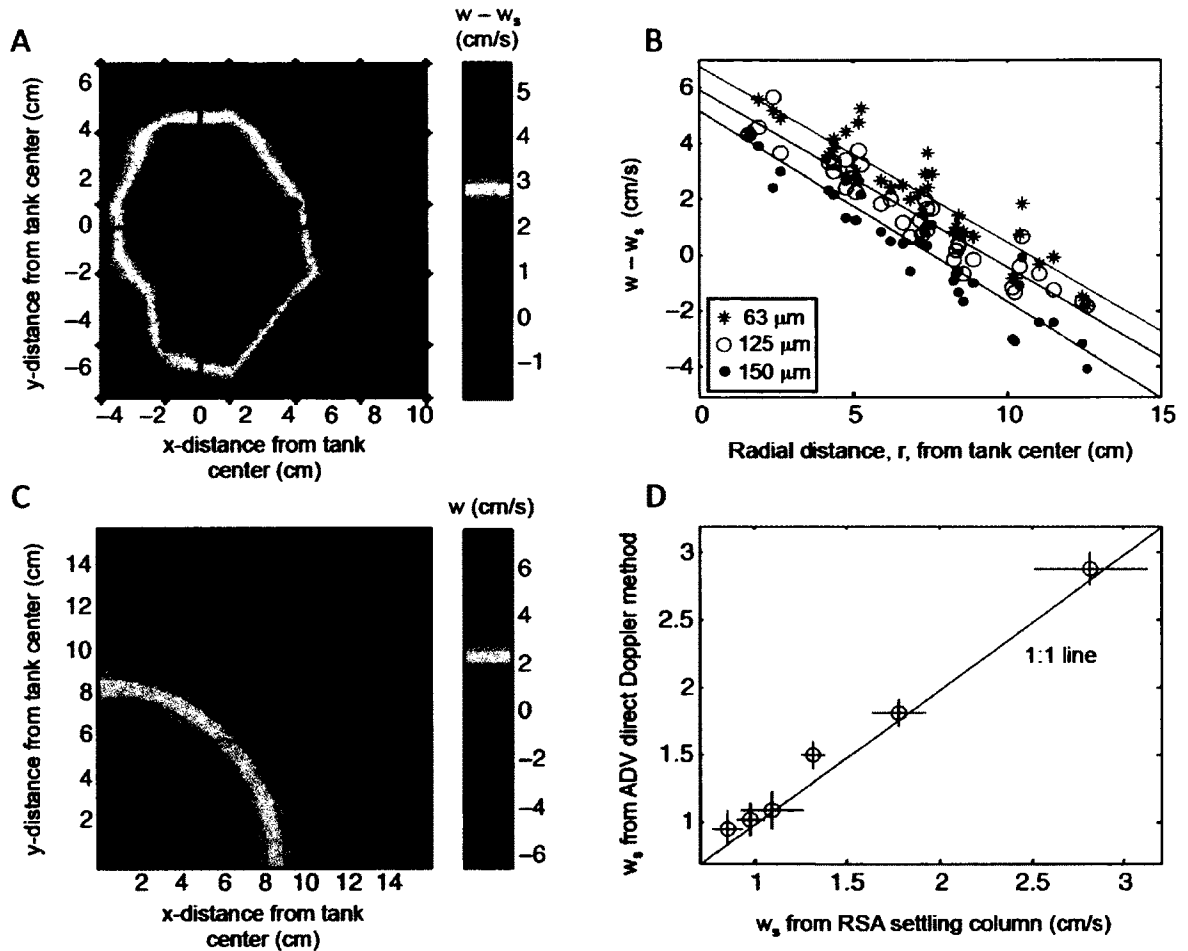
Figure 6.5 A) Vertical velocity of scatters $(w - w_s)$ as recorded by the ADV for the 125 μm sieve case, measured over a cross-section of the VIMS sediment mixing tank 18 cm from the top of the tank (measurement locations indicated by *); **B)** $w - w_s$ as recorded by the ADV versus radial distance from the center of the tank for 63, 125 and 150 μm cases, along with best-fit linear regressions; **C)** spatial distribution of vertical water velocity, w, over a quadrant of the tank based on averaging the regression slope for all 6 size classes, with the offset chosen to conserve water mass; **D)** averaged w_s calculated from the ADV determined by removing interpolated values of w from observations of $w - w_s$, plotted versus w_s measured by the RSA. Error bars are +/- one standard error about each mean. Both axis in cm/s.

6.4 Results

Direct Doppler Method

Figure 6.5A displays an example map of the burst-averaged vertical velocity of scatterers ($w - w_s$) as output by the ADV for a horizontal plane 18 cm below the top of the mixing tank, in this case for 125 mm sand. The jets from the four pump circulation outlets (see Figure 6.4) meet in the center of the chamber, 7 cm below the level of the plane sampled by the ADV, and cause a mean flow up the center of tank that exceeds 5 cm/sec. This upward flux is balanced by a downward flowalong the edges of the chamber. Because of the size and shape of the SonTek ADVOcean, it was not possible to directly measure velocities all the way to the far edges of the tank (as seen in figure 6.5A). Nonetheless, when the ADV burst-averaged values for $w - w_s$ were plotted versus radial distance, $r = (x^2 + y^2)^{1/2}$, relative to the center of the tank (Figure 6.5B), linear relations of the form

$$w - w_s = A\ r + B(w_s) \tag{6.3}$$

were obtained which were extrapolated farther out toward the walls of the chamber.

The slopes of the best-fit regressions of $w - w_s$ versus r (i.e., A in Eq. 6.3) did not vary much between sand sizes (Figure 6.5B), presumably because the axially-symmetric pattern of water circulation did not itself depend on w_s. However, each sand size was associated with a different offset of the best-fit regression. Assuming w_s to be independent of the local hydrodynamics and, thus, constant for a given sand size, the shift in offset provided a measure of the change in w_s between sand samples.

A global best-fit slope for $w = A\,r + B_0$ (i.e., for the spatial distribution of vertical velocity without sand) was assigned by averaging the slopes found individually for the six cases with sand present. Conservation of mass for water was then used to set the constant offset, B_0, needed to predict w over the entire horizontal plane. In other words, the final function for w was defined such that the integration of $(A\,r + B_0)$ over the entire horizontal plane equalled zero. The resulting flow pattern for predicted w over a quadrant of the mixing tank is shown in Figure 6.5C.

Subtracting the observed, burst-averaged vertical velocities of the scatterers $(w - w_s)$ from the predicted values of vertical water velocity (w) gave 36 realizations of w_s for each of the six sand sizes. The best estimate for w_s for each sand size was then the average of those 36 observations with an uncertainty provided by the standard error on that mean. Figure 6.5D compares the final values of w_s determined by this "direct Doppler method" against those for the same sand samples determined by the RSA settling column. Overall, the values for w_s determined by these two independent methods were highly consistent, despite the varying hydrodynamic conditions across the width of the mixing tank and the lack of turbulence in the RSA settling column.

Reynolds Flux Method

Pump samples collected by the VIMS profiler throughout the water column on 6 October 2012 at the same height and within a minute of each ADV burst were utilized to calibrate ADV backscatter for mass concentration (Figure 6.6). Although there was significant scatter in the regression of log(TSS) versus burst-averaged ADV backscatter among individual pump samples, the best-fit line for 6 October 2012 was remarkably similar to overall best-fit found for the same model SonTek ADVOcean by Cartwright et al. (2009) (see dashed line in Figure 6.6), that also utilized *in situ* York River pump samples.
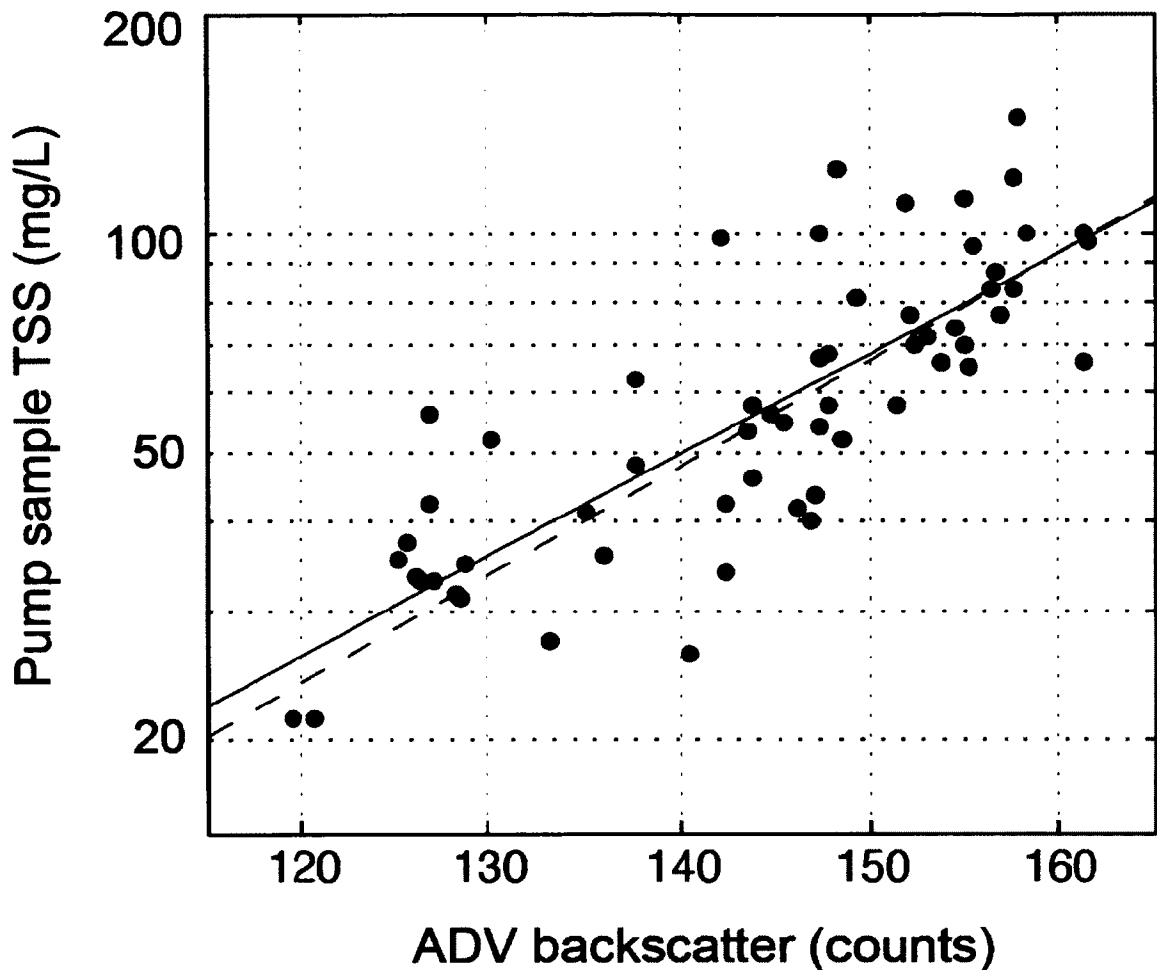
Figure 6.6 ADV backscatter measured by the VIMS profiler and corresponding total suspended solids concentrations determined from pump samples collected throughout the water column at the MUDBED site in the York River Estuary over the course of a flood tide on 6 October 2012. The solid line is the best-fit semilog regression for these samples, while the dotted line is the best-fit line for 100s of York River Estuary TSS vs. ADV backscatter samples analyzed in 2007 and 2008 by Cartwright et al. 2009.

The stability of the best-fit line combined with such large scatter suggests that much of the "noise" in Figure 6.6 is due to significant, but short-term (i.e., < 10s of sec), turbulent variations in concentration. This degree of short-term variability was also resolved by the ADV: the range in ADV backscatter incorporated into each burst-average value displayed in Fig. 6, based on +/- 2 standard deviations, averaged 15 counts. But given the short-term duration of the pump samples (~ 5 sec to fill a liter
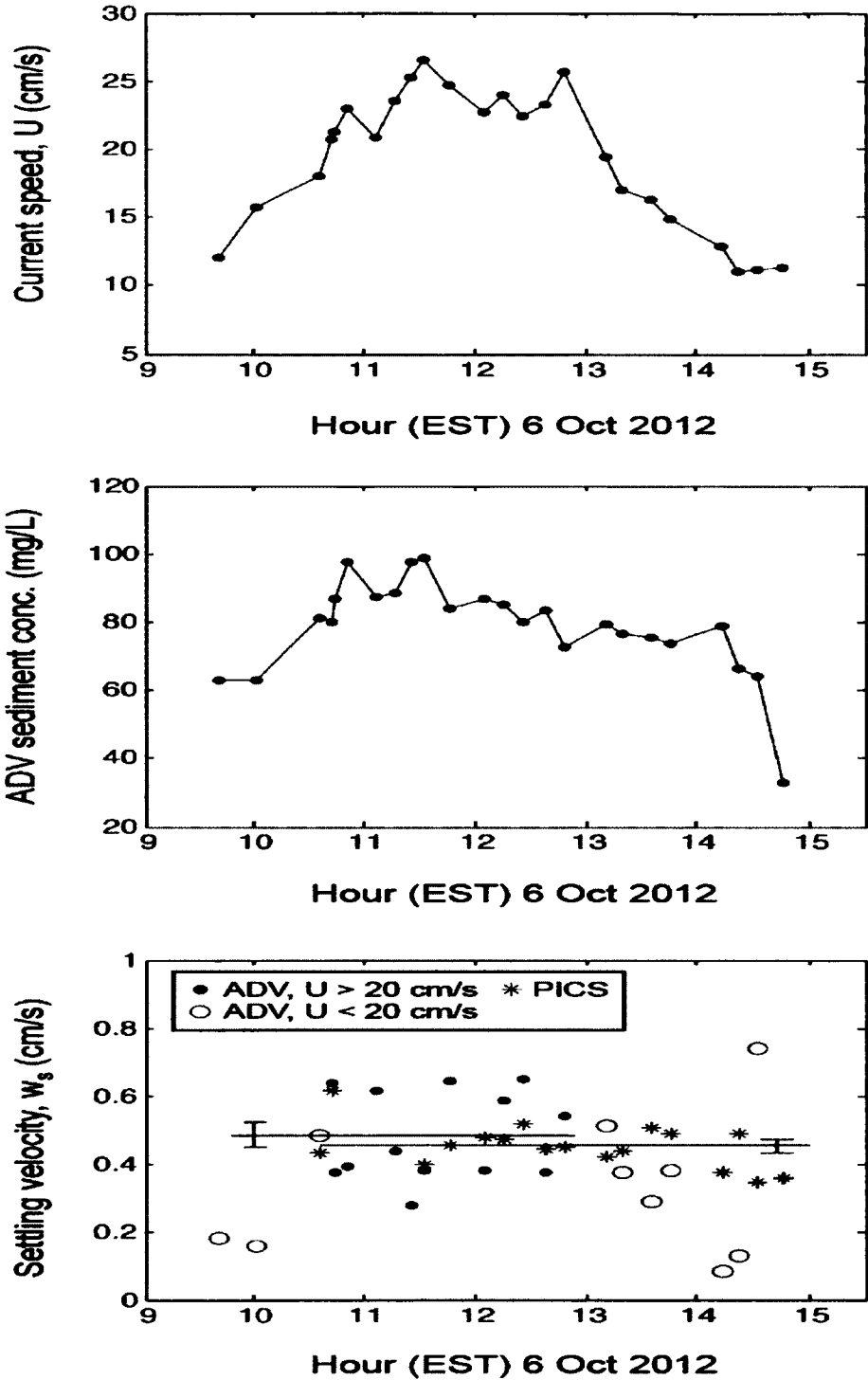
Figure 6.7 Near-bed observations of **(A)** current speed from ADV; **(B)** suspended suspended sediment concentration from ADV backscatter; **(C)** particle settling velocity (w_s) from both ADV and PICS observations. Also shown are standard errors for w_s for all the PICS observations as well as for w_s for ADV cases with U > 20 cm/s.

bottle) and the horizontal separation of the pump intake and the ADV on the profiler, it was not possible to exactly co-locate the ADV and TSS samples in space and time.

Results for burst-averaged current speed and sediment concentration 37 cm above the bed, as determined by the ADV for times that the profiler rested on the bottom, are displayed in Figures 6.7A and 6.7B. Observations were collected through "slack" after flood, although lateral circulation at the end of flood created near-bed current speed of at least about 10 cm/s. The lowest value inferred near the bed for burst-averaged sediment concentration was 33 mg/L. Thus this value was taken to approximate C_{wash}. Fig. 6.7C displays the resulting "instantaneous" ADV-based estimates of settling velocity determined by solving for w_s in Eq. (6.2) along with observations of w_s collected by the PICS video settling column. Note that several PICS observations are missing from early in the field experiment due to technical glitches.

The ADV Reynolds method for w_s is most consistent with the PICS setting column results for samples collected around peak tidal flow. This makes sense because this is the part of the tidal cycle when the steady-state Rouse balance assumed by Eqs. (6.1)-(6.2) is most justified. Based on several months of ADV tripod data from the York River, Fall (2012) found that noise in ADV-based estimates of w_s began to increase substantially for currents speeds less than about 20 cm/s. Thus ADV-based estimates of w_s for U > 20 cm/s are highlighted in Figure 6.7C as being relatively more reliable. The average of the estimates of w_s based on the ADV (0.48+/-0.04 mm/s) and based on the PICS (0.45+/-0.02 mm/s) are then highly consistent (Figure 6.7C). It is worth noting that for the period around peak tidal flow in Figure 6.7, the "slope-intercept" method, of Fugate and Friedrichs (2002), for estimating w_s failed, in that there was not enough systematic co-variation in <w'C'> and <C> to resolve a stable estimate of w_s.

The sensitivity of the "prescribed washload" method to the overall ADV calibration was tested by reducing all of the TSS values by 50% in Figure 6.6 and repeating the full

analysis. The resulting ADV-based estimates of w_s in Figure 6.7C changed by less than 1%. This follows because the calibration for C appears proportionately in all three terms in Eq. (6.2)., so that the effect of the "absolute" calibration effectively cancels out. In contrast, the "prescribed washload" method (as its name suggests) is indeed sensitive to the choice of C_{wash}. If one reduces C_{wash} by 50%, but otherwise keeps the ADV calibration the same, the average value of ADV-based w_s is reduced in this case by 24%. *From (6.2) it is easily seen that the closer C_{wash} is to $<C>$, the more sensitive w_s is to changes in the choice of C_{wash}.*

6.5 Discussion and Conclusions

Two distinct ADV-based approaches for estimating w_s have been verified, one which utilizes direct Doppler measurements of sediment motion, and the second which balances upward Reynolds flux and downward settling assuming a Rouse balance. The former can be useful when w_s is relatively large (~ cm/s) and has potential for future approaches for measuring w_s in the laboratory under a variety of flow conditions. The latter is particularly useful when w_s is relatively small (~ mm/s) and is especially useful for non-obtrusive, *in situ* field measurements.

ADV-based estimates of sediment settling velocity (w_s) have been confirmed here by independent measurements of the same particle populations within settling columns. Advantages of the ADV include its relatively simple operation and robustness under high-energy conditions, its resilience to biofouling, and, especially, the fact that its ability for *in situ* observation does not affect local flow conditions within its remote sampling volume.

Both ADV-based methods presented here are relatively insensitive to the calibration of acoustic backscatter to mass concentration (C). In the first case, w_s is determined directly by Doppler shift and thus is, by definition, independent of the acoustic backscatter calibration. In the latter case, calibrated concentration appears within each term of the relevant equation such that sensitivities to the calibration of the acoustic signal tend to cancel.

Two approaches to Reynolds flux approach for estimating ADV-based w_s have been outlined, one that regresses $<C>$ vs. $<C'w'>$ to derive w_s, and the second which divides $<C'w'>$ by $(<C> - C_{wash})$, where C_{wash} is a non-settling washload component of sediment concentration. The former is approach limited by its low-pass nature and by the likelihood that bursts might be included that do not individually satisfy a Rouse balance. The second method is limited by the need to specify C_{wash} and by its overall sensitivity to the choice of C_{wash}. However, an operational definition of C_{wash}, as the lowest concentration observed at a given height over a tidal cycle, is relatively simple to objectively implement and produced reasonable estimates of w_s.

An important corollary of this study's agreement between ADV-based *in situ* measurements of w_s under turbulent flow, and w_s measured in settling columns under nearly quiescent conditions is that, for conditions under which the particles themselves do not evolve, *relatively diverse hydrodynamic conditions do not appear to fundamentally affect w_s*. Other investigators have previously suggested that w_s can be highly dependent on turbulence, even for resilient, non-cohesive particles (Kawanisi and Shiozaki, 2008).

It is possible that in the past, some confusion may have arisen over the definition of w_s being applied in various situations. Here we define w_s as the particle settling velocity within a reference frame moving within local turbulent eddies. So local slowing or speeding of overall settlement flux by eddies does not necessarily impact w_s by our

definition. In fact, it is the very correlations between eddy motion and fluctuations in the concentration field that create the Reynolds flux that ultimately balances settling by $w_s<C>$.

The successful comparison of w_s inferred from ADVs with w_s inferred from settling columns supports the use of both of these methods. For non-cohesive sediment in the lab, it appears that gravimetric settling columns such as the Rapid Sediment Analyzer produce values for w_s equivalent to those observed under turbulent conditions, at least for w_s up to several cm/s and turbulenc and concentration levels typical in the York River. For *in situ* video settling columns such as the PICS, we conclude that flocs can potentially be sampled quickly enough to avoid significant flow-induced changes in particle properties with in the camera chamber.

6.6 Acknowledgements

6.7 References

Buchholz, F., Buchholz, C., Reppin, J., & Fischer, J. (1995). Diel vertical migrations of Meganyctiphanes norvegica in the Kattegat: Comparison of net catches and measurements with Acoustic Doppler Current Profilers. Helgoländer Meeresuntersuchungen, 49(1-4), 849-866.

Cartwright, G. M., Friedrichs, C. T., Dickhudt, P. J., Gass, T., & Farmer, F. H. (2009). Using the acoustic Doppler velocimeter (ADV) in the MUDBED real-time observing system. In: OCEANS 2009, Institute of Electrical and Electronics Engineers, ISBN: 978-1-4244-4960-6, p. 1428-1436.

Cartwright, G. M., Friedrichs, C. T., & Sanford, L. P. (2011). *In situ* characterization of estuarine suspended sediment in the presence of muddy flocs and pellets. In: P. Wang, P., Rosati, J. D., & Roberts, T. M. (eds.), Coastal Sediments 2011, World Scientific, ISBN 978-981-4355-52-0, p. 642-655.

Fall, K. A. (2012). Relationships among fine sediment settling and suspension, bed erodibility, and particle type in the York River estuary Virginia. M.S. Thesis, School of Marine Science, College of William & Mary, Gloucester Point, VA, 144 p.

Friedrichs, C. T., Cartwright, G. M., & Dickhudt, P. J. (2008). Quantifying benthic exchange of fine sediment via continuous, noninvasive measurements of settling velocity and bed erodibility. Oceanography, 21(4), 168-172.

Fugate, D. C., & Friedrichs, C. T. (2002). Determining concentration and fall velocity of estuarine particle populations using ADV, OBS and LISST. Continental Shelf Research, 22(11), 1867-1886.

Halka, J. P., Conkwright, R. D., Kerhin, R. T., & Wells, D. V. (1980). The design and calibration of a rapid sediment analyzer and techniques for interfacing to a dedicated computer system: Maryland Geological Survey Information Circular No. 32, 32 p.

Harris, C. K., Sherwood, C. R., Signell, R. P., Bever, A. J., & Warner, J. C. (2008). Sediment dispersal in the northwestern Adriatic Sea. Journal of Geophysical Research: Oceans, 113(C11), doi:10.1029/2006JC003868, 18 p.

Jay, D. A., Orton, P. M., Chisholm, T., Wilson, D. J., & Fain, A. M. (2007). Particle trapping in stratified estuaries: application to observations. Estuaries and Coasts, 30(6), 1106-1125.

Kawanisi, K., & Shiozaki, R. (2008). Turbulent effects on the settling velocity of suspended sediment. Journal of Hydraulic Engineering, 134(2), 261-266.

Kraus, N. C., Lohrmann, A., & Cabrera, R. (1994). New acoustic meter for measuring 3D laboratory flows. Journal of Hydraulic Engineering, 120(3), 406-412.

Maa, J. Y., & Kwon, J. I. (2007). Using ADV for cohesive sediment settling velocity measurements. Estuarine, Coastal and Shelf Science, 73(1), 351-354.

Mantovanelli, A., & Ridd, P. V. (2006). Devices to measure settling velocities of cohesive sediment aggregates: a review of the *in situ* technology. Journal of Sea Research, 56(3), 199-226.

McCave, I. N., & Hall, I. R. (2006). Size sorting in marine muds: processes, pitfalls, and prospects for paleoflow speed proxies. Geochemistry, Geophysics, Geosystems, 7(10), doi:10.1029/2006GC001284, 37 p.

McLean, S. R. (1992). On the calculation of suspended load for noncohesive sediments. Journal of Geophysical Research: Oceans, 97(C4), 5759-5770.

Sanford, R. B., & Swift, D. J. (1971). Comparison of sieving and settling techniques for size analysis, using a Benthos Rapid Sediment Analyzer. Sedimentology, 17(3-4), 257-264.

Smith, J. J. (2010). Fine sediment dynamics in dredge plumes. PhD Thesis, School of Marine Science, College of William and Mary, Gloucester Point, VA, 130 p.

Smith, S. J., & Friedrichs, C. T. (2011). Size and settling velocities of cohesive flocs and suspended sediment aggregates in a trailing suction hopper dredge plume. Continental Shelf Research, 31(10), S50-S63.

Smith, S. J., & Friedrichs, C. T. (2013). Image processing methods for *in situ* estimation of cohesive sediment floc size, settling velocity and density. Submitted to Limnology and Oceanography Methods.

Smyth, C., Hay, A. E., Hill, P. S., & Schillinger, D. (2006). Acoustic observations of vertical and horizontal swimming velocities of a diel migrator. Journal of Marine Research, 64(5), 723-743.

SonTek (2001). SonTek/YSI ADVField/Hydra Acoustic Doppler Veocimeter (Field) technical documentation ADVOcean/Hydra expanded description. SonTek/YSI, Inc., 228 p.

Rehman, S. S., & Vincent, C. E. (1990). Underwater acoustic measurement of suspended sediments: the calibration of a high-frequency acoustic backscatter meter. Geological Bulletin, University of Peshawar, 23, 161-173.

Voulgaris, G., & Meyers, S. T. (2004). Temporal variability of hydrodynamics, sediment concentration and sediment settling velocity in a tidal creek. Continental Shelf Research, 24(15), 1659-1683.

Voulgaris, G., & Trowbridge, J. H. (1998). Evaluation of the Acoustic Doppler Velocimeter (ADV) for turbulence measurements. Journal of Atmospheric and Oceanic Technology, 15(1), 272-289.

CHAPTER 7

CONCLUSIONS AND Suggestions for FUTURE WORK

7. Recommendations for Future Work

This last chapter, which addresses recommendations for future work, serves two purposes. First, it suggests logical next steps in the line of investigation associated with this dissertation, namely productive avenues for the continued application of acoustic and optics for characterizing estuarine suspended particulate matter. Second, it provides an opportunity to add additional commentary addressing the "fixed" content of Chapters 2, 3 and 5. Because these three chapters of the dissertation have already been published in their "final" form, it would not be productive to further edit them. Some of the most likely future work to follow on soon after this dissertation is completed includes:

7.1. MUDBED Data Report

An electronic data report (CHSD2013-01) will be created summarizing all the tripod and calibration cruise data which were collected between 2006-2012 for the MUDBED project on the York River. Before doing so the burst concentrations and bulk settling velocities will need to be recalculated using the procedures developed in Chapters 4 and 6.

7.2. Corrected Concentrations

The concentrations in Chapter 2 of this dissertation were calculated based on a "universal" regression to convert the burst averaged acoustic backscatter to

concentration. This universal regression was generated using all the acoustic bursts which correspond to pumped water samples collected during calibration cruises in 2007 and 2008. The backscatter collected for each of the calibration cruises can be "normalized" by adjusting the acoustic response measured by the ADV to a reference ADV as described in Chapter 4. Once this is done, the regressions generated for each of the 30+ cruises can be compared to either: 1) generate a new "universal" regression or 2) see if the suspended population is changing enough to warrant a "seasonal" regression. It would be interesting to see how much "bias" in the original concentrations was introduced by using the single 2007-2008 "universal" regression. The scatter in the data (Figure 2.10) around this universal regression curve was large. While some of the scatter is due to the natural variation particle properties and the limited ability of a pump sample to fully represent the ADV sample volume, normalizing the ADV backscatter to a reference ADV is still expected to reduce that scatter significantly.

7.3 Corrected Bulk Settling Velocities

Once the best concentration regressions are determined and generated, the tripod concentrations can be recalculated. These concentrations can then be used to determine how the "background" concentration described in Chapter 6 changes over time. I would expect a tidal, seasonal and yearly change in this concentration. As well as possibly a change due to episodic events. As shown in Chapter 6, it is critical to determine the

most realistic background concentration before calculating settling velocity for the non-washload component of the concentration field. Once the settling velocities for the actively settling component are more properly and carefully calculated, they can more effectively be used to compare the suspended sediment population changes in the bottom meter over tidal, seasonal, and yearly times-scales, and in response to consistent weather changes and episodic events.

7.4 ADV response to suspended sediment population changes

More laboratory work needs to be done in order to better understand how the ADV responds to mixed sediment concentrations. A logical next step is to see how the ADV responds to different percentages of silt and/or sand size in the suspended mud fraction. With the success of being able to generate a model for the response of the ADV to changing sand in a mud concentration in Chapter 4, it would be interesting to see how that model changes with 1) changing concentrations of silt in the mud fraction, and 2) changes in the sand grain-size.

More work also needs to be done to understand the acoustic response to flocculation/de-flocculation of the "natural" fine sediment in suspension. One possibility could be to increase the salinity of the mud solution in the laboratory. Tap water was used for the laboratory calibration experiments done for this dissertation to discourage the

flocculation of the fine sediment. Increasing the salinity would enhance the flocculation tendencies. A series of calibrations of sediment with different silt/clay ratios could be run in various salinities to create different floc populations. It might be possible to verify the floc size distributions with the PICS camera settling column.

APPENDICES

Appendix 1. 2006-2012 Tripod Schedule and Metadata

Appendix 1 (Table A1) contains information (metadata) such as of when the tripods were deployed, retrieved, including what instruments were used between 2006-2012. Data are available in Data Report CHSD2013-01.

The columns in Table A1 are as follows:

Column 1: General location Tripod deployed in the York River, Virginia (Gloucester Point or Clay Bank)

Column 2: Date tripod deployed

Column 3: Date tripod retrieved

Column 4: minutes of latitude of tripod deployment site (37° N + minutes)

Column 5: minutes of longitude of tripod deployment site (-76° W + minutes)

Columns 6-9: Serial number of each instrument deployed on the tripod

Table A1. 2006-2012 Tripod Schedule and Metadata

					Vendor Sensor Serial Number			
Location (York River)	Deploy date	Retrival date	Lattitude 37° N	Longitude -76° W	Sontek ADV (downward)	Sontek ADV (upward)	LISST 100X	YSI CTD
Gloucester Point	12/4/06	1/30/07	14.875	29.918	B337			03H1988
Clay Bank	2/27/07	6/8/07	20.403	37.461	B337			0001341A
Clay Bank	6/12/07	8/31/07	20.418	37.458	B337			
Gloucester Point	7/31/07	8/30/07	14.681	29.939	B337		1232	03K0492
Gloucester Point	8/31/07	11/12/07	14.687	29.970	B337		1232	03K0492
Clay Bank	8/31/07	11/12/07	20.390	37.430	B336		1239	07B1391
Clay Bank	12/5/07	2/4/07	20.397	37.434	B337		1185	03K0492
Gloucester Point	12/5/07	4/2/08	14.692	29.961	B338		1239	07B1391
Clay Bank	2/8/08	6/23/08	20.411	37.341	B336		1232	03H1988
Gloucester Point	4/2/08	7/11/08	14.695	29.941	B337		1185	03K0492
Clay Bank	6/23/08	9/22/08	20.448	37.448	B338		1239	07B1391
Gloucester Point	7/11/08	12/9/08	14.692	29.940	B336		1232	03H1988
Clay Bank	9/30/08	2/11/09	20.446	37.476	B337		1185	03K0492
Gloucester Point	12/8/08	3/19/09	14.692	29.940	B338		1239	07B1391
Clay Bank	2/25/09	4/29/09	20.463	37.476	B337		1232	03H1988
Clay Bank	5/12/09	8/25/09	20.499	37.484	B337		1185	03H1988
Clay Bank	7/22/09	10/20/09	20.446	37.476	B338		1232	07B1391
Clay Bank	11/5/09	2/24/10	20.446	37.476	B336		1185	03K0492
Clay Bank	12/22/09	2/19/10	20.449	37.467		B338		
Clay Bank	2/24/10	9/8/10	20.449	37.476	B337		1239	03H1988
Clay Bank	9/27/11	3/13/11	20.449	37.476	B338			03K0492

Table A1. 2006-2012 Tripod Schedule and Metadata   (cont)

| Location | Deploy date | Retrival date | Latitude | Longitude | Vendor Sensor Serial Number | | | |
(York River)			37° N	-76° W	Sontek ADV (downward)	Sontek ADV (upward)	LISST 100X	YSI CTD
Clay Bank	5/6/11	7/5/11	20.482	37.513	B337	B336		03H1988
Clay Bank	7/19/11	12/1/11	20.490	37.520	B338	B337		07B1391
Clay Bank	12/9/11	2/29/12	20.490	37.520	B338	B337		07B1391
Clay Bank	3/19/12	6/7/12	20.492	37.497	B338			04K17251AB
Clay Bank	6/27/12	9/24/12	20.490	37.500	B336	B337		03K0492
Clay Bank	9/24/12	2/12/13	20.485	37.510	B3084	B338		03H1988

Appendix 2. 2006-2012 Calibration Cruise Schedule and Metadata

Appendix 2 contains information (metadata) such as of when the calibration cruises occurred, instruments used, number of "bursts" from which instruments, and number of pump samples collected. Table A2.1 is a list of all the calibration cruises conducted that correspond to tripods deployed as listed in table. Tables A2.2-A2.34 contain information for each cruise. Data are available in Data Report CHSD2013-01.

The columns in Table A2.1 are as follows:

Column 1: The unique cruise identification number

Column 2: Date calibration cruise conducted

Column 3: General location of the calibration cruise (either Clay Bank or Gloucester Point)

Column 4: Unique station numbers collected during the cruise that correspond to individual file names collected by each of the instruments

Column 5: Stage of the tide the cruise was conducted over. Usually a 6 hour time period from slack to slack bracketing either an ebb or flood tide.

Columns 6-8: Serial number of each instrument deployed on the profiler. Additionally, a downward looking RDI 1200 kHz ADCP was mounted to the bow of the vessel. The same one was used from 2006-2012.

Table A2.1 Calibration Cruises associated with Tripod Deployments

Cruise	Date	Location	Station Numbers	Stage of tide	YSI CTD SN	Sequia LISST SN	Sontek ADV SN
					Vendor Sensor Serial Number		
YR070129	1/29/07	Gloucester Pt	4254-4269		03K0492	1075	B338
YR070329	3/29/07	Clay Bank	4270-4314	Ebb	01J0035	1075	B338
YR070718	7/18/07	Clay Bank	4315-4356	Flood	07B1391	1075	B336
YR070724	7/24/07	Clay Bank	4357-4389	Ebb-Flood	07B1391	1075	B336
YR070821	8/21/07	Gloucester Pt	4390-4407	Flood	07B1391	1239	B336
YR071217	12/17/07	Gloucester Pt	4408-4420	Flood	03H1988	1232	B336
YR071218	12/18/07	Clay Bank	4421-2257	Flood	03H1988	1232	B336
YR080415	4/15/08	Clay Bank	4461-4488	Ebb	07B1391	1239	B338
YR080416	4/16/08	Gloucester Pt	4489-4497	Ebb	07B1391	1239	B338
YR080418	4/18/08	Clay Bank	4498-4514	Slack-Ebb	07B1391	1239	B338
YR080505	5/5/08	Clay Bank	4515-4525	Slack-Ebb	07B1391	1239	B338
YR080507	5/7/08	Clay Bank	4526-4540	Slack-Flood	07B1391	1239	B338
YR080514	5/14/08	Clay Bank	4541-4564	Slack-Ebb	07B1391	1239	B338
YR080515	5/15/08	Clay Bank	4565-4591	Slack-Ebb	07B1391	1239	B338
YR080603	6/3/08	Clay Bank	4582-4601	Slack-Ebb	07B1391	1239	B338
YR080606	6/6/08	Clay Bank	4602-4620	Slack-Flood	07B1391	1239	B338
YR080609	6/9/08	Clay Bank	4621-4635	Slack-Flood	07B1391	1239	B338
YR080610	6/10/08	Clay Bank	4636-4650	Slack-Flood	07B1391	1239	B338
YR080729	7/29/08	Clay Bank	4651-4676	Ebb	03K0492	1185	B337
YR080731	7/31/08	Gloucester Pt	4677-4700	Ebb	03K0492	1185	B337

Table A2.1 Calibration Cruises associated with Tripod Deployments   **(cont)**

					Vendor Sensor Serial Number		
Cruise	Date	Location	Station Numbers	Stage of tide	YSI	Sequia	Sontek
					CTD SN	LISST SN	ADV SN
YR081016	10/16/08	Clay Bank	4701-4729	Flood	07B1391	1239	B338
YR090108	1/8/09	Gloucester Pt	4730-4757	Ebb	03H1988	1232	B336
YR090226	2/26/09	Clay Bank	4758-4781	Flood	03K0492	1185	B339
YR090514	5/14/09	Clay Bank	4802-4819	Flood	07B1391	1232	B339
YR090811	8/11/09	Clay Bank	4820-4846	Flood	04K17251	1185	B336
YR091125	11/25/09	Clay Bank	4847-4872	Ebb	04K17251	1232	B338
YR110816	8/16/11	Clay Bank	4941-4946	Flood	04K17251	1185	B339
YR110818	8/18/11	Clay Bank	4949-4967	Flood	04K17251	1185	B339
YR110901	9/1/11	Clay Bank	4976-4995	Flood	04K17251	1185	B339
YR111220	12/20/11	Clay Bank	4989-5004	Ebb	11H100740	1239	B339
YR120430	4/30/12	Clay Bank	4998-5014	Ebb	11H100740	1239	B339
YR120724	7/24/12	Clay Bank	5026-5040	Flood	11H100740	1239	B308H
YR121006	10/6/12	Clay Bank	5038-5077	Flood	11H100740	1239	B336

The columns in Table2 A2.2-A2.34 are as follows:

Column 1: Unique station numbers collected during the cruise that correspond to individual file names collected by each of the instruments

Column 2: A description of what is collected. "Profile" usually consists of a full downward profile of the instruments and then "sample bursts" at distinct heights on the way up. Each "sample burst" is when the instruments are held at one height for a period of 2-5 minutes".

Column 3: Date of calibration cruise

Column 4: Time of the start of each station using the CTD data. It is always collected in EST. All computers and instruments are synced to time provided by a GPS or cell phone (to the nearest second).

Column 5: Minutes of latitude of tripod deployment site (37° N + minutes) at the beginning of the station

Column 6: Minutes of longitude of tripod deployment site (-76° W + minutes) at the beginning of the station

Column 7: Total water depth as recorded by the bottom tracking feature of the ADCP at the beginning of the station.

Columns 8: A "1" indicates a "real-time" data file was collected by the CTD. If the station number is 4254 the filename collected by the CTD is C4254.

Column 9: The number indicates the water samples collected during the station. This is also number of "bursts" collected if the station is a profile.

Column 10: A "1" indicates a "real-time" data file was collected by the LISST. If the station number is 4254 the filename collected by the LISST is L4254.

230

Column 11: A "1" indicates a "real-time" data file was collected by the ADCP during a profile station. The ADCP filename is in column 15.

Column 12: A "1" indicates a "real-time" data file was collected by the ADV during a profile. If the station number is 4254 the filename collected by the ADV is A4254.

Column 13: A "1" indicates a "real-time" data file was collected by the ADV while the profiler is sitting on the bottom. If the station number is 4254 the filename collected by the ADV is A4254.

Column 14: A "1" indicates that a transect was collected using the ADCP. Information in columns 4-7 correspond to the beginning of the transect. A linked GPS and bottom tracking can be used to identify location along the transect. The ADCP filename is in column 15.

Table A2.2. YR070129 (Gloucester Point - Jan 29, 2007) Calibration Cruise

Station	Description	Date	Time (EST)	Lat 37° N	Long 76° W	depth (m)	CTD	TSS	LISST	ADCP profile	ADV profile	ADV bottom	ADCP transect	ADCP filename
4254	Proflile	1/29/07	847	14.678	29.923	7.26	1	3	1	1	1			YR0701000
4255	Bottom		854	14.676	29.924	7.31	1	1	1	1	1			YR0701001
4256	Proflile		1040	14.678	29.222	6.96	1	0	1	1	1			YR0701002
4257	Proflile		1113	14.676	29.920	6.99	1	3	1	1	1			YR0701003
4258	Bottom		1126	14.677	29.920	6.89	1	1	1	1	1			YR0701004
4259	Proflile		1201	14.678	29.920	6.82	1	3	1	1	1			YR0701005
4260	Bottom		1215	14.676	29.920	6.87	1	1	1	1	1			YR0701006
4261	Proflile		1252	14.678	29.920	6.89	1	3	1	1	1			YR0701007
4262	Bottom		1301	14.679	29.920	6.86	1	0	1	1	1			YR0701008
4263	Proflile		1339	14.678	29.921	6.94	1	3	1	1	1			YR0701009
4264	Bottom		1350	14.680	29.922	6.94	1	0	1	1	1			YR0701010
4265	Proflile		1426	14.675	29.924	6.97	1	3	1	1	1			YR0701011
4266	Bottom		1437	14.677	29.921	6.96	1	1	1	1	1			YR0701012
4267	Proflile		1514	14.676	29.923	7.07	1	3	1	1	1			YR0701013
4268	Bottom		1524	14.684	29.924	6.93	1	1	1	1	1			YR0701014
4269	Proflile		1600	14.677	29.935	7.16	1	3	1	1	1			YR0701015

Table A2.3. YR070329 (Clay Bank, March 29, 2007) Calibration Cruise

Station	Description	Date	Time (EST)	Lat 37° N	Long 76° W	depth (m)	CTD	TSS	LISST	ADCP profile	ADV profile	ADV bottom	ADCP transect	ADCP filename
4270	Full Transect	3/29/07	805	20.796	36.656								1	YR0702000
4271	A- SE shoal profile		829	20.110	38.046	1.67	1	1	1	1	1			YR0702002
4272	Transect A-B		844	20.246	37.851								1	YR0702004
4273	B- Second Channel		849	20.405	37.511	5.69	1	1	1	1	1			YR0702005
4274	Transect B-C		902	20.408	37.504								1	YR0702006
4275	C- Interfluv profile		910	20.496	37.228	4.62	1	1	1	1	1			YR0702007
4276	Transect C-D		915	20.498	37.217								1	YR0702008
4277	D- Main Channel		920	20.743	36.762	13.3	1	3	1	1	1			YR0702009
4278	Transect D-E		930	20.741	36.74								1	YR0702010
4279	E- NW shoal profile		932	20.786	36.657	1.49	1	1	1	1	1			YR0702011
4280	Full Transect (NW-SE)		940	20.784	36.67								1	YR0702012
4281	A- SE shoal profile		1003	20.181	38.056	2.61	1	1	1	1	1			YR0702013
4282	Transect A-B		1011	20.221	37.964								1	YR0702014
4283	B- Secondary Channel		1016	20.403	37.478	5.9	1	2	1	1	1			YR0702015
4284	Transect B-C		1024	20.493	37.333								1	YR0702016
4285	C- Interfluv profile		1027	20.478	37.228	4.47	1	1	1	1	1			YR0702017
4286	Transect C-D		1037	20.487	37.212								1	YR0702018
4287	D- Main Channel		1042	20.741	36.742	12.83	1	3	1	1	1			YR0702019
4288	Transect D-E		1054	20.739	36.695								1	YR0702020
4289	E- NW shoal		1100	20.784	36.666	1.6	1	1	1	1	1			YR0702022
4290	Full Transect (NW-SE)		1107	20.787	36.676								1	YR0702023

Table A2.3. YR070329 (Clay Bank, March 29, 2007) Calibration Cruise (Cont)

Station	Description	Date	Time (EST)	Lat 37° N	Long 76° W	depth (m)	CTD	TSS	LISST	ADCP profile	ADV profile	ADV bottom	ADCP transect	ADCP filename
4291	Transect A-B		1122	20.184	38.109								1	YR0702024
4292	B- Secondary Channel		1128	20.392	37.47	5.58	1	2	1	1	1			YR0702025
4293	Transect B-C		1140	20.398	37.459								1	YR0702026
4294	C- Interfluv profile		1142	20.492	37.217	4.18	1	1	1	1	1			YR0702027
4295	Transect C-D		1148	20.500	37.211								1	YR0702028
4296	D- Main Channel		1152	20.713	36.741	12.15	1	3	1	1	1			YR0702029
4297	Transect D-E		1203	20.721	36.695								1	YR0702030
4298	Full Transect (NW-SE)		1205	20.786	36.666								1	YR0702031
4299	Transect A-B		1219	20.193	38.101								1	YR0702032
4300	B- Secondary Channel		1226	20.388	37.475	5.23	1	2	1	1	1			YR0702033
4301	Transect B-C		1235	20.373	37.462								1	YR0702034
4302	C- Interfluv profile		1239	20.488	37.21	3.99	1	1	1	1	1			YR0702035
4303	Transect C-D		1245	20.437	37.153								1	YR0702036
4304	D- Main Channel		1250	20.725	36.74	12.51	1	3	1	1	1			YR0702037
4305	Transect D-E		1302	20.731	36.744								1	YR0702038
4306	Full Transect (NW-SE)		1304	20.784	36.673								1	YR0702039
4307	Transect A-B		1318	20.192	38.104								1	YR0702040
4308	B- Secondary Channel		1323	20.396	37.472		1	2	1	1	1			YR0702041
4309	Transect B-C		1331	20.407	37.464								1	YR0702042
4310	C- Interfluv profile		1334	20.500	37.215		1	1	1	1	1			YR0702043
4311	Transect C-D		1339	20.501	37.209								1	YR0702044

234

Table A2.23 YR070329 (Clay Bank, March 29, 2007) Calibration Cruise   (Cont)

Station	Description	Date	Time (EST)	Lat 37° N	Long 76° W	depth (m)	CTD	TSS	LISST	ADCP profile	ADV profile	ADV bottom	ADCP transect	ADCP filename
4312	**D-** Main Channel		1344	20.723	36.727	12.4	1	3	1	1	1			YR0702045
4313	Transect D-E		1354	20.719	36.696								1	YR0702046
4314	Full Transect (NW-SE)		1355	20.783	36.675								1	YR0702047

Table A2.4. YR070718 (Clay Bank, July 18, 2007) Calibration Cruise

Station	Description	Date	Time (EST)	Lat 37° N	Long 76° W	depth (m)	CTD	TSS	LISST	ADCP profile	ADV profile	ADV bottom transect	ADCP bottom transect	ADCP filename
4315	Full Transect (	7/18/07	801	20.793	36.667								1	YR0707000
4316	A- SE shoal profile		818	20.285	37.865	2.6	1	1	1	1	1			YR0707001
4317	Transect A-B		829	20.302	37.844								1	YR0707002
4318	B- Secondary Channel		833	20.414	37.486	5.46	1	3	1	1	1			YR0707003
4319	Transect B-C		846	20.429	37.469								1	YR0707004
4320	C- Interfluv profile		849	20.497	37.248	4.34	1	2	1	1	1			YR0707005
4321	Transect C-D		858	20.400	37.200								1	YR0707006
4322	D- Main Channel		903	20.734	36.755	12.62	1	3	1	1	1			YR0707007
4323	Full Transect (NW-SE)		920	20.797	36.678								1	YR0707008
4324	A- SE shoal profile		936	20.276	37.852	2.81	1	1	1	1	1			YR0707009
4325	Transect A-B		944	20.298	37.820								1	YR0707010
4326	B- Secondary Channel		948	20.436	37.485	5.84	1	3	1	1	1			YR0707011
4327	Transect B-C		959	20.428	37.495								1	YR0707012
4328	C- Interfluv		1003	20.499	37.226	4.51	1	2	1	1	1			YR0707013
4329	Transect C-D		1012	20.500	37.229								1	YR0707014
4330	D- Main Channel		1016	20.732	36.765	12.41	1	3	1	1	1			YR0707015
4331	Full Transect (NW-SE)		1028	20.799	36.679								1	YR0707016
4332	A- SE shoal profile		1044	20.268	37.835	2.96	1	1	1	1	1			YR0707017
4333	Transect A-B		1052	20.266	37.837								1	YR0707018
4334	B- Secondary Channel		1055	20.427	37.491	5.93	1	3	1	1	1			YR0707019
4335	Transect B-C		1107	20.420	37.489								1	YR0707020

Table A2.4. YR070718 (Clay Bank, July 18, 2007) Calibration Cruise

Station	Description	Date	Time (EST)	Lat 37° N	Long 76°W	depth (m)	CTD	TSS	LISST	ADCP profile	ADV profile	ADV bottom	ADCP transect	ADCP filename
4341	Transect A-B		1218	20.292	37.743								1	YR0707026
4342	B- Secondary Channel		1221	20.434	37.481	6.32	1	3	1	1	1			YR0707027
4343	Transect B-C		1236	20.420	37.449								1	YR0707028
4344	C- Interfluv profile		1238	20.506	37.211	4.95	1	2	1	1	1			YR0707029
4345	Transect C-D		1246	20.503	37.214								1	YR0707030
4346	D- Main Channel		1251	20.735	36.753	13.14	1	3	1	1	1			YR0707031
4347	Transect D-end		1303	20.727	36.760								1	YR0707032
4348	Full Transect (NW-SE)		1306	20.793	36.670								1	YR0707033
4349	A- SE shoal profile		1322	20.268	37.844	3.21	1	3	1	1	1			YR0707034
4350	Transect A-B		1331	20.322	37.685								1	YR0707035
4351	B- Secondary Channel		1338	20.426	37.484	6.12	1	3	1	1	1			YR0707037
4352	Transect B-C		1350	20.437	37.480								1	YR0707038
4353	C- Interfluv profile		1352	20.509	37.244	4.85	1	2	1	1	1			YR0707039
4354	Transect C-D		1405										1	YR0707040
4355	D- Main Channel		1408	20.748	36.738	13.79	1	3	1	1	1			YR0707041
4356	Full Transect (NW-SE)		1422	20.789	36.665								1	YR0707042

237

Table A2.5. YR070724 (Clay Bank, July 24, 2007) Calibration Cruise

Station	Description	Date	Time (EST)	Lat 37° N	Long 76° W	depth (m)	CTD	TSS	LISST	ADCP profile	ADV profile	ADV bottom	ADCP transect	ADCP filename
4357	Full Transect (NW	7/24/07	802	20.791	36.679								1	YR070702001
4358	A- SE shoal profile		821	20.275	37.836	2.69	1	1		1	1			YR070702002
4359	Transect A-B		835										1	YR070702003
4360	B- Secondary Channel		839	20.412	37.478	5.54	1	3		1	1			YR070702004
4361	Transect B-C		851	20.442	37.451								1	YR070702005
4362	C- Interfluv profile		854	20.500	37.222	4.24	1	2		1	1			YR070702006
4363	Transect C-D		912	20.575	37.103								1	YR070702007
4364	D- Main Channel		917	20.737	36.738	12.75	1	3		1	1			YR070702008
4365	Full Transect (NW-SE)		933	20.791	36.672								1	YR070702009
4366	A- SE shoal profile		1025	20.280	37.829	2.59	1	1		1	1			YR070702010
4367	Transect A-B		1034	20.314	37.739								1	YR070702011
4368	B- Secondary Channel		1038	20.415	37.484	5.45	1	3		1	1			YR070702012
4369	Transect B-C			20.500	37.200								1	YR070702013/4
4370	C- Interfluv profile		1058	20.500	37.200	4.24	1	2		1	1			YR070702015
4371	Transect C-D		1109	20.500	37.200								1	YR070702016
4372	D- Main Channel		1114	20.700	36.800	13.1	1	3		1	1			YR070702017
4373	Full Transect (NW-SE)		1128	20.787	36.686								1	YR070702018
4374	A- SE shoal profile		1145	20.274	37.855	2.65	1	1		1	1			YR070702019
4375	Transect A-B		1152	20.285	37.832								1	YR070702020
4376	B- Secondary Channel		1158	20.423	37.500	5.32	1	3		1	1			YR070702021
4377	Transect B-C		1209	20.415	37.484								1	YR070702022

Table A2.5. YR070724 (Clay Bank, July 24, 2007) Calibration Cruise (cont)

Station	Description	Date	Time (EST)	Lat 37° N	Long 76° W	depth (m)	CTD	TSS	LISST	ADCP profile	ADV profile	ADV bottom	ADCP transect	ADCP filename
4378	C- Interfluv profile		1215	20.504	37.240	4.31	1	2		1	1			YR070702023
4379	Transect C-D		1223	20.500	37.209								1	YR070702024
4380	D- Main Channel		1231	20.742	36.749	12.81	1	3		1	1			YR070702025
4381	Full Transect (NW-SE)		1248	20.794	36.686								1	YR070702026
4382	A- SE shoal profile		1302	20.280	37.857	2.75	1	1		1	1			YR070702027
4383	Transect A-B		1312	20.285	37.811								1	YR070702028
4384	B- Secondary Channel		1318	20.426	37.500	5.5	1	3		1	1			YR070702029
4385	Transect B-C		1330	20.425	37.468								1	YR070702030
4386	C- Interfluv profile		1333	20.497	37.227	4.46	1	2		1	1			YR070702031
4387	Transect C-D		1342	20.501	37.206								1	YR070702032
4388	D- Main Channel		1347	20.759	36.758	13.4	1	3		1	1			YR070702033
4389	Full Transect (NW-SE)		1402	20.793	36.690								1	YR070702034

Table A2.6. YR070821 (Gloucester Point,August 21, 2007) Calibration Cruise

Station	Description	Date	Time (EST)	Lat 37° N	Long 76°W	depth (m)	CTD	TSS	LISST	ADCP profile	ADV profile	ADV bottom	ADCP transect	ADCP filename
4390	1- profile	1/29/06	1032	14.675	29.914	7.62	1	3	1	1	1			YR0708000
4391	2- profile		1103	14.678	29.915	7.6	1	3	1	1	1			YR0708001
4392	3- profile		1126	14.678	29.916	7.63	1	3	1	1	1			YR0708002
4393	4- profile		1158	14.680	29.915	7.71	1	3	1	1	1			YR0708003
4394	5- profile		1230	14.681	29.917	7.7	1	3	1	1	1			YR0708004
4395	6- profile		1245	14.678	29.916	7.8	1	3	1	1	1			YR0708005
4396	7- profile		1300	14.678	29.916	7.79	1	3	1	1	1			YR0708006
4397	8- profile		1315	14.679	29.916	7.97	1	3	1	1	1			YR0708007
4398	9- profile		1330	14.681	29.914	7.93	1	3	1	1	1			YR0708008
4399	10- profile		1345	14.679	29.916	8	1	3	1	1	1			YR0708009
4400	11- profile		1400	14.679	29.916	8	1	3	1	1	1			YR0708010
4401	12- profile		1417	14.679	29.915	8.02	1	3	1	1	1			YR0708011
4402	13- profile		1430	14.679	29.916	8.03	1	3	1	1	1			YR0708012
4403	14- profile		1500	14.679	29.915	8.02	1	3	1	1	1			YR0708013
4404	15- profile		1530	14.680	29.917	8	1	3	1	1	1			YR0708014
4405	16- profile		1559	14.683	29.917	7.9	1	3	1	1	1			YR0708015
4406	17- profile		1630	14.675	29.913	8.08	1	3	1	1	1			YR0708016
4407	18- profile		1701	14.677	29.915	8.04	1	3	1	1	1			YR0708017
														YR0708018

Table A2.7. YR071217 (Gloucester Point, December 17, 2007) Calibration Cruise

Station	Description	Date	Time (EST)	Lat 37° N	Long 76°W	depth (m)	CTD	TSS	LISST	ADCP profile	ADV profile	ADV bottom	ADCP transect	ADCP filename
4408	1- profile	12/17/07	1101	14.641	29.929	8.24	1	3	1	2	1			YR0712000&1
4409	2- profile		1131	14.640	29.927	8.21	1	3	1	1	1			YR0712002
4410	3- profile		1202	14.648	29.924	7.88	1	3	1	1	1			YR0712003
4411	4- profile		1234	14.642	29.928	8.21	1	3	1	1	1			YR0712004
4412	5- profile		1301	14.644	29.925	8.3	1	3	1	1	1			YR0712005
4413	6- profile		1331	14.641	29.926	8.45	1	3	1	1	1			YR0712006
4414	7- profile		1402	14.638	29.942	8.65	1	3	1	1	1			YR0712007
4415	8- profile		1433	14.640	29.931	8.53	1	3	1	1	1			YR0712008
4416	9- profile		1502	14.641	29.928	8.51	1	3	1	1	1			YR0712009
4417	10- profile		1531	14.645	29.927	8.27	1	3	1	1	1			YR0712010
4418	11- profile		1602	14.647	29.925	8.33	1	3	1	1	1			YR0712011
4419	12- profile		1640	14.649	29.924	8.11	1	3	1	1	1			YR0712012
4420	13- profile		1715	14.651	29.924	7.96	1	3	1	1	1			YR0712013

Table A2.8. YR071218 (Clay Bank, December 18, 2007) Calibration Cruise

Station	Description	Date	Time (EST)	Lat 37° N	Long 76° W	depth (m)	CTD	TSS	LISST	ADCP profile	ADV profile	ADV bottom	ADCP transect	ADCP filename
4421	1- Full Transec	12/18/07	1104	20.789	36.670								1	YR071218000
4422	Transect End-A		1120	20.214	38.072								1	YR071218001
4423	A- SE shoal		1128	20.289	37.845	2.14	1	2		1	1			YR071218002
4424	Transect A-B		1138	20.299	37.829								1	YR071218003
4425	B- Secondary Channel		1143	20.417	37.454	5.53	1	3		1	1			YR071218004
4426	Transect B-C		1159	20.424	37.456								1	YR071218005
4427	C- Interfluv		1202	20.488	37.282	4.22	1	2		1	1			YR071218006
4428	Transect C-D		1213	20.497	37.280								1	YR071218007
4429	D- Main Channel		1224	20.724	36.724	11.53	1	3		1	1			YR071218008
4430	Transect D-end		1238	20.750	36.745								1	YR071218009
4431	2- Full Transect (NW-SE		1239	20.789	36.670								1	YR071218010
4432	Transect end-B		1300	20.199	38.075								1	YR071218011
4433	B- Secondary Channel		1307	20.426	37.461		1	3		1	1			YR071218012
4434	Transect B-C		1326	20.419	37.457								1	YR071218013
4435	C- Interfluv		1331	20.503	37.281	4.36	1	2		1	1			YR071218014
4436	Transect C-D		1344	20.505	37.285								2	YR071218015
4437	D- Main Channel		1354	20.740	36.785	12.02	1	3		1	1			YR071218017
4438	Transect D-end		1410	20.729	36.778								1	YR071218018
4439	3- Full Transect (NW-SE		1413	20.784	36.685								1	YR071218019
4440	Transect end-B		1427	20.202	38.073								1	YR071218020
4441	B- Secondary Channel		1436	20.423	37.464		1	3		1	1			YR071218021

Table A2.8. YR071218 (Clay Bank, December 18, 2007) Calibration Cruise (cont)

Station	Description	Date	Time (EST)	Lat 37° N	Long 76° W	depth (m)	CTD	TSS	LISST	ADCP profile	ADV profile	ADV bottom	ADCP transect	ADCP filename
4442	Transect B-C		1452	20.420	37.457								1	YR071218022
4443	C- Interfluv		1455	20.507	37.271		1	2		1	1			YR071218023
4444	Transect C-D		1508	20.509	37.275									YR071218024
4445	D- Main Channel		1516	20.737	36.783		1	3		1	1			YR071218025
4446	Transect D-end		1536	20.736	36.772								1	YR071218026
4447	4- Full Transect (NW-SE	1539	20.784	36.677								1	YR071218027
4448	Transect End-A		1555	20.202	38.073								1	YR071218028
4449	A- SE shoal		1559	20.277	37.848		1	1		1	1			YR071218029
4450	Transect A - B		1610	20.277	37.848								1	YR071218030
4451	B- Secondary Channel		1615	20.425	37.458	6.02	1	3		1	1			YR071218031
4452	Transect B-C		1632	20.431	37.452								1	YR071218032
4453	C- Interfluv		1635	20.513	37.269		1	3		1	1			YR071218033
4454	Transect C-D		1653	20.513	37.267								1	YR071218034
4455	D- Main Channel		1701	20.733	36.782	12.09	1	3		1	1			YR071218035
4456	Transect D-end		1719	20.730	36.760								1	YR071218036
4457	5- Full Transect (NW-SE	1720	20.778	36.695								1	YR071218037
														YR071218038

243

Table A2.9. YR080415 (Clay Bank, April 15, 2008) Calibration Cruise

Station	Description	Date	Time (EST)	Lat 37° N	Long 76° W	depth (m)	CTD	TSS	LISST	ADCP profile	ADV profile	ADV bottom	ADCP transect	ADCP filename
4461	Full Transect (	4/15/08	822	20.780	36.695								1	YR00804000
4462	Transect End-B		834	20.178	37.977								1	YR00804001
4463	B- Secondary Channel		840	20.406	37.459	6.4	1	3		1	1			YR00804002
4464	C- Interfluv profile		911	20.547	37.103	4.7	1	3		1	1			YR00804003
4465	Transect C-D		928	20.547	37.103								1	YR00804004
4466	D- Main Channel		934	20.736	36.771	12.81	1	3		1	1			YR00804005
4467	Transect D-end		946	20.740	36.746								1	YR00804006
4468	Full Transect (NW-SE)		947	20.789	36.677								1	YR00804007
4469	Transect end-B		958	20.277	37.875								1	YR00804008
4470	B- Secondary Channel		1003	20.402	37.444	6.13	1	3		1	1			YR00804009
4471	Transect B-C		1015	20.402	37.444								1	YR00804010
4472	C- Interfluv profile		1021	20.575	37.104	4.5	1	3		1	1			YR00804011
4473	Transect C-D		1030	20.518	37.063								2	YR00804012
4474	D- Main Channel		1035	20.761	36.771	13.2	1	3		1	1			YR00804013
4475	Full Transect (NW-SE)		1048	20.769	36.697								1	YR00804014
4476	Transect end-B		1101	20.227	37.904								1	YR00804015
4477	B- Secondary Channel		1107	20.402	37.437	5.94	1	3		1	1			YR00804016
4478	Transect B-C		1119	20.461	37.360								1	YR00804017
4479	C- Interfluv profile		1123	20.572	37.118	4.3	1	3		1	1			YR00804018
4480	D- Main Channel		1146	20.724	36.744	12.6	1	3		1	1			YR00804019
4481	Full Transect (NW-SE)		1203	20.783	36.681								1	YR00804020

244

Table A2.9. YR080415 (Clay Bank, April 15, 2008) Calibration Cruise (conc)

Station	Description	Date	Time (EST)	Lat 37° N	Long 76°W	depth (m)	CTD	TSS	LISST	ADCP profile	ADV profile	ADV bottom	ADCP transect	ADCP filename
4482	Transect end - B		1216	20.226	37.913								1	YR00804021
4483	B- Secondary Channel		1223	20.404	37.446	5.93	1	3		1	1			YR00804022
4484	Transect B-C		1233	20.422	37.416								1	YR00804023
4485	C- Interfluv profile		1238	20.577	37.093	4.36	1	3		1	1			YR00804024
4486	Transect C-D		1250	20.630	37.005								1	YR00804025
4487	D- Main Channel		1254	20.743	36.759	12.88	1	3		1	1			YR00804026
4488	Full Transect (NW-SE)		1306	20.772	36.711								1	YR00804027
														YR00804028

245

Table A2.10. YR080416 (Gloucester Point, April 16, 2008) Calibration Cruise

Station	Description	Date	Time (EST)	Lat 37° N	Long 76° W	depth (m)	CTD	TSS	LISST	ADCP profile	ADV profile	ADV bottom	ADCP transect	ADCP filename
4489	1- profile	4/16/08	813	14.686	29.911	7.25	1	3	1	2	1			YR080415000
4490	2- profile		830	14.688	29.909	7.15	1	3	1	1	1			YR080415001
4491	3- profile		900	14.690	29.909	7.05	1	3	1	1	1			YR080415002
4492	4- profile		930	14.691	29.910	6.83	1	3	1	1	1			YR080415003
4493	5- profile		1000	14.690	29.909	6.89	1	3	1	1	1			YR080415004
4494	6- profile		1032	14.693	29.909	6.67	1	3	1	1	1			YR080415005
4495	7- profile		1100	14.687	29.910	6.66	1	3	1	1	1			YR080415006
4496	8- profile		1130	14.689	29.911	6.62	1	3	1	1	1			YR080415007
4497	9- profile		1200	14.695	29.930	6.57	1	3	1	1	1			YR080415008

246

Table A2.11. YR080418 (Gloucester Point, April 18, 2008) Calibration Cruise

Station	Description	Date	Time (EST)	Lat 37° N	Long 76° W	depth (m)	CTD	TSS	LISST	ADCP profile	ADV profile	ADV bottom	ADCP transect	ADCP filename
4498	bottom	4/18/08	933	20.825	36.947	12.19	1	1	1	1			1	YR080418001
4499	bottom		953	20.823	36.947	12.03	1	1	1	1			1	YR080418002
4500	bottom		1015	20.823	36.947	11.85	1	1	1	1			1	YR080418003
4501	bottom		1136	20.815	36.939	11.82	1	1	1	1			1	YR080418004
4502	bottom		1145	20.814	36.938	11.74	1	1	1	1			1	YR080418005
4503	bottom		1059	20.812	36.934	11.79	1	1	1	1			1	YR080418006
4504	bottom		1115	20.812	36.933	11.8	1	1	1	1			1	YR080418007
4505	bottom		1129	20.811	36.933	11.71	1	1	1	1			1	YR080418008
4507	bottom		1150	20.812	36.931	11.71	1	1	1	1			1	YR080418009
4508	bottom		1200	20.813	36.927	11.73	1	1	1	1			1	YR080418010
4509	bottom		1216	20.811	36.929	11.76	1	1	1	1			1	YR080418011
4510	bottom		1230	20.812	36.928	11.7	1	1	1	1			1	YR080418012
4511	bottom		1245	20.812	36.928	11.64	1	1	1	1			1	YR080418013
4512	bottom		1300	20.811	36.929	11.6	1	1	1	1			1	YR080418014
4513	bottom		1315	20.811	36.929	11.61	1	1	1	1			1	YR080418015
4514	bottom		1330	20.812	36.930	11.56	1	1	1	1			1	YR080418016

Table A2.12. YR0080505 (Claybank Erosion Study Anchor station May 5, 2008) Calibration Cruise

Station	Description	Date	Time (EST)	Lat 37° N	Long 76° W	depth (m)	CTD	TSS	LISST	ADCP profile	ADV profile	ADV bottom	ADCP transect	ADCP filename
4515	bottom	5/5/08	1015	20.827	36.827	10.19	1	1	1	1		1		YR080505001
4516	bottom		1030	20.827	36.991	10.11	1	1	1	1		1		YR080505002
4517	bottom		1039	20.825	36.990	10.12	1	1	1	1		1		YR080505003
4518	bottom		1048	20.823	36.987	10.07	1	1	1	1		1		YR080505004
4519	bottom		1102	20.816	36.981	9.97	1	1	1	1		1		YR080505005
4520	bottom		1116	20.821	36.974	10.41	1	1	1	1		1		YR080505006
4521	bottom		1133	20.818	36.973	10.15	1		1	1		1		YR080505007
4522	bottom		1146	20.819	36.972	10.13	1	1	1	1		1		YR080505008
4523	bottom		1201	20.818	36.973	9.9	1	1	1	1		1		YR080505009
4524	bottom		1216	20.820	36.970	10.07	1	1	1	1		1		YR080505010
4525	bottom		1233	20.823	36.965	10.39	1	1	1	1		1		YR080505011

248

Table A2.13. YR080507 (Claybank Erosion Study Anchor station May 7, 2008) Calibration Cruise

Station	Description	Date	Time (EST)	Lat 37° N	Long 76°W	depth (m)	CTD	TSS	LISST	ADCP profile	ADV profile	ADV bottom transect	ADCP	ADCP filename
4526	profile	5/7/08					1		1	1	1			YR080507000
4527	bottom		622	20.588	36.672	9.22	1	1	1	1		1		YR080507001
4528	bottom		636	20.589	36.673	9.23	1	1	1	1		1		YR080507002
4529	bottom		645	20.589	36.673	9.27	1	1	1	1		1		YR080507003
4530	bottom		701	20.589	36.672	9.32	1	1	1	1		1		YR080507004
4531	bottom		715	20.589	36.673	9.38	1	1	1	1		1		YR080507005
4532	bottom		732	20.590	36.672	9.42	1	1	1	1		1		YR080507006
4533	bottom		747	20.590	36.674	9.45	1	1	1	1		1		YR080507007
4534	bottom		8	20.594	36.677	9.47	1	1	1	1		1		YR080507008
4535	bottom		815	20.592	36.678	9.52	1	1	1	1		1		YR080507009
4536	bottom		838	20.631	36.696	10.34	1	1	1	1		1		YR080507010
4537	bottom		9	20.628	36.700	10.39	1	1	1	1		1		YR080507011
4538	bottom		930	20.629	36.700	10.45	1	1	1	1		1		YR080507012
4539	bottom		946	20.631	36.699	10.64	1	1	1	1		1		YR080507013

Table A2.14. YR080514 (Claybank Erosion Study Anchor station May 14, 2008) Calibration Cruise

Station	Description	Date	Time (EST)	Lat 37° N	Long 76° W	depth (m)	CTD	TSS	LISST	ADCP profile	ADV profile	ADV bottom	ADCP transect	ADCP filename
4541	bottom	5/14/08	706	20.804	36.918	11.68	1	1	1	1		1		YR080514000
4542	bottom		721	20.803	36.919	11.58	1	1	1	1		1		YR080514001
4543	bottom		730	20.802	36.919	11.51	1	1	1	1		1		YR080514002
4544	1- profile		745	20.801	36.920	11.61	1			1	1	1		YR080514003
4545	bottom		746	20.801	36.919	11.66	1	1	1	1		1		YR080514004
4546	bottom		801	20.801	36.918	11.64	1	1	1	1		1		YR080514005
4547	bottom		819	20.803	36.910	12.16	1	1	1	1		1		YR080514006
4548	bottom		848	20.804	36.912	11.9	1	1	1	1		1		YR080514007
4549	bottom		901	20.801	36.913	11.77	1	1	1	1		1		YR080514008
4550	bottom		921	20.804	36.912	11.96	1	1	1	1		1		YR080514009
4551	bottom		936	20.803	36.913	11.75	1	1	1	1		1		YR080514011
4552	bottom		947	20.802	36.914	11.73	1	1	1	1		1		YR080514012
4553	bottom		1000	20.801	36.915	11.5	1	1	1	1		1		YR080514013
4554	bottom		1017	20.800	36.916	11.5	1	1	1	1		1		YR080514014
4555	bottom		1031	20.801	36.915	11.48	1	1	1	1		1		YR080514015
4556	bottom		1100	20.736	36.790	12.3	1	1	1	1		1		YR080514018
4557	bottom		1122	20.736	36.789	12.27	1	1	1	1		1		YR080514019
4558	bottom		1134	20.738	36.789	12.29	1	1	1	1		1		YR080514020
4559	bottom		1148	20.737	36.791	12.25	1	1	1	1		1		YR080514021
4560	bottom		1200	20.737	36.791	12.25	1	1	1	1		1		YR080514022
4561	bottom		1216	20.739	36.789	12.39	1	1	1	1		1		YR080514023

Table A2.14. YR080514 (Claybank Erosion Study Anchor station May 14, 2008) Calibration Cruise   (cont)

Station	Description	Date	Time (EST)	Lat 37° N	Long 76° W	depth (m)	CTD	TSS	LISST	ADCP profile	ADV profile	ADV bottom	ADCP transect	ADCP filename
4562	2- profile		1232	20.740	36.789	12.45	1		1	1	1			YR080514024
4563	bottom		1235	20.738	36.790	12.36	1	1	1	1			1	YR080514025
4564	bottom		1247	20.738	36.790	12.42	1	1	1	1			1	YR080514026

Table A2.15. YR080515 (Claybank Erosion Study Anchor station May 15, 2008) Calibration Cruise

Station	Description	Date	Time (EST)	Lat 37° N	Long 76° W	depth (m)	CTD	TSS	LISST	ADCP profile	ADV profile	ADV bottom	ADCP transect	ADCP filename
4565	1- profile	5/15/08	804	20.834	36.943	12.19	1		1	1	1			YR080515000
4566	bottom		806	20.833	36.943	12.16	1	1	1	1			1	YR080515001
4567	bottom		821	20.830	36.942	11.22	1	1	1	1			1	YR080515002
4568	bottom		831	20.830	36.942	12.07	1	1	1	1			1	YR080515003
4569	bottom		844	20.829	36.941	12.07	1	1	1	1			1	YR080515004
4570	2- profile		900	20.824	36.936	12.04	1		1	1	1			YR080515005
4571	bottom		901	20.824	36.937	12.02	1	1	1	1			1	YR080515006
4572	bottom		915	20.822	36.938	11.81	1	1	1	1			1	YR080515007
4573	3- profile		930	20.819	36.939	11.58	1		1	1	1			YR080515008
4574	bottom		931	20.819	36.940	11.57	1	1	1	1			1	YR080515009
4575	bottom		946	20.819	36.941	11.5	1	1	1	1			1	YR080515010
4576	4- profile		1002	20.818	36.940	11.36	1		1	1	1			YR080515011
4577	bottom		1003	20.810	36.940	11.31	1	1	1	1			1	YR080515012
4578	bottom		1018	20.817	36.942	11.22	1	1	1	1			1	YR080515013
4579	5- profile		1033	20.818	36.942	11.39	1		1	1	1			YR080515014
4580	bottom		1034	20.818	36.940	11.39	1	1	1	1			1	YR080515015
4581	bottom		1046	20.817	36.941	11.16	1	1	1	1			1	YR080515016
4582	6- profile		1102	20.817	36.940	11.94	1		1	1	1			YR080515017
4583	bottom		1103	20.818	36.940	11.17	1	1	1	1			1	YR080515018
4584	bottom		1116	20.817	36.939	11.34	1	1	1	1			1	YR080515019
4585	7- profile		1134	20.818	36.939	11.32	1		1	1	1			YR080515020

Table A2.15. YR080515 (Claybank Erosion Study Anchor station May 15, 2008) Calibration Cruise

Station	Description	Date	Time (EST)	Lat 37° N	Long 76°W	depth (m)	CTD	TSS	LISST	ADCP profile	ADV profile	ADV bottom	ADCP transect	ADCP filename
4586	bottom		1135	20.819	36.939	11.33	1	1	1	1			1	YR080515021
4587	bottom		1146	20.818	36.938	11.2	1	1	1	1			1	YR080515022
4588	8- profile		1201	20.819	36.938	11.32	1		1	1	1			YR080515023
4589	bottom		1202	20.819	36.937	11.32	1	1	1	1			1	YR080515024
4590	bottom		1218	20.818	36.939	11.28	1	1	1	1			1	YR080515025
4591	bottom		1230	20.818	36.940	11.23	1	1	1	1			1	YR080515026

253

Table A2.16. YR080603 (Claybank Erosion Study Anchor station June 3, 2008) Calibration Cruise

Station	Description	Date	Time (EST)	Lat 37° N	Long 76° W	depth (m)	CTD	TSS	LISST	ADCP profile	ADV profile	ADV bottom	ADCP transect	ADCP filename
4582	1- profile	6/3/08	916	20.861	36.978	12.38	1		1	1	1			YR080603000
4583	bottom		920	20.863	36.975	12.44	1	1	1	1		1		YR080603001
4584	bottom		933	20.863	36.973	12.55	1	1	1	1		1		YR080603002
4585	2- profile		952	20.861	36.974	12.36	1	1	1	1	1	1		YR08603003
4586	bottom		955	20.861	36.974	12.43	1	1	1	1		1		YR080603004
4587	3- profile		926	20.861	36.972	12.47	1		1	1	1			YR080603005
4588	bottom		1030	20.860	36.970	12.42	1	1	1			1		YR080603006
4589	bottom		1046	20.860	36.974	12.17	1	1	1	1		1		YR080603007
4590	4- profile		1105	20.862	36.970	12.28	1		1	1	1			YR080603008
4591	bottom		1108	20.862	36.969	12.34	1	1	1	1		1		YR080603009
4592	bottom		1127	20.862	36.971	12.24	1	1	1	1		1		YR080603010
4593	5- profile		1143	20.864	36.963	12.31	1		1	1	1			YR080603011
4594	bottom		1145	20.865	36.963	12.36	1	1	1	1		1		YR080603012
4595	bottom		1157	20.857	36.957	12.24	1	1	1	1		1		YR080603013
4596	6- profile		1204	20.851	36.957	11.94	1		1	1	1			YR080603014
4597	bottom		1206	20.848	36.957	11.76	1	1	1	1		1		YR080603015
4598	7- profile		1225	20.847	36.955	11.87	1		1	1	1			YR080603016
4599	bottom		1227	20.847	36.955	11.79	1	1	1	1		1		YR080603017
4600	bottom		1238	20.848	36.953	12	1	1	1	1		1		YR080603018
4601	bottom		1253	20.846	36.954	11.74	1	1	1	1		1		YR080603019

254

Table A2.17. YR080606 (Claybank Erosion Study Anchor Station June 6, 2008) Calibration Cruise

Station	Description	Date	Time (EST)	Lat 37° N	Long 76° W	depth (m)	CTD	TSS	LISST	ADCP profile	ADV profile	ADV bottom	ADCP transect	ADCP filename
4602	ADCP only	6/6/08	629	20.812	36.972	11.42				1				YR080606000
4603	ADCP only		653	20.813	36.927	11.47				1				YR080606001
4604	1- profile		659	20.813	36.925	11.66	1		1	1	1			YR080606002
4605	bottom		704	20.813	36.926	11.7	1	2	1	1			1	YR080606003
4606	bottom		720	20.815	36.927	11.63	1	2	1	1			1	YR080606004
4607	bottom		736	20.814	36.927	11.46	1	2	1	1			1	YR080606005
4608	2- profile and bottom		802	20.816	36.928	11.65	1	2	1	1	1		1	YR080606006
4609	bottom		816	20.820	36.931	11.93	1	2	1	1			1	YR080606007
4610	bottom		831	20.818	36.933	11.58	1	2	1	1			1	YR080606008
4611	3- profile		855	20.839	36.957	11.62	1		1	1	1			YR080606009
4612	bottom		859	20.838	36.959	11.65	1	2	1				1	
4613	bottom		916	20.840	36.956	11.82	1	2	1	1			1	YR080606010
4614	bottom		933	20.841	36.957	11.94	1	2	1	1			1	YR080606011
4615	bottom		946	20.840	36.957	12.02	1	2	1	1			1	YR080606012
4616	4- profile		1001	20.839	36.959	11.88	1		1	1	1			YR080606013
4617	bottom		1003	20.841	36.958	11.94	1	2	1	1			1	YR080606014
4618	bottom		1017	20.840	36.958	12	1	2	1	1			1	YR080606015
4619	bottom		1032	20.839	36.959	11.88	1	2	1	1			1	YR080606016
4620	bottom		10.46	20.839	36.960	12.02	1	2	1	1			1	YR080606017

Table A2.18. YR080696 (Claybank Erosion Study Anchor Station June 9, 2008) Calibration Cruise

Station	Description	Date	Time (EST)	Lat 37° N	Long 76° W	depth (m)	CTD	TSS	LISST	ADCP profile	ADV profile	ADV bottom	ADCP transect	ADCP filename
4621	1- profile	6/9/08	941	20.751	36.824	11.83	1		1	1	1			YR080606018
4622	bottom		944	20.750	36.824	11.77	1	2	1	1			1	YR080609000
4623	bottom		1004	20.752	36.824	11.87	1	2	1	1			1	YR080609001
4624	bottom		1017	20.749	36.828	11.57	1	2	1	1			1	YR080609002
4625	2- profile		1038	20.751	36.824	11.94	1		1	1	1			YR080609003
4626	bottom		1039	20.752	36.826	11.94	1	2	1	1			1	YR080609004
4627	bottom		1117	20.763	36.828	12.24	1	2	1	1			1	YR080609005
4628	bottom		1134	20.762	36.833	12.24	1	2	1	1			1	YR080609006
4629	3- profile		1144	20.762	36.839	12.31	1		1	1	1			YR080609007
4630	bottom		1147	20.764	36.841	12.07	1	2	1	1			1	YR080609008
4631	bottom		1205	20.765	30.842	12.23	1	2	1	1			1	YR080609009
4632	bottom		1222	20.766	36.843	12.33	1	2	1	1			1	YR080609010
4633	bottom		1240	20.767	36.846	12.34	1	2	1	1			1	YR080609011
4634	bottom		1303	20.769	36.855	12.88	1	2	1	1			1	YR080609012
4635	bottom		1308	20.771	36.859	12.35	1	2	1	1			1	YR080609013

Table A2.19. YR080610 (Claybank Erosion Study Anchor Station June 10, 2008) Calibration Cruise

Station	Description	Date	Time (EST)	Lat 37° N	Long 76° W	depth (m)	CTD	TSS	LISST	ADCP profile	ADV profile	ADV bottom	ADCP transect	ADCP filename
4636	1- profile	6/10/08	1019	20.742	36.846	10.77	1		1	1	1			YR080610000
4637	bottom		1021	20.741	36.848	10.7	1	2	1	1			1	YR080610001
4638	bottom		1036	20.742	36.849	10.72	1	2	1	1			1	YR080610002
4639	bottom		1049	20.741	36.850	10.6	1	2	1	1			1	YR080610003
4640	bottom		1106	20.741	36.852	10.46	1	2	1	1			1	YR080610004
4641	2- profile		1126	20.741	36.850	10.77	1		1	1	1			YR080610005
4642	bottom		1136	20.742	36.855	10.47	1	2	1	1			1	YR080610006
4643	3- profile		1205	20.755	36.857	11.07	1		1	1	1			YR080610007
4644	bottom		1207	20.756	36.855	11.17	1	2	1	1			1	YR080610008
4645	bottom		1231	20.761	36.855	11.33	1	2	1	1			1	YR080610009
4646	bottom		1256	20.760	36.860	11.3	1	2	1	1			1	YR080610010
4647	bottom		1315	20.762	36.870	11.2	1	2	1	1			1	YR080610011
4648	bottom		1343	20.762	36.869	11.34	1	2	1	1			1	YR080610012
4649	4- profile		1407	20.767	36.885	11.16	1	2	1	1			1	YR080610013
4650	bottom		1410	20.767	36.885	11.14	1		1	1	1			YR080610014

257

Table A2.20. YR080729 (Clay Bank Anchor Station, July 29, 2008) Calibration Cruise

Station	Description	Date	Time (EST)	Lat 37° N	Long 76° W	depth (m)	CTD	TSS	LISST	ADCP profile	ADV profile	ADV bottom	ADCP transect	ADCP filename
4651		7/29/08	748	20.437	37.484	6.35	1		1	1	1			YR080729000
4652	1- profile		801	20.438	37.483	6.26	1	3	1	1	1			YR080729001
4653	2- profile		812	20.437	37.485	6.29	1		1	1	1			YR080729002
4654	bottom		813	20.437	37.485	6.27	1	2	1	1			1	YR080729003
4655	bottom		836	20.437	37.484	6.13	1	2	1	1			1	YR080729004
4656	3- profile		902	20.431	37.476	6.18	1	3	1	1	1			YR080729005
4657	4- profile		911	20.430	37.476	6.16	1		1	1	1			YR080729006
4658	bottom		913	20.430	37.477	6.07	1	2	1	1			1	YR080729007
4659	bottom		935	20.429	37.477	6.04	1	2	1	1			1	YR080729008
4660	5- profile		946	20.420	37.471	6.02	1	3	1	1	1			YR080729009
4661	6- profile		953	200.420	37.472	6	1		1	1	1			YR080729010
4662	bottom		956	20.419	37.473	5.94	1	2	1	1			1	YR080729011
4663	bottom		1020	20.419	37.473	5.88	1	2	1	1			1	YR080729012
4664	bottom		1041	20.418	37.474	5.76	1	2	1	1			1	YR080729013
4665	7- profile		1107	20.418	37.470	5.85	1	3	1	1	1			YR080729014
4666	8- profile		1115	20.418	37.471	5.76	1		1	1	1			YR080729015
4667	bottom		1116	20.418	37.473	5.74	1	2	1	1			1	YR080729016
4668	bottom		1141	20.417	37.472	5.67	1	2	1	1			1	YR080729017
4669	9- profile		1205	20.419	37.470	5.78	1	3	1	1	1			YR080729018
4670	10- profile		1212	20.419	37.470	5.76	1		1	1	1			YR080729019
4671	bottom		1214	20.417	37.471	5.72	1	2	1	1			1	YR080729020

Table A2.20. YR080729 (Clay Bank Anchor Station, July 29, 2008) Calibration Cruise (cont)

Station	Description	Date	Time (EST)	Lat 37° N	Long 76° W	depth (m)	CTD	TSS	LISST	ADCP profile	ADV profile	ADV bottom	ADCP transect	ADCP filename
4672	bottom		1231	20.417	37.473	5.63	1	2	1	1		1		YR080729021
4673	11- profile		1302	20.420	37.472	5.83	1	3	1	1	1			YR080729022
4674	12- profile		1310	20.422	37.475	5.77	1		1	1	1			YR080729023
4675	bottom		1312	20.421	37.473		1	2	1	1		1		YR080729024
4676	13- profile		1350	20.434	37.490	5.79	1		1	1	1			YR080729026

Table A2.21. YR080731 (Gloucester Point Anchor Station, July 31, 2008) Calibration Cruise

Station	Description	Date	Time (EST)	Lat 37° N	Long 76° W	depth (m)	CTD	TSS	LISST	ADCP profile	ADV profile	ADV bottom	ADCP transect	ADCP filename
4677	ADCP only	7/31/08	826	14.656	29.979	9.04				1				YR080801000
4678	1- profile		906	14.655	29.966	8.90	1	3	1	1	1			YR080801001
4679	2- profile		918	14.684	29.965	9.06	1		1	1	1			YR080801002
4680	bottom		920	14.653	26.966	9.02	1	2	1	1			1	YR080801003
4681	bottom		942	14.654	29.966	8.92	1	2	1	1			1	YR080801004
4682	3- profile		1002	14.660	29.955	8.59	1	3	1	1	1			YR080801005
4683	4- profile		1011	14.662	29.956	8.37	1		1	1	1			YR080801006
4684	bottom		1014	14.660	29.955	8.40	1	2	1	1			1	YR080801007
4685	bottom		1035	14.660	29.954	8.31	1	2	1	1			1	YR080801008
4686	5- profile		1105	14.661	29.954	8.24	1	3	1	1	1			YR080801009
4687	6- profile		1112	14.658	29.949	8.24	1		1	1	1			YR080801010
4688	bottom		1114	14.656	29.946	8.22	1	2	1	1			1	YR080801011
4689	bottom		1142	14.657	29.943	7.97	1	2	1	1			1	YR080801012
4690	7- profile		1204	14.659	29.943	7.93	1	3	1	1	1			YR080801013
4691	8- profile		1212	14.658	29.944	7.94	1		1	1	1			YR080801014
4692	bottom		1215	14.657	29.945	8.04	1	2	1	1			1	YR080801015
4693	bottom		1238	14.658	29.945	7.91	1	2	1	1			1	YR080801016
4694	9- profile		1300	14.656	29.945	7.66	1	3	1	1	1			YR080801017
4695	10- profile		1312	14.657	29.952	7.69	1		1	1	1			YR080801018
4696	bottom		1313	14.656	29.954	7.95	1	2	1	1			1	YR080801019
4697	bottom		1338	14.659	29.956	7.68	1	2	1	1			1	YR080801020

Table A2.21. YR080731 (Gloucester Point Anchor Station, July 31, 2008) Calibration Cruise (Cont)

Station	Description	Date	Time (EST)	Lat 37° N	Long 76° W	depth (m)	CTD	TSS	LISST	ADCP profile	ADV profile	ADV bottom	ADCP transect	ADCP filename
4698	11- profile		1407	14.659	29.972	8.35	1	3	1	1	1			YR080801021
4699	12- profile		1415	14.660	29.943	8.00	1		1	1	1			YR080801022
4700	bottom		1416	14.655	29.974	8.47	1	2	1	1		1		YR080801023

Table A2.22. YR0801016 (Clay Bank Anchor Station, Oct 16, 2008) Calibration Cruise

Station	Description	Date	Time (EST)	Lat 37° N	Long 76° W	depth (m)	CTD	TSS	LISST	ADCP profile	ADV profile	ADV bottom	ADCP transect	ADCP filename
4701	**Profile**	10/16/08	4:53:00	20.405	37.494	5.25	1			1	1			YR081016000
4702	Bottom		4:59:00	20.408	37.493	5.28	1	2		1		1		YR081016001
4703	**Profile**		5:30:00	20.408	37.495	5.46	1	3		1				YR081016002
4704	**Profile**		5:55:00	20.418	37.500	5.47	1			1	1			YR081016003
4705	**Bottom**		5:58:00	20.418	37.500	5.47	1	2		1		1		YR081016004
4706	**Profile**		6:03:00	20.423	37.508	5.63	1	3		1				YR081016005
4707	**Profile**		6:37:00	20.422	37.509	5.66	1			1	1			YR081016006
4708	**Bottom**		6:40:00	20.422	37.508	5.6	1	2		1		1		YR081016007
4709	**Bottom**		7:12:00	20.424	37.509	5.77	1	2		1		1		YR081016008
4710	**Profile**		7:40:00	20.436	37.518	5.93	1	3		1				YR081016009
4711	**Profile**		7:58:00	20.427	37.495	6.22	1			1	1			YR081016010
4712	**Bottom**		8:00:00	20.427	37.496	6.19	1	2		1		1		YR081016011
4713	**Bottom**		8:21:00	20.427	37.495	6.27	1	2		1		1		YR081016012
4714	**Profile**		8:42:00	20.427	37.496	6.36	1	3		1				YR081016013
4715	**Profile**		8:49:00	20.427	37.496	6.36	1			1	1			YR081016014
4716	**Bottom**		8:50:00	20.427	37.496	6.38	1	2		1		1		YR081016015
4717	**Bottom**		9:10:00	20.428	37.495	6.39	1	2		1		1		YR081016016
4718	**Profile**		9:37:00	20.428	37.494	6.5	1	3		1				YR081016017
4719	**Profile**		9:40:00	20.427	37.494	6.52	1			1	1			YR081016018
4720	**Bottom**		9:45:00	20.428	37.493	6.5	1	2		1		1		YR081016019
4721	**Bottom**		10:11:00	20.429	37.491	6.58	1	2		1		1		YR081016020

Table A2.22. YR0801016 (Clay Bank Anchor Station, Oct 16, 2008) Calibration Cruise (cont)

Station	Description	Date	Time (EST)	Lat 37° N	Long 76° W	depth (m)	CTD	TSS	LISST	ADCP profile	ADV profile	ADV bottom	ADCP transect	ADCP filename
4727	**Bottom**		11:32:00	20.426	37.480	6.55	1	2		1		1		YR081016026
4728	**Bottom**		11:54:00	20.427	37.479	6.52	1	2		1		1		YR081016027
4729	**Profile**		12:21:00	20.423	37.475	6.5	1	3		1	1			YR081016028

Table A2.23. YR090108 (Gloucester Point Anchor Station, January 08, 2009) Calibration Cruise

Station	Description	Date	Time (EST)	Lat 37° N	Long 76° W	depth (m)	CTD	TSS	LISST	ADCP profile	ADV profile	ADV bottom	ADCP transect	ADCP filename
4730	profile	1/8/09	7:56:00	14.6769	29.9436	7.4	1	3	1	1	1			YR090108001
4731	profile		8:03:20	14.6772	29.9351	7.45	1		1	1	1			YR090108002
4732	bottom		8:08:10	14.6775	29.9354	7.37	1	2	1	1		1		YR090108003
4733	bottom		8:26:45	14.6504	29.9389	7.31	1	2	1	1		1		YR090108004
4734	profile		8:43:00	14.6800	29.9369	7.31	1	3	1	1	1			YR090108005
4735	profile		8:55:30	14.6800	29.9370	7.24	1		1	1	1			YR090108006
4736	bottom		9:00:40	14.6810	29.9384	7.25	1	2	1	1		1		YR090108007
4737	bottom		9:32:20	14.6801	29.9356	7.19	1	2	1	1		1		YR090108008
4738	profile		9:47:20	14.6779	29.9349	7.14	1	3	1	1	1			YR090108009
4739	profile		9:57:30	14.6766	29.9341	7.17	1		1	1	1			YR090108010
4740	bottom		10:01:20	14.676	29.9339	7.11	1	2	1	1		1		YR090108011
4741	bottom		10:22:20	14.6776	29.935	7.09	1	2	1	1		1		YR090108012
4742	profile		10:56:20	14.6759	29.9338	7.07	1	3	1	1	1			YR090108013
4743	profile		11:05:50	14.6767	29.9337	7.01	1		1	1	1			YR090108014
4744	bottom		11:09:30	14.6700	29.9343	6.94	1	2	1	1		1		YR090108015
4745	bottom		11:36:00	14.6752	29.9324	7.04	1	2	1	1		1		YR090108016
4746	profile		11:53:40	14.6745	29.9319	7.05	1	3	1	1	1			YR090108017
4747	profile		12:01:20	14.6706	29.9309	7.06	1		1	1	1			YR090108018
4748	bottom		12:05:00	14.6737	29.932	7.01	1		1	1		1		YR090108019
4749	bottom		12:29:20	14.6717	29.9304	7.2	1		1	1		1		YR090108020
4750	bottom		12:32:45	14.6690	29.9930	7.11		2						YR090108021

Table A2.23. YR090108 (Gloucester Point Anchor Station, January 08, 2009) Calibration Cruise   (cont)

Station	Description	Date	Time (EST)	Lat 37° N	Long 76° W	depth (m)	CTD	TSS	LISST	ADCP profile	ADV profile	ADV bottom	ADCP transect	ADCP filename
4751	profile		12:55:00	14.6733	29.9319	7.01	1	3	1	1	1			YR090108022
4752	profile		13:03:30	14.6734	29.9318	7.01	1		1	1	1			YR090108023
4753	bottom		13:06:30	14.6746	29.9319	6.95	1	2	1	1			1	YR090108024
4754	bottom		13:17:20	14.6694	29.9305	6.94	1	2	1	1			1	YR090108025
4755	profile		13:37:00	14.6651	29.9312	7.27	1		1	1	1			YR090108026
4756	bottom		13:39:50	14.6671	29.9305	7.18	1		1	1			1	YR090108027
4757	profile		14:06:20	14.6710	29.9306	7.11	1	2	1	1	1			YR090108028

Table A2.24. YR090226 (Clay Bank Anchor Station, February 26, 2009) Calibration Cruise

Station	Description	Date	Time (EST)	Lat 37° N	Long 76° W	depth (m)	CTD	TSS	LISST	ADCP profile	ADV profile	ADV bottom	ADCP transect	ADCP filename
4759	**Profile**	2/26/09	7:50:00	20.499	37.506	6.28	1		1		1			
4760	**Bottom**		7:54:00	20.499	37.507	6.34	1	2	1	1			1	YR090226000
4761	**Bottom**		8:18:00	20.499	37.507	6.19	1	2	1	1			1	YR090226001
4762	**Profile**		8:38:00	20.499	37.507	6.28	1	3	1	1	1			YR090226002
4763	**Profile**		8:48:00	20.500	37.507	6.32	1		1	1	1			YR090226003
4764	**Bottom**		8:51:00	20.499	37.507	6.27	1	2	1	1			1	YR090226004
4765	**Bottom**		9:09:00	20.500	37.509	6.34	1	2	1	1			1	YR090226005
4766	**Profile**		9:38:00	20.499	37.509	6.43	1	3	1	1	1			YR090226006
4767	**Profile**		9:47:00	20.500	37.508	6.44	1		1	1	1			YR090226007
4768	**Bottom**		9:51:00	20.499	37.508	6.39	1	2	1	1			1	YR090226008
4769	**Bottom**		10:17:00	20.499	37.508	6.46	1	2	1	1			1	YR090226009
4770	**Profile**		10:41:00	20.500	37.503	6.54	1	3	1	1	1			YR090226010
4771	**Profile**		10:49:00	20.550	37.502	6.56	1		1	1	1			YR090226011
4772	**Bottom**		10:52:00	20.500	37.503	6.5	1	2	1	1			1	YR090226012
4773	**Bottom**		11:13:00	20.501	37.498	6.52	1	2	1	1			1	YR090226014
4774	**Profile**		11:40:00	20.500	37.495	6.45	1	3	1	1	1			YR090226015
4775	**Profile**		11:48:00	20.500	37.497	6.5	1		1	1	1			YR090226016
4776	**Bottom**		11:52:00	20.501	37.500	6.45	1	2	1	1			1	YR090226017
4777	**Bottom**		12:09:00	20.501	37.498	6.37	1	2	1	1			1	YR090226018
4778	**Profile**		12:39:00	20.500	37.494	6.35	1	3	1	1	1			YR090226019
4779	**Profile**		12:48:00	20.501	37.497	6.35	1		1	1	1			YR090226020

Table A2.24. YR090226 (Clay Bank Anchor Station, February 26, 2009) Calibration Cruise (cont)

Station	Description	Date	Time (EST)	Lat 37° N	Long 76° W	depth (m)	CTD	TSS	LISST	ADCP profile	ADV profile	ADV bottom	ADCP transect	ADCP filename
4780	**Bottom**		12:51:00	20.501	37.494	6.28	1	2	1	1			1	YR090226021
4781	**Bottom**		13:19:00	20.494	37.485	6.24	1	2	1	1			1	YR090226022

Table A2.25. YR090514 (Clay Bank Anchor Station, May 14, 2009) Calibration Cruise

Station	Description	Date	Time (EST)	Lat 37° N	Long 76° W	depth (m)	CTD	TSS	LISST	ADCP profile	ADV profile	ADV bottom	ADCP transect	ADCP filename
4802	Profile	5/14/09	4:51:00	20.523	37.510	6.16	1	3	1	1	1			YR090514001
4803	Profile		5:03:00	20.523	37.510	6.06	1		1	1	1			YR090514002
4804	Bottom		5:09:00	20.523	37.510	6.00	1	2	1	1		1		YR090514003
4805	Bottom		5:31:00	20.522	37.509	5.95	1	2	1	1		1		YR090514004
4806	Profile		5:46:00	20.523	37.508	6.00	1	3	1	1	1			YR090514005
4807	Profile		5:55:00	20.523	37.508	5.95	1		1	1	1			YR090514006
4808	Bottom		5:59:00	20.524	37.508	6.94	1	2	1	1		1		YR090514007
4809	Bottom		6:19:00	20.522	37.510	6.93	1	2	1	1		1		YR090514008
4810	Profile		6:45:00	20.521	37.502	9.95	1	3	1	1	1			YR090514009
4811	Profile		6:55:00	20.522	37.510	5.93	1		1	1	1			YR090514010
4812	Bottom		6:58:00	20.523	37.510	5.88	1	2	1	1		1		YR090514011
4813	Bottom		7:23:00	20.525	37.508	5.87	1		1	1		1		YR090514012
4814	Bottom		7:34:00	20.525	37.511	6.10	1	2	1	1		1		YR090514013
4815	Profile		7:59:00	20.541	37.512	5.89	1	3	1	1	1			YR090514014
4816	Profile		8:28:00	20.553	37.527	5.91	1		1	1	1			YR090514015
4817	Bottom		8:31:00	20.552	37.531	5.90	1		1	1		1		YR090514016
4818	Profile		9:03:00	20.553	37.528	6.00	1	3	1	1	1			YR090514017
4819	Profile		9:24:00	20.556	37.529	6.73	1	3	1	1	1			YR090514018

Too rough to continue

Table A2.26. YR090811 (Clay Bank Anchor Station, August 11, 2009) Calibration Cruise

Station	Description	Date	Time (EST)	Lat 37° N	Long 76° W	depth (m)	CTD	TSS	LISST	ADCP profile	ADV profile	ADV bottom	ADCP transect	ADCP filename
4820	**Profile**	8/11/09	8:34:00	20.508	37.505	5.88	1	3	1		1			No ADCP
4821	**Profile**		8:41:00	20.508	37.505	5.82	1		1		1			No ADCP
4822	**Bottom**		8:43:00	20.509	37.506	5.85	1	1	1			1		No ADCP
4823	**Bottom**		9:02:00	20.509	37.504	5.94	1		1			1		No ADCP
4824	**Profile**		9:33:00	20.508	37.503	6	1	3	1		1			No ADCP
4825	**Profile**		9:39:00	20.510	37.501	6	1		1		1			No ADCP
4826	**Bottom**		9:40:00	20.509	37.502	6	1	1	1			1		No ADCP
4827	**Profile**		10:13:00	20.516	37.517	6.12	1	3	1		1			No ADCP
4828	**Bottom**		10:23:00	20.518	37.518	6.19	1	1	1			1		No ADCP
4829	**Bottom**		10:45:00	20.519	37.518	6.19	1	1	1			1		No ADCP
4830	**Profile**		11:01:00	20.521	37.520	6.25	1	3	1		1			No ADCP
4831	**Profile**		11:08:00	20.526	37.524	6.31	1		1		1			No ADCP
4832	**Bottom**		11:11:00	20.525	37.524	6.34	1	1	1			1		No ADCP
4833	**Bottom**		11:33:00	20.527	37.527	6.52	1	1	1			1		No ADCP
4834	**Profile**		12:01:00	20.527	37.524	6.4	1	3	1		1			No ADCP
4835	**Profile**		12:08:00	20.529	37.526	6.44	1		1		1			No ADCP
4836	**Bottom**		12:10:00	20.529	37.526	6.43	1	1	1			1		No ADCP
4837	**Bottom**		12:32:00	20.529	37.524	6.49	1	1	1			1		No ADCP
4838	**Profile**		13:09:00	20.530	37.524	6.49	1	3	1		1			No ADCP
4839	**Profile**		13:15:00	20.530	37.524	6.43	1		1		1			No ADCP
4840	**Bottom**		13:17:00	20.529	37.523	6.46	1	1	1			1		No ADCP

Table A2.26. YR090811 (Clay Bank Anchor Station, August 11, 2009) Calibration Cruise

Station	Description	Date	Time (EST)	Lat 37° N	Long 76°W	depth (m)	CTD	TSS	LISST	ADCP profile	ADV profile	ADV bottom	ADCP transect	ADCP filename
4841	**Bottom**		13:39:00	20.530	37.523	6.52	1	1	1				1	No ADCP
4842	**Profile**		14:03:00	20.530	37.524	6.4	1	3	1		1			No ADCP
4843	**Profile**		14:09:00	20.530	37.524	6.4	1		1		1			No ADCP
4844	**Bottom**		14:11:00	20.530	37.523	6.43	1	1	1				1	No ADCP
4845	**Bottom**		14:33:00	20.529	37.522	6.4	1	1	1				1	No ADCP
4846	**Profile**		15:08:00	20.529	37.521	6.28	1	3	1		1			No ADCP

270

Table A2.27. YR091125 (Clay Bank Anchor Station, November 25, 2009) Calibration Cruise

Station	Description	Date	Time (EST)	Lat 37° N	Long 76° W	depth (m)	CTD	TSS	LISST	ADCP profile	ADV profile	ADV bottom	ADCP transect	ADCP filename
4847	Profile	11/25/09	7:32:00	20.399	37.423	6.41	1	3	1	1	1			YR091125000
4848	Profile		7:48:00	20.399	37.422	6.39	1		1	1	1			YR091125001
4849	Bottom		7:50:00	20.400	37.422	6.39	1	2	1	1		1		YR091125002
4850	Bottom		8:09:00	20.400	37.423	6.35	1	2	1	1		1		YR091125003
4851	Profile		8:40:00	20.401	37.422	6.38	1	3	1	1	1			YR091125004
4852	Profile		8:48:00	20.401	37.421	6.34	1		1	1	1			YR091125005
4853	Bottom		8:50:00	20.401	37.421	6.31	1	2	1	1		1		YR091125006
4854	Bottom		9:16:00	20.401	37.422	6.29	1	2	1	1		1		YR091125007
4855	Profile		9:32:00	20.400	37.422	6.3	1	3	1	1	1			YR091125008
4856	Profile		9:40:00	20.400	37.423	6.3	1		1	1	1			YR091125009
4857	Bottom		9:41:00	20.400	37.423	6.3	1	2	1	1		1		YR091125009
4858	Bottom		9:51:00	20.399	37.423	6.27	1	2	1	1		1		YR091125010
4859	Bottom		10:04:00	20.399	37.425	6.3	1	2	1	1		1		YR091125011
4860	Profile		10:32:00	20.400	37.425	6.32	1	3	1	1	1			YR091125012
4861	Profile		10:42:00	20.400	37.422	6.31	1		1	1	1			YR091125013
4862	Bottom		10:43:00	20.400	37.422	6.31	1	2	1	1		1		YR091125014
4863	Bottom		11:10:00	20.401	37.442	6.35	1	2	1	1		1		YR091125015
4864	Profile		11:38:00	20.402	37.419	6.41	1	3	1	1	1			YR091125016
4865	Profile		11:46:00	20.402	37.419	6.43	1		1	1	1			YR091125017
4866	Bottom		11:48:00	20.402	37.420	6.4	1	2	1	1		1		YR091125018
4867	Bottom		12:16:00	20.405	37.419	6.46	1	2	1	1		1		YR091125019

271

Table A2.27. YR091125 (Clay Bank Anchor Station, November 25, 2009) Calibration Cruise

Station	Description	Date	Time (EST)	Lat 37° N	Long 76° W	depth (m)	CTD	TSS	LISST	ADCP profile	ADV profile	ADV bottom	ADCP transect	ADCP filename
4868	**Profile**		12:38:00	20.406	37.419	6.55	1	3	1	1	1			YR091125020
4869	**Profile**		12:47:00	20.408	37.419	6.55	1		1	1	1			YR091125021
4870	**Bottom**		13:04:00	20.410	37.419	6.58	1	2	1	1			1	YR091125022
4871	**Bottom**		13:25:00	20.410	37.420	6.58	1	2	1	1			1	YR091125023
4872	**Profile**		14:12:00	20.414	37.423	6.74	1	3	1	1	1			YR091125024

split 4856 and 4857 both as 4856

272

Table A2.28. **YR110816 (Clay Bank Anchor Station, August 16, 2011) Calibration Cruise**

Station	Description	Date	Time (EST)	Lat 37° N	Long 76° W	depth (m)	CTD	TSS	LISST	ADCP profile	ADV profile	ADV bottom	ADCP transect	ADCP filename
4941	**Profile**	8/16/11	7:13:00	20.571	37.584	6.1	1	3	1	1	2			YR081116000
4942	**Bottom**		7:25:00	20.573	37.583	6.2	1	2	1	1			2	YR081116001
4943	**Bottom**		7:40:00	20.575	37.583	6.31	1	2	1	1			2	YR081116002
4944	**Profile**		8:03:00	20.583	37.596	6.36	1	3	1	1	2			YR081116003
4945	**Bottom**		8:16:00	20.588	37.512	6.38	1	2	1	1			2	YR081116004
4946	**Bottom**		8:43:00	20.583	37.593	6.47	1	2	1	1			2	YR081116005

Got too rough... had to abort

Table A2.29. YR110818 (Clay Bank Anchor Station, August 18, 2011) Calibration Cruise

Station	Description	Date	Time (EST)	Lat 37° N	Long 76° W	depth (m)	CTD	TSS	LISST	ADCP profile	ADV profile	ADV bottom	ADCP transect	ADCP filename
4949	Profile	8/18/11	805	20.582	37.604	5.92	1	3	1	1	1			YR110818000&1
4950	Bottom		828	20.583	37.605	5.94	1	1	1	1		1		YR110818002
4951	Bottom		841	20.583	37.608	5.97	1	1	1	1		1		YR110818003
4952	Profile		906	20.587	37.613	6.04	1	3	1	1	1			YR110818004
4953	Bottom		918	20.586	37.615	6.04	1	1	1	1		1		YR110818005
4954	Bottom		941	20.586	37.615	6.12	1	1	1	1		1		YR110818006
4955	Profile		1007	20.590	37.618	6.27	1	3	1	1	1			YR110818008
4956	Bottom		1022	20.588	37.620	6.28	1	2	1	1		1		YR110818009
4957	Bottom		1041	20.590	37.618	6.34	1	2	1	1		1		YR110818010
4958	Profile		1107	20.589	37.620	6.43	1	3	1	1	1			YR110818011
4959	Bottom		1117	20.589	37.619	6.44	1	2	1	1		1		YR110818012
4960	Bottom		1140	20.588	37.620	6.45	1	2	1	1		1		YR110818013
4961	Profile		1205	20.589	37.620	6.55	1	3	1	1	1			YR110818014
4962	Bottom		1218	20.589	37.621	6.51	1	2	1	1		1		YR110818015
4963	Bottom		1244	20.592	37.613	6.62	1	2	1	1		1		YR110818016
4964	Profile		1308	20.590	37.616	6.59	1	3	1	1	1			YR110818017
4965	Bottom		1317	20.491	37.614	6.54	1	2	1	1		1		YR110818018
4966	Bottom		1341	20.590	37.615	6.5	1	1	1	1		1		YR110818019
4967	Profile		1410	20.590	37.615	6.48	1	3	1	1	1			YR110818020

274

Table A2.30. YR110901 (Clay Bank Anchor Station, Sept 1, 2011) Calibration Cruise

Station	Description	Date	Time (EST)	Lat 37° N	Long 76° W	depth (m)	CTD	TSS	LISST	ADCP profile	ADV profile	ADV bottom	ADCP transect	ADCP filename
4976	Profile	9/1/11	725	20.562	37.593	5.77	1	3	1	1	1			YR110901000
4977	ADCP only		749	20.563	37.594	5.87				1				YR110901001
4978	Profile		755	20.564	37.593	5.89	1	3	1	1	1			YR110901002
4979	Bottom		805	20.566	37.596	5.9	1	2	1	1		1		YR110901003
4980	Bottom		836	20.574	37.602	5.97	1	2	1	1		1		YR110901004
4981	Profile		904	20.579	37.610	6.07	1	3	1	1	1			YR110901005
4982	Bottom		916	20.504	37.614	6.1	1	2	1	1		1		YR110901006
4983	Bottom		942	20.584	37.614	6.26	1	2	1	1		1		YR110901007
4984	Profile		1007	20.586	37.616	6.43	1	3	1	1	1			YR110901008
4985	Bottom		1019	20.587	37.616	6.43	1	2	1	1		1		YR110901009
4986	Bottom		1042	20.588	37.614	6.5	1	2	1	1		1		YR110901010
4987	Profile		1105	20.589	37.614	6.59	1	3	1	1	1			YR110901011
4988	Bottom		1117	20.589	37.614	6.63	1	2	1	1		1		YR110901012
4989	Bottom		1143	20.589	37.613	6.63	1	2	1	1		1		YR110901013
4990	Profile		1207	20.588	37.635	6.66	1	3	1	1	1			YR110901014
4991	Bottom		1216	20.587	37.616	6.65	1	1	1	1		1		YR110901015
4992	Bottom		1244	20.586	37.616	6.6				1				YR110901016
4993	Profile		1305	20.586	37.662	6.6	1	3	1	1	1			YR110901017
4994	Bottom		1320	20.586	37.616	6.54	1	2	1	1		1		YR110901018
4995	Profile		1349	20.585	37.616	6.5	1	3	1	1	1			YR110901019

Table A2.31. YR111220 (Clay Bank Anchor Station, December 20, 2011) Calibration Cruise

Station	Description	Date	Time (EST)	Lat 37° N	Long 76° W	depth (m)	CTD	TSS	LISST	ADCP profile	ADV profile	ADV bottom	ADCP transect	ADCP filename
4989	Profile	12/20/11	752	20.433	37.506	5.72	1	3	1	1	1			YR111220000
4990	Bottom		819	20.432	37.506	5.62	1	2	1	1			1	YR111220001
4991	Bottom		832	20.433	37.506	5.61	1	2	1	1			1	YR111220002
4992	Profile		859	20.430	37.510	5.53	1	3	1	1	1			YR111220003
4993	Bottom		916	20.431	37.509	5.45	1	2	1	1			1	YR111220004
4994	Bottom		943	20.431	37.508	5.35	1	2	1	1			1	YR111220005
4995	Profile		959	20.431	37.508	5.35	1	3	1	1	1			YR111220006
4996	Bottom		1017	20.431	37.508	5.27	1	2	1	1			1	YR111220007
4997	Bottom		1045	20.431	37.507	5.21	1	2	1	1			1	YR111220008
4998	Profile		1101	20.432	37.506	5.26	1	3	1	1	1			YR111220009
4999	Bottom		1116	20.431	37.507	5.14	1	2	1	1			1	YR111220010
5000	Bottom		1146	20.431	37.507	5.12	1	2	1	1			1	YR111220011
5001	Profile		1206	20.432	37.406	5.17	1	3	1	1	1			YR111220012
5002	Bottom		1221	20.431	37.507	5.13	1	2	1	1			1	YR111220013
5003	Bottom		1247	20.431	37.507	5.14	1	2	1	1			1	YR111220014
5004	Profile		1305	20.432	37.508	5.26	1	3	1	1	1			YR111220015

Table A2.32. YR120430 (Clay Bank Anchor Station, April 30, 2012) Calibration Cruise

Station	Description	Date	Time (EST)	Lat 37° N	Long 76° W	depth (m)	CTD	TSS	LISST	ADCP profile	ADV profile	ADV bottom	ADCP transect	ADCP filename
4998	Profile	4/30/12	542	20.741	37.484	6.3	1	3	1	1	1			YR120430000
4999	Bottom		556	20.470	37.482	6.27	1	2	1	1			1	YR120430001
5000	Bottom		617	20.463	37.480	6.24	1	2	1	1			1	YR120430002
5001	Profile		647	20.462	37.482	6.15	1	3	1	1	1			YR120430003
5002	Bottom		700	20.462	37.482	6.01	1	2	1	1			1	YR120430004
5003	Bottom		728	20.452	37.484	5.88	1	2	1	1			1	YR120430005
5004	Profile		751	20.452	37.482	5.9	1	3	1	1	1			YR120430006
5005	Bottom		804	20.543	37.480	5.9	1	2	1	1			1	YR120430007
5006	Bottom		828	20.453	37.481	5.8	1	2	1	1			1	YR120430008
5007	Profile		908	20.454	37.478	5.85	1	3	1	1	1			YR120430009
5008	Bottom		922	20.455	37.477	5.79	1	2	1	1			1	YR120430010
5009	Bottom		938	20.455	37.478	5.74	1	2	1	1			1	YR120430011
5010	Profile		950	20.455	37.479	5.79	1	3	1	1	1			YR120430012
5011	Bottom		1002	20.455	37.480	5.75	1	2	1	1			1	YR120430013
5012	Bottom		1022	20.455	37.472	5.74	1	2	1	1			1	YR120430014
5013	Profile		1048	20.457	37.477	5.76	1	3	1	1	1			YR120430016
5014	Profile		1250	20.476	37.499	5.98	1	3	1	1	1			YR120430017

Table A2.33. YR120724 (Clay Bank Anchor Station, July 24, 2012) Calibration Cruise

Station	Description	Date	Time (EST)	Lat 37° N	Long 76° W	depth (m)	CTD	TSS	LISST	ADCP profile	ADV profile	ADV bottom	ADCP transect	ADCP filename
P5026	profile 1	7/24/12	900	20.5160	37.5090	5.92	1	3	1	1	1			YR120724000
P5027	bottom		934	20.5192	37.5111	6.02	1	2	1	1		1		YR120724001
P5028	profile 2		1000	20.5206	37.5148	6.05	1	3	1	1	1			YR120724002
P5029	bottom		1019	20.5206	37.5756	6.06	1	2	1	1		1		YR120724003
P5030	bottom		1044	20.5229	37.5193	6.18	1	2	1	1		1		YR120724004
P5031	profile 3		1107	20.5272	37.5250	6.28	1	3	1	1	1			YR120724005
P5032	bottom		1125	20.5268	37.5264	6.38	1	2	1	1		1		YR120724006
P5033	bottom		1148	20.5271	37.5253	6.42	1	2	1	1		1		YR120724007
P5034	profile 4		1202	20.5268	37.5279	6.48	1	3	1	1	1			YR120724008
P5035	bottom		1220	20.5274	37.5245	6.54	1	2	1	1		1		YR120724009
P5036	bottom		139	20.5279	37.5230	6.55	1	2	1	1		1		YR120724010
P5037	profile 5		1304	20.5284	37.5206	6.63	1	3	1	1	1			YR120724011
P5038	bottom		1322	20.5279	37.5195	6.65	1	2	1	1		1		YR120724012
P5039	bottom		1341	20.5275	37.5176	6.65	1	2	1	1		1		YR120724013
P5040	profile 6		1351	20.5275	37.5185	6.65	1	3	1	1	1			YR120724014

Table A2.34. YR121006 (Clay Bank Anchor Station, October 6, 2012) Calibration Cruise

Station	Description	Date	Time (EST)	Lat 37° N	Long 76° W	depth (m)	CTD	TSS	LISST	ADCP profile	ADV profile	ADV bottom	ADCP transect	ADCP filename
5038	bottom	10/6/12	818	20.5300	37.5400	5.87	1		1	1			1	none
5039	profile 1		838	20.5302	37.5405	5.92	1		1	1	1			YR121006000
5040	bottom		841	20.5309	37.5440	5.88	1	2	1	1			1	YR121006001
5041	sample depths		853	20.5390	37.5433	5.89	1	5	1	1	1			YR121006002
5042	profile 2		909	20.5326	37.5440	5.92	1		1	1	1			YR121006003
5043	bottom		910	20.5867	37.5408	5.97	1	2	1	1			1	YR121006004
5044	bottom		917	20.5317	37.5419	5.97	1	2	1	1			1	YR121006005
5045	bottom		927	20.5303	37.5388	6.02	1	3	1	1			1	YR121006006
5046	bottom		939	20.5309	37.5406	6.02	1	1	1	1			1	YR121006007
5047	sample depths		952	20.5328	37.5443	6.02	1	5	1	1	1			YR121006008
5048	Sediment Grab		1016	20.5328	37.5443	6.02								
5049	profile 3		1031	20.5033	37.5045	6.09	1		1	1	1			YR121006009
5050	bottom		1035	20.5337	37.5479	6.1	1	3	1	1			1	YR121006010
5051	bottom		1042	20.5333	37.5514	6.11	1	3	1	1			1	YR121006011
5052	bottom		1045	20.5332	37.5505	6.07	1	3	1	1			1	YR121006012
5053	sample depths		1051	20.5334	37.5519	6.15	1	5	1	1	1			YR121006013
5054	profile 4		1106	20.5342	37.5493	6.27	1		1	1	1			YR121006014
5055	bottom		1108	20.5336	37.5492	6.22	1	3	1	1			1	YR121006015
5056	bottom		1115	20.5333	37.5337	6.22	1	3	1	1			1	YR121006016
5057	bottom		1125	20.5338	37.5518	6.22	1	3	1	1			1	YR121006017
5058	bottom		1133	20.5373	37.5500	6.3	1	3	1	1			1	YR121006018

Table A2.34. YR121006 (Clay Bank Anchor Station, October 6, 2012) Calibration Cruise

Station	Description	Date	Time (EST)	Lat 37° N	Long 76° W	depth (m)	CTD	TSS	LISST	ADCP profile	ADV profile	ADV bottom	ADCP transect	ADCP filename
5059	profile 5		1144	20.5345	37.5500	6.3	1		1	1	1			YR121006019
5060	sample depths		1146	20.5342	37.5501	6.34	1	5	1	1	1			YR121006020
5061	bottom		1206	20.5345	37.5501	6.35	1	3	1	1			1	YR121006021
5062	bottom		1214	20.5341	37.5506	6.4			1	1			1	YR121006022
5063	bottom		1216	20.5344	37.5491	6.42	1	3	1	1			1	YR121006023
5064	bottom		1226	20.5344	37.5490	6.39	1	3	1	1			1	YR121006024
5065	bottom		1238	20.5348	37.5509	6.4	1	3	1	1			1	YR121006025
5066	sample depths		1249	20.5345	37.5466	6.42	1	5	1	1	1			YR121006026
5067	profile 6		1310	20.5330	37.5437	6.47	1		1	1	1			YR121006027
5068	bottom		1311	20.5335	37.5464	6.44	1	3	1	1			1	YR121006028
5069	bottom		1320	20.5335	37.5441	6.51	1	3	1	1			1	YR121006029
5070	bottom		1336	20.5309	37.5407	6.5	1	2	1	1			1	YR121006030
5071	sample depths		1345	20.5315	37.5405	6.5	1	6	1	1			1	YR121006031
5072	profile 7		1409	20.5278	37.5375	6.4	1		1	1	1			YR121006032
5073	bottom		1413	20.5291	37.5390	6.48	1	2	1	1			1	YR121006033
5074	bottom		1421	20.5262	37.5369	6.47	1	2	1	1			1	YR121006034
5075	bottom		1433	20.5312	37.5410	6.5	1	2	1	1			1	YR121006035
5076	sample depths		1446	20.524	37.536	6.46	1	5	1	1	1			YR121006036
5077	Sediment Grab		1446	20.524	37.536	6.46								

VITA

Grace M. Cartwright

Born Grace M. Hornby in Portsmouth, VA, on June 13 1960, Grace was raised as a military dependent, including 10 years on Guam and the Philippines, until her father retired from the Navy in Yorktown, VA. She worked as a lab tech at James R. Reed and Associates in Newport News, VA, from 1980 until receiving her B.S. in Chemistry as from Christopher Newport College, Newport News, in January 1983. She then worked as a drinking/waste water analytical chemist at Reed and Associates and at Jennings Laboratory in Virginia Beach, VA. In 1987, Grace started her over 25 years, to date, of service for the Virginia Institute of Marine Science, Gloucester Point, VA, beginning in the Analytical Services Center. In 1996 she switched career paths and started working as a laboratory specialist for the Coastal Hydrodynamic and Sediment Dynamics (CHSD) lab in the Physical Sciences department. Soon thereafter she started utilizing the W&M employee benefit program, and she graduated with her M.S. in Marine Science from the College of William & Mary as Grace M. Battisto in 2000. In 2004 she was accepted into the School of Marine Science's Ph.D. program. Limiting herself to one class a semester, also as part of the employee benefit program, she completed her dissertation in June 2013, and she will graduate in August 2013 with a Ph.D. in Marine Science, with a concentration in physical oceanography.

While working for CHSD, Grace has been promoted to a Professional Faculty position and program manager for CHSD and has earned the VIMS 2009 Outstanding Classified (Technical) Employee award. To date, she has managed several million dollars in CHSD grants and contacts and has been either a PI or Co-PI of almost $250,000. She has been first or second author on 39 posters and abstracts, 12 journal papers and conference proceedings and 21 technical reports. Grace has taught 6 semesters of GEOL 160 "Introductory Geology Lab" for the William and Mary Undergraduate Program (2 sessions each semester) and has mentored or co-mentored 22 high school and college students, including W&M undergraduates, REUs, Governor School students, and visiting students from the University of Utrecht, The Netherlands. She has also supervised 7 part-time employees during her service for CHSD. She has served at VIMS on the Professional/Professional Faculty Council since 2009, on the Field Operations Advisory Committee from 2010-2012, and on the Database User's Group from 2009-2011. Outside of VIMS, she has advised the US Integrated Ocean Observing System (US IOOS) through her invited attendance at the Quality Assurance of Real Time Data (QARTOD) workshop for the development of QARTOD manual for Real-Time Quality Control of Dissolved Oxygen Observations and was on the Review Team the QARTOD manual for Real-Time Quality Control of currents (both published by US IOOS).